THE BELL SYSTEM
TECHNICAL JOURNAL

VOLUME XLV SEPTEMBER 1966 NUMBER 7

An Experimental 224 Mb/s Digital Repeatered Line

By I. DORROS, J. M. SIPRESS, and F. D. WALDHAUER

(Manuscript received May 12, 1966)

An experimental digital repeatered line has been developed which transmits information at a rate of 224 Mb/s as part of an experimental high-speed digital transmission system. The PCM terminals and time division multiplex portions were described by J. S. Mayo and others in the November 1965 issue of the Bell System Technical Journal. The repeatered line is described in this paper. The performance of this line is shown to be suitable for coast-to-coast operation.

The line utilizes 0.270-inch copper coaxial transmission lines and regenerative repeaters at one-mile intervals. Ten repeaters have been operated in tandem to form ten miles of repeatered line. Each repeater uses 25 transistors, most of them a new germanium design with a cutoff frequency, f_t, of 4 GHz. Esaki diodes provide the decision thresholds for the regeneration. Power to the repeaters is supplied by dc over the center coaxial conductor. The pulse transmission code is paired selected ternary (PST).

I. INTRODUCTION

Digital transmission of information is becoming increasingly attractive in the telephone plant because it competes favorably both in performance and in cost for telephone service and it allows all kinds of other services such as data and television to share the transmission media with virtually no interaction among the various signals. The digital transmission process[1] is based on (*i*) pulse code modulation of the analog signals to be transmitted, (*ii*) time interleaving of the resultant pulse streams to form a composite pulse stream, and (*iii*) regeneration

in the repeatered line to nullify the effects of noise and distortion encountered in transmission.

The T1 carrier system,[2,3] extremely successful since its introduction in the Bell System in 1962, provided the first wide use of the digital transmission concept. In T1, 24 exchange area voice signals are pulse code modulated, time division multiplexed, and transmitted over cable pairs at a rate of 1.544 megabauds. T1 repeatered lines are now also in use for short-haul data services,[4] since these lines are virtually insensitive to the source of the pulse streams transmitted.

There has also been interest in making use of the features of digital transmission for long-haul transmission. Recently, at Bell Telephone Laboratories, a 224 megabits/second (Mb/s) experimental system was constructed to demonstrate the feasibility of a coast-to-coast system. The PCM terminals and time division multiplex portions of this system were described by J. S. Mayo and others in the November 1965 Bell System Technical Journal.[5,6,7] It was there indicated that the 224 Mb/s information rate would serve either four coded 600 channel mastergroups for a total of 2400 voice channels, 144 T1 signals representing 24 channels each for a total of 3456 voice channels, two coded network TV signals, or some combination of these and other digital signals. In this paper, we describe the experimental repeatered line. The significant accomplishment is the realization of repeater circuits with suitable operating margins that detect and regenerate pulses at a 224 megabaud rate (a baud interval of 4.5 nanoseconds) when each pulse is dispersed by the transmission medium into more than 30 baud intervals and also attenuated to a level limited by thermal noise considerations.

In Section II we give a general description of the line and a summary of performance. In Section III we describe the design of the overall line leading to the requirements on each of the repeaters. The design considerations include the pulse transmission code, the equalization for the loss-frequency characteristic of the coaxial transmission medium and the control of the accumulation of jitter in a chain of repeaters. In Section IV, the design of the repeater is described with emphasis on critical circuits such as the Esaki diode regenerator. Section V reports on performance under laboratory conditions.

II. GENERAL DESCRIPTION

2.1 *Brief Description of the Experimental Repeatered Line*

The configuration of the experimental repeatered line is shown in Fig. 1. The overall performance of such a line is characterized by the

rate of errors introduced into the transmitted stream of information and by the amount of pulse jitter introduced into this stream.

The line operates at error rates below 10^{-10} through ten repeatered links. A coast-to-coast system of about 4000 repeatered links requires an overall error rate below 10^{-6}, or below 2.5×10^{-10} per link. Hence, 4000 mile error performance has been achieved under laboratory conditions.

The pulse jitter measured through ten repeatered links under laboratory conditions was 13 degrees rms. From the model for the accumulation of jitter in a chain of repeaters,[8] this 13 degrees implies that the significant component of jitter introduced *per repeater* is about 3 degrees rms. As will be discussed in Section 3.3.2, 3 degrees is an entirely acceptable performance level in a coast-to-coast system.

An arbitrary stream of binary unipolar pulses from the multiplex at a rate of 223.880 Mb/s is introduced into the line at a binary-to-PST translator as shown in Fig. 1. This translator converts the 2-level pulses into a selected ternary code, called paired selected ternary (PST), for transmission. The details of this code are described in Section 3.1 and also in an earlier paper.[9] Briefly, the ternary transmission of the binary information provides sufficient redundancy (*i*) to allow the transmission of unrestricted binary sequences while still providing timing information to the repeaters, (*ii*) to eliminate dc components from the transmitted spectrum, thus permitting ac coupling in the repeaters and powering at dc, and (*iii*) to allow in-service error monitoring for maintenance purposes.

The ternary signal from the translator has its positive and negative pulses represented as positive pulses on separate leads. These are applied to the transmitting repeater which adjusts levels, combines the two streams, and adds dc power to the signal for serial powering of the repeaters.

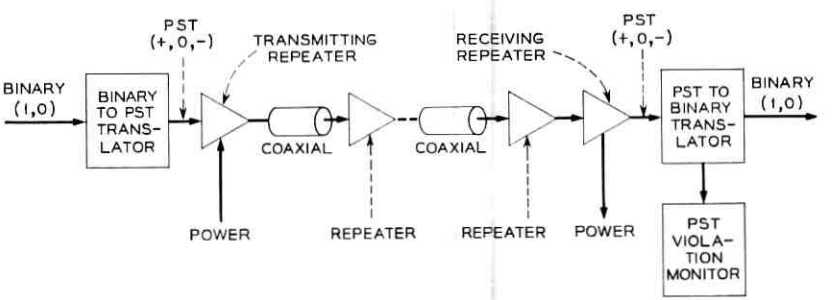

Fig. 1 — Experimental repeatered line.

This system utilizes essentially one mile of an experimental cable with eighteen 0.270-inch coaxials, designed at Bell Laboratories and fabricated at the Western Electric Company's Baltimore Works. The cable design will be reported on separately. Each repeatered link uses one of the 18 coaxials in the cable. Electrically, the coaxial line inserts a loss that is proportional in dB to the square root of frequency ($\sqrt{f}$) over the frequency range of interest. At a nominal temperature, the loss of a mile of 0.270-inch coaxial line is 57 dB at 112 MHz, one-half the baud rate. The propagation characteristics of the experimental cable are essentially equivalent to those of standard Bell System coaxial cables used for L-carrier transmission.[10] Hence, the spacing of the repeaters on the 0.375-inch standard coaxials now generally being installed would be that of the experimental system modified by the ratio of the diameters [(1.0 miles) $\times$ (0.375/0.270) = 1.4 miles].

The regenerative repeater, of the forward acting complete retiming variety,[11] performs the three R's — reshaping, retiming, and regeneration. To reshape, an equalizer compensates for the $\sqrt{f}$ propagation characteristic of the transmission medium in such a manner as to compromise among the intersymbol interference, the noise entering at the repeater preamplifier, and other important degrading effects. The repeater spacing is controlled by this compromise. To retime, a sine wave with average frequency equal to the baud rate is extracted from the pulse train by nonlinear means. This sine wave in turn generates regularly spaced pulses of short duration for sampling the equalized waveform. To regenerate, a 3-level decision is made at each sampling instant to determine whether a +, 0, or − pulse is to be emitted in each baud interval. A detailed description of the repeater is given in Section IV.

In the experimental system, 10 such repeatered links have been operated in tandem, looping through 10 coaxials of the 18-coaxial cable to form 10 miles of line.

In the receiving repeater, the dc powering circuit is completed, the levels are adjusted, and the positive and negative pulses are separated into two unipolar streams for application to the PST-to-binary translator. Finally, a PST violation monitor makes use of a redundant property of the PST code to monitor errors as described in Section 3.1.4.[9]

2.2 *Main Stations*

An actual long-haul repeatered line would have main stations spaced at appropriate intervals to house equipment for (*i*) powering the line repeaters through the transmitting and receiving repeaters, (*ii*) isolating and automatically switching out a section of line for maintenance pur-

poses, (*iii*) controlling the accumulation of pulse jitter in a long repeatered line,[5,7] and (*iv*) dropping and adding information-bearing pulse streams (multiplexing).

The main station spacing appears to be determined primarily by the multiplexing considerations. The limitation due to powering is based on the power required by the repeaters and the maximum practical voltage which can be applied to the coaxials and the repeaters. The limitation due to section isolation considerations depends on the combined reliability of the cable and the repeaters. We will not deal with the power and section isolation questions in this paper, but we will show in Section 3.3 that jitter control is required only at very distant spacings, and hence is not a consideration in the spacing of main stations.

III. DESIGN OF THE LINE

The overall design of the experimental 224 Mb/s digital repeatered line is described in this section; the repeater itself is described in Section IV. We discuss the pulse transmission code in Section 3.1, the equalization of a link of repeatered line in Section 3.2, and the retiming of such a link in Section 3.3. The derivation of performance objectives for a single repeater from the overall objectives for a 4000-mile system is included; we treat error rate in Section 3.2 and jitter in Section 3.3.

3.1 *Pulse Transmission Code*

3.1.1 *Purposes of a Transmission Code*

The binary information from the multiplex must be coded into a sequence of signal symbols that is readily transmitted over a practical line. The transmission code adds redundancy to the binary information to permit the three specific functions described below.

Conceptually, the simplest pulse transmission code is unipolar in which the binary marks and spaces are coded for transmission as presence and absence of pulses. There are three significant practical problems associated with this unipolar format:

(*i*) Timing information must be extracted from the pulse train at each repeater to determine when the pulse, no-pulse decisions should be made and to retime the regenerated pulses emitted by each repeater. Long sequences of binary spaces result in long periods without pulses and hence, without timing information. This in turn yields poor timing performance, leading to increased error rate and pulse position jitter.

(*ii*) Since the repeaters are serially powered by means of dc trans-

mitted on the center conductors of the coaxials, the signal path in the repeaters cannot be dc coupled to the cable medium. Consequently, the transmission of varying densities of marks results in dc wander of the pulse stream, thereby reducing drastically the margins in the detection process. DC restoration circuits which could eliminate this wander appeared unfeasible for the experimental repeater because of the high baud rate.

(*iii*) Some method of determining error performance without the interruption of service is essential for maintenance purposes. In-service monitoring of the line error rate with the unipolar format as described above is impossible because each unipolar binary symbol carries exactly 1 bit of information with no redundancy.

All three of these problems can be eliminated by introducing redundancy into the coding process. In the experimental line, the required redundancy is obtained by employing 3-level transmission (+,0,−) at a line baud rate equal to that of the binary information rate. This redundancy is $\log_2 3 - 1 = 0.59$ bits/symbol.

Another means of achieving the necessary redundancy is to utilize polar binary transmission at a line baud rate higher than the information rate. This appears to be an unattractive alternative for a coaxial medium because the higher baud rate, resulting from a compromise satisfying the above three constraints with reasonable coding complexity, more than offsets the potential signal-to-noise advantage of detecting 2-level signals rather than 3-level signals.

3.1.2 *The Paired Selected Ternary (PST) Code*

The pulse transmission code is paired selected ternary (PST).[9] In this code, the binary sequence to be transmitted is framed into pairs and translated into a ternary format according to Table I. There are two modes in the PST code and the mode is changed after each occurrence of either a 10 or a 01 binary pair. As an example of PST coding, consider the following binary sequence and the corresponding PST sequence.

BINARY	10	01	00	01	11	01
PST	+0	0−	−+	0+	+−	0−

Note the change of mode after each occurrence of a 10 or a 01 pair in the binary sequence.

Six of the nine possible ternary symbol pairs are used to represent the four possible binary symbol pairs. The remaining three unused ternary symbol pairs are used for framing the pairs at the receiver.

TABLE I—THE PAIRED SELECTED TERNARY CODE

Binary	PST	
	+ Mode	− Mode
11	+−	+−
10	+0	−0
01	0+	0−
00	−+	−+

Change mode after each 10 or 01

The alternation of modes produces a null in the power spectrum at dc when the positive and negative pulses are balanced (identical except for sign). This enables dc powering of the repeaters. The PST power spectrum, $W(f)$, normalized to the baud interval, T, is presented in Fig. 2 for the case of equally likely marks and spaces in the original binary sequence [$p(1) = p(0)$], cosine-squared pulses one baud interval in duration at the base, and balanced positive and negative pulses. For other than this idealized situation, see Ref. 9.

The coding of the 00 binary pair into the −+ PST pair eliminates the timing problems associated with the transmission of long sequences of 0's. An additional feature of the PST code is that timing information

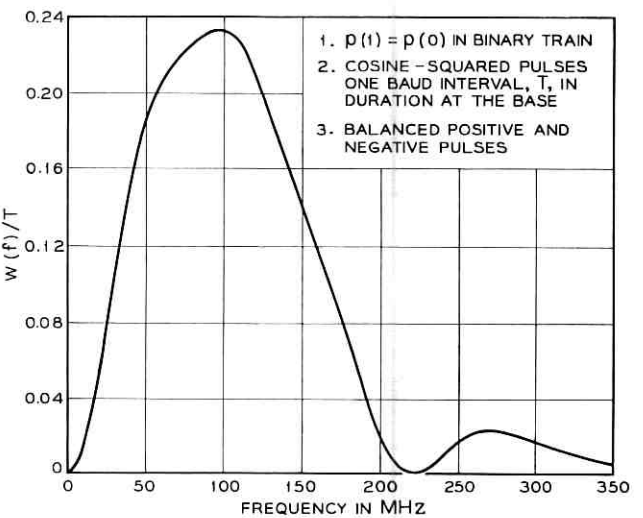

Fig. 2 — PST power spectrum for a random binary sequence.

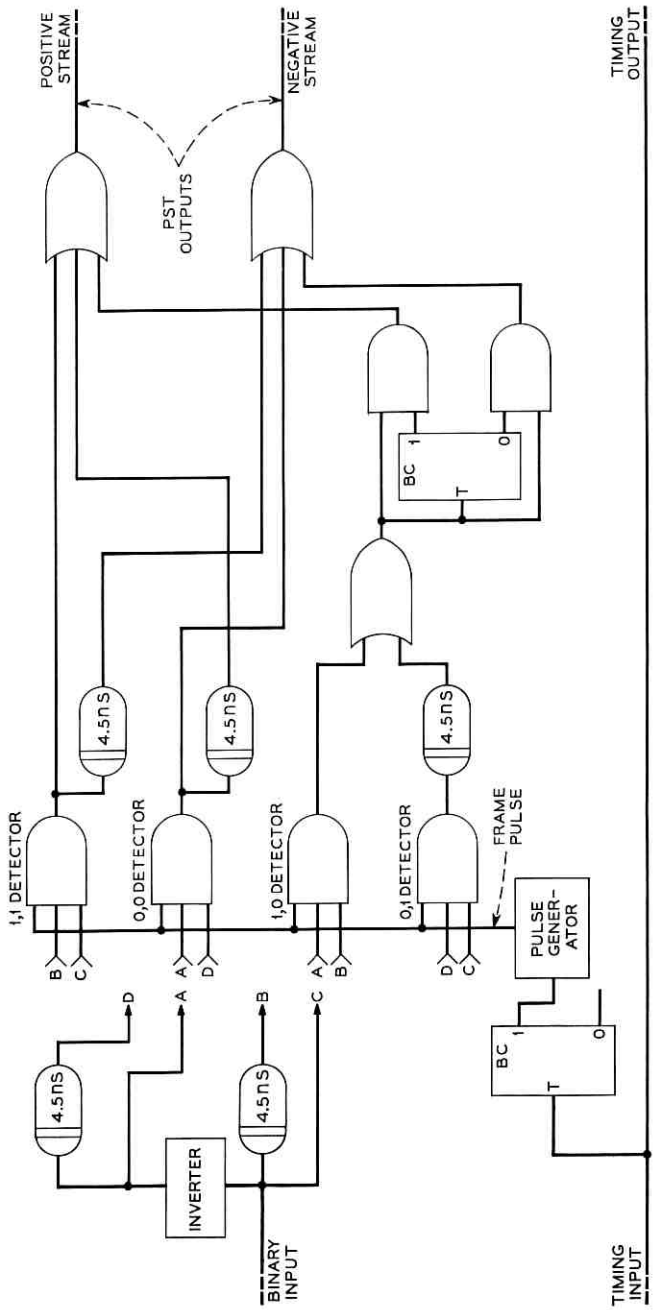

Fig. 3 — Logical diagram of the binary-to-PST translator.

at the repeaters can be extracted by nonlinear means (rectification). This avoids the harmonic and phase distortion problems associated with other schemes involving the linear extraction of timing information from the low-level components received at the baud frequency.

A logical diagram of the binary-to-PST translator is shown in Fig. 3.

3.1.3 *Translation of PST Sequences Back Into Binary*

At the receiving end of the line, the original binary sequence is recovered from the selected ternary sequence in the PST-to-binary translator.

Framing is essential to associate the symbols which are part of the same PST pair. The effect of incorrect framing is demonstrated below.

Binary		1	0	0	1	0	0	0	1	1	1	0	1	
PST		+0		0−		−+		0+		+−		0−		
Incorrectly framed PST	+		0	0	−	−		+0		++		−0		−
Incorrect binary			?		?			1	0		?		1	0

The unused ++, −−, and 00 ternary pairs are detected to indicate an out-of-frame condition.

The PST-to-binary translator is shown in Fig. 4. Out-of-frame indications are applied to a flywheel circuit which prevents randomly occurring line errors from initiating a change in frame. The flywheel requires that three out-of-frame indications occur within 19 consecutive pairs (38 baud intervals or 170 nanoseconds) to initiate a change in frame. The cumulative probability of obtaining three out-of-frame indications within J consecutive pairs after going out of frame is given by the $N = 3$ curve in Fig. 5 for the case of equally likely marks and spaces in the original binary sequence. The mean time (in PST pairs) to occurrence of N out-of-frame indications is shown as M.

To reduce the effect of erroneous frame shifts due to line errors, the flywheel is disabled for a period of 19 pairs after a change in frame. During this period, only one out-of-frame indication is required to initiate a second frame shift pulse, thereby reestablishing the original framing condition. The cumulative probability of obtaining one out-of-frame indication within J pairs is indicated by the $N = 1$ curve in Fig. 5. The mean time to an incorrect initiation of a change of frame due to randomly occurring line errors is shown in Fig. 6 as a function of error rate, assuming $p(1) = p(0) = \frac{1}{2}$. For the required error rates of 10^{-6}, such false misframes are extremely unlikely.

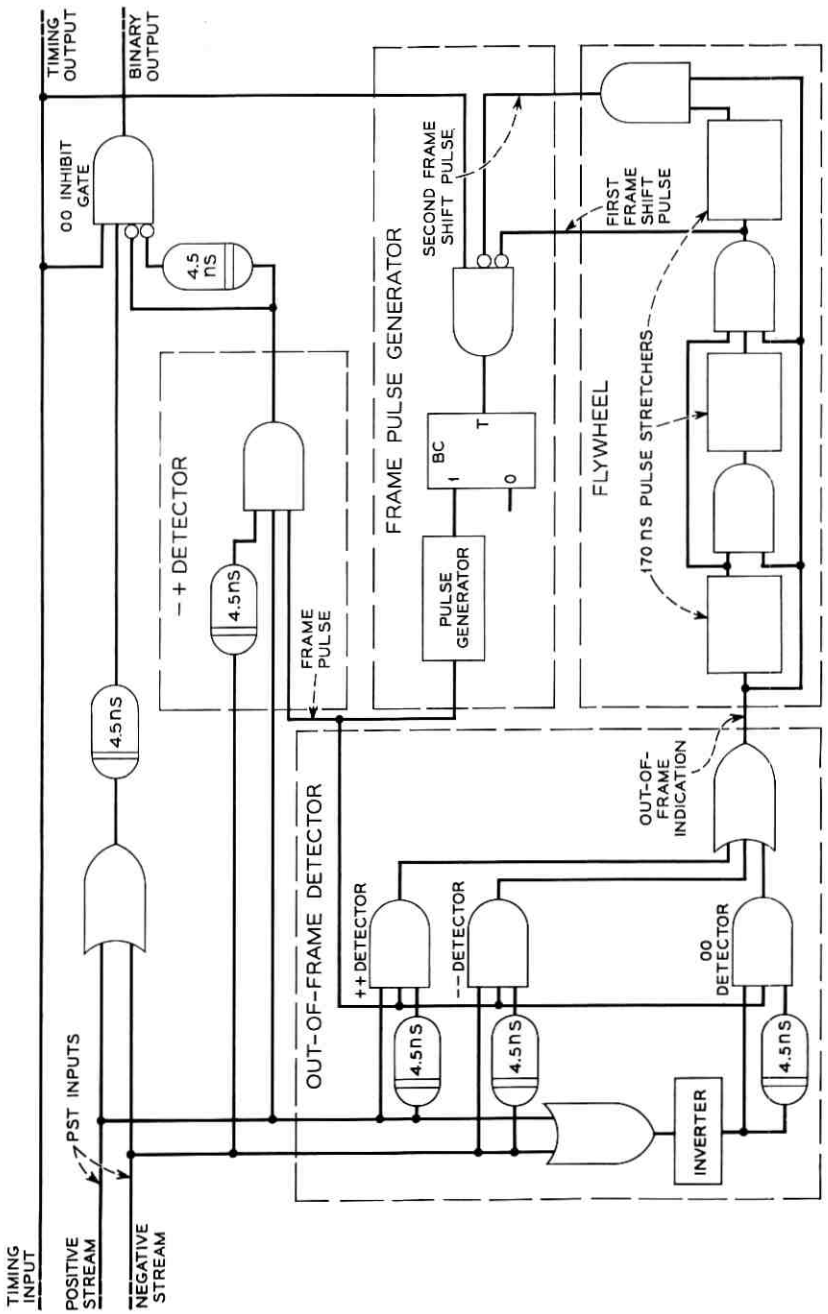

Fig. 4 — Logical diagram of the PST-to-binary translator.

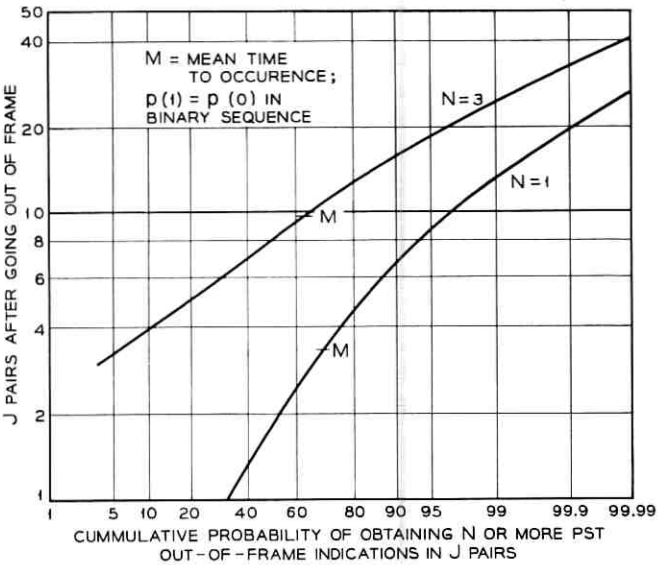

Fig. 5 — Probability of obtaining N or more PST out-of-frame indications in J pairs.

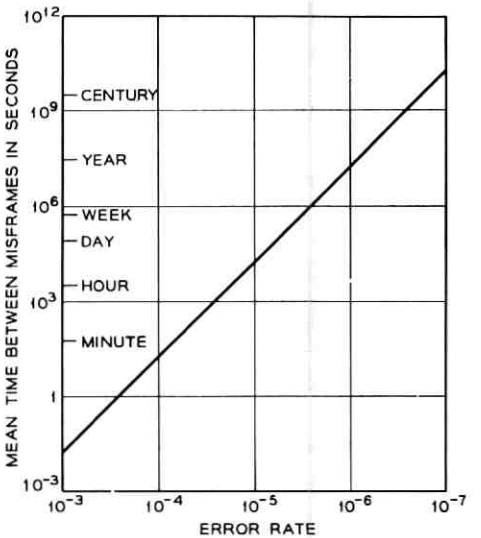

Fig. 6 — Misframes due to random line errors.

3.1.4 *In-Service Error Performance Monitoring*

A method of monitoring line error performance without interrupting service is a necessary maintenance feature of a long-haul digital transmission system. PST sequences contain certain properties which are violated only when errors occur. Violations of these properties can be monitored to determine the error performance on an in-service basis.

Four different properties whose violation provide means of error monitoring are given in Ref. 9. One of these, the *bipolar property* of PST, is employed in the experimental line.

To error monitor with the bipolar property, we first remove all of the $+-$ and $-+$ ternary pairs from the pulse stream. The remaining pulses, which come from coding the binary 10 and 01 pairs, alternate in polarity. An error causes a violation of this alternation or bipolar property, as in the example below.

PST pulse stream	+0 0− −+ 0+ +− 0−
PST with $+-$ and $-+$ removed	+0 0− 0 0 0+ 0 0 0−
	Error
PST with error	+0 +− −+ 0+ +− 0−
	Violation
PST with error and $+-$ and $-+$ removed	+0 0 0 0 0 0+ 0 0 0−

The violation can occur some time after the error, but all singly occurring errors* are detected.

A logical diagram of the PST violation monitor is shown in Fig. 7.

Since this form of violation monitoring requires framing common to PST-to-binary translation, these two functions have been combined in one circuit in the experimental system.

3.1.5 *Circuit Techniques for PST Code Translation*

The laboratory realization of the PST code translation equipment has made extensive use of Schottky barrier diodes and emitter-coupled current-routing pairs using transistors having an f_T of 3 GHz. The diodes perform the logic and the current routing pairs provide isolation, amplification, amplitude regeneration, and, when appropriately connected, logical inversion. Fig. 8 shows one of the four binary pair detectors in the

* For the low error rates we are interested in, the rate of singly occurring errors is essentially the total error rate.

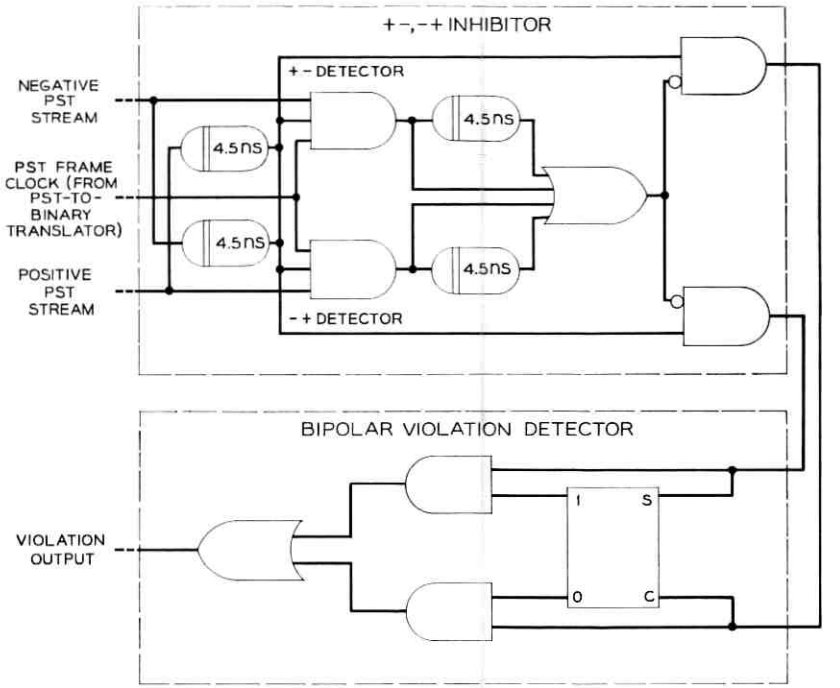

Fig. 7 — Logical diagram of the PST violation monitor.

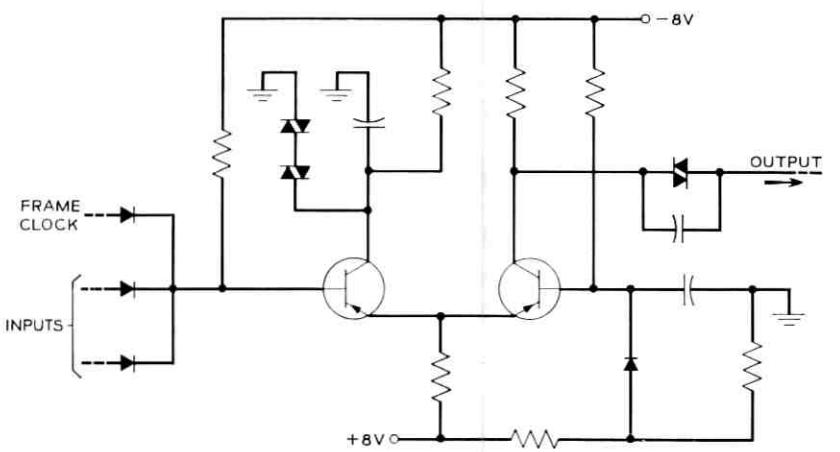

Fig. 8 — Binary pair detector at the input of the PST-to-binary translator — typical of the logic gates in the code conversion equipment.

binary-to-PST translator, a circuit typical of the logic gates used throughout the translation equipment. The input signals to the gates are at least one-half volt to insure complete switching of the emitter current from one transistor to the other.

Another circuit used extensively in the code translation equipment is the Goto pair binary counter, shown in Fig. 9, which employs two Esaki diodes.

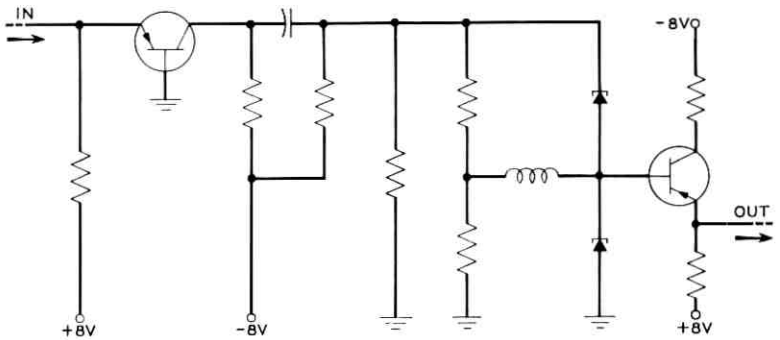

Fig. 9 — Goto pair binary counter using two Esaki diodes.

3.2 *Equalization of a Link of the Repeatered Line*

3.2.1 *The Error Rate Objective*

The preliminary overall error rate objective for a 4000-mile digital repeatered line is a maximum of 10^{-6}, based upon subjective testing and computation of noise power in the terminal signals due to line errors. Such an error rate will introduce negligible degradation into analog signals arising from services such as message, television, *Picturephone** and voiceband data, and will yield high performance for signals already in digital form such as computer outputs.[12] If we assume an approximate repeater spacing of one mile, we obtain a maximum error rate objective of 2.5×10^{-10} per repeatered link, or approximately 10^{-10}. This calculation assumes uniform operation of all repeaters. In a field situation, we would expect to permit somewhat poorer performance in several repeaters since the bulk of the repeaters normally would be operating at substantially better than this level. To place an objective on this, however, requires more knowledge of uniformity of repeater operation than is presently available.

* Service mark of the Bell System.

3.2.2 *Model of the Signal Path*

A model of the signal path in a link of a repeatered line is shown in Fig. 10. The signal path begins at the regenerator output in a repeater and ends at the regenerator input in the next repeater. The overall transmission of the signal path from $S_N(f)$ to $R_N(f)$ is denoted $T(f)$.

The loss of a coaxial tube in a cable, $C(f)$, is primarily dependent on the skin effect in the conductors and therefore this loss in dB is essentially proportional to the square root of frequency in the range of interest to us, and linearly proportional to the cable length. A single pulse through $C(f)$ alone is highly attenuated and severely dispersed and therefore gain and equalization are required to amplify and shape the pulse stream prior to detection in the regenerator. In the model, there are two equalizing blocks, $E_1(f)$ and $E_2(f)$, and two amplifying blocks, $A_1(f)$ and $A_2(f)$. The details of this separation will be discussed later, but it can briefly be stated here that the amplifier split is to sectionalize the required high gain, and the equalizer split is a compromise to limit the noise bandwidth, to prevent overload of the preamplifier, and to provide surge protection for the repeater output. The power separation filters at the input and output of the repeater are included in $A_1(f)$ and $E_1(f)$.

Our analyses have been carried out with cosine-squared regenerator output pulses one-half baud interval in duration at half-amplitude. This is a good approximation for the experimental system. The detailed shape of these pulses is not important because the spectrum of such a narrow pulse is nearly flat over the important frequencies in $T(f)$, which only go up to about three-fourths of the baud frequency. Hence, it is

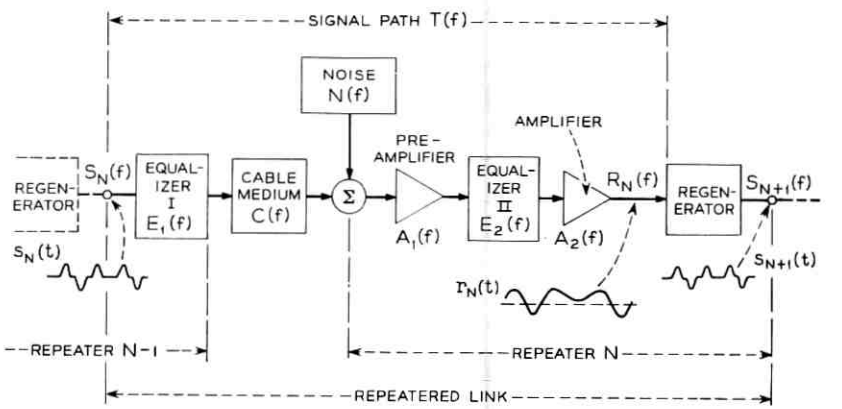

Fig. 10 — Signal path model.

only the total *area* of these pulses that is important. The pulse duration used was chosen for convenience in implementation.

The outer conductor of the coaxial is 0.005-inch thick copper with a soldered seam. The conductor thickness is sufficient to essentially isolate the signals inside the coaxial from the outside world. Hence, the controlling disturbance to the signal is the sum of the thermal noise of the cable and the noise generated in the preamplifier. This is shown in the model as an equivalent noise source at the preamplifier input, $N(f)$.

The key measure of the performance of a repeater is the error rate. This rate, in turn, is dependent on the ability of the regenerator to decide correctly whether +, 0, or − pulses were transmitted in each of the baud intervals. We are, therefore, highly concerned about the details of the waveform at the regenerator input, $r_N(t)$. Equalization $E_1(f)E_2(f)$ compensates for the shape of $C(f)$ and the imperfections in the transmission characteristic of $A_1(f)A_2(f)$. Also, the bandwidth of the noise entering the regenerator is primarily determined by $E_2(f)$. The optimum equalization maximizes the repeater spacing for a given error rate objective by means of a compromise between intersymbol interference and noise, while taking into account variations in coaxial loss due to temperature variations, sampling amplitude threshold offset, sampling timing misalignment, and other practical degradations.

An analytical solution for the optimum equalization in the face of all of the practical degradations in the repeatered link is not tractable. The general problem of optimum equalization for pulse detection has been treated in the literature,[13,14] but nowhere, including in analyses of our own, is there a solution to an applicable model. Consequently, we simulated the repeatered link on a digital computer in such a manner as to allow examination of the effects of the following:

(*i*) variations in the transmission characteristics of the coaxial, $C(f)$, the amplifiers, $A_1(f)$ and $A_2(f)$, and the equalizers, $E_1(f)$ and $E_2(f)$;
(*ii*) Gaussian noise with arbitrary power spectrum;
(*iii*) static and dynamic sampling time misalignment;
(*iv*) variations in detection threshold;
(*v*) variations in the statistics of the input binary sequence;
(*vi*) variations in the regenerator output pulse shape.

3.2.3 *Signal-to-Noise Ratio and Error Rate*

The theoretical error rate in the detection of a signal in the presence of Gaussian noise follows the well-known curve shown in Fig. 11.[15] Note that we have plotted peak signal-to-rms-noise. It is the *peak* signal that is of interest to us since the power limitation is in the repeater

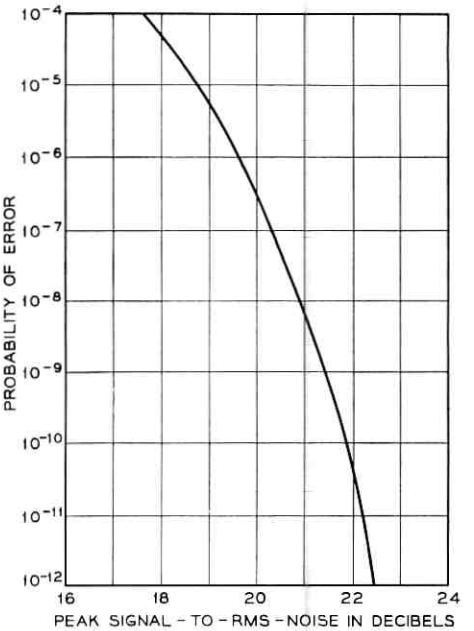

Fig. 11 — Theoretical error rate as a function of peak signal-to-rms-noise ratio.

peak output capability, not in its average signal power. Also, because of the shielded nature of the coaxial medium, transmitted signals do not interfere with any other signals.

The interpretation of Fig. 11 is that the average error rate indicated by the ordinate will prevail if the ratio of the peak of an isolated pulse to rms Gaussian noise, with no interfering signals or other degrading effects at the time of detection, is the quantity in dB indicated by the abscissa. Under practical conditions with a high baud rate there *will* be intersymbol interference and other degradations. Hence, at the decision instants the signal will depart from the ideal case, where there is either a full peak or no signal at all, and where the decision time instant and threshold are perfect. Fig. 11 must, therefore, be interpreted appropriately.

To avoid the difficulty of dealing with statistical intersymbol interference and other degradations, we conservatively design for the worst case. Hence, Fig. 11 may be used to determine the upper bound on the error rate if the *peak signal* is interpreted as the difference at the sampling instant between the minimum amplitude of all received pulse signals and the maximum amplitude of all received no-pulse signals.

The worst case is the combination of the worst intersymbol interference resulting principally from cable temperature changes and circuit imperfections, and the other degradations such as nonideal sampling where both the time instant and the threshold are imperfect. The lumping of the other degradations with intersymbol interference is illustrated in Fig. 12 using the ternary eye. This eye represents the inner boundaries of all possible pulse sequences superimposed and synchronized with the baud rate; in addition, the boundaries have been displaced inward vertically and horizontally to account for the other degradations. Resulting eye heights H_+ and H_- now represent the peak signal for use on Fig. 11, and the time and amplitude crosshairs now are of zero width. In what follows, H is taken to represent either H_+ or H_-.

From Fig. 11, we see that in order to maintain the per repeater 10^{-10} error rate objective indicated in Section 3.2.1, under extreme conditions (due to pulse sequences, cable temperature, parameter drifts, and sampling time and threshold displacements), the ratio of H to the rms noise must be 22 dB. It follows then that the ratio of the peak of the pulse, P, to the rms noise is greater than the theoretical value of 22 dB by an impairment defined as

$$I = 20 \log (P/H).$$

The impairment, I, is the excess peak-signal-to-rms-noise ratio in dB required to compensate for the worst case degraded eye due to the total of the intersymbol interference and other degradations. Due to the rapid increase with frequency of the loss of the coaxial, a small increase in equalized bandwidth for the purpose of reducing intersymbol interference produces a large increase in noise. The compromise between intersymbol interference and noise, therefore, is balanced in favor of reduced bandwidth. Our specific compromise allows enough intersymbol interference and other degradations to reduce H to 0.2 P, which corresponds to an I of 14 dB.

It should be pointed out that the eye opening, H, is an artificial one with idealized crosshairs and, therefore, is not what is seen on an oscilloscope at the regenerator input. What is seen on an oscilloscope is the eye with all degradations up to the input to the practical detector. The detector, however, has its own degradations which *are* included in the artificial eye.

3.2.4 *Signal Path Parameters for the Experimental Line*

The digital computer simulation and actual circuit performance achievements have led to the signal path parameters of Table II for a

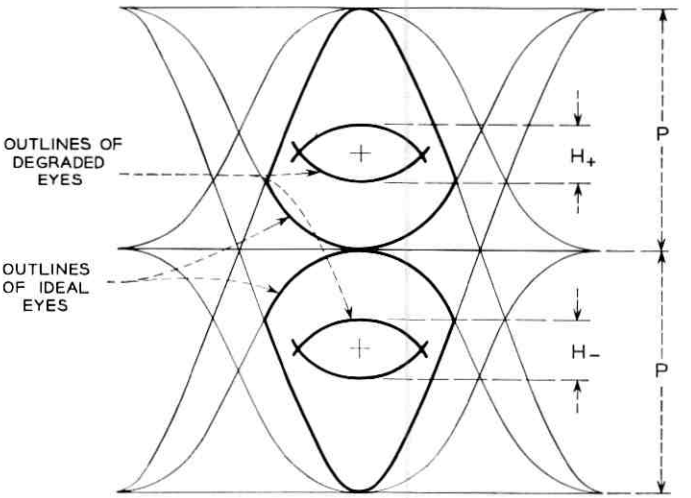

Fig. 12 — Ideal and degraded eyes.

repeatered link. These parameters have been realized, but under laboratory degraded conditions rather than worse case conditions.

Table III gives an example of the extreme conditions simultaneously permitted by the design implied by Table II.

The signal path parameters of Table II impose the requirements on the design of the repeater itself, to be discussed in detail in Section IV. For the present, we have specified, (*i*) the loss of the cable at the half

TABLE II — SIGNAL PATH PARAMETERS OF A REPEATERED LINK

Worst case error rate		10^{-10}
Repeater peak output power		+14 dBm
Preamplifier noise figure		6 dB
Theoretical peak signal-to-rms-noise ratio for 10^{-10} error rate		22 dB
Impairment, I, for worst case degradations		14 dB
Ratio of peak equalized single pulse to rms noise under nominal conditions		36 dB
Loss of coaxial between repeaters (Corresponding length of 0.270-inch coaxial at nominal 55°F)		57 dB at 112 MHz (5320 ft)
Equalizer singularities	Zeros:	11 MHz
		15 MHz
		70 MHz
	Poles:	94 MHz
		161 MHz $\angle \pm 117°$
		196 MHz $\angle \pm 114°$

TABLE III — EXAMPLE OF EXTREME CONDITIONS SIMULTANEOUSLY PERMITTED

Cable temperature rise	21°F (maximum expected)
Equivalent echo at the sampling instant	20% of the pulse peak
Sampling amplitude threshold offset	10% of the pulse peak
Static sampling timing misalignment*	20°
Dynamic sampling timing misalignment distribution*	$\cos^4$ with 60° base width
Noise figure	7 dB

* 360° is one baud interval.

baud rate which bears on the gain in the repeater,† (*ii*) the required output power and noise figure of the repeater, (*iii*) the equalizer singularities, and (*iv*) the allowed impairment. The repeater design will take up from there.

As an indication of the significance of these signal path parameters, we refer to Figs. 13 through 17. First, the loss at 55°F of a coaxial be-

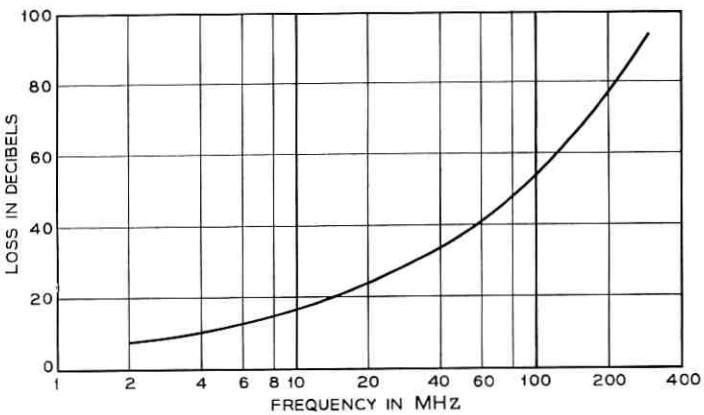

Fig. 13 — Loss of 5320 feet of 0.270-inch coaxial at 55°F on the usual log f scale.

tween repeaters is shown in Fig. 13 plotted on the usual log frequency scale in accordance with conventional characterization of transmission media. This curve (loss in dB) follows essentially the square root of frequency and goes through 57 dB at 112 MHz.

The nominal losses of the cable, the equalization including the effect of the amplifiers, and the overall channel with 50 dB net effective flat gain, are shown in Fig. 14.

† The loss of the peak of a pulse through the signal path is given approximately by the loss of this path at a frequency corresponding to half the baud rate.[16]

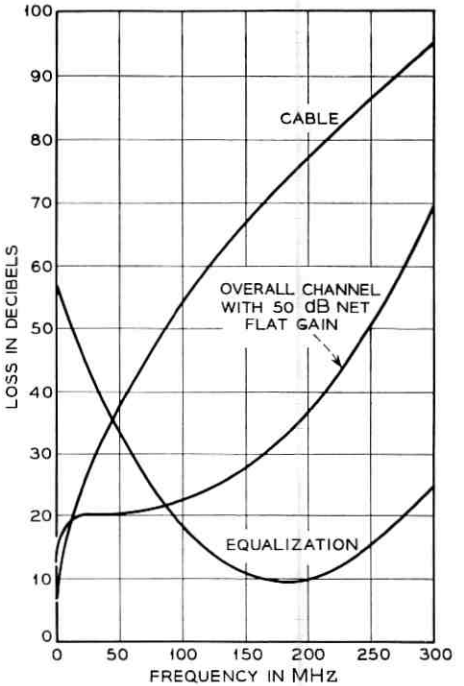

Fig. 14 — Cable, equalization, and overall channel loss characteristics.

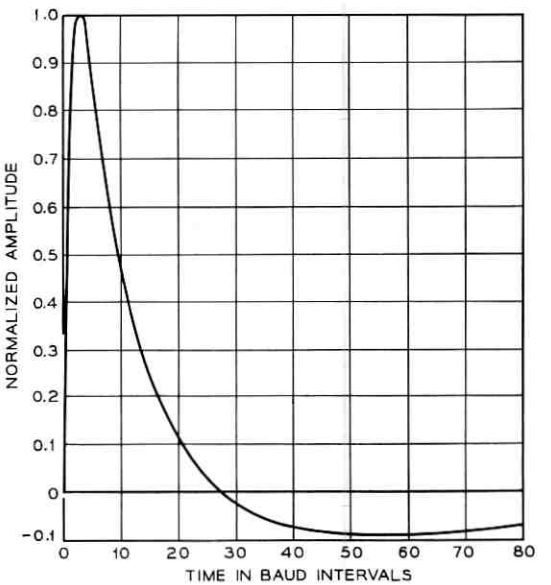

Fig. 15 — Nominal isolated pulse without equalization.

Due to the great variation of the cable loss over the frequency band of interest, the nominal isolated pulse without benefit of equalization is severely dispersed as shown, normalized to its own peak, in Fig. 15. It has a rise time of about 3 baud intervals and a fall time of about 25 baud intervals. The undershoot is due to the lack of dc transmission in the power separation filters and is of little significance since there are balanced numbers of positive and negative pulses in the PST code. As a result of the dispersion, the peak amplitude of all possible unequalized pulse sequences varies over a 28-dB range. The problem of dealing with the resulting large dynamic range in the repeater is discussed further in Section 4.1.

The nominal single equalized pulse is shown in Fig. 16. It is apparent that the amplitudes at -1.0, $+1.0$, $+2.0$, and $+3.0$ baud intervals are small. Under degraded conditions, however, these amplitudes are substantial. The low amplitude negative tail of such an isolated pulse, which obviously must be present in the response of a channel without dc transmission, is off the chart. The inner boundary of the superposition of this single pulse in all possible PST sequences forms the nominal eye shown in Fig. 17. The uppermost curve in this figure is the envelope of the maximum values of all pulse sequences. The slow-acting automatic

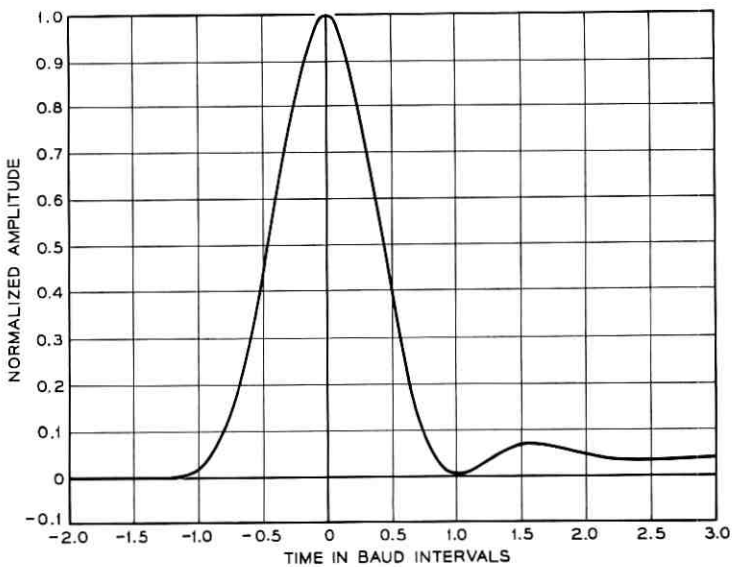

Fig. 16 — Nominal single equalized pulse.

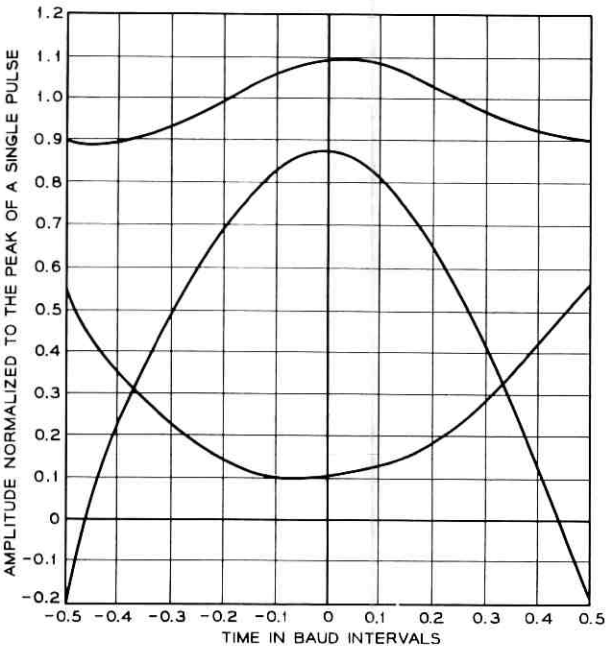

Fig. 17 — Nominal positive eye at the regenerator — inner boundary of the superposition of all possible PST sequences using the nominal single equalized pulse shown in Fig. 16.

gain control (AGC) in the repeater operates substantially on the peak of this curve. It should be emphasized that this nominal eye is the one seen on an oscilloscope and does not include the effects of the finite crosshair widths.

3.3 *Retiming in the Repeatered Line*

3.3.1 *Timing Extraction at Each Repeater*

The function of the repeater timing path is to extract timing information from the equalized ternary pulse stream. As discussed previously, this timing information is used to determine when the pulse, no-pulse decisions should be made as well as to retime the pulses transmitted from the repeater.

The repeater uses forward acting complete retiming[11] with nonlinear extraction of the timing component from the PST sequence. The equalized pulse stream is full-wave rectified and the upper portion of the

resulting unipolar stream is amplified and applied to a simple tuned circuit. The output of this is amplified and limited to produce a constant amplitude sinusoid which, in turn, drives a timing pulse generator.

Each repeater introduces phase variation, or timing noise, called jitter, into the extracted timing information. This jitter contains a systematic component which is a function of the transmitted pulse pattern and accumulates in a chain of repeaters considerably faster than the pattern independent, nonsystematic component.

The amounts of jitter introduced in and transmitted through each repeater can be kept low by a small effective bandwidth in the timing path. The smaller this bandwidth, however, the larger the static sampling timing misalignment for a given and inevitable mistuning of the timing extraction circuit.

The jitter accumulation and the objective for the jitter introduced in each repeater are discussed next.

3.3.2 *Control of Jitter Accumulation and the Requirements on a Single Repeater*

The preliminary objective for band-limited jitter at the end of a 4000-mile line is as shown in Fig. 18. This was derived on the basis of coded mastergroup message service in which the top frequency is 2.788 MHz, such as in an L600 mastergroup or a U600 mastergroup shifted down in frequency for more efficient sampling.* Based upon preliminary analysis and subjective testing, however, this objective is probably controlling for all digital and analog type services including data and network television. These two latter services, however, require further study.[12] The effect of low-frequency jitter within the objective shown is a signal-to-distortion ratio in the message channels in the frequency multiplexed mastergroup of greater than 30 dB; the effect of high-frequency jitter is crosstalk between channels less than theoretical 9-digit quantizing noise.

In order to meet this objective with an economical repeater design, appropriately spaced high Q jitter reducers[7] are required along the line. A jitter reducer includes an automatic phase control (APC) loop to smooth the jittered timing wave, and buffer storage for the information pulses. The information pulses are read into the store by the jittered timing wave and read out by the smoothed wave.

The jitter performance required of each repeater is a function of the

* In Ref. 5, this objective was given for a coded U600 mastergroup in which the top frequency is 3.084 MHz.

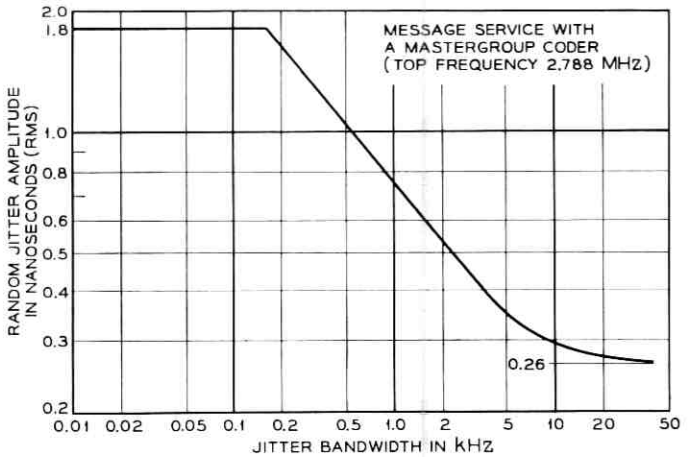

Fig. 18 — Objective for the maximum overall band-limited jitter due to random pulse sequences in a 4000-mile digital repeatered line.

overall jitter objective, the number of jitter reducers in the overall line, the effective Q of each of the jitter reducers, and the effective Q of the timing circuits in the repeaters.

The accumulation of jitter in a chain of repeaters with uniformly spaced jitter reducers can be analyzed by an extension of the technique developed for the analysis of jitter accumulation in the T1 system.[8,17] The analysis is based on a model in which the following assumptions are made:

(*i*) The significant jitter at the end of a chain of repeaters arises from the addition of the systematic, or pulse pattern dependent, jitter introduced in each repeater.

(*ii*) At the end of a long chain of repeaters, the accumulated jitter due to a random pattern is gaussian.

(*iii*) With respect to the transmission of accumulated jitter, the repeaters and jitter reducers may be replaced by the low-pass equivalents of their timing paths.

(*iv*) In each repeater, the effect of all sources of jitter due to random patterns is equivalent to the effect of a single, band-limited, white timing-noise source at the input to the equivalent low pass network.

(*v*) The timing noise introduced in the jitter reducers is negligible.

The model has successfully predicted experimental results for the T1 system,[8] and there is every indication that the same will be true for a high-speed repeatered line with jitter reducers. The model for the high-speed line is shown in Fig. 19. $F_R(s)$ and $F_J(s)$ are the low-pass equiva-

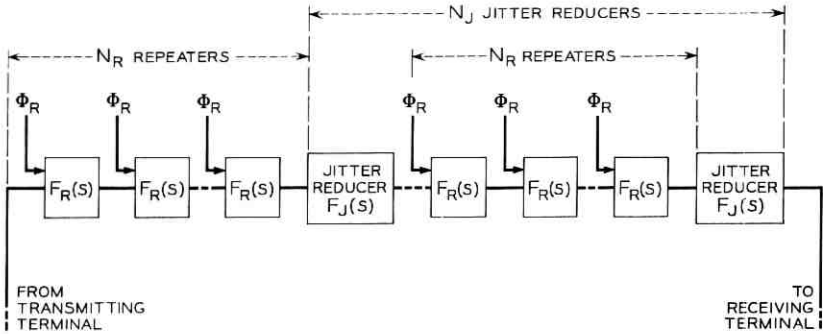

Fig. 19 — Model of a chain of repeaters and equally spaced jitter reducers for the analysis of the accumulation of jitter.

lents of the repeater and jitter reducer timing paths, and Φ_R is the power spectral density of the equivalent band-limited white timing noise source.

The results of an analysis are presented in Fig. 20 for a transcontinental system containing 3600 repeaters each with an effective Q of 80, and uniformly spaced jitter reducers each with an effective Q of 10^6. In this

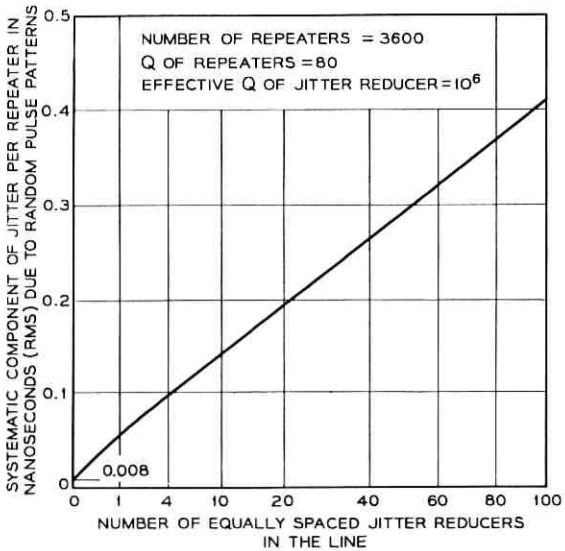

Fig. 20 — Objective for the systematic component of jitter (rms) contributed by a single repeater versus number of equally spaced jitter reducers.

figure, the requirement is given for the systematic component of jitter (rms) contributed by a single repeater due to random pulse patterns as a function of the number of equally spaced jitter reducers. If no jitter reducers were to be used, the repeater objective would be 0.008 ns rms or 0.6° rms, which when properly scaled is more stringent than the approximately 1° measured in T1.[8] Because of the higher-speed technology here, a practical requirement should be more liberal than the reported T1 performance. Based on our laboratory experience, a reasonable objective for the contribution of a single repeater to the systematic jitter due to random patterns is 0.1 ns rms or 8° rms. This leads to a need for four jitter reducers, each with a Q of 10^6, in 4000 miles, or one jitter reducer every 1000 miles. In an actual system, jitter reduction is required at all multiplex points. These occur, on the average, at intervals substantially smaller than 1000 miles, so that jitter reduction does not influence the main station spacing. Further, jitter reducers with Q's of less than 10^6 would be used.

IV. DESIGN OF THE REPEATER

A block diagram of the repeater is shown in Fig. 21. As briefly described in Section 2.1, the regenerative repeater performs the functions known as the three R's—reshaping, retiming, and regeneration. The

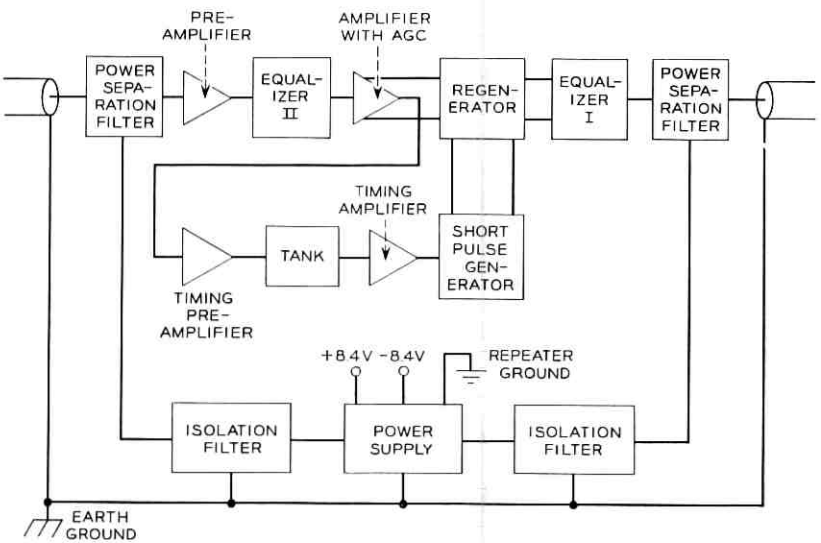

Fig. 21 — Functional block diagram of the repeater.

linear signal path (Fig. 10), comprising Equalizer I in the previous repeater, the preamplifier, Equalizer II, and the amplifier, reshapes and amplifies the pulse in preparation for detection. The timing path extracts a periodic timing wave from the signal train and generates a train of short sampling pulses occurring near the centers of the baud intervals, where the eye has its maximum opening. The regenerator provides crosshair pulse detection; at a time established by the sampling pulses, the signal pulse is compared with a threshold voltage, and if the threshold is exceeded, a new pulse is generated and transmitted to the next repeater. Since this is a ternary repeater, two such thresholds are provided. A second set of short periodic pulses controls the output signal pulse duration by turning off the regenerator after one-half baud interval.

The circuits shown on the block diagram of Fig. 21 were constructed on printed wiring boards and interconnected by sections of shielded transmission line on a printed interconnecting board. The development of the individual circuits was carried out independently between resistive terminations equal to the characteristic impedance of the transmission line used. Good cascading behavior was insured by controlling the forward transmission and the input impedance with load.

The complete repeater uses 25 transistors; 14 of these are a Bell System pnp germanium planar design with a cutoff frequency, f_T, of 4 GHz; 9 are a Bell System npn silicon design with an f_T of 1 GHz; and the remaining two are lower-frequency transistors of standard codes. A pair of gallium arsenide Esaki diodes provide the decision thresholds; a pair of charge storage diodes are used to generate the short sampling and turn-off pulses. Schottky barrier diodes are used in many circuits where high speed and low capacitance are required.

The description of the repeater circuits is organized into four sections: *reshaping* by the linear signal path, *retiming* by the timing path, *regeneration*, and *secondary features* such as powering and surge protection.

4.1 *Reshaping: The Linear Signal Path*

4.1.1 *Equalization*

The overall shape of the equalization is specified by the singularities indicated in Table II. Since the peak output power of the repeater is limited, minimum noise reaches the decision point in the regenerator if all of the passive equalization is placed beyond the preamplifier, a source of the noise. It is advantageous, however, to sacrifice a small amount of noise performance by placing a portion of the low-frequency attenu-

ating equalization ahead of the preamplifier to prevent its overload by certain pulse sequences strong in low-frequency content. With the PST code, the peak amplitude of the unequalized sequence varies over a 28-dB range, as stated earlier.

Once placed in front of the preamplifier, there is further advantage in placing this low frequency attenuating portion of the equalizer at the output of the previous repeater. This aids in protecting the regenerator against lightning and power surges, both rich in low frequencies relative to our band of interest.

The response characteristics and circuit configurations of Equalizers I and II are shown in Figs. 22 and 23. Equalizer I consists of a single

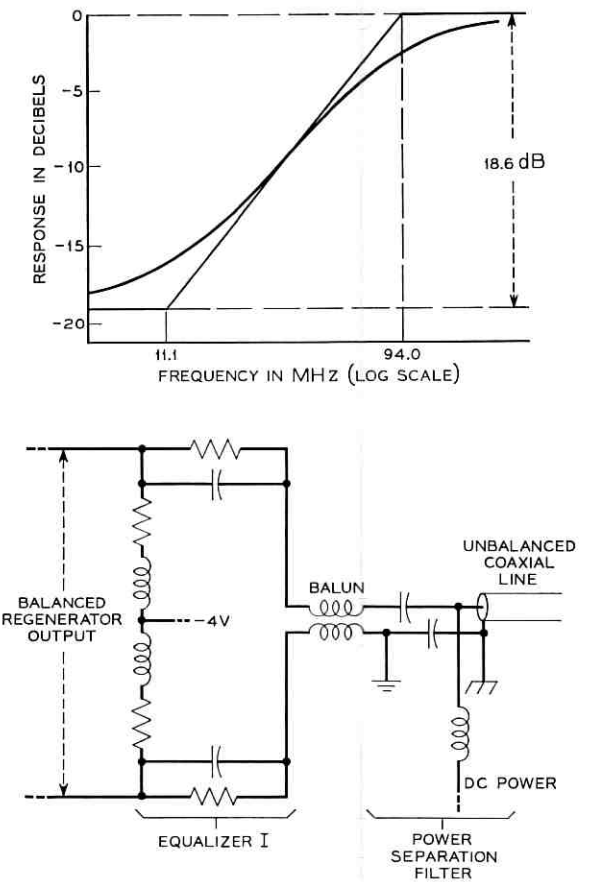

Fig. 22 — Equalizer I—attenuation characteristic and circuit configuration.

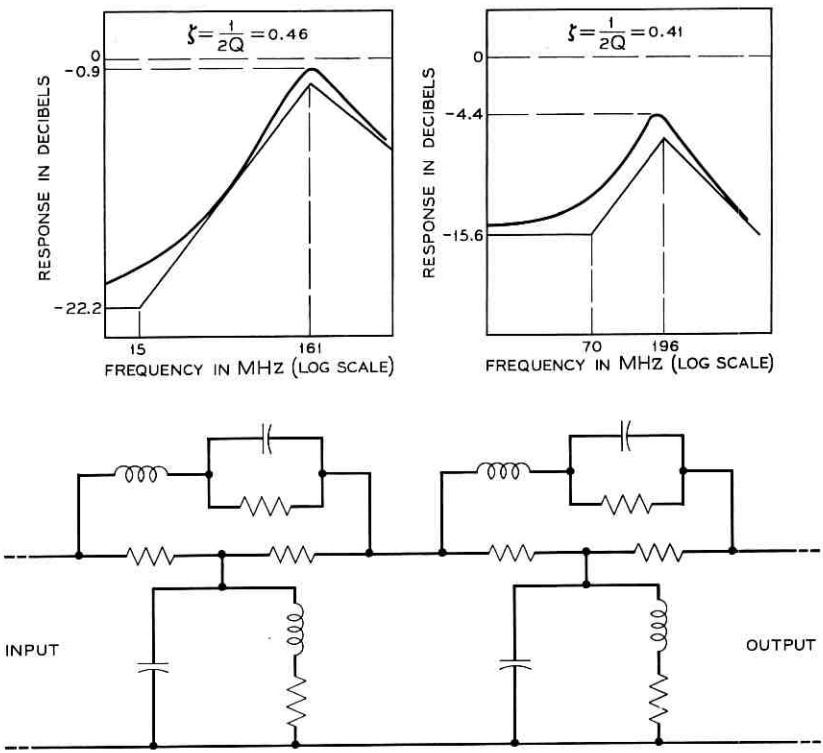

Fig. 23 — Equalizer II — attentuation characteristic and circuit configuration.

doublet with the zero at 11 MHz and the pole at 94 MHz. Notice the balanced nature of Equalizer I, which couples the balanced regenerator outputs to the unbalanced coaxial line through a balun and the unbalanced power separation filter.

Equalizer II comprises two constant R sections, each with a real zero and a complex pole pair. The first section has a zero at 15 MHz and poles at 161 MHz $\angle \pm 117°$ and the second section has a zero at 70 MHz and poles at 196 MHz $\angle \pm 114°$.

4.1.2 *Amplification*

It is the function of the preamplifier and amplifier to provide essentially flat gain while maintaining the desired equalized pulse shape. To accomplish this without complex delay equalization requires a bandwidth exceeding 300 MHz. The phase characteristic of this gain was

taken into account in the computer simulation that led to the equalization choice. A calculation of the gain required in the preamplifier and amplifier at 112 MHz is as follows:

Cable loss	57 dB
Equalization loss at 112 MHz relative to minimum loss	6 dB
Minimum loss of equalization	9 dB
Matching padding at amplifier input to achieve adequate return loss	6 dB
Nominal loss of variolosser (in amplifier for AGC)	5 dB
Effective ratio of amplifier to regenerator peak power outputs	−4 dB
Total gain required	79 dB

This gain is split with 26 dB in the preamplifier, and 53 dB in the amplifier.

The preamplifier curcuit, shown in Fig. 24, uses three transistors, each having a 4-GHz f_T, in common emitter configurations with collector to base feedback. The series diode gate at the input provides surge protection for the input transistor, and in the process loses 1 dB in noise figure and in gain. The overall circuit shown has a 6-dB noise figure at the frequencies of interest and a gain of 26 dB.

The amplifier functions (*i*) to terminate Equalizer II accurately in 50 ohms, (*ii*) to amplify the signal 48 dB nominally, with an AGC range of ±5 dB from nominal, (*iii*) to provide balanced outputs of 1 volt across each of the two regenerator 50 ohm inputs, and (*iv*) to rectify the bal-

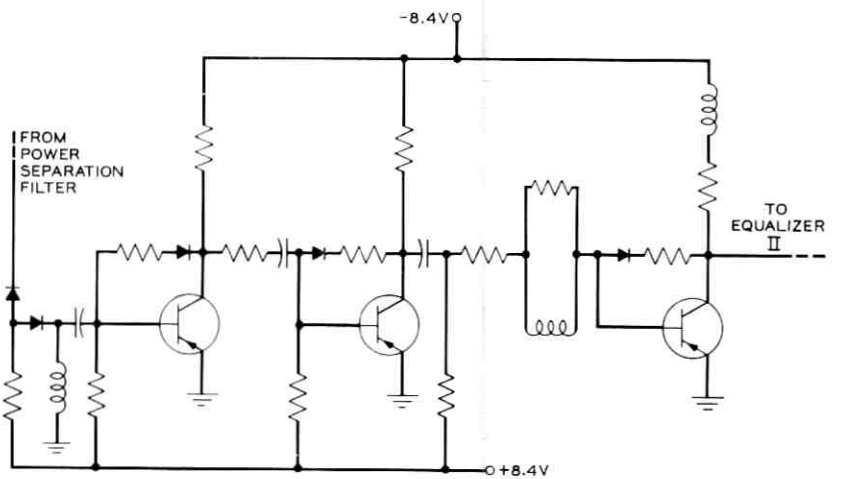

Fig. 24 — Preamplifier circuit.

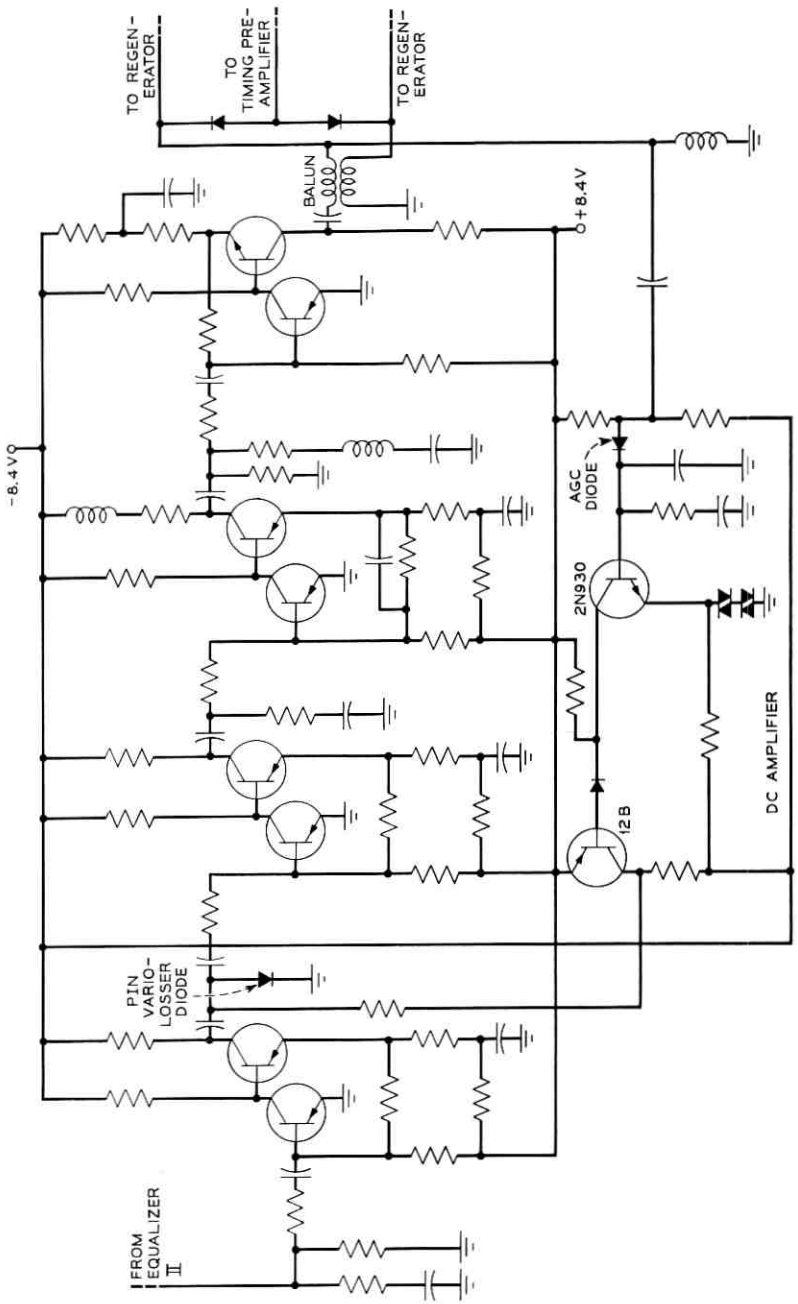

Fig. 25 — Amplifier circuit.

anced output to provide signals for the timing path. A circuit diagram of the amplifier is shown in Fig. 25. The basic gain stages are two-transistor doublets.[18] All transistors in the forward signal path are the 4-GHz pnp type, except the final transistor which is the 1-GHz npn type. The two transistors in the dc amplifier for the AGC are standard codes as noted.

The AGC diode compares the positive peak equalized signal amplitude with a reference derived from the power supply. When the amplitude is too large (small) the difference is amplified and the PIN variolosser diode current is increased (reduced). The advantage of a PIN diode over a pn-junction diode is that variolosser action is not obtained by the nonlinear conductance of a junction, but rather by the conductivity of the intrinsic region, determined by the dc control current. In this manner, currents of tenths of milliamperes are used to control signal power up to 1 milliwatt. The AGC loop gain is 40 dB at midrange.

4.2 *Retiming*

The timing path generates two trains of periodic subnanosecond pulses from information extracted from the equalized pulse stream. One train is for timing the decisions in the regenerator; the other, of opposite polarity, is for control of the duration of the regenerator output pulses. The relative phase between the sampling pulses and the information pulses at the regenerator input is determined by the timing path.

The timing path begins with the full-wave rectifier at the output of the amplifier (Fig. 25). The diodes are biased to transmit the upper 65 per cent of the rectified signals. This clipping level was shown to give best jitter performance both in an analog computer simulation of the timing path and in tests on the actual circuits. As indicated in Fig. 21, the clipped signal drives the timing preamplifier, which in turn drives a resonant tank tuned to the baud frequency. The output has pulse pattern dependent amplitude variations of approximately 14 dB; the $+0-0+0-\cdots$ sequence gives minimum amplitude and the $+-+-+-\cdots$ sequence gives maximum amplitude. This signal is amplified and limited to obtain a uniform high-amplitude sine wave, which in turn is coupled to a pair of oppositely poled charge storage diodes to generate the two required subnanosecond pulse trains.

4.2.1 *The Resonant Tank*

The tank is a loaded cavity with inductive loops for input and output coupling. The loaded Q is 80. An exploded view in Fig. 26(a) shows its

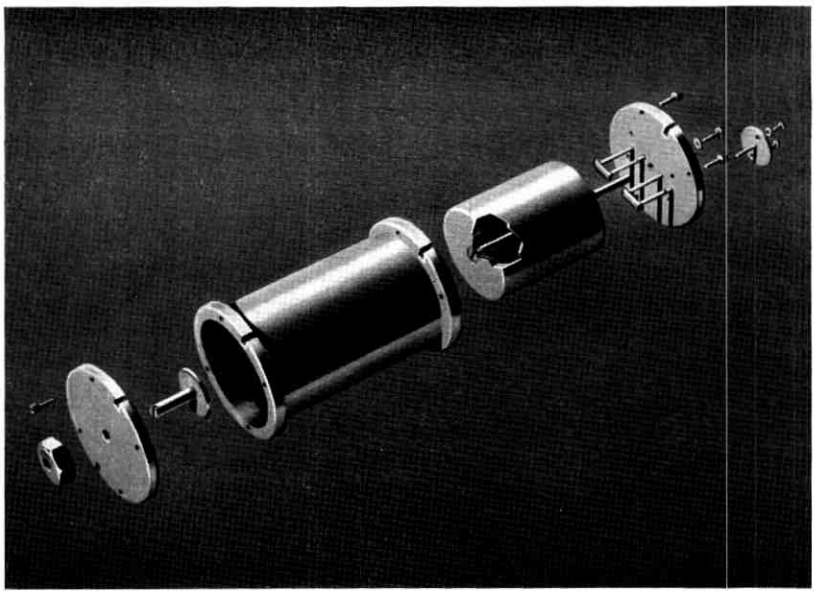

(a)

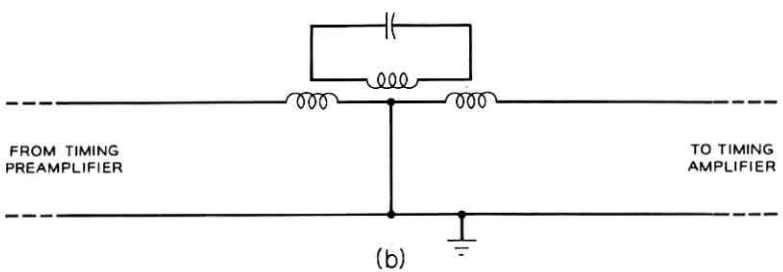

(b)

Fig. 26 — The resonant tank; (a) exploded view; (b) equivalent circuit.

construction, and the equivalent circuit in Fig. 26(b) shows its operation. The resonant frequency is stabilized with respect to temperature by the use of invar for the center post. This frequency can be adjusted over a narrow range by trimming the capacitance of the tank by adjusting the position of the disc attached to the trimming screw shown at the left end of Fig. 26(a).

We allow a maximum of ± 0.1 radian (5.7°) of static timing misalignment due to tank mistuning with age (20 years), and temperature (a range of 40°F). The phase shift, φ, of a high Q resonant circuit is

given for small values by

$$\varphi \approx 2Q \frac{\Delta f}{f}$$

where f is the resonant frequency and Δf is the mistuning. Hence, for a Q of 80, the tolerance on the resonant frequency is

$$\frac{\Delta f}{f} = \frac{\pm 0.1}{160} \quad \text{or} \quad \pm 0.0625\,\%$$

This level of performance is attained with the machined structure of Fig. 26, provided that it is operated between well-controlled impedances.

4.2.2 *Amplification in the Timing Path*

For the pulse sequence with maximum timing energy, the baud frequency component of the rectified timing signal has a peak amplitude of 150 mV. For the sequence with minimum energy, this component is 30 mV, or 14 dB lower. The peak amplitude of the required timing amplifier output is 3 volts, or 40 dB above 30 mV. In addition, as will be shown in Section 4.2.3, a minimum of 8 dB of limiting for the lowest level signal is required for good performance. Further, the tank has a loss of 0.5 dB at the baud frequency. Thus, linear gain of 40 + 8 + 0.5 = 48.5 dB is required in the timing path.

The 3-stage timing preamplifier, shown in Fig. 27, provides 22.5 dB of gain, and the 5-stage timing amplifier, shown in Fig. 28, provides 26

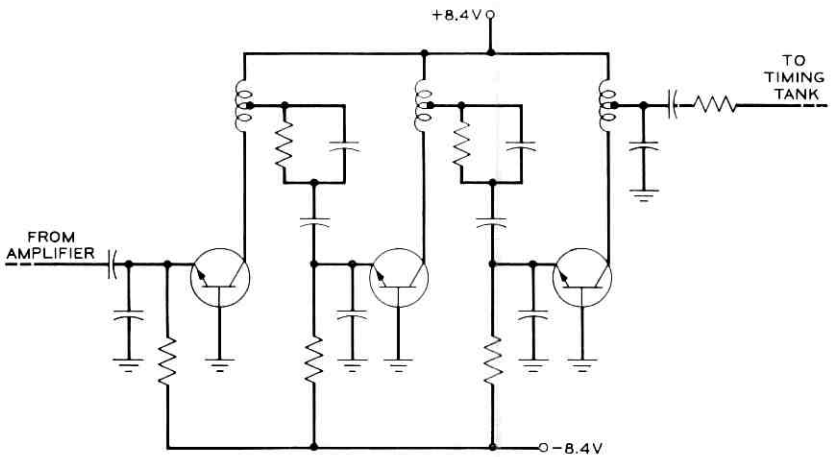

Fig. 27 — Timing preamplifier circuit.

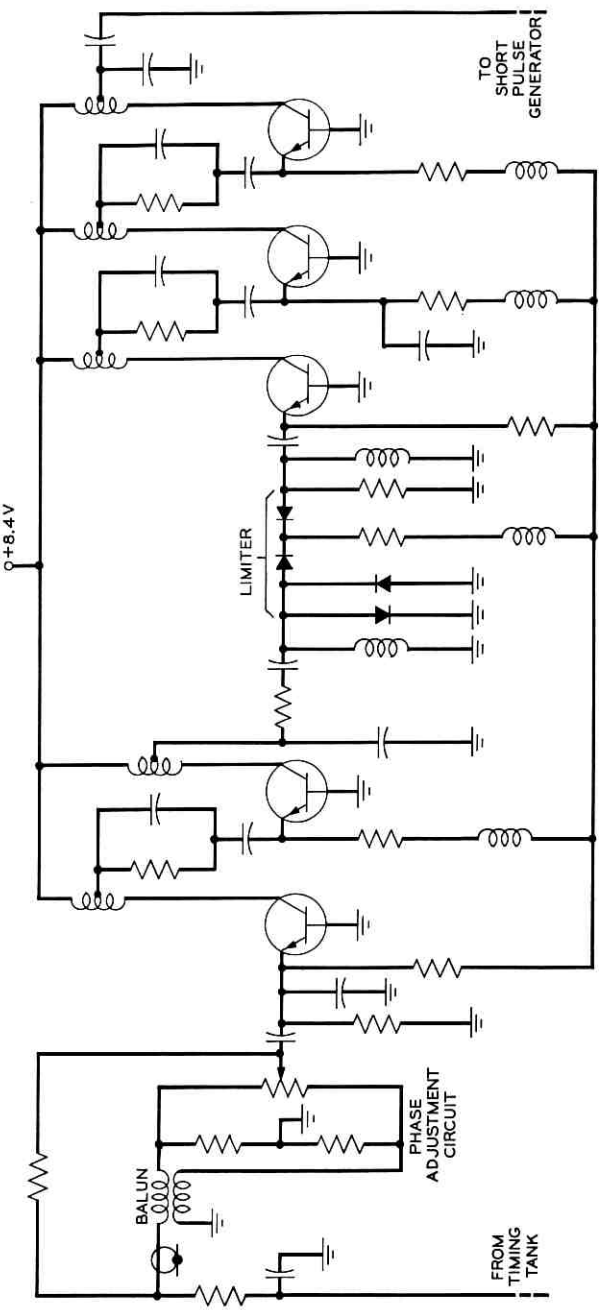

Fig. 28 — Timing amplifier circuit.

dB of gain at levels low enough not to produce limiting. Each stage has about 8 dB of gain, but the amplifier includes a phase adjustment circuit with 13 dB of loss, as described in Section 4.2.4. Both amplifiers employ common base stages coupled by bifilar-wound transmission line auto-transformers to provide current gain. All eight transistors are the 1-GHz npn silicon type.

As indicated in the composite frequency response of Fig. 29, the bandwidths of the timing path amplifiers are quite broad. This broadband design reduces the sensitivity of the timing path phase response to variations in amplifier reactive elements with age and temperature.

4.2.3 *Limiting*

A series gate employing Schottky barrier diodes at the output of the second stage of the amplifier is used to perform limiting, as shown on Fig. 28. Transistor limiting was avoided in order to keep amplitude-to-phase conversion at a minimum. The main cause of amplitude-to-phase conversion in this series type of limiter comes from diode shunt capacitance. With very large signals, significant reactive current flows through this capacitance and advances the phase of the output wave. This effect is kept small by the use of the shunt diodes to reduce the voltages reaching the series diodes. The amplitude-to-phase conversion of the limiter for the 7-mA diode current used is shown in Fig. 30(a).

Since the phases of the pulse trains generated by the charge storage diodes are heavily dependent upon the sine wave amplitude, the flatness of limiting shown in Fig. 30(b) is also important. Notice that an input of 0.35 volts at the lower end of the 17-dB range results in an output of

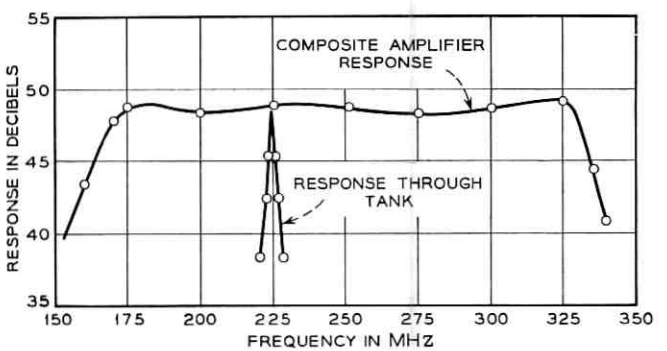

Fig. 29 — Composite frequency response of the timing path amplifiers.

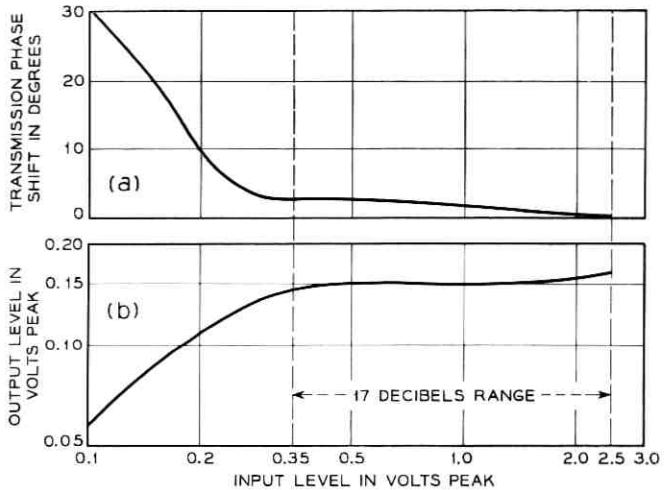

Fig. 30 — Limiter performance; (a) transmission phase shift vs input signal; (b) output signal vs input signal.

0.14 volts. This corresponds to the 8 dB of minimum limiting referred to earlier. The 17-dB range is the sum of 14 dB due to timing wave amplitude variations and 3 dB due to loss variations in the phase adjustment circuit to be described next.

4.2.4 *Phase Adjustment Circuit*

In order to set the sampling pulse at the center of the eye, a phase adjustment is required in the timing path. The circuit at the input to the timing amplifier (Fig. 28) was designed to permit a $\pm 45°$ adjustment range on the phase of the timing wave. The coaxial transmission line provides 90° of phase shift between the input and the upper end of the potentiometer. Due to the balun, there is 180° phase difference between the upper and lower ends. Two currents are summed at the emitter of the first amplifier stage. One current, I_R, at reference phase in the vector diagram of Fig. 31, comes directly from the input; a quadrature current, I_Q, comes from the movable tap. By moving the tap upward in the diagram, more phase lag is introduced and vice-versa. Over the extreme range of the potentiometer, for which I_Q is indicated by the dashed lines, 3 dB of amplitude variation is introduced, an amount which the limiter removes.

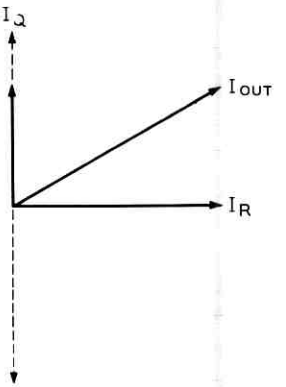

Fig. 31 — Vector diagram for phase adjustment circuit.

4.2.5 *The Short-Pulse Generator*

The circuit to generate the subnanosecond sampling and turn-off pulses is shown in Fig. 32. A sine wave of current from the timing amplifiers flows through the diode in the forward direction, storing charge. During this portion of the operation, the rather small forward voltage drop appears across the diode. When the sinusoidal current reverses polarity, the stored charge permits reverse conduction until the charge is depleted, whereupon the diode current abruptly falls to zero.[19,20] The feed inductor current is abruptly switched from the diode to the load to produce a rapid rise of current. The decay transient determining the short pulse duration is established by the coupling network with the diode open-circuited.

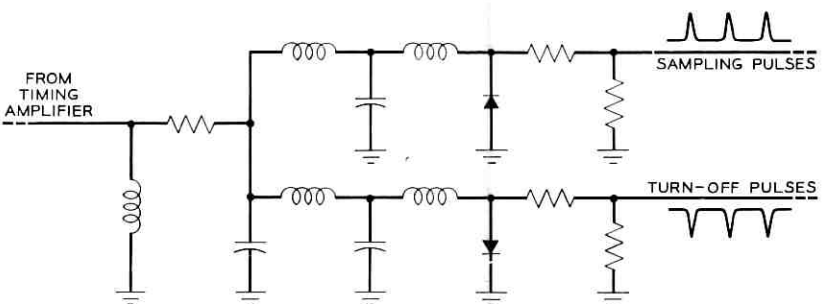

Fig. 32 — Short-pulse generator circuit.

4.3 *Regeneration*

In the regenerator, the ternary signal requires two amplitude thresholds, which are obtained by providing two identical decision circuits driven with oppositely phased signals from the balanced amplifier output. Each decision circuit incorporates a two-input AND gate and an Esaki diode, shown as part of Fig. 33. The signal is applied to one input of the gate and subnanosecond sampling pulses to the other. With a positive signal pulse present, the sampling pulse diverts the AND gate current from the sampling pulse diode to the AND gate output, where the Esaki diode is triggered to its high-voltage state. With either a zero or negative input signal, the gate current flows toward the signal source, and the Esaki diode remains untriggered. A subnanosecond negative turn-off pulse, one-half baud interval after the sampling pulse, returns the Esaki diode to its low-voltage state, establishing the repeater output pulse duration of 2.2 nanoseconds.

The Esaki diode voltages of the two decision circuits are amplified in a pair of current routing output stages, employing the 4-GHz germanium transistors. The resulting balanced outputs of these stages are combined to give the appropriate signal polarities at the repeater output.

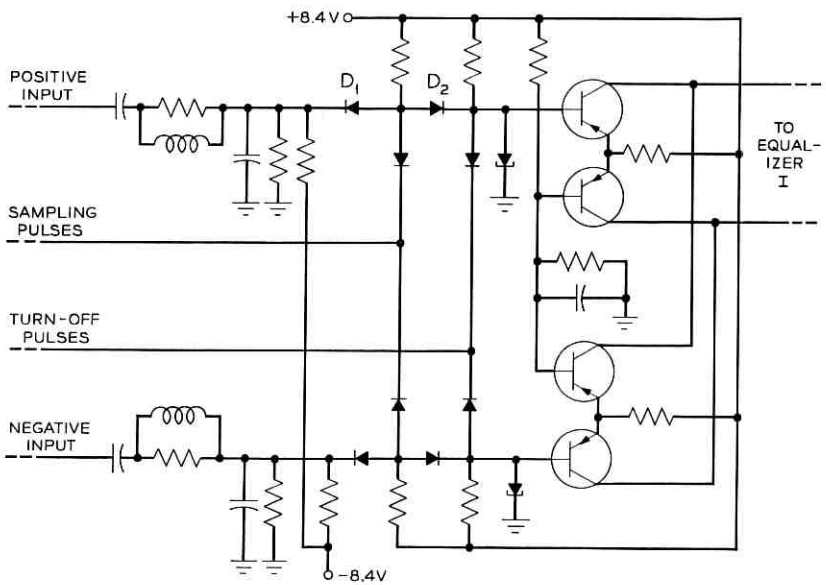

Fig. 33 — Regenerator circuit.

4.3.1 *Input Networks*

The inputs to the regenerator are ac coupled. The shunt capacitors (Fig. 33) reduce timing energy coupling onto the input signal leads. Since the timing path begins at the amplifier output, such coupling feeds energy back into the timing path, thereby increasing pattern dependent jitter. The other elements of the input networks provide good 50-ohm terminations for the amplifier signals.

4.3.2 *The Threshold Circuits*

A biasing circuit fixes the dc level of the signal relative to the threshold voltage, which is established by the Esaki diode. This threshold voltage and the signal bias are related through the back-to-back diodes of the AND gate to provide temperature tracking. The signal bias is chosen to place the Esaki diode threshold *voltage* at the center of the eye.

A discussion of the operation of the threshold circuit follows. At the threshold of triggering the Esaki diode, with the sampling pulse present, equal current flows through diodes D_1 and D_2 of the AND gate. It can be shown that this condition corresponds to maximum signal transmission, which provides maximum regenerator sensitivity.

An applicable model of the Esaki diode and its sources, shown in Fig. 34(a), is the parallel combination of a signal current source, I_S, a bias current source, I_B, a linear source resistance, a capacitance, and a nonlinear resistance whose static characteristic is shown in Fig. 34(b). The difference between the load line current and the static characteristic current is capacitive current I_C of our model. Threshold voltage V_A is the voltage at point A, the unstable intersection of the load line and the diode static characteristic. Initially, the voltage is V_C, the low voltage state. The subnanosecond sampled signal pulse charges the capacitance, raising the voltage. If after this pulse has passed, the resulting voltage is greater than V_A, excess current is available to further charge the capacitance, stable point B will be reached, and the decision will be that a pulse was present. If the voltage is less than V_A, the capacitance will discharge, operation will return to point C, and the decision will be that no pulse was present.

For good dynamic performance — that is, high circuit speed at the threshold level — the load line should intersect the diode negative resistance at a steep part. For high circuit gain, on the other hand, the load line should be raised toward the peak so that smaller AND gate current can be used (the amplifier must supply a peak-to-peak signal current equal to the gate current) and larger voltage can be obtained to

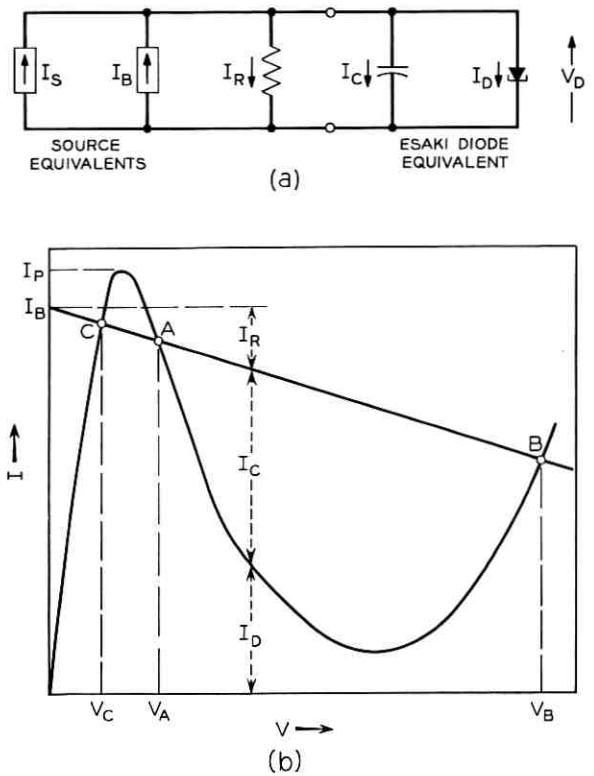

Fig. 34 — Esaki diode model; (a) equivalent circuit; (b) volt-ampere characteristic of nonlinear resistance.

drive the current routing stages. Further, for stability against changes in diode peak current with age and temperature, biasing current I_B should be small and the gate current should be large. As a suitable compromise among these factors, a bias current of 8 mA and a gate current of 4.5 mA were chosen in conjunction with a gallium arsenide Esaki diode having a peak current, I_P, of 10 mA.

The input-output dynamic regenerator characteristic was calculated using the equivalent circuit of Fig. 34(a) and a piece-wise linear approximation to the diode characteristic of Fig. 34(b). The performance was measured for six regenerators in the experimental setup of Fig. 35(a). A comparison of the limits of the measured characteristics and the calculated characteristic is shown in Fig. 35(b). It was indicated in Section 3.2.2 that the total area and not the amplitude of the regenerator output pulse primarily controls the amplitude of the pulse arriving at the sub-

sequent regenerator after transmission and equalization. Hence, the use of the simulated equalized line for $T(f)$ permits the proper comparison of equalized amplitudes, V_{out}.

4.3.3 *Output Amplifiers*

The emitter-coupled current routing pair of Fig. 33, which amplifies the Esaki diode voltage, has five important features. First, the circuit is fast because of the prevention of saturation. Second, it performs the inversion required for the negative pulse decision circuit. Third, its nonlinear forward transmission characteristic provides additional amplitude regeneration. Fourth, it has good dc temperature stability due

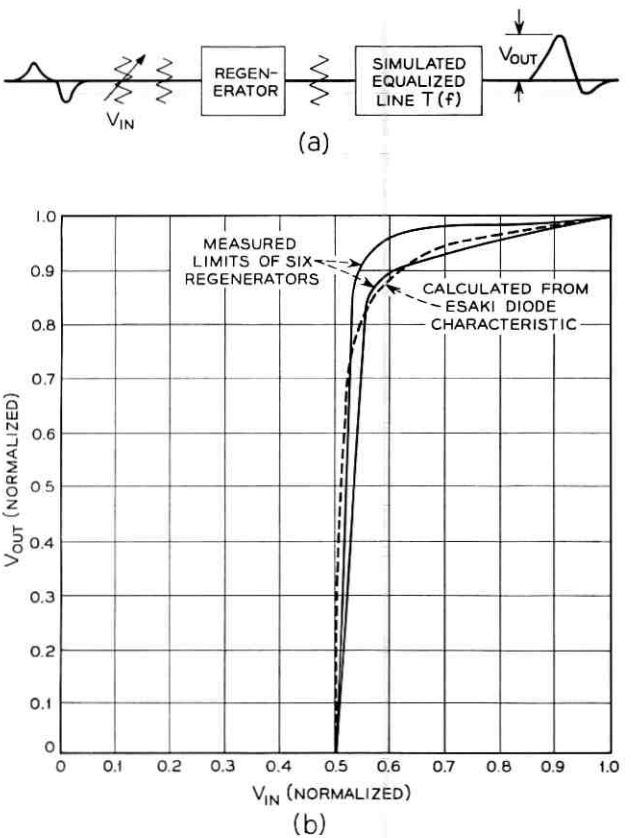

Fig. 35 — Input-output dynamic regenerator characteristic; (a) experimental setup; (b) measured and calculated characteristic.

to the oppositely poled emitter junctions between the signal and the reference inputs. (The Esaki diode signal voltage is a unipolar pulse stream which includes a dc component.) Fifth, to a first approximation, signal currents flow equally and oppositely in the two output leads and thus no current from the output flows through the ground system of the repeater. Many kinds of repeaters powered serially over the transmission line suffer from feedback problems due to such currents.

The output collectors of the two current-routing circuits are paralleled into balanced 75-ohm loads, to which they deliver peak output voltages of 1.5 volts of each polarity.

4.4 *Secondary Features*

4.4.1 *Power Arrangement*

Repeaters are powered serially by dc over the center conductor of the coaxial. The line current is 450 mA. Power supply voltages in the repeater are obtained by passing about 50 mA of this current through a series pair of 8.4-volt Zener diodes as shown in Fig. 36. Thus, each repeater consumes 7.5 watts.

In Fig. 36, we show only the circuit elements required to separate the dc power from the signal. Feedback from output to input is attenuated

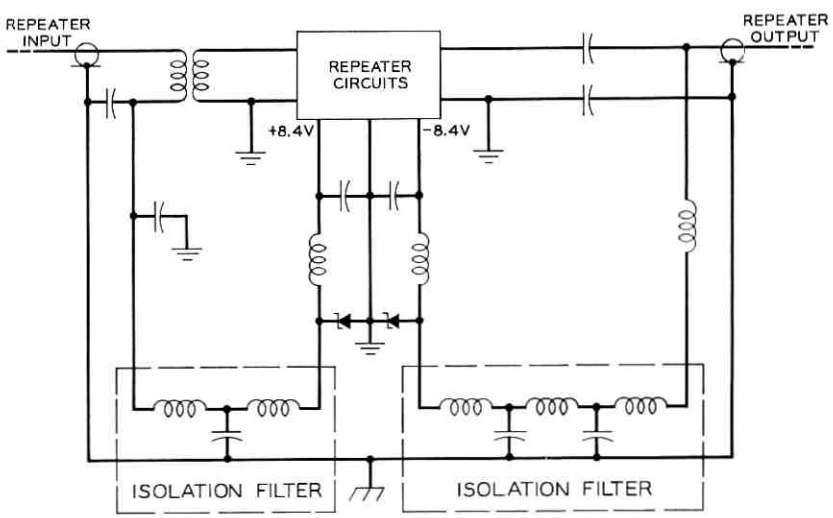

Fig. 36 — Repeater powering circuit.

in the power circuits by greater than 130 dB over the signal frequency range.

It is difficult to prevent spurious signals from appearing between earth ground and local repeater ground. In a long system, these two grounds may differ by as much as 1000 volts dc and capacitors with adequate voltage rating have appreciable impedance at frequencies of interest. Filtering inductors are required to prevent these ground-to-ground voltages from affecting the sensitive repeater circuits. The philosophy here is to isolate the repeater circuits from earth ground as much as possible.

4.4.2 *Surge Protection*

Partial surge protection has been provided at both the input and the output of the repeater. At the input, a series diode gate (Fig. 24), with 4 mA of current through each diode, limits the surge at the base of the first transistor. At the output, Equalizer I reduces the low frequency power which could harm the transistor collectors. These surge protection features are laboratory precautions only. Complete protection against lightning and power surges has not been accomplished in this experimental repeater.

4.4.3 *Repeater Equipment Design*

The repeater circuits shown on Fig. 21 were constructed on printed wiring boards which plug into a 3-layer printed wiring interconnecting board. The plug-in boards are attached to aluminum backing plates which provide support and an electrical ground plane for the circuits. The plates slide into the grooved sides of pockets in an aluminum investment casting. Fig. 37 is a photograph of a repeater showing the circuit boards in place in the casting, except for the amplifier board which has been removed. Shielding covers have been removed and are not shown.

Printed wiring carries shielded dc power to the individual circuit boards from the power supply on the interconnecting board (at the back of the casting in the photograph). Signal interconnections are made by miniature coaxial transmission lines to provide shielding.

Tantalum thin-film integrated techniques were considered for the circuits of the repeater, and there appear to be no fundamental obstacles to their use. A thin film version of the preamplifier was built and performance was equal to or better than the printed wiring version.

The size of this repeater is approximately 4x5x11 inches for a volume

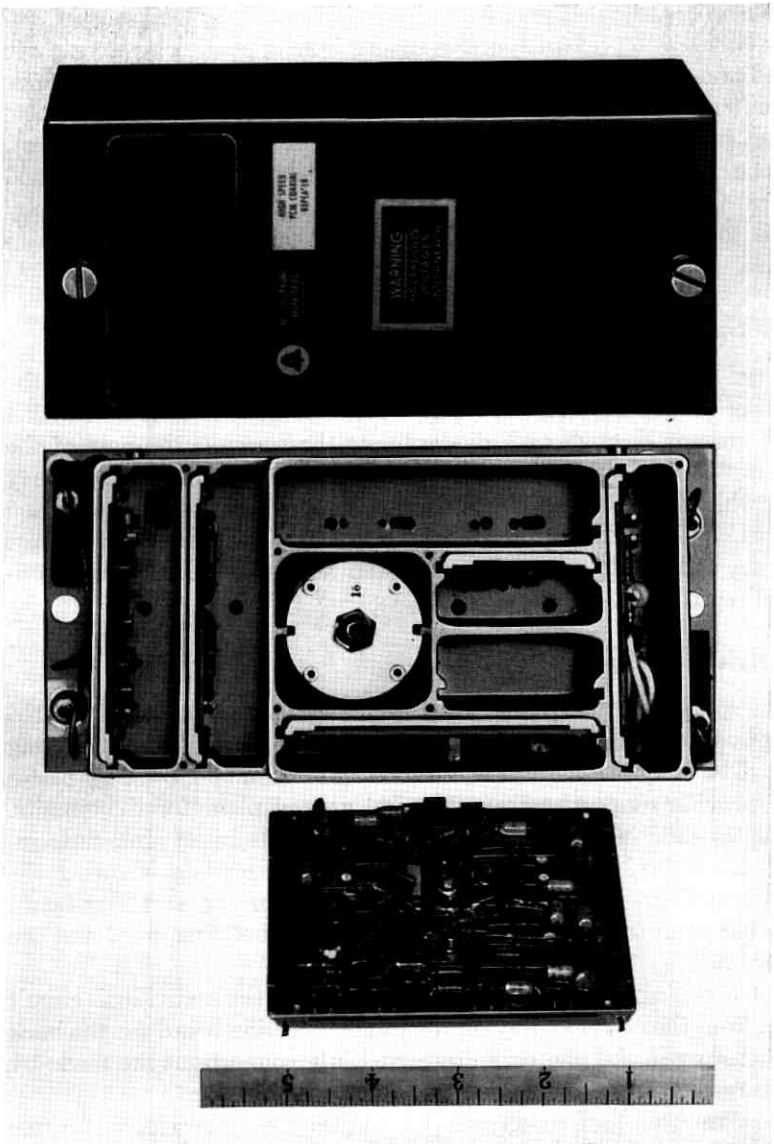

Fig. 37—Photograph of repeater with the amplifier printed circuit board removed. Shielding covers have been removed and are not shown.

of 220 cubic inches. By design, there is access space for testing of the experimental repeaters. It is anticipated that the use of integrated circuits and the elimination of excess space will result in a design occupying about one-quarter of the volume.

V. EXPERIMENTAL PERFORMANCE

In this section, we report on the performance of the line under laboratory conditions. In general, the line has met all performance expectations under these conditions. For volume manufacture, however, and for operation under field conditions for many years, further development is required. By the work reported on here, we have established the technical feasibility upon which a design for service can be based.

5.1 *Error Rate*

The line operates at error rates below 10^{-10} errors per baud through ten repeatered links.

5.2 *Jitter*

According to our model, each repeatered link introduces a pattern dependent, or systematic, component of jitter which is dominant. Pattern independent jitter tends to be random at each repeater; hence, it accumulates much more slowly and is negligible at the end of a long chain.

Since pattern dependent and pattern independent jitter are indistinguishable by measurement of a single link, we measure the jitter at the end of the chain. To determine the systematic component for the single link, we apply an equation derived from the model:[8]

$$\theta_1 = \sqrt{\frac{P(1)}{P(N)}}\,\theta_N$$

where θ_1 is the systematic rms jitter arising in each link, θ_N is the systematic rms jitter at the end of N links, and $P(N)$ is given by

$$P(N) = \frac{N}{2} - \frac{(2N-1)!}{4^N[(N-1)!]^2}$$

This function is tabulated in Ref. 8. For ten links, the above expression becomes

$$\theta_1 = 0.247\ \theta_{10}\,.$$

For only ten repeaters, the nonsystematic component may not be negligible, so that this calculation gives only an approximation to the systematic jitter contribution per link.

The total measured jitter at the end of our ten links is 13.3° rms. If we assume this to be all systematic, we calculate a per-link systematic jitter contribution of 3.3° rms. This laboratory measurement is well within the 8° objective of Section 3.3.2.

Fig. 38 shows the measured accumulated jitter versus the number of repeatered links. The intercept ($N = 0$) accounts for jitter introduced in the transmitting and receiving repeaters at the ends of the line.

5.3 *Waveforms*

In Fig. 39 we show some of the key waveforms in the repeater. All the waveforms are aligned in time for clarity. Fig. 39(a) shows the regenerator output before Equalizer I; 39(b), the signal input to the positive decision threshold of the regenerator; 39(c), the eye at this point when the line is driven by a random binary sequence; and 39(d), the subnanosecond sampling and turn-off pulses. For instructional purposes, the eye diagram has been synchronized at an even submultiple of the baud frequency to show the paired nature of the PST signal. The timing extractor causes the distortion in the negative eye. This distortion is of no consequence since only the positive eye is used by the positive threshold.

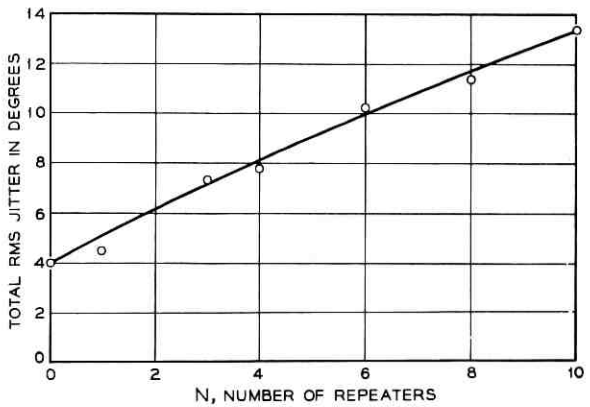

Fig. 38 — Measured accumulated jitter (rms) vs the number of repeatered links in the experimental line.

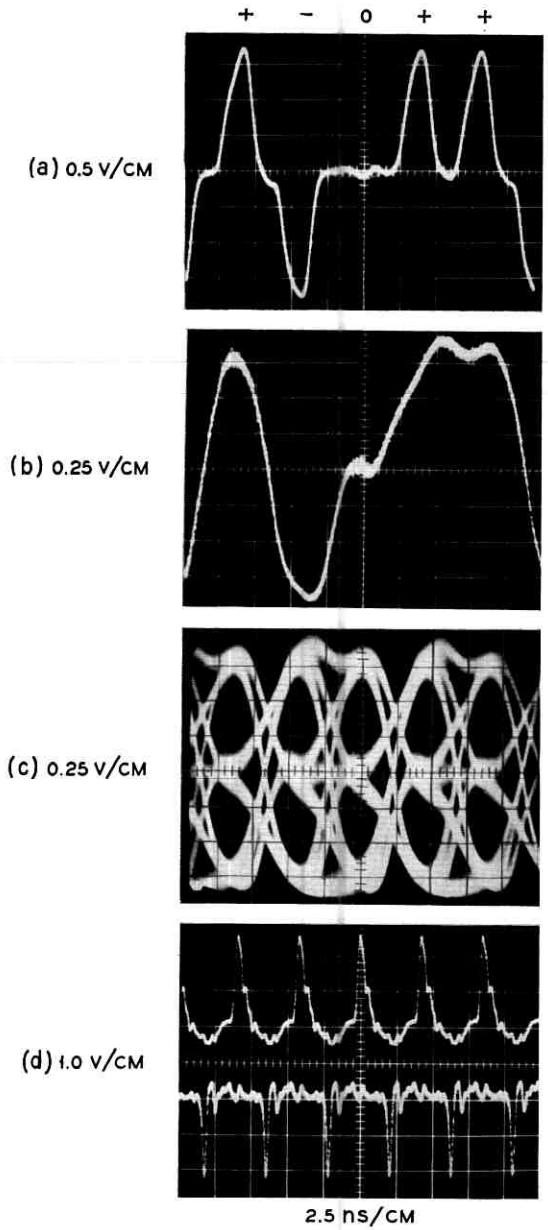

Fig. 39 — Key waveforms in the repeater; (a) regenerator output before Equalizer I; (b) signal input to the positive decision threshold; (c) the eye at the positive decision threshold; (d) the subnanosecond sampling and turn-off pulses.

VI. CONCLUSION

Ten 224-Mb/s experimental digital repeaters and associated code translation equipment have been developed, constructed, and operated over 10 miles of 0.270-inch coaxial line under laboratory conditions. The resulting performance has indicated that such a line 4000 miles in length is feasible for actual service and can be designed with existing techniques.

The transmission code is paired selected ternary (PST) which provides the essential features for the repeater operation as well as for in-service error monitoring.

Each repeater employs 25 transistors, most of them of a pnp germanium planar epitaxial design with an f_T of 4 GHz. The decision elements are gallium arsenide Esaki diodes.

The repeaters are serially powered by dc over the line with 450 mA of current, and each repeater consumes 7.5 watts.

Good agreement among theory, simulation, and laboratory performance has been achieved throughout. The error rate per repeatered link under laboratory conditions is less than 10^{-11} and the systematic jitter introduced in each link is about 3° rms.

VII. ACKNOWLEDGMENT

The work reported on herein was performed over a period of several years primarily by the members of the PCM repeater department under supervision of the authors. Many individuals have made significant contributions, but specific mention of these is not practical here. Prior work under the supervision of R. V. Sperry is gratefully acknowledged. The experimental cable was designed and manufactured through the efforts of Bell Laboratories' Outside Plant Laboratory, and Western Electric Company's Engineering Research Center and Baltimore Works. Support is also appreciated from many other departments within Bell Laboratories that have made contributions in areas such as systems engineering, components, devices, networks, and power. The work is based on earlier efforts over many years in the research department.

REFERENCES

1. Oliver, B. M., Pierce, J. R., and Shannon, C. E., The Philosophy of PCM, Proc. IRE, *36*, November, 1948, pp. 1324–1331.
2. Davis, C. G., An Experimental Pulse Code Modulation System for Short Haul Trunks, B.S.T.J., *41*, January, 1962, pp. 1–24.
3. Fultz, K. E. and Penick, D. B., The T1 Carrier System, B.S.T.J., *44*, September, 1965, pp. 1405–1451.
4. Travis, L. F. and Yaeger, R. E., Wideband Data on T1 Carrier, B.S.T.J., *44*, October, 1965, pp. 1567–1604.

5. Mayo, J. S., Experimental 224 Mb/s PCM Terminals, B.S.T.J., *44,* November, 1965, pp. 1813–1841.
6. Edson, J. O. and Henning, H. H., Broadband Codecs for an Experimental 224 Mb/s PCM Terminal, B.S.T.J., *44,* November, 1965, pp. 1887–1940.
7. Witt, F. J., An Experimental 224 Mb/s Digital Multiplexer Using Pulse Stuffing Synchronization, B.S.T.J., *44,* November, 1965, pp. 1843–1886.
8. Byrne, C. J., Karafin, B. J., and Robinson, D. B., Jr., Systematic Jitter in a Chain of Digital Regenerators, B.S.T.J., *42,* November, 1963, pp. 2679–2714.
9. Sipress, J. M., A New Class of Selected Ternary Pulse Transmission Plans for Digital Transmission Lines, IEEE Trans. Com. Tech., *Com-13,* September, 1965, pp. 366-372.
10. Elmendorf, C. H., et al., The L3 Coaxial System, B.S.T.J., *32,* July, 1953, pp. 781–1005.
11. Aaron, M. R., PCM Transmission in the Exchange Plant, B.S.T.J., *41,* January, 1962, pp. 99–141.
12. Ross, W. L., Private Communication.
13. Aaron, M. R. and Tufts, D. W., Intersymbol Interference and Error Probability, IEEE Trans. Inform. Theor., *IT-12,* January, 1966, pp. 26–34.
14. Smith, J. W., The Joint Optimization of Transmitted Signal and Receiving Filter for Data Transmission Systems, B.S.T.J., *44,* December, 1965, pp. 2363–2392.
15. Bennett, W. R., Methods of Solving Noise Problems, Proc. IRE, *44,* May, 1956, pp. 609–638.
16. Cravis, H. and Crater, T. V., Engineering of T1 Carrier System Repeatered Lines, B.S.T.J., *42,* March, 1963, p. 436.
17. Chapman, R. C., Private Communication.
18. Waldhauer, F. D., Wideband Feedback Amplifiers, IRE Trans. Circuit Theor., *CT-4,* September, 1957, pp. 178–190.
19. Goodall, W. M. and Dietrich, A. F., Fractional Millimicrosecond Electrical Stroboscope, Proc. IRE, *48,* September, 1960, pp. 1591–1594.
20 Moll, J. L., Krakauer, S., and Shen, R., *P-N* Junction Charge-Storage Diodes, Proc. IRE, *50,* January, 1962, pp. 43–53.

Difference-Set Cyclic Codes

By E. J. WELDON, JR.

(Manuscript received January 14, 1966)

Codes exist which are capable of correcting large numbers of random errors. Such codes are rarely used in practical data transmission systems, however, because the equipment necessary to realize their capabilities — that is, to actually correct the errors — is usually prohibitively complex and expensive. The problem of finding simply implemented decoding algorithms or, equivalently, codes which can be decoded simply with existing methods, is perhaps the outstanding unsolved problem in coding theory today.

In this paper, a new class of random-error-correcting cyclic codes is defined. These codes have two very desirable features: the binary members of the class are nearly as powerful as the best-known codes in the range of interest, and they can be decoded with the simplest known decoding algorithm. Unfortunately there are relatively few codes with useful parameters in this class, despite the fact that the class is infinite.

I. INTRODUCTION

The Bose-Chaudhuri[1]-Hocquenghem[2] (BCH) cyclic codes are, as a class, the best of the known, constructive, random-error-correcting codes. Fortunately a decoding algorithm, which can be implemented with a reasonable amount of equipment, has been found for these codes.[3,4,5]

In this paper, a new class of random-error-correcting cyclic codes is presented. These codes can be implemented much more simply than the BCH codes and are approximately as powerful. Unfortunately, the class is a small one.

II. DIFFERENCE-SET CYCLIC CODES

A simple perfect difference set of order l and modulus $n = l(l - 1) + 1$ is defined as a collection of l integers chosen from the set $\{0, 1, \cdots, l(l - 1)\}$ such that no two of the $l(l - 1)$ ordered differences modulo n are identical. That is, each occurs once. Singer[6] has shown

how to construct such sets when $l = p^s + 1$, p prime, s a positive integer, while Evans and Mann[7] have shown that a perfect difference set cannot be constructed for any other value of $l \leqq 1600$.

Since adding a fixed integer to every element of a perfect difference set clearly results in another such set, no loss of generality is suffered by considering only sets containing the element 0. In what follows, all perfect difference sets will be of this type.

Denote the elements of a perfect difference set of order $p^s + 1$ by $d_1 = 0, d_2, \cdots, d_{p^s+1}$ and let

$$\theta(x) = x^{d_1} + x^{d_2} + \cdots + x^{d_{p^s+1}}$$

be a polynomial in the algebra of polynomials modulo $x^n - 1$. The coefficients of all polynomials are taken from $GF(p^r)$, $r \leqq s$. Consider the n-by-n cyclic matrix Θ over $GF(p^r)$ whose rows are the coefficient vectors of $\theta(x), x\theta(x), \cdots, x^{n-1}\theta(x)$. For reasons which will become apparent shortly, the subspace of n-tuples generated by the rows of this matrix, which is an ideal in the algebra of polynomials modulo $x^n - 1$, will be considered to be the null space of a cyclic code of length n. The rank of this matrix, which will be shown to be the number of check symbols in the code, can be determined as follows. Consider the product

$$\begin{aligned}\theta(x)\theta(x^{-1}) = 1 &+ x^{d_1-d_2} &&+ x^{d_1-d_3} + \cdots + x^{d_1-d_{p^s+1}} \\ &+ x^{d_2-d_1} + 1 &&+ x^{d_2-d_3} + \cdots + x^{d_2-d_{p^s+1}} \\ &\vdots \\ &+ x^{d_{p^s+1}-d_1} + x^{d_{p^s+1}-d_2} + \cdots &&+ 1. \end{aligned} \tag{1}$$

Since the d_i are elements of a perfect difference set, each integer 1, 2, $\cdots$, $n - 1$ appears as an exponent in this polynomial exactly once. Thus, in the algebra of polynomials modulo $x^n - 1$,

$$\theta(x)\theta(x^{-1}) \equiv p^s + 1 + x + x^2 + \cdots x^{n-1}. \tag{2}$$

The reciprocal polynomial of $\theta(x)$, which is denoted by $\theta^*(x)$, is equal to $x^{(\text{degree of } \theta(x))} \cdot \theta(x^{-1})$. Since $p^s \equiv 0 \bmod p^r$, (2) reduces to

$$\begin{aligned}(x - 1)\theta(x)\theta^*(x) &\equiv 0 \\ &= q(x)(x^n - 1) \end{aligned} \tag{3}$$

for some polynomial $q(x)$.† Let $\theta(x) = f(x)h(x)$ where $h(x)$ is the

† If the code symbols are chosen from $GF((p')^r)$, p' a prime not equal to p, then $GCD(\theta(x), x^n - 1)$ equals a nonzero ground-field element, and the code specified by $h(x)$ is the trivial code which has n parity checks and no information symbols.

greatest common divisor of $\theta(x)$ and $x^n - 1$. That is,

$$h(x) = GCD(\theta(x), x^n - 1). \tag{4}$$

As a result the ideals (cyclic codes) in the algebra of polynomials modulo $x^n - 1$ generated by $\theta(x)$ and $h(x)$ are identical. Thus, the rank of the matrix θ is simply n minus the degree of $h(x)$, i.e., the number of check digits in the code generated by $g(x) = (x^n - 1)/h(x)$.

In an accompanying paper,[8] Graham and MacWilliams prove that there are exactly

$$n - k = \left[\binom{p+1}{2}\right]^s + 1 \tag{5}$$

check symbols in a difference-set cyclic (n,k) code over $GF(p)$. But since $\theta(x)$ and $x^n - 1$ are both polynomials over $GF(p)$, so are $h(x)$ and $g(x)$, regardless of the field from which the code symbols are chosen. Thus, (5) holds over $GF(p^r)$, $r \leqq s$, as well.

Although the derivation of (5) is fairly involved, it is easy to see that $n - k \leqq (n+1)/2$. For each zero of $x^n - 1$ except unity must be a zero of either $\theta(x)$, $\theta^*(x)$ or both, so it must also be a zero of either $h(x)$, $h^*(x)$ or both. That is,

$$(x - 1)h(x)h^*(x) = r(x)(x^n - 1)$$

where $r(x)f(x)f^*(x) = q(x)$. Therefore, the degree of $h(x)$ that is, k, cannot be less than $(n-1)/2$ and $n - k \leqq (n+1)/2$.

As defined, $g(x)$ is the generator polynomial of the code whose null space is generated by $h(x)$. Two polynomials multiply to zero in the algebra of polynomials modulo $x^n - 1$ only if the dot product of their coefficient vectors, with the order of the components reversed in one of them, is zero. Thus, the coefficient vectors of $\theta^*(x)$, $x\theta^*(x)$, $\cdots$, $x^{n-1}\theta^*(x)$ are in the null space of the code generated by $g(x)$. Each of these vectors represents a generalized parity check equation on certain symbols in each code word. Since each of these equations has $p^s + 1$ nonzero terms, each of the n symbols in every code vector is involved in exactly $p^s + 1$ equations. This follows from the fact that all the rows of the matrix θ are cyclically shifted versions of the first row and thus all columns and rows have the same weight. Furthermore, because a perfect difference set generates each difference exactly once, no two of the $p^s + 1$ equations which check a particular symbol can both check any other symbol. For if they could, this would imply that some differ-

ence was generated twice by the perfect difference set, which is impossible.

Consequently, these equations form an "orthogonal check set" of order $p^s + 1$ on the symbol in question. Massey[9] has defined such a set to consist of a collection of equations, all of which check a particular symbol, with the property that no two symbols appear together in more than one equation. He has shown that if it is possible to form an orthogonal check set of order $d - 1$ on any symbol in a cyclic code, then the code has minimum distance at least d and can be decoded with majority-logic decoding. Thus, difference-set codes have minimum distance at least $p^s + 2$ and, as described in Section III, can be decoded in a very straightforward manner.

Although codes exist over all finite fields, binary codes are, from a practical viewpoint, the most interesting. Table I contains a list of the first few binary difference-set codes and their generator polynomials. These codes have several interesting properties. For example, let d' denote the minimum distance of a code which can be realized by threshold decoding and let $\bar{d}$ denote the minimum distance of its dual code.

TABLE I — LIST OF BINARY DIFFERENCE-SET CYCLIC CODES

s	$n = 2^{2s} + 2^s + 1$	k	$d = 2^s + 2$	$t = 2^{s-1}$	Generator polynominal, $g(x)$	Difference—set polynomial $\theta(x)$
1	7	3	4	1	4,3,2,0	3,2,0
2	21	11	6	2	10,7,6,4,2,0	11,8,7,2,0
3	73	45	10	4	28,25,22,16,12,8,6,4,2,0	45,42,36,29,25,24,10,2, 0
4	273	191	18	8	82,77,76,71,67,66,56,52,48, 40,36,34,24,22,18,10,4,0	201,196,186,167,166, 159,128,126,115,112, 103,67,50,46,24,18,0
5	1057	813	34	16	244,242,236,234,232,228, 226,224,222,216,214,212, 211,210,209,208,203,202, 201,200,199,198,195,194, 193,191,189,188,186,184, 183,182,181,180,179,178, 177,176,175,174,169,167, 166,165,164,161,160,158, 155,154,153,151,150,149, 147,146,142,141,138,137, 135,132,131,129,126,124, 123,122,121,120,116,115, 114,111,108,106,105,103, 101,98,96,95,88,83,81, 79,76,75,74,72,71,70,68, 62,59,55,52,51,48,47,45, 43,41,39,37,35,33,32,28, 27,26,23,22,18,17,14,11, 5,4,3,1,0	1023,990,924,905,879, 792,754,702,697,677, 597,555,528,511,452, 439,348,338,298,277, 255,219,138,127,109, 63,54,31,15,7,3,1,0

Since any symbol appears in all equations orthogonal on that symbol and no other symbol appears in more than one of these equations, it is clear that the following bound holds for all block codes decoded with threshold decoding:

$$(d' - 1)(\bar{d} - 1) \leqq n - 1. \tag{6}$$

For difference-set codes $d' = 2^s + 2$, and in the binary case at least, $\bar{d} = 2^s + 1$, the weight of $\theta(x)$.[8] Thus, the equality holds in (6) and the codes are, in this peculiar sense, optimal.

In summation, it has been shown that there exists a class of cyclic codes of length $n = p^{2s} + p^s + 1$, i.e., those generated by $g(x) = (x^n - 1)/h(x)$ where $h(x) = GCD(\theta(x), x^n - 1)$, which have

$$\left[\binom{p+1}{2}\right]^s + 1$$

parity symbols[8] and which have the polynomials $\theta(x)$ and its multiples in their null spaces. Because of this latter property, the codes have minimum distance of at least $p^s + 2$. Also, in what follows, it is shown that this property can be used to implement these codes as random-error correctors in a remarkably simple manner.

III. IMPLEMENTATION

Because the codes are cyclic they can be encoded simply. See pages 148 and 149 in Peterson.[10]

Massey's majority-logic implementation of Meggitt's[11] general decoder for cyclic codes can be used to decode difference-set cyclic codes. A decoder of this type is shown in Fig. 1; it operates as follows. With the switch in the D position, the k-symbol data sequence is shifted into the syndrome and data registers simultaneously. When the entire data block has been entered, the switch is thrown to position P and the n-k received parity checks are shifted into the syndrome register, forming the syndrome. At this time, the output of the majority gate equals the additive inverse of the noise digit which was added to the first data symbol by the channel, provided that fewer than p^{s-1} errors occurred in the word.† Consequently, all that must be done to correct the first symbol is to add the output of the majority gate to the received symbol. This is done by the adder ($\oplus$) during the first shift of the registers.

† The majority gate has the following characteristics: Its output equals the additive inverse of the ground-field element which occurs most frequently among its $p^s + 1$ inputs, provided that that element occurs at least $p^{s-1} + 1$ times. Otherwise it equals zero.

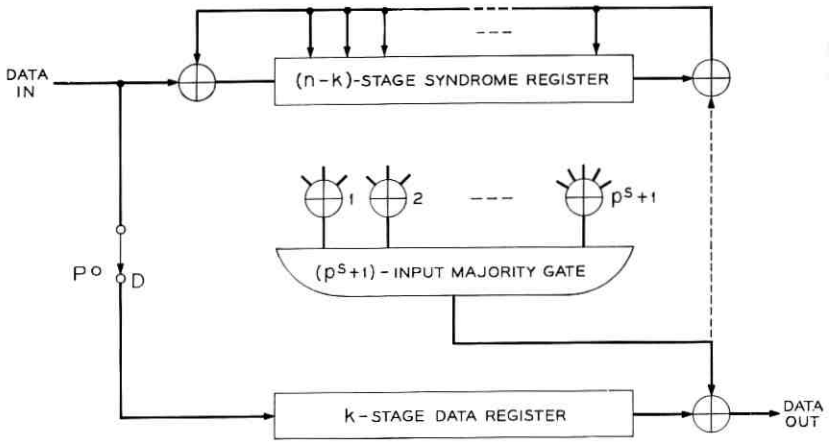

Fig. 1 — Fixed threshold majority-logic decoder for difference-set cyclic codes.

Because of the cyclic nature of the codes, repeating this process k times corrects all errors in the data section of the word.

Performance can be improved slightly at virtually no cost by the addition of the dotted connection and its associated adder to the decoder. This circuit removes the effects of corrected errors from the syndrome as the errors are corrected. This can be seen as follows. The first (highest-order) data symbol is checked by the parity check symbols stored in the shift register stages just to the left of the feedback connections. (This can be seen by examining the generator matrix of the code in systematic form.) If a particular ground-field element is added to the first information symbol to correct it, in order to remove the error from the parity check equations which checked that symbol, it is necessary to add the same ground-field element to each of these parity check symbols. This can be accomplished by adding the symbol to the feedback signal and shifting the register once. Successive corrections can be made in exactly the same manner.

Although a code will correct all error patterns of weight not greater than p^{s-1} and some of greater weight if this connection is omitted, many more patterns of weight greater than p^{s-1} will be corrected if it is included.

The presence of this connection also enables the decoder to detect undecodable error patterns. This is done by shifting the syndrome register $n - k$ times after the data symbols are corrected. A decodable pattern will have an all-zero syndrome after correction, while an undecodable pattern will not.

The connections from the syndrome register to the $p^s + 1$ summing circuits are made as follows. Each of the $p^s + 1$ equations orthogonal on the first information symbol involves one or more parity check symbols. The sum modulo p^r of all check symbols involved in the ith equation, $i = 1, 2, \cdots, p^s + 1$, equals the ith check sum orthogonal on the first information symbol. Thus, the inputs to the ith summing circuit are simply those parity check symbols involved in the ith equation.

This point is illustrated in Fig. 2 in which the decoder for the (73,45) binary code listed in Table I is depicted. Table II lists the 28-bit parity check sections of the nine composite parity check equations orthogonal on the first information symbol. Each of these equations manifests itself as one of the nine inputs to the majority gate of Fig. 2.†

A modification of threshold decoding, Variable Threshold Decoding, has been used to decode quasi-cyclic codes.[12] It can also be used here to improve performance somewhat, at the cost of a slight increase in complexity. Instead of keeping the threshold set at $p^{s-1} + 1$, it is initially set at its maximum value, $p^s + 1$, and an attempt is made to decode each of the n symbols of the received word. When an n-symbol cyclic revolution of the syndrome has been completed without any changes being made, the threshold is reduced by one and another attempt is made. If another complete revolution is made with no changes, the threshold is lowered again. If a change is made, however, the threshold is immediately raised by one and decoding continues. Upon the completion of the revolution, the threshold is again lowered by one.

Eventually one of two things must occur. Either the threshold will drop to its minimum value and remain there, or it will enter into some sort of limit cycle wherein it changes repetitively between two or more levels. In a practical system this latter difficulty can be obviated by terminating decoding after a fixed number of attempts, and if it is appropriate, signaling a detected error if the syndrome is not all zeros. It seems likely that roughly $2d$ cyclic revolutions of the word will suffice to decode nearly all decodable error patterns.

IV. A COMPARISON

In an unpublished report,[13] the author estimated that approximately 3600 transistors would be required to instrument a decoder for the (273,200), $d = 18$, code formed by shortening the (511,438) primitive BCH code.‡ Also it was estimated that the decoder's internal circuitry

† Using a combination of sequential and combinational circuits, rather than strictly combinational circuits, would undoubtedly result in a slightly cheaper, but conceptually more complex decoder.

‡ This was before Berlekamp's work.[5, 10]

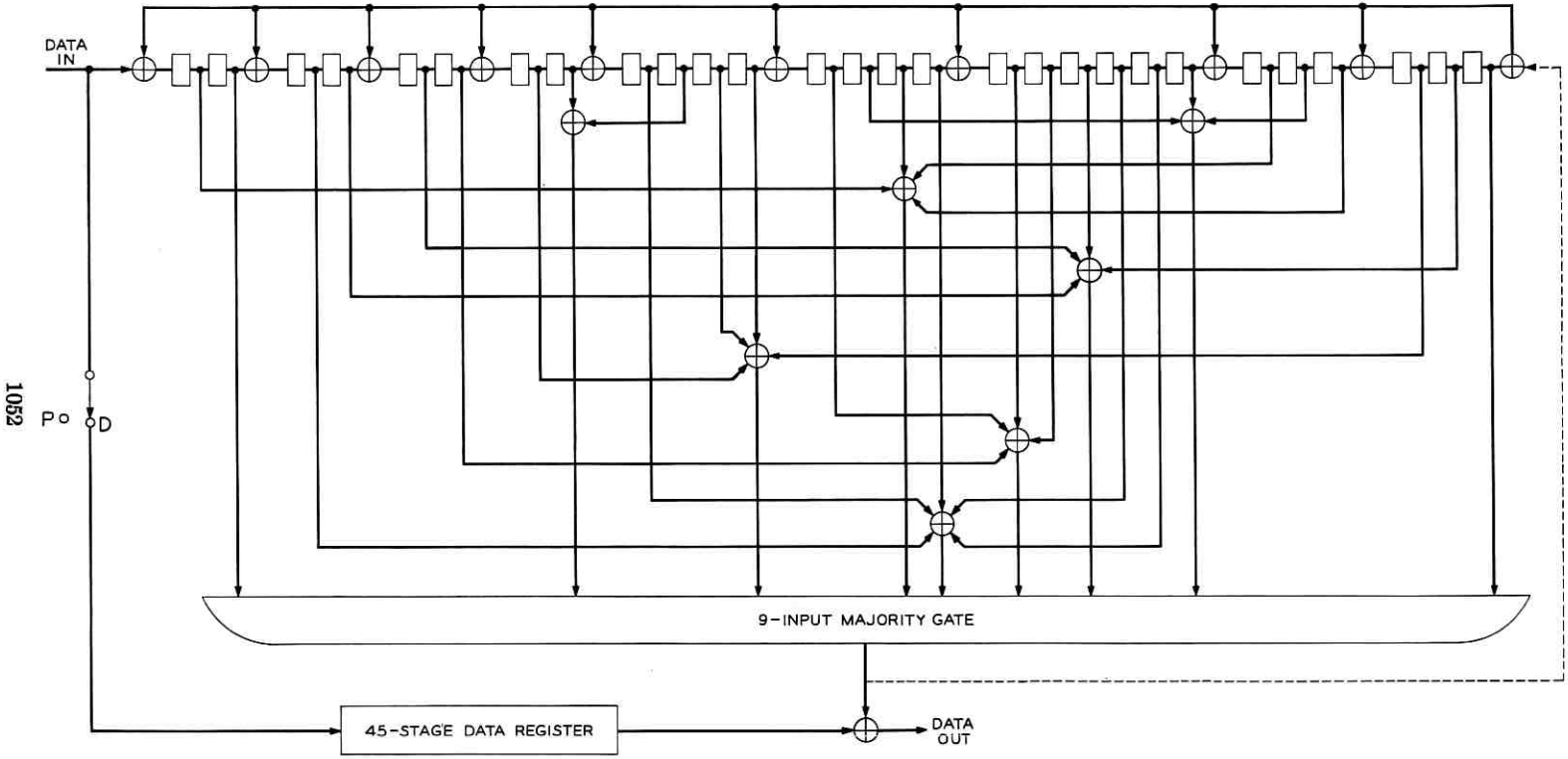

Fig. 2 — Decoder for (73, 45), $d = 10$, binary difference-set cyclic code.

TABLE II—PARITY SECTIONS OF THE NINE COMPOSITE PARITY CHECK EQUATIONS ORTHOGONAL ON FIRST INFORMATION SYMBOL IN (73, 45) CODE.

Eq Number	Bit position																											
	0	1	2	3	4	5	6	7	8	9	10	11	12	13	14	15	16	17	18	19	20	21	22	23	24	25	26	27
1																												1
2		1																										
3								1		1																		
4													1									1		1				
5	1													1									1		1			
6				1	1														1								1	
7							1				1	1															1	
8						1							1				1	1										
9			1						1						1				1		1							

would have to operate roughly 85 times faster than line speed to enable it to keep up with the data. These estimates were based on the assumptions that only transistor storage was used and that speed would be sacrificed to reduce the number of transistors needed whenever practical. For example, the decoder is a serial, rather than parallel, device.

Assuming that the syndrome register, exclusive-OR circuits and majority gate are duplicated, the internal circuitry of the decoder for the (273,191), $d = 18$, binary difference set code can operate at line speed. The numbers of transistors required for the various decoder components are tabulated below.

Circuit Function	Number of Transistors
Data register	382
Syndrome registers (2)	328
Exclusive-OR's	400
Majority gates (2)	40
Clock and switches	30
Miscellaneous	20
Total	1200

The complexity of the two decoders is compared in the following table.

Decoder for	Code Efficiency	Number of Transistors	Decoder Clock Rate (multiples of line bit rate)	Ease of Design, Construction, & Testing
BCH Code	0.73	3600	85	difficult
Difference-Set Code	0.70	1200	1	very simple

This type of comparison is quite crude and is admittedly chosen to illustrate the strong points of difference-set codes. Also, in light of Berlekamp's work,[5, 16] it may be possible to reduce the number of transistors required for the BCH decoder by as much as a factor of two and its speed by twice that. However, despite these facts, the difference-set decoder remains a much simpler piece of equipment than the BCH decoder. Also, a comparison of longer, more powerful codes would demonstrate the relative simplicity of the difference-set decoder even more dramatically.

This comparison is not intended to demean the BCH codes or their very elegant and general decoding algorithm. There are certainly many cases, in fact nearly all cases involving long, relatively efficient random-error-correcting codes, in which they are by far the most easily implemented codes. Rather, the comparison is simply intended to point out that, in certain cases, difference-set codes are much easier to implement that the BCH codes, and to suggest that there may be other classes of cyclic codes for which the same is true.

V. CONCLUSIONS

A new, relatively small, class of random-error-correcting cyclic codes has been presented. These codes, which are approximately as powerful as the best cyclic codes for given values of efficiency and length, are very easily implemented. Consequently, they are concluded to be attractive for use in error-control systems where forward-acting random-error-correction is required.

VI. ADDENDA

Subsequent to the discovery of these codes, the author became aware of the unpublished, but earlier, work of L. D. Rudolph.[14] In it a class of threshold-decodable codes, which contains the class of difference-set cyclic codes, is described. Also, (6) has been derived by Mitchell in Ref. 15.

REFERENCES

1. Bose, R. C. and Ray-Chaudhuri, D. K., On a Class of Error Correcting Binary Group Codes, Inform. Control, *3*, 1960, pp. 68–79.
2. Hocquenghem, A., Codes Correcteurs d'erreurs, Chiffres, *2*, 1959, pp. 147–156.
3. Peterson, W. W., Encoding and Error-Correction Procedures for the Bose-Chaudhuri Codes, IRS Trans., *IT-6*, 1960.
4. Chien, R. T., Cyclic Decoding Procedures for Bose-Chaudhuri-Hocquenghem Codes, IEEE Trans., *IT-10*, No. 4, 1964.

5. Berlekamp, E. R., On Decoding Binary Bose-Chaudhuri-Hocquenghem Codes, IEEE Trans., *IT-11*, No. 4, 1965.
6. Singer, J., A Theorem in Finite Projective Geometry and Some Applications to Number Theory, AMS Trans., *43*, 1938, pp. 377–385.
7. Evans, T. A. and Mann, H. B., On Simple Difference Sets, Sankhya, *11*, 1955, pp. 464–481.
8. Graham, R. L. and Mac Williams, Jessie, On the Number of Parity Checks in Difference-Set Cyclic Codes, B.S.T.J., this issue, pp. 1057–1070.
9. Massey, J. L., *Threshold Decoding*, MIT Press, 1963.
10. Peterson, W. W., *Error Correcting Codes*, MIT Press, 1961.
11. Meggitt, J. E., Error-Correcting Codes and Their Instrumentation for Data Transmission Systems, IRE Trans., *IT-7*, No. 4 1961.
12. Townsend, R. L. and Weldon, E. J., Jr., Self-Orthogonal Quasi-Cyclic Codes, To be published, IEEE Trans., *IT-12*, 1966.
13. Weldon, E. J., Jr., Complexity of Peterson-Chien Decoders, unpublished memorandum, 1965.
14. Rudolph, L. D., A Class of Majority Logic Decodable Codes, To be published, IEEE Trans., *IT-12*, 1966.
15. Mitchell, M. E., et al., Coding and Decoding Operations Research, Final Report on Contract AF 19 (604)-6183, AFCRL8, 1961.
16. Berlekamp, E. R., Practical BCH Decoders, IEEE Trans., *IT-13*, to be published, 1967.

On the Number of Information Symbols in Difference-Set Cyclic Codes

By R. L. GRAHAM and JESSIE MACWILLIAMS

(Manuscript received April 28, 1966)

The concept of a difference-set cyclic code has been described previously. It was shown that such a code is almost as powerful as a Bose-Chaudhuri code and considerably simpler to implement. It is the purpose of this paper to determine some of the more important properties of this code and its dual code (cf. Sec. IV). It may be pointed out that the problems we consider are equivalent to determining certain properties of incidence matrices associated with a class of balanced incomplete block designs formed from simple difference sets.

I. INTRODUCTION

The concept of a difference-set cyclic code has been described by E. J. Weldon, Jr. in the preceding paper.[1] In Ref. 1 it is shown that such a code is almost as powerful as a Bose-Chaudhuri code and considerably simpler to implement. It is the purpose of this paper to determine some of the more important properties of this code and its dual code (cf. Sec. IV). It may be pointed out that the problems we consider are equivalent to determining certain properties of incidence matrices of Desarguesian planes.

II. SIMPLE DIFFERENCE SETS AND ASSOCIATED CYCLIC CODES

A simple difference set S is a collection of l integers $\{d_1, \cdots, d_l\}$ modulo n such that every $a \not\equiv 0 \pmod{n}$ can be *uniquely* expressed in the form

$$d_i - d_j \equiv a \pmod{n},$$

for some d_i, d_j in S. Of course, $n = l(l-1) + 1$. If $\theta(x)$ (the difference-set polynomial) is defined by

$$\theta(x) = \sum_{i=1}^{l} x^{d_i},$$

then it follows that

$$\theta(x)\theta(x^{-1}) = l + \sum_{i=1}^{n-1} x^i \pmod{(x^n - 1)}.$$

This may be written

$$\theta(x)\theta(x^{-1}) = (l - 1) + (x^n - 1)/(x - 1) \pmod{(x^n - 1)}.$$

Changing to arithmetic over the finite field $GF(p)$, where p is a prime that divides $l - 1$, we have

$$(x - 1)\theta(x)\theta(x^{-1}) \equiv 0 \pmod{(x^n - 1)}.$$

This means that $\theta(x)$ has a nontrivial highest common factor $h(x)$ in common with $x^n - 1$ over $GF(p)$.

Let R be the ring of polynomials modulo $x^n - 1$ over $GF(p)$. The ideal $R \cdot \theta(x)$ is the same ideal as $R \cdot h(x)$ and is a proper ideal in R, and, in fact a cyclic code (see Ref. 5, Section 8.1). The dimension of this code is $(n - \deg h(x))$.*

The only known simple difference sets are obtained by a construction due to Singer.[2] For this construction, n must be of the form $p^{2s} + p^s + 1$. Hence, $l - 1 = p^s$, which determines the finite field one must use. For $p = 2$ and $1 \leqq s \leqq 5$, the dimension of $R \cdot \theta(x)$ was found by E. J. Weldon, Jr. to be $3^s + 1$. In this paper it is shown that in general the dimension of $R \cdot \theta(x)$ is $\binom{p+1}{2}^s + 1$.

III. AN EQUIVALENT PROBLEM

Let $n = p^{2s} + p^s + 1$, $r = p^s - 1$. $\{d_1, d_2, \cdots, d_l\}$ is a Singer difference set modulo n, and $\theta(x)$ the difference-set polynomial. In this section all arithmetic will be in $GF(p)$ (addition and multiplication mod p) unless otherwise specified.

The degree of $h(x)$ is the number of zeros of $x^n - 1$ which are also zeros of $\theta(x)$. Hence, the following odd-sounding theorem is relevant.

Theorem 1: The number of nth *roots of unity (over* $GF(p)$*) which are not zeros of* $\theta(x)$ *is the number of integers* t, $1 \leqq t \leqq n$, *such that for some* j, $1 \leqq j \leqq t - 1$, *the binomial coefficient* $\binom{tr}{jr}$ *is not zero (mod* p*).*

* This roundabout approach is usual in coding theory. Appendix B contains a direct proof that the dimension of $R \cdot \theta(x)$ is the number of zeros of $x^n - 1$ which are not zeros of $\theta(x)$.

The purpose of this section is to prove Theorem 1. Several preliminary steps are needed.

Let ν be a primitive nrth root of unity over $GF(p)$; $\omega = \nu^n$ is a primitive rth root of unity, $\zeta = \nu^r$ is a primitive nth root of unity. The first n powers of ζ are the zeros of $x^n - 1$; the degree of the highest common factor of $\theta(x)$ and $x^n - 1$ is the number of integers $t \leqq n$ for which $\theta(\zeta^t) = 0$.

The powers of ω generate $GF(p^s)$, and, since $nr = p^{3s} - 1$, the powers of ν generate $GF(p^{3s})$. Since $GF(p^{3s}) \supset GF(p^s)$, any linear combination $\sum_{i,j} \omega^i \nu^j$ is again a power of ν.

To construct a Singer difference set modulo n, one picks two arbitrary distinct integers d_1, d_2 (less than n), forms all linear combinations $\omega^i \nu^{d_1} + \omega^j \nu^{d_2} = \nu^b$, and replaces ν^b by $\omega^{h_f} \nu^{d_f}$ $(d_f \leqq n)$ by using $\nu^n = \omega$ (cf., Ref. 2). The distinct exponents of ν which are obtained in this way form a Singer difference set.* Since $\omega^h(\omega^i \nu^{d_1} + \omega^j \nu^{d_2}) = \omega^{h_f + h} \nu^{d_f}$, each exponent d_f will be produced r times; we can get each one exactly once by using the equations

$$\begin{aligned} \nu^{d_1} + \nu^{d_2} &= \omega^{h_3} \nu^{d_3}, \\ \omega \nu^{d_1} + \nu^{d_2} &= \omega^{h_4} \nu^{d_4}, \\ &\cdots \\ \omega^{r-1} \nu^{d_1} + \nu^{d_2} &= \omega^{h_l} \nu^{d_l}, \end{aligned} \tag{1}$$

where

$$l = p^s + 1 = r + 2.$$

Lemma 1: ζ^t *is a zero of* $\theta(x)$ *if and only if*

$$\sum_{j=1}^{t-1} \binom{tr}{jr} \zeta^{(d_1 - d_2) j} = 0.$$

Proof: Raising (1) to the power tr gives the set of equations

$$\begin{aligned} (\nu^{d_1} + \nu^{d_2})^{tr} &= (\omega^{h_3} \nu^{d_3})^{tr} = (\nu^{d_3})^{tr} = \zeta^{t d_3} \\ (\omega \nu^{d_1} + \nu^{d_2})^{tr} &= (\nu^{d_4})^{tr} = \zeta^{t d_4} \\ &\cdots \\ (\omega^{r-1} \nu^{d_1} + \nu^{d_2})^{tr} &= (\nu^{d_l})^{tr} = \zeta^{t d_l}. \end{aligned}$$

---

* An example is given in the appendix.

Thus,

$$\theta(\zeta^t) = \sum_{i=1}^{l} (\zeta^t)^{d_i} = 0$$

if and only if

$$(\nu^{d_1})^{tr} + (\nu^{d_2})^{tr} + \sum_{i=0}^{r-1} (\omega^i \nu^{d_1} + \nu^{d_2})^{tr} = 0.$$

This may be rewritten as

$$(r+1)(\nu^{d_1})^{tr} + (r+1)(\nu^{d_2})^{tr} + \sum_{i=0}^{r-1} \sum_{h=1}^{tr-1} \binom{tr}{h} \nu^{\sigma_h} \omega^{ih},$$

where

$$\sigma_h = d_1 h + d_2(tr - h).$$

Since $r + 1 = p^s$ the first two terms are zero; the remainder is

$$\sum_{h=1}^{tr-1} \binom{tr}{h} \nu^{\sigma_h} \sum_{i=0}^{r-1} (\omega^h)^i.$$

Now,

$$\sum_{i=0}^{r-1} (\omega^h)^i = \begin{cases} 0 & \text{if } h \not\equiv 0 \bmod r, \\ r & \text{if } h = jr. \end{cases}$$

In particular (for $t = 1$) ζ is a zero of $\theta(x)$. Since

$$r \equiv -1 \bmod p, \quad \nu^r = \zeta, \quad \text{and} \quad \sigma_{jr} = (d_1 - d_2)jr + tr\, d_2,$$

the expression for $\theta(\zeta^t)$ becomes

$$-\nu^{t r d_2} \sum_{j=1}^{t-1} \binom{tr}{jr} \zeta^{j(d_1 - d_2)},$$

which proves the lemma.

Lemma 2:

$$\sum_{j=1}^{t-1} \binom{tr}{jr} \zeta^{(d_1 - d_2)j} = 0$$

if and only if

$$\binom{tr}{jr} \equiv 0 \pmod{p} \quad \textit{for} \quad j = 1, \cdots, t-1.$$

Proof: The difference set $\{d_1, d_2, \cdots, d_l\}$ may be obtained by picking

any two distinct d_i, d_j contained in it, and applying the construction previously described to ν^{d_i}, ν^{d_j}. By the definition of a difference set we may choose $d_i - d_j$ to be any number $1, 2, \cdots, n-1$. Thus, $\theta(\zeta^t) = 0$ implies

$$\sum_{j=1}^{t-1} \binom{tr}{jr} \zeta^{uj} = 0 \quad \text{for} \quad u = 1, 2, \cdots, n-1,$$

and the equation

$$\sum_{j=1}^{t-1} \binom{tr}{jr} x^j = 0$$

will have $(n-1)$ nonzero roots. Since $t \leqq n$ this is impossible unless all the coefficients are zero. This proves the lemma.

The experimental evidence (for $p = 2$, $1 \leqq s \leqq 5$) showed that the number of ζ^t which are *not* zeros of $\theta(x)$ is $3^s + 1$. We guess (it turns out correctly) that "+1" corresponds to $t = n$,—ζ^n is not a zero of $\theta(x)$, since $\theta(1) \equiv 1 \pmod{p}$ —, and that it will be simpler to count binominal coefficients which are not divisible by p. The information contained in Lemmas 1 and 2 is rephrased in the form of Theorem 1.

The following corollary is immediate.

Corollary 1: The degree of the highest common factor (over GF(p)) of $\theta(x)$ and $x^n - 1$ is the same for every Singer difference set.

IV. A THEOREM ON BINOMIAL COEFFICIENTS

In this section, we change to ordinary arithmetic (instead of mod p) and count the number of integers t which satisfy the conditions of Theorem 1. In particular, our goal is to establish

Theorem 2: The number of t, $1 \leqq t \leqq p^{2s} + p^s$, for which

$$\binom{tr}{jr} \not\equiv 0 \pmod{p} \tag{2}$$

for $r = p^s - 1$ and some j, $1 \leqq j < t$, is just $\binom{p+1}{2}^s$.

The proof of this result will depend upon several lemmas. We first need some notation. Let $P_p(u)$ denote the greatest power of p which divides u. If u is written to the base p, i.e.,

$$u = \sum_{i=1}^{h} u_i p^i, \qquad 0 \leqq u_i < p,$$

for some h, then $D(u)$ will denote* the sum of the "digits" of u, i.e.,

$$D(u) = \sum_{i=1}^{h} u_i .$$

As usual, we let $[u]$ represent the greatest integer not exceeding u.

Lemma 3:

$$\binom{u+v}{u} \not\equiv 0 \pmod{p}$$

if and only if

$$u_j + v_j \leqq p - 1, \qquad j = 0, 1, 2, \cdots .$$

Proof: It is well known that

$$P_p(m!) = \sum_{i=1}^{\infty} \left[\frac{m}{p^i}\right]$$

(the upper limit ∞ is convenient, but not necessary). Since

$$P_p\left(\binom{u+v}{u}\right) = P_p((u+v)!) - P_p(u!) - P_p(v!),$$

we have

$$P_p\left(\binom{u+v}{u}\right) = 0$$

if and only if

$$\sum_{i=1}^{\infty} \left[\frac{u+v}{p^i}\right] = \sum_{i=1}^{\infty} \left[\frac{u}{p^i}\right] + \sum_{i=1}^{\infty} \left[\frac{v}{p^i}\right]. \tag{3}$$

But it is always true that

$$[x + y] \geqq [x] + [y] ,$$

so that (3) holds if and only if

$$\left[\frac{u+v}{p^i}\right] = \left[\frac{u}{p_i}\right] + \left[\frac{v}{p^i}\right], \qquad i = 1, 2, 3, \cdots . \tag{4}$$

Noting that, in general, $[x/p^i]$ is just one of the "digits" in the representation of x to the base p, we see that (4) is exactly the condition that,

* We should more accurately denote this by $D_p(u)$ but since p is fixed in this argument, no confusion will arise.

for each j, the jth digit in the representation of $u + v$ to the base p is just the sum of the jth digits of u and v. Hence, (4) holds if and only if

$$u_j + v_j \leqq p - 1, \qquad j = 0, 1, 2, \cdots,$$

and the lemma is proved.

We note as a

Corollary:

$$D(u + v) \leqq D(u) + D(v)$$

with equality if and only if

$$u_j + v_j \leqq p - 1, \qquad j = 0, 1, 2, \cdots.$$

We recall that the numbers of particular interest are

$$u = jr, \qquad v = tr - jr,$$

where

$$r = p^s - 1 = \sum_{i=0}^{s-1} wp^i \qquad (\text{where } w = p - 1).$$

Lemma 4:

$$D(tr) = sw \quad \textit{for} \quad 1 \leqq t \leqq r.$$

Proof: Set

$$t = \sum_{i=1}^{s-1} a_i p^i + a_0,$$

where we may take $a_0 \neq 0$, since $D(p^x u) = D(u)$. Now,

$$a_0 r = (a_0 - 1)p^s + \sum_{i=1}^{s-1} wp^i + (p - a_0).$$

Consequently,

$$\begin{aligned} tr &= (p^s - 1) \sum_{i=1}^{s-1} a_i p^i + a_0 r \\ &= \sum_{i=1}^{s-1} a_i p^{i+s} - \sum_{i=1}^{s-1} a_i p^i + (a_0 - 1)p^s + \sum_{i=1}^{s-1} wp^i + (p - a_0) \\ &= \sum_{i=1}^{s-1} a_i p^{i+s} + (a_0 - 1)p^s + \sum_{i=1}^{s-1} (w - a_i)p^i + (p - a_0). \end{aligned}$$

Thus,

$$D(tr) = \sum_{i=1}^{s-1} a_i + (a_0 - 1) + (s-1)w - \sum_{i=1}^{s-1} a_i + (p - a_0)$$

$$= sw \qquad \text{for} \qquad 1 \leqq t \leqq r = p^s - 1,$$

which proves the lemma.

Note that if $1 < t < n$, there is a 1 to 1 correspondence between t such that $D(tr) = u$ and t such that $D(tr) = 3sw - n$. For

$$0 < (p^{3s} - 1) - tr = (n - t)r$$

and clearly

$$D((n - t)r) = 3sw - D(tr).$$

Lemma 5:

$$sw \leqq D(tr) \leqq 2sw, \quad \text{for} \quad 1 \leqq t < n.$$

Proof: We show that $D(tr) \leqq 2sw$; the other inequality is then immediate by the preceding remark.

Since $t \leqq p^{2s} + p^s$ we have either

$$t = p^{2s} + \sum_{i=0}^{s-1} a_i p^i$$

or

$$t = p^s \sum_{i=0}^{s-1} b_i p^i + \sum_{i=0}^{s-1} a_i p^i.$$

In either case, let t_1 denote the first summand and t_2 denote the second summand (so that $t = t_1 + t_2$).

By Lemma 4

$$D(t_1 r) = D(t_2 r) = sw.$$

Hence,

$$D(tr) = D(t_1 r + t_2 r) \leqq D(t_1 r) + D(t_2 r) = 2sw$$

and the lemma is proved.

We recall now that in Theorem 2 we are considering integers t which satisfy (2). By Lemma 3, this is equivalent to finding j and t, with $1 \leqq j < t < n$, such that

$$D(tr) = D(jr) + D((t - j)r).$$

But Lemma 5 implies

$$2sw \geqq D(tr) = D(jr) + D((t-j)r) \geqq sw + sw = 2sw.$$

Hence, we must have

$$D(tr) = 2sw, \qquad D(jr) = D((t-j)r) = sw.$$

On the other hand, suppose for some u, $1 \leqq u < n$, we have

$$D(ur) = 2sw.$$

Let h denote $P_p(u)$ and set $u = p^h u'$. As in Lemma 5, set

$$u' = u_1' + u_2',$$

where $u_2' \leqq r$ and $D(u_2' r) = sw$. Since

$$D(u'r) = D(ur) = 2sw$$

then we must have $D(u_1' r) = sw$. Thus for $j = p^h u_2'$,

$$\binom{ur}{jr} \not\equiv 0 \pmod{p}.$$

We can summarize this discussion in

Lemma 6: The number of t which satisfy (2) is exactly the number of t for which

$$D(tr) = 2sw.$$

By a previous remark, this is just the number of t such that

$$D(tr) = sw.$$

This problem is equivalent to finding the number of u, $1 \leqq u < p^{3s} - 1$, such that

$$D(u) = sw \quad \text{and} \quad u \equiv 0 \pmod{r}. \tag{5}$$

We state the result in

Lemma 7: The number of integers u which satisfy (5) is $\binom{p+1}{2}^s$.

Proof: Write u in the form

$$u = \sum_{i=0}^{s-1} a_i p^i + p^s \sum_{i=0}^{s-1} b_i p^i + p^{2s} \sum_{i=0}^{s-1} c_i p^i$$

$$= A + p^s B + p^{2s} C,$$

where

$$0 \leqq A, B, C \leqq r = p^s - 1.$$

Then

$$u = A + B + C + (p^s - 1)B + (p^{2s} - 1)C$$

and so we have

$$u \equiv 0 \pmod{r}$$

if and only if

$$A + B + C = 0 \pmod{r}.$$

Since $u > 0$, then by Lemma 5,

$$D(A + B + C) \geqq sw.$$

But

$$D(A + B + C) \leqq D(A) + D(B) + D(C) = D(u) = sw$$

by the corollary to Lemma 3. Hence, we must have

$$D(A + B + C) = sw = D(A) + D(B) + D(C).$$

This implies that

$$a_i + b_i + c_i \leqq w, \qquad i = 0, 1, \cdots, s - 1,$$

and consequently

$$A + B + C \leqq r.$$

However, the requirement that r divides u implies

$$A + B + C = r,$$

so the only possibility left is

$$a_i + b_i + c_i = w, \qquad i = 0, 1, \cdots, s - 1.$$

Since the number of ways (cf. Ref. 4, 6.6) of obtaining w as the ordered sum of three nonnegative integers is $\binom{w+2}{2} = \binom{p+1}{2}$ then the total number of choices for A, B, and C (and hence for u) is just $\binom{p+1}{2}^s$. This completes the proof of Lemma 7.

By combining the preceding lemmas, Theorem 2 is proved.

V. CODING THEORY

It has been shown[1] that the minimum distance of the dual code of the cyclic code $R \cdot \theta(x)$ is at least $p^s + 2$. It is now easy to show that the minimum distance of $R \cdot \theta(x)$ itself is $p^s + 1$.

Since $R \cdot \theta(x)$ contains $\theta(x)$, $p^s + 1$ is an upper bound for its minimum distance; it suffices to show that it is also a lower bound.

By Theorems 1 and 2, ζ^t is a zero of $\theta(z)$ if $D(tr) = sw$ (this is, of course, only a sufficient condition). By Lemma 4, the $p^s - 1$ numbers $t = 1, 2, \cdots, p^s - 1$ have the property that $D(tr) = sw$; clearly $t = p^s$ also has this property. Thus there are at least p^s consecutive powers of ζ which are zeros of $\theta(x)$. By the usual proof of the Bose-Chaudhuri bound* (See Ref. 5, Section 9.1) the minimum distance of $R \cdot \theta(x)$ is at least $p^s + 1$.

Theorem 2′ is a summary of known results about difference-set cyclic codes.

Theorem 2′: Let $d_1, d_2, \cdots, d_l$ be a Singer difference-set modulo n, where $n = p^{2s} + p^s + 1$. Set

$$\theta(x) = \sum_{i=1}^{l} x^{d_i}.$$

Let R be the ring of polynomials modulo $x^n - 1$ over $GF(p)$. Then $R \cdot \theta(x)$ is a cyclic code of dimension $\binom{p+1}{2}^s + 1$, and minimum distance $p^s + 1$.

It has been shown that for every Singer difference-set modulo n, there exists a set of integers t such that ζ^t is a zero of the difference-set polynomial. The set of such t is the same for every difference set, but this of course does not mean that every $\theta(x)$ has the same zeros in common with $x^n - 1$. The difference set is constructed by means of a primitive nrth root of unity ν; ν determines the choice of ζ, and a different choice may or may not lead to a different set of zeros for $\theta(x)$.

APPENDIX A

Example

Take $p = 2$, $s = 2$, $n = 2^4 + 2^2 + 1 = 21$, $nr = 2^6 - 1 = 63$. The polynomial $x^6 + x + 1$ is an irreducible factor of $x^{63} + 1$ over $GF(2)$

* The proof applies although $R \cdot \theta(x)$ is not necessarily a BCH code.

[see Ref. 6, p. 309, polynomial f_{10}]. In this case, ω is a cube root of unity and the above polynomial factors over $GF(4)$ into

$$(x^3 + x^2 + \omega^2 x + \omega)(x^3 + x^2 + \omega x + \omega^2).$$

We take a zero of the first polynomial for ν, and for purposes of calculation it is convenient to express it as

$$\nu = \begin{bmatrix} 1 & 1 & 0 \\ \omega^2 & 0 & 1 \\ \omega & 0 & 0 \end{bmatrix}.$$

It is readily checked that the characteristic equation of this matrix is $x^3 + x^2 + \omega^2 x + \omega$. A table of the relevant powers of ν follows.

$$\nu = \begin{bmatrix} 1 & 1 & 0 \\ \omega^2 & 0 & 1 \\ \omega & 0 & 0 \end{bmatrix} \quad \nu^2 = \begin{bmatrix} \omega & 1 & 1 \\ 1 & \omega^2 & 0 \\ \omega & \omega & 0 \end{bmatrix} \quad \nu^3 = \begin{bmatrix} \omega^2 & \omega & 1 \\ \omega^2 & 1 & \omega^2 \\ \omega^2 & \omega & \omega \end{bmatrix}$$

$$\nu^6 = \begin{bmatrix} 0 & 1 & 0 \\ \omega^2 & 1 & 1 \\ \omega & 0 & 1 \end{bmatrix} \quad \nu^{12} = \begin{bmatrix} \omega^2 & 1 & 1 \\ 1 & \omega & 0 \\ \omega & \omega & 1 \end{bmatrix}$$

$$\nu^7 = \begin{bmatrix} \omega^2 & 0 & 1 \\ \omega & \omega^2 & 1 \\ 0 & \omega & 0 \end{bmatrix} \quad \nu^{14} = \begin{bmatrix} \omega & \omega & \omega^2 \\ 0 & 0 & 1 \\ \omega^2 & 1 & \omega \end{bmatrix}$$

Take $d_1 = 3$, $d_2 = 6$.

$$\nu^3 + \nu^6 = \begin{bmatrix} \omega^2 & \omega^2 & 1 \\ 0 & 0 & \omega \\ 1 & \omega & \omega^2 \end{bmatrix} = \omega\nu^{14}$$

$$\omega\nu^3 + \nu^6 = \begin{bmatrix} 1 & \omega & \omega \\ \omega & \omega^2 & 0 \\ \omega^2 & \omega^2 & \omega \end{bmatrix} = \omega\nu^{12}$$

$$\omega^2\nu^3 + \nu^6 = \begin{bmatrix} \omega & \omega & \omega^2 \\ 1 & \omega & \omega^2 \\ 0 & 1 & 0 \end{bmatrix} = \omega\nu^7.$$

Hence, 3, 6, 7, 12, 14 is a difference-set modulo 21. In this case, $r = 2^2 - 1 = 3$, and the appropriate values of t are 5, 10, 20, 19, 17, 13; 9, 18, 15. ($tr = 15, 30, 60$ etc.) It is readily checked that each tr has a digit sum (to base 2) of $2s = 4$.

APPENDIX B

Let $\theta(x) = a_0 + a_1x + \cdots + a_{n-1}x^{n-1}$. The ideal $R \cdot \theta(x)$ consists of all linear combinations over $GF(p)$ of the n polynomials $x^i\theta(x)$ (mod $(x^n - 1)$), $i = 0, 1, \cdots, n - 1$. Its dimension is therefore the rank over $GF(p)$ of the matrix

$$A = \begin{pmatrix} a_0 & a_1 & a_2 & \cdots & a_{n-1} \\ a_{n-1} & a_0 & a_1 & \cdots & a_{n-2} \\ \cdots & \cdots & \cdots & \cdots & \cdots \\ a_1 & a_2 & a_3 & \cdots & a_0 \end{pmatrix}.$$

Let $\alpha_1, \alpha_2, \cdots, \alpha_n$ be the n zeros of $x^n - 1$ over $GF(p)$; they are all distinct since p does not divide n. Let Δ be the matrix

$$\Delta = \begin{pmatrix} 1 & 1 & \cdots & 1 \\ \alpha_1 & \alpha_2 & \cdots & \alpha_n \\ \alpha_1^2 & \alpha_2^2 & \cdots & \alpha_n^2 \\ \cdots & \cdots & \cdots & \cdots \\ \alpha_1^{n-1} & \alpha_2^{n-1} & \cdots & \alpha_n^{n-1} \end{pmatrix}.$$

Then

$$\det \Delta = \prod_{i<j\leqq n} (\alpha_i - \alpha_j) \neq 0,$$

and the rank of A is the same as the rank of $A\Delta$. Now,

$$A\Delta = \begin{vmatrix} \theta(\alpha_1) & \theta(\alpha_2) & \cdots & \theta(\alpha_n) \\ \alpha_1\theta(\alpha_1) & \alpha_2\theta(\alpha_2) & \cdots & \alpha_n\theta(\alpha_n) \\ \cdots & \cdots & \cdots & \cdots \\ \alpha_1^{n-1}\theta(\alpha_1) & \alpha_2^{n-1}\theta(\alpha_2) & \cdots & \alpha_n^{n-1}\theta(\alpha_n) \end{vmatrix}.$$

Suppose the a_i are arranged so that $\theta(\alpha_i) \neq 0$, $i = 1, \cdots, t$, and $\theta(\alpha_i) = 0$ $i = t + 1, \cdots, n$. The last $n - t$ columns of $A\Delta$ contain only zeros, so that the rank of $A\Delta$ is $\leqq t$. The t by t matrix in the upper left hand corner of $A\Delta$ is

$$\begin{vmatrix} \theta(\alpha_1) & \theta(\alpha_2) & \cdots & \theta(\alpha_t) \\ \alpha_1\theta(\alpha_1) & \alpha_2\theta(\alpha_2) & \cdots & \alpha_t\theta(\alpha_t) \\ \cdots & \cdots & \cdots & \cdots \\ \alpha_1^{t-1}\theta(\alpha_1) & \alpha_2^{t-1}\theta(\alpha_2) & \cdots & \alpha_t^{t-1}\theta(\alpha_t) \end{vmatrix},$$

and the determinant of this is

$$\theta(\alpha_1)\cdot\theta(\alpha_2)\cdots\theta(\alpha_t)\prod_{i<j\leqq t}(\alpha_i - \alpha_j) \neq 0.$$

Thus, the rank of $A\Delta$ (hence, the dimension of $R\cdot\theta(x)$) is exactly t.

REFERENCES

1. Weldon, E. J., Jr., Difference-Set Cyclic Codes. B.S.T.J. this issue, pp. 1045–1055.
2. Singer, J., A Theorem in Finite Projective Geometry and Some Applications to Number Theory, Trans., AMS *43*, 1938, pp. 377–385.
3. Evans, T. A. and Mann, H. B., On Simple Difference Sets, Sankhya, *11*, 1955, pp. 464–481.
4. Riordan, J., *An Introduction to Combinatorial Analysis*, John Wiley and Sons, 1958.
5. Peterson, W. W., *Error Correcting Codes*, M.I.T. Press, 1961.
6. MacWilliams, Jessie, The Structure and Properties of Binary Cyclic Alphabets, B.S.T.J., *44*, 1965, pp. 303–332.

Simultaneously Orthogonal Expansion of Two Stationary Gaussian Processes — Examples

By T. T. KADOTA

(Manuscript received April 20, 1966)

This paper presents two examples of the simultaneously orthogonal expansion of the sample functions of a pair of stationary Gaussian processes. The pair of Gaussian processes are specified by zero means and covariances $exp\ (-\alpha\,|\,s-t\,|\,)$, $exp\ (-\beta\,|\,s-t\,|\,)$ *in Example 1 and by* $1-|\,s-t\,|\,/2T$, $exp\ (-|\,s-t\,|\,/T)$ *in Example 2. The expansion takes the form of a trigonometric series where the coefficients are mutually independent Gaussian variables for both processes, and the series converges, both with probability one for every* t *and in the stochastic mean uniformly in* t, *for both processes. This type of expansion is an extension of the Karhunen-Loéve expansion to the case of a pair of processes, and no concrete example has been given previously.*

The general theory of the orthogonal expansions is briefly reviewed in Section I, while concrete results for the two examples are tabulated in Section II with a brief outline of the method of derivation. The complete derivation, which constitutes the principal part of this paper, is presented in full detail in Appendices.

I. GENERAL THEORY

Orthogonal expansion of Gaussian processes has been used extensively for both theoretical investigation and application in communication engineering. In the case of a single process, the expansion is a modified version of the Karhunen-Loéve expansion.[1,2] Specifically, if $x(t)$, $-T \leqq t \leqq T$, is the sample function of a Gaussian process with zero mean and a continuous covariance $R(s,t)$, $-T \leqq s, t \leqq T$, then $x(t)$ can be expanded in terms of the (orthonormalized) eigenfunctions f_k, $k = 0, 1, 2,$

$\cdots$, of R as follows:*

$$x(t) = \sum_k \xi_k(x) f_k(t), \qquad \text{a.e. } [P],$$

$$\xi_k(x) = (x, f_k), \qquad \text{a.e. } [P],\dagger$$

where P is the Gaussian measure induced by the process with zero mean and the covariance R.

This expansion has two desirable properties: (i) for every measurable set specified by the sample function $x(t)$, there is an equivalent measurable set specified by the coefficients, $\{\xi_k\}$, and (ii) $\{\xi_k\}$ are mutually independent Gaussian variables with zero means and variances equal to the eigenvalues of R. Thus, many problems concerning the sample function can often be reduced to equivalent problems concerning the coefficients alone, and they in turn can be decomposed into a collection of effectively "one-dimensional problems".

In the case of two Gaussian processes, the sample functions can be expanded relative to a single set of functions such that their coefficients are mutually independent with respect to the two finite dimensional distributions.‡ Such "simultaneously orthogonal" expansions have often been used to prove the equivalence-singularity dichotomy of two Gaussian measures.[3,4,5] The particular expansion theorem used here is due to Pitcher.[5] It goes as follows: Let P_1 and P_2 be the probability measures induced by two Gaussian processes with zero means and continuous, positive-definite covariances $R_1(s,t)$ and $R_2(s,t)$, $-T \leqq s, t \leqq T$.§ If $R_1^{-\frac{1}{2}} R_2 R_1^{-\frac{1}{2}}$ is densely defined and bounded on $\mathfrak{L}_2$ and its extension to the

* R denotes both the covariance and the integral operator generated by it, namely,

$$(Rf)(t) = \int_{-T}^{T} R(s,t) f(s) ds, \qquad f \in \mathfrak{L}_2,$$

where $\mathfrak{L}_2$ is the space of square-integrable functions on $[-T,T]$.

† Without loss of generality, the process under consideration is assumed to be separable and measurable. (f,g) denotes the usual scalar product of two elements f and g in $\mathfrak{L}_2$.

‡ Instead of regarding "two Gaussian processes" as two *one-parameter families* of random variables, we consider a *single* one-parameter family of measurable functions x_t, $-T \leqq t \leqq T$, with *two* probability measures P_1 and P_2.

§ We assume that P_1 and P_2 are extended to $\mathfrak{B}$ and complete on $\mathfrak{B}_{P_1}$ and $\mathfrak{B}_{P_2}$, where $\mathfrak{B}$ is the minimal σ-field with respect to which x_t is measurable for every $t \in [-T,T]$. Since $R_1(s,t)$ and $R_2(s,t)$ are both continuous, we consider only the separable and measurable version of $\{x_t, -T \leqq t \leqq T\}$ without loss of generality, where the separability is with respect to $\frac{1}{2}(P_1 + P_2)$ while the measurability is with respect to $\mathfrak{B}_{\frac{1}{2}(P_1+P_2)} \times \mathfrak{A}$ and $\mathfrak{A}$ is the Lebesgue field of the subsets of $[-T,T]$. Note that such a version is also separable with respect to both P_1 and P_2 and measurable with respect to $\mathfrak{B}_{P_1} \times \mathfrak{A}$ and $\mathfrak{B}_{P_2} \times \mathfrak{A}$.

whole of $\mathfrak{L}_2$ has a set of eigenfunctions which spans $\mathfrak{L}_2$, then

$$x(t) = \text{l.i.m.}_{n\to\infty} \sum_{k=0}^{n} \eta_k(x)(R_1^{\frac{1}{2}}\varphi_k)(t), \qquad [P_1 \times \mu, P_2 \times \mu],$$

$$\eta_k(x) = \text{l.i.m.}_{j\to\infty} (x, R_1^{-\frac{1}{2}}\varphi_{kj}), \qquad [P_1, P_2],$$

where φ_k, $k = 0, 1, 2, \cdots$, are the orthonormalized eigenfunctions of the extension of $R_1^{-\frac{1}{2}}R_2R_1^{-\frac{1}{2}}$, and μ is the Lebesgue measure defined on the subsets of $[-T,T]$, and φ_{kj}, $j = 0, 1, 2, \cdots$, are a sequence of $\mathfrak{L}_2$-functions in the domain of $R^{-\frac{1}{2}}$ that converges strongly to φ_k for each k, namely,

$$\varphi_{kj} \in \mathfrak{D}(R_1^{-\frac{1}{2}}), \qquad \lim_{j\to\infty} \| \varphi_k - \varphi_{kj} \| = 0, \qquad k = 0, 1, 2, \cdots.$$

As in the case of a single process, this expansion also has two desirable properties:

(*i*) for every measurable* set Λ specified by $x(t)$, there exists another measurable set Λ' specified by $\{\eta_k\}$ such that

$$P_1(\Lambda \,\Delta\, \Lambda') = 0 = P_2(\Lambda \,\Delta\, \Lambda'),\dagger$$

(*ii*) $E_1\{\eta_k\eta_j\} = \delta_{kj}$, $\quad E_2\{\eta_k\eta_j\} = \lambda_k\delta_{kj}$, $\quad k, j = 0, 1, 2, \cdots$,

where λ_k is the eigenvalue of the extension of $R_1^{-\frac{1}{2}}R_2R_1^{-\frac{1}{2}}$ corresponding to φ_k. As seen from the definition and the property (*ii*), η_k, $k = 0, 1, 2, \cdots$, are, with respect to both P_1 and P_2, mutually independent Gaussian variables with zero means, and their variances are all unity with respect to P_1 and λ_k with respect to P_2.

Unfortunately, the above theorem is not a suitable method of actually obtaining the simultaneous expansion for a given pair of covariances $R_1(s,t)$ and $R_2(s,t)$. As the result of defining the expansion coefficients η_k and the expanding functions $R_1^{\frac{1}{2}}\varphi_k$ in terms of φ_k, $k = 0, 1, \cdots$, one must first of all solve the homogeneous equation involving the extension of $R_1^{-\frac{1}{2}}R_2R_1^{-\frac{1}{2}}$. Yet, there is no standard method of solution available for this type of equation, since $R_1^{-\frac{1}{2}}R_2R_1^{-\frac{1}{2}}$ is not, in general, a simple operator as R_1 and R_2 are. This may partly account for the fact that no concrete example for the simultaneous expansion has been given previously. In the next section and Appendices, we give two examples to illustrate an indirect method of obtaining φ_k first and then calculating η_k and $R_1^{\frac{1}{2}}\varphi_k$.

* The measurability is with respect to $\mathfrak{B}_{\frac{1}{2}(P_1+P_2)}$.
† Δ denotes symmetric difference, namely, $\Lambda \,\Delta\, \Lambda' = (\Lambda - \Lambda') \cup (\Lambda' - \Lambda)$.

II. EXAMPLES

The two examples we consider here are stationary Gaussian processes with zero means and the pair of covariances

$$R_1(s,t) = \exp(-\alpha \mid s - t \mid), \qquad R_2(s,t) = \exp(-\beta \mid s - t \mid)$$

in Example 1, and

$$R_1(s,t) = 1 - \frac{\mid s - t \mid}{2T}, \qquad R_2(s,t) = \exp\left(-\frac{\mid s - t \mid}{T}\right)$$

in Example 2.

The method we employ to obtain the expansions may be outlined as follows: First, we prove that $R_1^{-\frac{1}{2}} R_2 R_1^{-\frac{1}{2}}$ is densely defined and bounded, by showing that $R_2^{\frac{1}{2}} R_1^{-\frac{1}{2}}$ is bounded. Next, we consider solutions of the homogeneous equation

$$R_2\psi_k = \lambda_k R_1\psi_k .$$

If ψ_k is a square-integrable solution with a real number λ_k, then $R_1^{\frac{1}{2}}\psi_k$ is seen to be an eigenfunction of $R_1^{-\frac{1}{2}} R_2 R_1^{-\frac{1}{2}}$. Thus, the function $R_1^{\frac{1}{2}}\varphi_k$ in the desired expansion is simply $R_1\psi_k$.* Unfortunately, there are no such solutions in Example 1, and there are only half of what is needed in Example 2. However, suppose we consider "formal solutions" of the homogeneous equation and expand them relative to the set of eigenfunctions of R_1, which forms an orthonormal basis of $\mathfrak{L}_2$. Let ψ_{kj} be the sum of the first j terms of such an expansion. Then, it turns out that the normalized version of $\{R_1^{\frac{1}{2}}\psi_{kj}\}_j$ is the desired sequence $\{\varphi_{kj}\}$ used for defining η_k. That is, we show that (*i*) the normalized version of $\{R_1^{\frac{1}{2}}\psi_{kj}\}_j$ forms a Cauchy sequence and its limit in the mean is an eigenfunction of the extension of $R_1^{-\frac{1}{2}} R_2 R_1^{-\frac{1}{2}}$ with λ_k as the corresponding eigenvalue for each k, (*ii*) the collection of all such limits forms an orthonormal basis of $\mathfrak{L}_2$, hence they are the only eigenfunctions of the extension. Thus, the desired expansion is obtained simply by calculating $R_1^{\frac{1}{2}}\varphi_k$, $k = 0, 1, 2, \ldots$.

Finally, that the expansion series in both examples converge both a.e. $[P_1, P_2]$ for every t and in the mean $[P_1, P_2]$ uniformly in t, is deduced as follows: We first observe that the t-functions of the series are uniformly bounded in i and t, and the sum of the variances of the coefficients is finite with respect to both P_1 and P_2. Thus, by virtue of mutual independence of the coefficients, the partial sum of the series, denoted by

* The expansion in terms of $R_1\psi_k$ is suggested in Ref. 6 without the connection with $R_1^{-\frac{1}{2}} R_2 R_1^{-\frac{1}{2}}$.

$x_n(t)$, converges both a.e. $[P_1, P_2]$ for every t and in the mean $[P_1, P_2]$ uniformly in t to some Gaussian variable $\tilde{x}(t)$, $E_1\{\tilde{x}(t)\} = 0 = E_2\{\tilde{x}(t)\}$. Now, since $x_n(t)$ converges to $x(t)$ in the mean $[P_1 \times \mu, P_2 \times \mu]$, $E_1\{x_n(s)x_n(t)\}$ and $E_2\{x_n(s)x_n(t)\}$ converge in the mean $[\mu \times \mu]$ to $R_1(s,t)$ and $R_2(s,t)$ which are continuous. Hence, they converge uniformly to $R_1(s,t)$ and $R_2(s,t)$, respectively, which implies that

$$E_1\{\tilde{x}(s)\tilde{x}(t)\} = R_1(s,t) \qquad \text{and} \qquad E_2\{\tilde{x}(s)\tilde{x}(t)\} = R_2(s,t).$$

That is, $\{\tilde{x}(t), -T \leqq t \leqq T\}$ is a Gaussian process with zero mean and covariances $R_1(s,t)$ and $R_2(s,t)$ corresponding to P_1 and P_2, respectively. Hence, $\tilde{x}(t) = x(t)$, a.e. $[P_1, P_2]$ for every t. Thus, it follows that $x_n(t)$ converges to $x(t)$ both a.e. $[P_1, P_2]$ for every t and in the mean $[P_1, P_2]$ uniformly in t.

The results are tabulated in the following summary. In both examples, the orthogonal expansions of the sample function take the form of trigonometric series, which asymptotically behave like harmonic series for large indices. The coefficients are mutually independent Gaussian variables with zero means, and their variances are explicitly given, together with the asymptotic values for large indices. In addition, we include for future reference the eigenvalues and the (orthonormalized) eigenfunctions of the extension of $R_1^{-\frac{1}{2}}R_2R_1^{-\frac{1}{2}}$ to the whole of $\mathfrak{L}_2$, though they are not of the primary interest here.

III. SUMMARY

3.1 *Example 1*

$$R_1(s,t) = \exp(-\alpha \mid s - t \mid), \qquad R_2(s,t) = \exp(-\beta \mid s - t \mid), \qquad \alpha > \beta > 0$$

$$x(t) = \sum_{i=0}^{\infty} [\eta_i(x) \cos \theta_i t + \hat{\eta}_i(x) \sin \hat{\theta}_i t], \qquad \text{a.e. } [P_1, P_2],$$

where θ_i's and $\hat{\theta}_i$'s are positive solutions of*

$$(\alpha + \beta)\theta_i \tan \theta_i T = \alpha\beta - \theta_i^2,$$

$$-(\alpha + \beta)\hat{\theta}_i \operatorname{ctn} \hat{\theta}_i T = \alpha\beta - \hat{\theta}_i^2,$$

and η_i, $\hat{\eta}_i$, $i = 0, 1, 2, \cdots$, are mutually independent Gaussian variables with zero means and variances given by

* θ_i's and $\hat{\theta}_i$'s are indexed in the ascending order.

$$E_1\{\eta_i^2\} = 2\alpha/(\alpha^2 + \theta_i^2)\tau(\theta_i), \qquad E_1\{\hat{\eta}_i^2\} = 2\alpha/(\alpha^2 + \hat{\theta}_i^2)\tau(\hat{\theta}_i),$$

$$E_2\{\eta_i^2\} = 2\beta/(\beta^2 + \theta_i^2)\tau(\theta_i), \qquad E_2\{\hat{\eta}_i^2\} = 2\beta/(\beta^2 + \hat{\theta}_i^2)\tau(\hat{\theta}_i),$$

where

$$\tau(\theta) = T + \frac{(\alpha + \beta)\alpha\beta}{\theta^4 + (\alpha^2 + \beta^2)\theta^2 + \alpha^2\beta^2}.$$

For large i,

$$\theta_i \sim \left(i + \frac{1}{2}\right)\frac{\pi}{T}, \qquad \hat{\theta}_i \sim i\frac{\pi}{T},$$

$$E_1\{\eta_i^2\} \sim \frac{2\alpha T}{\left(i + \frac{1}{2}\right)^2\pi^2}, \qquad E_i\{\hat{\eta}_i^2\} \sim \frac{2\alpha T}{i^2\pi^2},$$

$$E_2\{\eta_i^2\} \sim \frac{2\beta T}{\left(i + \frac{1}{2}\right)^2\pi^2}, \qquad E_2\{\hat{\eta}_i^2\} \sim \frac{2\beta T}{i^2\pi^2}.$$

The extension of $R_1^{-\frac{1}{2}}R_2R_1^{-\frac{1}{2}}$ has eigenvalues

$$\lambda_{2i} = \frac{\beta}{\alpha}\frac{\alpha^2 + \theta_i^2}{\beta^2 + \theta_i^2}, \qquad \lambda_{2i+1} = \frac{\beta}{\alpha}\frac{\alpha^2 + \hat{\theta}_i^2}{\beta^2 + \theta_i^2},$$

and orthonormalized eigenfunctions

$$\varphi_{2i}(t) = \frac{2\alpha}{\alpha + \beta}\left[\frac{\alpha^2 + \theta_i^2}{\tau(\theta_i)}\right]^{\frac{1}{2}} \cos\theta_i T \text{ l.i.m.}_{n\to\infty} \sum_{j=0}^{n} \gamma(\sigma_j, \theta_i) \cos\alpha\sigma_j T \cos\alpha\sigma_j t,$$

$$\varphi_{2i+1}(t) = \frac{2\alpha}{\alpha + \beta}\left[\frac{\alpha^2 + \hat{\theta}_i^2}{\tau(\hat{\theta}_i)}\right]^{\frac{1}{2}} \sin\hat{\theta}_i T \text{ l.i.m.}_{n\to\infty} \sum_{j=0}^{n} \gamma(\hat{\sigma}_j, \hat{\theta}_i) \sin\alpha\hat{\sigma}_j T \sin\alpha\hat{\sigma}_j t,$$

where

$$\gamma(\sigma,\theta) = (1 + \sigma^2)^{\frac{1}{2}} \Big/ \left[T + \frac{\sigma^2}{\alpha(1 + \sigma^2)}\right](\alpha^2\sigma^2 - \theta^2),$$

and σ_j and $\hat{\sigma}_j$ are positive solutions of*

$$\sigma_j \tan\alpha\sigma_j T = 1, \qquad -\hat{\sigma}_j \operatorname{ctn}\alpha\hat{\sigma}_j T = 1.$$

---

* σ_i's and $\hat{}_i$'s are indexed in the ascending order.

3.2 *Example 2*

$$R_1(s,t) = 1 - \frac{|s-t|}{2T}, \qquad R_2(s,t) = \exp\left(-\frac{|s-t|}{T}\right).$$

$$x(t) = \sum_{i=0}^{\infty} [\eta_i(x) \cos \theta_i t + \hat{\eta}_i(x) \sin \theta_i t], \qquad \text{a.e. } [P_1, P_2]$$

where θ_i's are positive solutions of*

$$\theta_i T \tan \theta_i T = 1,$$

and η_i, $\hat{\eta}_i$, $i = 0, 1, 2, \cdots$, are mutually independent Gaussian variables with zero means and variances given by

$$E_1\{\eta_i^2\} = E_1\{\hat{\eta}_i^2\} = \frac{1 + \theta_i^2 T^2}{\theta_i^2 T^2 (2 + \theta_i^2 T^2)},$$

$$E_2\{\eta_i^2\} = E_2\{\hat{\eta}_i^2\} = \frac{2}{2 + \theta_i^2 T^2}.$$

For large i,

$$\theta_i \sim i\frac{\pi}{T}, \qquad E_1\{\eta_i^2\} \sim \frac{1}{i^2\pi^2}, \qquad E_2\{\eta_i^2\} \sim \frac{2}{i^2\pi^2}.$$

The extension of $R_1^{-\frac{1}{2}} R_2 R_1^{-\frac{1}{2}}$ has eigenvalues

$$\lambda_{2i} = \lambda_{2i+1} = \frac{2\theta_i^2 T^2}{1 + \theta_i^2 T^2},$$

and orthonormalized eigenfunctions

$$\varphi_{2i}(t) = \left(T\frac{2 + \theta_i^2 T^2}{1 + \theta_i^2 T^2}\right)^{-\frac{1}{2}} \cos \theta_i t$$

$$\varphi_{2i+1}(t) = 2\varphi_{2i}(T) \operatorname*{l.i.m.}_{n\to\infty} \sum_{j=0}^{n} \frac{(-1)^j (j + \frac{1}{2})\pi}{\theta_i^2 T^2 - (j + \frac{1}{2})^2 \pi^2} \sin (j + \tfrac{1}{2}) \frac{\pi}{T} t.$$

IV. ACKNOWLEDGMENT

The author acknowledges his deep indebtedness to D. Slepian for suggesting the examples and providing assistance.

* θ_i's are indexed in the ascending order.

APPENDIX A

Example 1

$$\begin{aligned} R_1(s,t) &= \exp(-\alpha \mid s-t \mid), \\ R_2(s,t) &= \exp(-\beta \mid s-t \mid), \end{aligned} \qquad -T \leqq s,t \leqq T, \qquad \alpha > \beta > 0.$$

A.1 *Eigenvalues and Eigenfunctions of R_1 and R_2*

Let μ_k and f_k, $k = 0, 1, 2, \cdots$, be the eigenvalues and the corresponding orthonormalized eigenfunctions of R_1. Then,

$$\mu_{2i} = \frac{2}{\alpha(1+\sigma_i^2)}, \qquad \mu_{2i+1} = \frac{2}{\alpha(1+\hat{\sigma}_i^2)}, \qquad i = 0, 1, 2, \cdots, \tag{1}$$

$$\begin{aligned} f_{2i}(t) &= \cos \alpha\sigma_i t \Big/ \left(T + \frac{\sin 2\alpha\sigma_i T}{2\alpha\sigma_i}\right)^{\frac{1}{2}}, \\ f_{2i+1}(t) &= \sin \alpha\hat{\sigma}_i t \Big/ \left(T - \frac{\sin 2\alpha\hat{\sigma}_i T}{2\alpha\hat{\sigma}_i}\right)^{\frac{1}{2}}, \end{aligned} \tag{2}$$

where σ_i and $\hat{\sigma}_i$ are positive solutions of

$$\sigma_i \tan \alpha\sigma_i T = 1, \qquad -\hat{\sigma}_i \operatorname{ctn} \alpha\hat{\sigma}_i T = 1, \tag{3}$$

respectively, indexed in ascending order.*

Similarly, the eigenvalues and eigenfunctions of R_2, denoted by ν_k and g_k, are given by

$$\nu_{2i} = \frac{2}{\beta(1+\rho_i^2)}, \qquad \nu_{2i+1} = \frac{2}{\beta(1+\hat{\rho}_i^2)}, \tag{4}$$

$$\begin{aligned} g_{2i}(t) &= \cos \alpha\rho_i t \Big/ \left(T + \frac{\sin 2\beta\rho_i T}{2\beta\rho_i}\right)^{\frac{1}{2}}, \\ g_{2i+1}(t) &= \sin \beta\hat{\rho}_i t \Big/ \left(T - \frac{\sin 2\beta\hat{\rho}_i T}{2\beta\hat{\rho}_i}\right)^{\frac{1}{2}}, \end{aligned} \tag{5}$$

where ρ_i and $\hat{\rho}_i$ are positive solutions of

$$\rho_i \tan \beta\rho_i T = 1, \qquad -\hat{\rho}_i \operatorname{ctn} \beta\hat{\rho}_i T = 1. \tag{6}$$

A.2 *Boundedness of $R_2^{\frac{1}{2}} R_1^{-\frac{1}{2}}$*

Since $\{f_k\}$ forms an orthonormal basis of $\mathfrak{L}_2[-T,T]$, we only have to show that $\| R_2^{\frac{1}{2}} R_1^{-\frac{1}{2}} f_k \|$ is uniformly bounded relative to the index k.

* See Ref. 7, pp. 99–101.

Namely, we must show existence of a constant c, $0 < c < \infty$, independent of k such that

$$\| R_2^{\frac{1}{2}} R_1^{-\frac{1}{2}} f_k \|^2 = \sum_l \frac{\nu_l}{\mu_k} (f_k, g_l)^2 < c.$$

Consider even k's, and put $k = 2i$, $i = 0, 1, 2, \cdots$. Observe

$$(f_{2i}, g_l) = 0, \qquad l: \text{odd}. \tag{7}$$

Hence, we shall consider only even l's. Note

$$(f_{2i}, g_{2j})^2 = \frac{\left(\int_{-T}^{T} \cos \alpha\sigma_i t \cos \beta\rho_j t \, dt\right)^2}{\left(T + \frac{\sin 2\alpha\sigma_i T}{2\alpha\sigma_i}\right)\left(T + \frac{\sin 2\beta\rho_i T}{2\beta\rho_i}\right)}, \qquad j = 0, 1, 2, \cdots,$$

$$\begin{aligned}\int_{-T}^{T} \cos \alpha\sigma_i t \cos \beta\rho_j t \, dt &= 2(\alpha\sigma_i \tan \alpha\sigma_i T - \beta\rho_j \tan \beta\rho_j T) \frac{\cos \alpha\sigma_i T \cos \beta\rho_j T}{\alpha^2\sigma_i^2 - \beta^2\rho_j^2} \qquad (8)\\ &= 2(\alpha - \beta) \frac{\cos \alpha\sigma_i T \cos \beta\rho_j T}{\alpha^2\sigma_i^2 - \beta^2\rho_j^2}\end{aligned}$$

where (3) and (6) are used for the last equality, and

$$(1 + \sigma_i^2) \cos^2 \alpha\sigma_i T = \sigma_i^2, \qquad (1 + \rho_j^2) \cos^2 \beta\rho_j T = \rho_j^2, \tag{9}$$

which also follow from (3) and (6). Thus,

$$\frac{\nu_{2i}}{\mu_{2j}} (f_{2i}, g_{2j})^2 = \frac{4\frac{\beta}{\alpha}(\alpha - \beta)^2 \cos^2 \beta\rho_j T}{T + \frac{\sin 2\alpha\sigma_i T}{2\alpha\sigma_i}} \frac{a(\beta\rho_j)\alpha^2\sigma_i^2}{\beta^2\rho_j^2(\alpha^2\sigma_i^2 - \beta^2\rho_j^2)^2}, \tag{10}$$

where

$$a(\theta) = \frac{\cos^2 \theta T}{T + \frac{\sin 2\theta T}{2\theta}}.$$

Also note that

$$\begin{aligned}\frac{\alpha^2\sigma_i^2}{\beta^2\rho_j^2(\alpha^2\sigma_i^2 - \beta^2\rho_j^2)^2} &= \frac{1}{(\alpha^2\sigma_i^2 - \beta^2\rho_j^2)^2} + \frac{1}{\alpha^2\sigma_i^2\beta^2\rho_j^2}\\ &\quad + \frac{1}{2\alpha^3\sigma_i^3}\left(\frac{1}{\alpha\sigma_i + \beta\rho_j} + \frac{1}{\alpha\sigma_i - \beta\rho_j}\right).\end{aligned}$$

First, through direct calculation with the use of (5) and (8),

$$\left[\int_{-T}^{T} \cos \alpha\sigma_i t\, g_{2j}(t)\, dt\right]^2 = 4(\alpha - \beta)^2 \cos^2 \alpha\sigma_i T \frac{a(\beta\rho_j)}{(\alpha^2\sigma_i^2 - \beta^2\rho_j^2)^2},$$

and from the fact that $\{g_k\}$ forms an orthonormal basis of $\mathfrak{L}_2$,

$$\sum_{j=0}^{\infty}\left[\int_{-T}^{T} \cos \alpha\sigma_i t\, g_{2j}(t)\, dt\right]^2 = \int_{-T}^{T} \cos^2 \alpha\sigma_i t\, dt$$

$$= T + \frac{\sin 2\alpha\sigma_i T}{2\alpha\sigma_i}.$$

Thus,

$$\sum_{j=0}^{\infty} \frac{4\frac{\beta}{\alpha}(\alpha - \beta)^2 \cos^2 \beta\rho_j T}{\left(T + \frac{\sin 2\alpha\sigma_i T}{2\alpha\sigma_i}\right)} \frac{a(\beta\rho_j)}{(\alpha^2\sigma_i^2 - \beta^2\rho_j^2)^2} \leqq \frac{\beta/\alpha}{\cos^2 \alpha\sigma_0 T}. \tag{11}$$

Secondly, it follows from (3) and (6) that

$$T + \frac{\sin 2\alpha\sigma_i T}{2\alpha\sigma_i} = T\left[1 + \frac{1}{\alpha T(1 + \sigma_i^2)}\right] > T,$$

$$T + \frac{\sin 2\beta\rho_j T}{2\beta\rho_j} > T, \tag{12}$$

and

$$\alpha^2\sigma_j^2 > \left(\frac{\pi}{T} j\right)^2, \qquad \beta^2\rho_j^2 > \left(\frac{\pi}{T} j\right)^2, \qquad j = 1, 2, \cdots. \tag{13}$$

Thus, $a(\beta\rho_j) < 1/T$. Hence,

$$\sum_{j=0}^{\infty} \frac{4\frac{\beta}{\alpha}(\alpha - \beta)^2 \cos^2 \beta\rho_j T}{\left(T + \frac{\sin 2\alpha\sigma_i T}{2\alpha\sigma_i}\right)} \frac{a(\beta\rho_j)}{\alpha^2\sigma_i^2\beta^2\rho_j^2}$$

$$< \frac{4\frac{\beta}{\alpha}(\alpha - \beta)^2}{\alpha^2\sigma_0^2}\left[\frac{1}{\beta^2\rho_0^2 T^2} + \frac{1}{\pi^2}\sum_{j=1}^{\infty}\frac{1}{j^2}\right]. \tag{14}$$

Thirdly, let $h_1(z)$ be a function of the complex variable z defined by

$$h_1(z) = \frac{z}{z \tan zT - \beta}.$$

Then, $h_1(z)$ satisfies the condition of a theorem on expansion in rational

functions,* and has poles $\pm\beta\rho_j$ and the residues $a(\beta\rho_j)$, $j = 0, 1, 2, \cdots$. Hence, according to the theorem,

$$\sum_{j=0}^{\infty} a(\beta\rho_j)\left(\frac{1}{\alpha\sigma_i + \beta\rho_j} + \frac{1}{\alpha\sigma_i - \beta\rho_j}\right) = h_1(\alpha\sigma_i) = \frac{\alpha\sigma_i}{\alpha - \beta}, \quad (15)$$

where (3) is used for the last equality. Thus,

$$\sum_{j=0}^{\infty} \frac{4\frac{\beta}{\alpha}(\alpha - \beta)^2 \cos^2 \beta\rho_j T}{\left(T + \frac{\sin 2\alpha\sigma_i T}{2\alpha\sigma_i}\right)} \frac{a(\beta\rho_j)}{2\alpha^3\sigma_i^3}\left(\frac{1}{\alpha\sigma_i + \beta\rho_j} + \frac{1}{\alpha\sigma_i - \beta\rho_j}\right) < \frac{2\beta(\alpha - \beta)}{\alpha^3\sigma_0^2 T} \quad (16)$$

where (12) is also used.

Therefore, upon combination of (11), (14), and (16), together with (7), we conclude that for even k's $\sum_l (\nu_l/\mu_k)(f_k, g_l)^2$ is bounded by the sum of the right-hand sides of (11), (14), and (16), which is obviously independent of k.

For odd k's, we can arrive at the same conclusion by following the similar steps.

A.3 *Formal Solutions of* $R_2\psi = \lambda R_1\psi$

The formal solutions of the homogeneous integral equation

$$\int_{-T}^{T} \exp(-\beta|s - t|)\psi_k(s)\,ds = \lambda_k \int_{-T}^{T} \exp(-\alpha|s - t|)\psi_k(s)\,ds$$

are

$$\lambda_{2i} = \frac{\beta}{\alpha}\frac{\alpha^2 + \theta_i^2}{\beta^2 + \theta_i^2}, \qquad \lambda_{2i+1} = \frac{\beta}{\alpha}\frac{\alpha^2 + \hat{\theta}_i^2}{\beta^2 + \hat{\theta}_i^2}, \qquad i = 0, 1, 2, \cdots, \quad (17)$$

$$\psi_{2i}(t) = \cos\theta_i t + \frac{\cos\theta_i T}{\alpha + \beta}[\delta(t - T) + \delta(t + T)],$$
$$\psi_{2i+1}(t) = \sin\hat{\theta}_i t + \frac{\sin\hat{\theta}_i T}{\alpha + \beta}[\delta(t - T) - \delta(t + T)], \quad (18)$$

where θ_i and $\hat{\theta}_i$ are positive solutions of

$$(\alpha + \beta)\theta_i \tan\theta_i T = \alpha\beta - \theta_i^2,$$
$$-(\alpha + \beta)\hat{\theta}_i \operatorname{ctn}\hat{\theta}_i T = \alpha\beta - \hat{\theta}_i^2, \quad (19)$$

* See Ref. 8, p. 134.

respectively, and they are indexed in ascending order. Namely, if θ_i and $\hat{\theta}_i$, $i = 0, 1, 2, \cdots$, are solutions of (19), then the following equalities hold for every i:

$$\begin{aligned}
&\int_{-T}^{T} \exp(-\beta|s-t|)\cos\theta_i s\,ds \\
&\qquad + \frac{\cos\theta_i T}{\alpha+\beta}\{\exp[-\beta(T-t)] + \exp[-\beta(T+t)]\} \\
&= \frac{\beta}{\alpha}\frac{\alpha^2+\theta_i^2}{\beta^2+\theta_i^2}\left[\int_{-T}^{T}\exp(-\alpha|s-t|)\cos\theta_i s\,ds\right. \\
&\qquad \left. + \frac{\cos\theta_i T}{\alpha+\beta}\{\exp[-\alpha(T-t)] + \exp[-\alpha(T+t)]\}\right], \qquad (20)\\
&\int_{-T}^{T} \exp(-\beta|s-t|)\sin\hat{\theta}_i s\,ds \\
&\qquad + \frac{\sin\hat{\theta}_i T}{\alpha+\beta}\{\exp[-\beta(T-t)] - \exp[-\beta(T+t)]\} \\
&= \frac{\beta}{\alpha}\frac{\alpha^2+\hat{\theta}_i^2}{\beta^2+\hat{\theta}_i^2}\left[\int_{-T}^{T}\exp(-\alpha|s-t|)\sin\hat{\theta}_i s\,ds\right. \\
&\qquad \left. + \frac{\sin\hat{\theta}_i T}{\alpha+\beta}\{\exp[-\alpha(T-t)] - \exp[-\alpha(T+t)]\}\right].
\end{aligned}$$

The above assertion can be verified through direct calculation.

A.4 *Eigenvalues and Eigenfunctions of* $R_1^{-\frac{1}{2}}R_2R_1^{-\frac{1}{2}}$

A.4.1 $\{R_1^{\frac{1}{2}}\psi_{kl}\}_l$ *form Cauchy sequences*

Let ψ_{kl}, $k, l = 0, 1, 2, \cdots$, be the lth partial sum of the series obtained by formally expanding ψ_k of (18) relative to $\{f_k\}$ of (2), the eigenfunctions of R_1. Namely, for $i = 0, 1, 2, \cdots$.

$$\begin{aligned}
\psi_{2i,2n}(t) &= \psi_{2i,2n+1}(t), \\
&= \sum_{j=0}^{n}\left[\int_{-T}^{T}\cos\theta_i s\, f_{2j}(s)\,ds + 2\frac{\cos\theta_i T}{\alpha+\beta}f_{2j}(T)\right]f_{2j}(t), \qquad (21)\\
\psi_{2i+1,2n+1}(t) &= \psi_{2i+1,2n+2}(t) \\
&= \sum_{j=0}^{n}\left[\int_{-T}^{T}\sin\hat{\theta}_i s\, f_{2j+1}(s)\,ds\right. \\
&\qquad \left. + 2\frac{\sin\hat{\theta}_i T}{\alpha+\beta}f_{2j+1}(T)\right]f_{2j+1}(t).
\end{aligned}$$

Then, $\{R_1^{\frac{1}{2}}\psi_{kl}\}_l$ forms a Cauchy sequence for every k.

Proof: It suffices to show that for every k

$$\lim_{l\to\infty} \| R_1^{\frac{1}{2}}\psi_{kl} \|^2 < \infty.$$

From (1) and (2) and through the use of (19),

$$\begin{aligned} \| R_1^{\frac{1}{2}}\psi_{2i,2n} \|^2 &= \sum_{j=0}^{n} \left[\int_{-T}^{T} \cos \theta_i s \, f_{2j}(s) \, ds \right. \\ &\qquad \left. + 2 \frac{\cos \theta_i T}{\alpha + \beta} f_{2j}(T) \right]^2 \frac{2}{\alpha(1 + \sigma_j^2)} \\ &= \frac{4\alpha}{(\alpha + \beta)^2} \cos^2 \theta_i T \sum_{j=0}^{n} a(\alpha\sigma_j) \frac{2\alpha^2(1 + \sigma_j^2)}{(\theta_i^2 - \alpha^2\sigma_j^2)^2}. \end{aligned}$$

Note also that

$$\frac{2\alpha^2(1 + \sigma_j^2)}{(\theta_i^2 - \alpha^2\sigma_j^2)^2} = 2 \frac{\alpha^2 + \theta_i^2}{(\theta_i^2 - \alpha^2\sigma_j^2)^2} - \frac{1}{\theta_i} \left(\frac{1}{\theta_i + 2\sigma_j} + \frac{1}{\theta_i - \alpha\sigma_j} \right).$$

Next, with the aid of (2), (3), and (19), we find

$$\left[\int_{-T}^{T} \cos \theta_i t \, f_{2j}(t) \, dt \right] = \frac{4(\alpha^2 + \theta_i^2)^2 \cos^2 \theta_k T}{(\alpha + \beta)^2} \frac{a(\alpha\sigma_j)}{(\theta_i^2 - \alpha^2\sigma_j^2)^2}.$$

Also observe that

$$\sum_{j=0}^{\infty} \left[\int_{-T}^{T} \cos \theta_i t \, f_{2j}(t) \, dt \right]^2 = \int_{-T}^{T} \cos^2 \theta_i t \, dt = T + \frac{\sin 2\theta_i T}{2\theta_i}.$$

Thus,

$$\frac{4\alpha}{(\alpha + \beta)^2} \cos^2 \theta_i T \sum_{j=0}^{\infty} a(\alpha\sigma_j) \frac{\alpha(\alpha^2 + \theta_i^2)}{(\theta_i^2 - \alpha^2\sigma_j^2)^2} = \frac{2\alpha}{\alpha^2 + \theta_i^2} \left(T + \frac{\sin 2\theta_i T}{2\theta_i} \right).$$

Next, following the procedure for obtaining (15),

$$\begin{aligned} &- \frac{4\alpha}{(\alpha + \beta)^2} \cos^2 \theta_i T \sum_{j=0}^{\infty} \frac{a(\alpha\sigma_j)}{\theta_i} \left(\frac{1}{\theta_i + \alpha\sigma_j} + \frac{1}{\theta_i - \alpha\sigma_j} \right) \\ &\qquad = \frac{4\alpha}{\alpha + \beta} \frac{\cos^2 \theta_i T}{\alpha^2 + \theta_i^2}, \end{aligned}$$

where (19) is also used. Hence,

$$\lim_{l\to\infty} \| R_1^{\frac{1}{2}}\psi_{2i,l} \|^2 = \frac{2\alpha}{\alpha^2 + \theta_i^2} \left(T + \frac{\sin 2\theta_i T}{2\theta_i} + \frac{2 \cos^2 \theta_i T}{\alpha + \beta} \right) = \frac{2\alpha\tau(\theta_i)}{\alpha^2 + \theta_i^2},$$

where

$$\tau(\theta) = T + \frac{(\alpha + \beta)\alpha\beta}{\theta^4 + (\alpha^2 + \beta^2)\theta^2 + \alpha^2\beta^2}, \tag{22}$$

and (19) is used for the second equality.

By following the same steps, we obtain

$$\lim_{l\to\infty} \| R_1^{\frac{1}{2}}\psi_{2i+1,l} \|^2 = \frac{2\alpha\tau(\hat{\theta}_i)}{\alpha^2 + \hat{\theta}_i^2}.$$

Thus, the assertion is proved.

A.4.2 *Orthornormality of* $\{\varphi_k\}$

Define φ_{km}, $k, m = 0, 1, 2, \cdots$, by

$$\begin{aligned} \varphi_{2i,2n} = \varphi_{2i,2n+1} &= \left(\lim_{l\to\infty} \| R_1^{\frac{1}{2}}\psi_{2i,l} \|^2\right)^{-\frac{1}{2}} R_1^{\frac{1}{2}}\psi_{2i,2n}, \\ \varphi_{2i+1,2n+1} = \varphi_{2i+1,2n+2} &= \left(\lim_{l\to\infty} \| R_1^{\frac{1}{2}}\psi_{2i+1,l} \|^2\right)^{-\frac{1}{2}} R_1^{\frac{1}{2}}\psi_{2i+1,2n+1}. \end{aligned} \tag{23}$$

Define φ_k by

$$\varphi_{2i} = \underset{n\to\infty}{\text{l.i.m.}}\ \varphi_{2i,2n}, \qquad \varphi_{2i+1} = \underset{n\to\infty}{\text{l.i.m.}}\ \varphi_{2i+1,2n+1}. \tag{24}$$

Then, $\{\varphi_k\}$ is a sequence of orthonormal functions.

Proof: Normality is obvious. To prove orthogonality, let us first write φ_k explicitly.

$$\begin{aligned} \varphi_{2i}(t) &= \underset{n\to\infty}{\text{l.i.m.}}\ b_i \sum_{j=0}^{n} \frac{[2\alpha^2(1 + \sigma_j^2)]^{\frac{1}{2}} \cos \alpha\sigma_j T}{\left(T + \dfrac{\sin 2\alpha\sigma_j T}{2\alpha\sigma_j}\right)(\alpha^2\sigma_j^2 - \theta_i^2)} \cos \alpha\sigma_j t, \\ \varphi_{2i+1}(t) &= \underset{n\to\infty}{\text{l.i.m.}}\ \hat{b}_i \sum_{j=0}^{n} \frac{[2\alpha^2(1 + \hat{\sigma}_j^2)]^{\frac{1}{2}} \sin \alpha\hat{\sigma}_j T}{\left(T - \dfrac{\sin 2\alpha\hat{\sigma}_j T}{2\alpha\hat{\sigma}_j}\right)(\alpha^2\hat{\sigma}_j^2 - \hat{\theta}_i^2)} \sin \alpha\hat{\sigma}_j t, \end{aligned} \tag{25}$$

where

$$b_i = \left[\frac{2(\alpha^2 + \theta_i^2)}{\tau(\theta_i)}\right]^{\frac{1}{2}} \frac{\cos \theta_i T}{\alpha + \beta}, \qquad \hat{b}_i = \left[\frac{2(\alpha^2 + \hat{\theta}_i^2)}{\tau(\hat{\theta}_i)}\right]^{\frac{1}{2}} \frac{\sin \hat{\theta}_i T}{\alpha + \beta}. \tag{26}$$

First, note

$$(\varphi_{2i}, \varphi_{2m+1}) = 0, \qquad i, m = 0, 1, 2, \cdots.$$

Secondly,

$$(\varphi_{2i}, \varphi_{2m}) = b_i b_m \sum_{j=0}^{\infty} a(\alpha\sigma_j) \frac{2\alpha^2(1 + \sigma_j^2)}{(\theta_i^2 - \alpha^2\sigma_j^2)(\theta_m^2 - \alpha^2\sigma_j^2)},$$

and

$$\frac{2\alpha^2(1+\sigma_j^2)}{(\theta_i^2-\alpha^2\sigma_j^2)(\theta_m^2-\alpha^2\sigma_j^2)} = \frac{1}{\theta_m^2-\theta_i^2}\left[\frac{\alpha^2+\theta_i^2}{\theta_1}\left(\frac{1}{\theta_i+\alpha\sigma_j}+\frac{1}{\theta_i-\alpha\sigma_j}\right) - \frac{\alpha^2+\theta_m^2}{\theta_m}\left(\frac{1}{\theta_m+\alpha\sigma_j}+\frac{1}{\theta_m-\alpha\sigma_j}\right)\right].$$

Again, following the same procedure for obtaining (15),

$$(\varphi_{2i}, \varphi_{2m}) = \frac{b_i b_m}{\theta_m^2-\theta_i^2}\left(\frac{\alpha^2+\theta_i^2}{\theta_i}\frac{\theta_i}{\theta_i\tan\theta_i T-\alpha} - \frac{\alpha^2+\theta_m^2}{\theta_m}\frac{\theta_m}{\theta_m\tan\theta_m T-\alpha}\right) = 0,$$

where (19) is used for the second equality.

By following the same steps, we also obtain

$$(\varphi_{2i+1}, \varphi_{2m+1}) = 0.$$

A.4.3 $\{\varphi_k\}$ *forms an orthonormal basis of* $\mathfrak{L}_2$

Since $\{\varphi_k\}$ is a sequence of orthonormal functions and $\{f_l\}$ is an orthonormal basis of $\mathfrak{L}_2$, it suffices to show that for every $l = 0, 1, 2, \cdots$,

$$\sum_{k=0}^{\infty}(f_l, \varphi_k)^2 = 1.$$

First, note that (f_l, φ_k) vanishes unless l and k have the same parity. Secondly, from (2) and (25),

$$\sum_{j=0}^{\infty}(f_{2i}, \varphi_{2j})^2 = \frac{1}{(\alpha+\beta)\left(T+\dfrac{\sin 2\alpha\sigma_i T}{2\alpha\sigma_i}\right)} \sum_{j=0}^{\infty}\frac{\cos^2\theta_j T}{(\alpha+\beta)\tau(\theta_j)}\frac{4\alpha^2\sigma_i^2(\alpha^2+\theta_j^2)}{(\alpha^2\sigma_i^2-\theta_j^2)^2},$$

and also note

$$\frac{4\alpha^2\sigma_j^2(\alpha^2+\theta_j^2)}{(\alpha^2\sigma_i^2-\theta_j^2)^2} = \alpha^2(1+\sigma_i^2)\left[\frac{1}{(\alpha\sigma_i+\theta_j)^2}+\frac{1}{(\alpha\sigma_i-\theta_j)^2}\right] + \frac{\alpha^2(1-\sigma_i^2)}{\alpha\sigma_i}\left(\frac{1}{\alpha\sigma_i+\theta_j}+\frac{1}{\alpha\sigma_i-\theta_j}\right).$$

Now, consider a function of the complex variable defined by

$$h_2(z) = \frac{z}{(\alpha+\beta)z\tan zT-\alpha\beta+z^2}.$$

$h_2(z)$ satisfies the condition of the previously quoted theorem and has poles $\pm\theta_j$ and the residues

$$\frac{\cos^2 \theta_j T}{(\alpha + \beta)\tau(\theta_j)}, \qquad j = 0, 1, 2, \cdots .$$

Also,

$$\frac{d}{dz} h_2(z) \mid_{z=\alpha\sigma_i} = \frac{1}{\alpha^2(1 + \sigma_i^2)} \left[\frac{1 - \sigma_i^2}{1 + \sigma_i^2} - (\alpha + \beta)\left(T + \frac{\sin 2\alpha\sigma_i T}{2\alpha\sigma_i}\right)\right].$$

Thus, according to the theorem,

$$\frac{\alpha^2(1 - \sigma_i^2)}{\alpha\sigma_i} \sum_{j=0}^{\infty} \frac{\cos^2 \theta_j T}{(\alpha + \beta)\tau(\theta_j)} \left(\frac{1}{\alpha\sigma_i + \theta_j} + \frac{1}{\alpha\sigma_i - \theta_j}\right)$$
$$= \frac{\alpha^2(1 - \sigma_i^2)}{\alpha\sigma_i} h_2(\alpha\sigma_i) = \frac{1 - \sigma_i^2}{1 + \sigma_i^2},$$

where (3) is used for the second equality. Also, through the use of a modified version of the theorem,*

$$\alpha^2(1 + \sigma_i^2) \sum_{j=0}^{\infty} \frac{\cos^2 \theta_j T}{(\alpha + \beta)\tau(\theta_j)} \left[\frac{1}{(\alpha\sigma_i + \theta_j)^2} + \frac{1}{(\alpha\sigma_i - \theta_j)^2}\right]$$
$$= -\alpha^2(1 + \sigma_i^2) \frac{d}{dz} h_2(z) \mid_{z=\alpha\sigma_i} = (\alpha + \beta)$$
$$\cdot\left(T + \frac{\sin 2\alpha\sigma_i T}{2\alpha\sigma_i}\right) - \frac{1 - \sigma_i^2}{1 + \sigma_i^2}.$$

Hence, upon combination of these two results,

$$\sum_{j=0}^{\infty} \frac{\cos^2 \theta_j T}{(\alpha + \beta)\tau(\theta_j)} \frac{4\alpha^2\sigma_i^2(\alpha^2 + \theta_j^2)}{(\alpha^2\sigma_i^2 - \theta_j^2)^2} = (\alpha + \beta)\left(T + \frac{\sin 2\alpha\sigma_i T}{2\alpha\sigma_i}\right).$$

---

* The modified version:
Let $f(z)$ be the function satisfying the condition of the theorem (Ref. 8, p. 134), having poles a_n and their residues b_n. Then,

$$\sum_n \frac{b_n}{(a_n - x)^2} = -\frac{d}{dz} f(z) \mid_{z=x}.$$

This is proved by noting that

$$\frac{1}{2\pi i} \int_{C_m} \frac{f(z)}{(z - x)^2} dz = \frac{d}{dz} f(z) \mid_{z=x} + \sum_n \frac{b_n}{(a_n - x)^2},$$

and the left-hand side vanishes as $m \to \infty$, where C_m is the contour defined in Ref. 8.

Thus,

$$\sum_{j=0}^{\infty} (f_{2i}, \varphi_{2j})^2 = 1, \qquad i = 0, 1, 2, \cdots.$$

By following similar steps, we obtain

$$\sum_{j=0}^{\infty} (f_{2i+1}, \varphi_{2j+1})^2 = 1, \qquad i = 0, 1, 2, \cdots,$$

and the assertion is proved.

A.4.4 *Closed form-expressions of* $R_1^{\frac{1}{2}}\varphi_k$

$$R_1^{\frac{1}{2}}\varphi_{2i}(t) = \left[\frac{2\alpha}{(\alpha^2 + \theta_i^2)\tau(\theta_i)}\right]^{\frac{1}{2}} \cos \theta_i t,$$

$$R_1^{\frac{1}{2}}\varphi_{2i+1}(t) = \left[\frac{2\alpha}{(\alpha^2 + \theta_i^2)\tau(\hat{\theta}_i)}\right]^{\frac{1}{2}} \sin \hat{\theta}_i t, \qquad i = 0, 1, 2, \cdots. \quad (27)$$

Proof: From (25) and (1),

$$-R_1^{\frac{1}{2}}\varphi_{2i}(t) = \lim_{n\to\infty} \frac{b_i\alpha^{\frac{1}{2}}}{\theta_i} \sum_{j=0}^{n} c_j(t) \left(\frac{1}{\theta_i + \alpha\sigma_j} + \frac{1}{\theta_i - \alpha\sigma_j}\right)$$

$$-R_1^{\frac{1}{2}}\varphi_{2i+1}(t) = \lim_{n\to\infty} \frac{\hat{b}_i\alpha^{\frac{1}{2}}}{\hat{\theta}_i} \sum_{j=0}^{n} \hat{c}_j(t) \left(\frac{1}{\hat{\theta}_i + \alpha\hat{\sigma}_j} + \frac{1}{\hat{\theta}_i - \alpha\hat{\sigma}_j}\right),$$

where b_i and $\hat{b}_i$ are given by (26) and

$$c_j(t) = \frac{\cos \alpha\sigma_j T \cos \alpha\sigma_j t}{T + (\sin 2\alpha\sigma_j T/2\alpha\sigma_j)}, \qquad \hat{c}_j(t) = \frac{\sin \alpha\hat{\sigma}_j T \sin \alpha\hat{\sigma}_j t}{T - (\sin 2\alpha\hat{\sigma}_j T/2\hat{\sigma}_j)}.$$

In order to sum the series, consider

$$h_3(z) = \frac{z \cos zt}{z \sin zT - \alpha \cos zT}.$$

Observe that $h_3(z)$ satisfies the condition of the previously quoted theorem, and has poles $\pm\alpha\sigma_j$ and the residues $c_j(t)$, $j = 0, 1, 2, \cdots$.* Thus, with the use of the theorem,

$$-R_1^{\frac{1}{2}}\varphi_{2i}(t) = \frac{b_i\alpha^{\frac{1}{2}}}{\theta_i} h_3(\theta_i) = -\frac{\alpha^{\frac{1}{2}}(\alpha + \beta)b_i}{(\alpha^2 + \theta_i^2) \cos \theta_i T} \cos \theta_i t,$$

* The residues of $h_3(z)$ are shown to be $c_j(t)$ through direct calculation with the use of (3).

where (19) is used for the second equality. Similarly,

$$-R_1^{\frac{1}{2}}\varphi_{2i+1}(t) = -\frac{\alpha^{\frac{1}{2}}(\alpha+\beta)\hat{b}_i}{(\alpha^2+\hat{\theta}_i^2)\sin\hat{\theta}_i T}\sin\hat{\theta}_i t.$$

Then, substitution of (26) into the above gives (27).

A.4.5 λ_k *and* φ_k *are eigenvalues and eigenfunctions of* $R_1^{-\frac{1}{2}}R_2R_1^{-\frac{1}{2}}$

λ_k and φ_k, $k = 0, 1, 2, \cdots$, are the eigenvalues and the corresponding orthonormalized eigenfunctions of the extension of $R_1^{-\frac{1}{2}}R_2R_1^{-\frac{1}{2}}$ to the whole of $\mathfrak{L}_2$.

Proof: It suffices to show that for every k

$$\lambda_k R_1^{\frac{1}{2}}\varphi_k = \underset{m\to\infty}{\text{l.i.m.}}\ R_2R_1^{-\frac{1}{2}}\varphi_{km},$$

where φ_{km}, $m = 0, 1, 2, \cdots$, are defined by (23), namely, φ_{km} is the mth partial sum of the series obtained by expanding φ_k relative to $\{f_l\}$.

Through direct calculation,

$$\int_{-T}^{T}\exp(-\beta|s-t|)\cos\theta_i s\,ds + \frac{\cos\theta_i T}{\alpha+\beta}\{\exp[-\beta(T-t)]+\exp[-\beta(T+t)]\} = \frac{2\beta}{\beta^2+\theta_i^2}\cos\theta_i t.$$

Thus, from (17) and (27),

$$\lambda_{2i}(R_1^{\frac{1}{2}}\varphi_{2i})(t) = \frac{(\alpha+\beta)b_i}{2\alpha^{\frac{1}{2}}\cos\theta_i T}\left[\int_{-T}^{T}\exp(-\beta|s-t|)\cos\theta_i s\,ds + \frac{\cos\theta_i T}{\alpha+\beta}\{\exp[-\beta(T-t)]+\exp[-\beta(T+t)]\}\right].$$

On the other hand, from (23) and (21),

$$\begin{aligned}(R_2R_1^{-\frac{1}{2}}\varphi_{2i,2n})(t) &= (R_2R_1^{-\frac{1}{2}}\varphi_{2i,2n+1})(t)\\ &= \frac{(\alpha+\beta)b_i}{2\alpha^{\frac{1}{2}}\cos\theta_i T}\sum_{j=0}^{n}(R_2f_{2j})(t)\left[\int_{-T}^{T}\cos\theta_i s\,f_{2j}(s)\,ds + 2\frac{\cos\theta_i T}{\alpha+\beta}f_{2j}(T)\right].\end{aligned}$$

But, since

$$\int_{-T}^{T}\exp(-\beta|s-t|)\cos\theta_i s\,ds = \underset{n\to\infty}{\text{l.i.m.}}\sum_{j=0}^{n}(R_2f_{2j})(t)\int_{-T}^{T}\cos\theta_i s\,f_{2j}(s)\,ds,$$

we only have to show

$$\exp[-\beta(T-t)] + \exp[-\beta(T+t)] = 2\lim_{n\to\infty}\sum_{j=0}^{n} f_{2j}(T)(R_2 f_{2j})(t),$$

i.e.,

$$R_2(T,t) + R_2(-T,t) = \text{l.i.m.}_{n\to\infty}\sum_{l=0}^{n}[f_l(T) + f_l(-T)](R_2 f_l)(t).$$

But this is certainly implied by

$$R_2^2(s,t) = \sum_{k,l=0}^{\infty}(f_k, R_2^2 f_l) f_k(s) f_l(t), \qquad -T \leqq s,t \leqq T, \tag{28}$$

where

$$R_2^2(s,t) = \int_{-T}^{T} R_2(s,u)R_2(u,t)\,du.$$

To prove (28), we first note that the series on the right converges to $R_2^2(s,t)$ in the mean. In addition,

$$|f_k(t)| < T^{-\frac{1}{2}},$$

as seen from (2) and (12). Hence, it suffices to show that

$$\sum_{k,l=0}^{\infty}|(f_k, R_2^2 f_l)| < \infty,$$

which is implied, through the Schwarz inequality, by

$$\sum_{k=0}^{\infty}\|R_2 f_k\|^2 < \infty.$$

Hence, we have shown that

$$\lambda_{2i} R_1^{\frac{1}{2}}\varphi_{2i} = \lim_{m\to\infty} R_2 R_1^{-\frac{1}{2}}\varphi_{2i,m}, \qquad i = 0, 1, 2, \cdots.$$

Through the same argument, (28) implies

$$\lambda_{2i+1} R_1^{\frac{1}{2}}\varphi_{2i+1} = \lim_{m\to\infty} R_2 R_1^{-\frac{1}{2}}\varphi_{2i+1,m}.$$

APPENDIX B

Example 2

$$R_1(s,t) = 1 - \frac{|s-t|}{2T}, \qquad -T \leqq s,t \leqq T.$$

$$R_2(s,t) = \exp\left(-\frac{|s-t|}{T}\right),$$

B.1 *Eigenvalues and Eigenfunctions of R_1 and R_2*

The eigenvalues and the orthonormalized eigenfunctions of R_1 are

$$\mu_{2i} = \frac{1}{T\theta_i^2}, \qquad \mu_{2i+1} = \frac{T}{(i + \frac{1}{2})^2\pi^2}, \qquad i = 0, 1, 2, \cdots, \tag{29}$$

$$f_{2i}(t) = \frac{\cos \theta_i t}{\left(T + \dfrac{\sin 2\theta_i T}{2\theta_i}\right)^{\frac{1}{2}}}, \qquad f_{2i+1}(t) = \frac{\sin\left(i + \dfrac{1}{2}\right)\dfrac{\pi}{T}t}{T^{\frac{1}{2}}}, \tag{30}$$

where θ_i, $i = 0, 1, 2, \cdots$, are positive solutions of

$$\theta_i T \tan \theta_i T = 1, \tag{31}$$

indexed in ascending order. Similarly, the eigenvalues and eigenfunctions of R_2 are

$$\nu_{2i} = \frac{2T}{1 + \theta_i^2 T^2}, \qquad \nu_{2i+1} = \frac{2T}{1 + \hat{\theta}_i^2 T^2}, \tag{32}$$

$$g_{2i}(t) = f_{2i}(t), \qquad g_{2i+1}(t) = \frac{\sin \hat{\theta}_i t}{\left(T - \dfrac{\sin 2\hat{\theta}_i T}{2\hat{\theta}_i}\right)^{\frac{1}{2}}}, \tag{33}$$

where $\hat{\theta}_i$, $i = 0, 1, 2, \cdots$, are positive solutions of

$$-\hat{\theta}_i T \operatorname{ctn} \hat{\theta}_i T = 1. \tag{34}$$

B.2 *Boundedness of $R_2^{\frac{1}{2}} R_1^{-\frac{1}{2}}$*

From (29), (32), and (33),

$$\| R_2^{\frac{1}{2}} R_1^{-\frac{1}{2}} f_{2i} \|^2 = \frac{2\theta_i^2 T^2}{1 + \theta_i^2 T^2} < 2, \qquad i = 0, 1, 2, \cdots.$$

Since

$$(f_{2i+1}, g_{2j}) = 0, \qquad j = 0, 1, 2, \cdots,$$

we have, through (29), (30), (32), and (33),

$$\| R_2^{\frac{1}{2}} R_1^{-\frac{1}{2}} f_{2i+1} \|^2 = \sum_{j=0}^{\infty} \frac{2\hat{\theta}_j^2 T^2}{1 + \hat{\theta}_j^2 T^2} \frac{4T \cos^2 \hat{\theta}_j T}{T - \dfrac{\sin 2\hat{\theta}_j T}{2\hat{\theta}_j}} \frac{(i + \frac{1}{2})^2\pi^2}{[\hat{\theta}_j^2 T^2 - (i + \frac{1}{2})^2\pi^2]^2},$$

and also note

$$\frac{(i+\frac{1}{2})^2\pi^2}{[\hat{\theta}_j^2T^2-(i+\frac{1}{2})^2\pi^2]^2}=\frac{\hat{\theta}_j^2T^2}{[\hat{\theta}_j^2T^2-(i+\frac{1}{2})^2\pi^2]^2}-\frac{1}{\theta_j^2T^2-(i+\frac{1}{2})^2\pi^2}. \tag{35}$$

Now

$$\sum_{j=0}^{\infty}\frac{4T\cos^2\hat{\theta}_jT}{T-\dfrac{\sin 2\hat{\theta}_jT}{2\hat{\theta}_j}}\frac{\hat{\theta}_j^2T^2}{[\hat{\theta}_jT^2-(i+\frac{1}{2})^2\pi^2]^2}=\sum_{j=0}^{\infty}(f_{2i+1},g_{2j+1})^2=1, \tag{36}$$

$$\left|\sum_{j=0}^{\infty}\frac{2\hat{\theta}_iT^2}{1+\hat{\theta}_j^2T^2}\frac{T\cos^2\hat{\theta}_jT}{T-\dfrac{\sin 2\hat{\theta}_jT}{2\hat{\theta}_j}}\frac{1}{\hat{\theta}_j^2T^2-(i+\frac{1}{2})^2\pi^2}\right|$$

$$\leqq\sum_{j=0}^{\infty}\frac{\hat{\theta}_j^2T^2}{(1+\hat{\theta}_j^2T^2)^2}\frac{T\cos^2\hat{\theta}_jT}{T-\dfrac{\sin 2\hat{\theta}_iT}{2\hat{\theta}_j}}<\infty,$$

where the first inequality follows from the Schwarz inequality and (36) while the second follows from (34).* Hence, $\| R_2^{\frac{1}{2}}R_1^{-\frac{1}{2}}f_{2i+1}\|^2$ is also bounded by a constant independent of i.

Thus, by using the argument in A.2, we conclude that $R_2^{\frac{1}{2}}R_1^{-\frac{1}{2}}$ is bounded.

B.3 *Formal Solutions of* $R_1\psi=\lambda R_0\psi$

Unlike Example 1, the even solutions of

$$\int_{-T}^{T}\exp\left(-\frac{|s-t|}{T}\right)\psi_k(s)\,ds=\lambda_k\int_{-T}^{T}\left(1-\frac{|s-t|}{2T}\right)\psi_k(s)\,ds \tag{37}$$

are bonafide functions while the odd remain formal. They are

$$\lambda_{2i}=\lambda_{2i+1}=\frac{2\theta^2T^2}{1+\theta_i^2T^2}, \tag{38}$$

$$\begin{aligned}\psi_{2i}(t)&=\cos\theta_it,\\ \psi_{2i+1}(t)&=\sin\theta_it+T\sin\theta_iT[\delta(t-T)-\delta(t+T)].\end{aligned} \tag{39}$$

* It follows from (34) that

$$T-\frac{\sin 2\hat{\theta}_iT}{2\hat{\theta}_j}=T\left(1+\frac{1}{1+\hat{\theta}_j^2T^2}\right)>T,$$

which corresponds to (12).

Again, the precise meaning of the odd solutions is that if θ_i, $i = 0, 1, 2, \cdots$, are positive solutions of (31) then

$$\int_{-T}^{T} \exp\left(-\frac{|s-t|}{T}\right) \sin \theta_i s \, ds + T \sin \theta_i T \cdot \left[\exp\left(-\frac{T-t}{T}\right) - \exp\left(-\frac{T+t}{T}\right)\right] \tag{40}$$

$$= \frac{2\theta_i^2 T^2}{1+\theta_i^2 T^2} \int_{-T}^{T} \left(1 - \frac{|s-t|}{2T}\right) \sin \theta_i s \, ds + t \sin \theta_i T$$

for every i. Again, the above assertions can be verified through direct calculation.

B.4 *Eigenvalues and Eigenfunctions of* $R_1^{-\frac{1}{2}} R_2 R_1^{-\frac{1}{2}}$

B.4.1 $\{R_1^{\frac{1}{2}}\psi_{2i+1,l}\}_l$ *form Cauchy sequences**

Define, for each $i = 0, 1, 2, \cdots$,

$$\psi_{2i+1,2n+1}(t) = \psi_{2i+1,2n+2}(t) = \sum_{j=0}^{n} \left[\int_{-T}^{T} \sin \theta_i s \, f_{2j+1}(s) \, ds + 2T \sin \theta_i T \, f_{2j+1}(T)\right] f_{2j+1}(t). \tag{41}$$

Then, $\{R_1^{\frac{1}{2}}\psi_{2i+1,l}\}_l$ forms a Cauchy sequence for every i.

Proof: From (29) and (30) and through the use of (31) and (35)

$$\| R_1^{\frac{1}{2}}\psi_{2i+1,2n+1} \|^2 = \sum_{j=0}^{n} \left[\int_{-T}^{T} \sin \theta_i s \, f_{2j+1}(s) \, ds + 2T \sin \theta_i T \, f_{2j+1}(T)\right] \frac{T}{\left(j+\frac{1}{2}\right)^2 \pi^2}$$

$$= 4 \frac{\cos^2 \theta_i T}{\theta_i^2} \sum_{j=0}^{n} \left(\frac{\theta_i^2 T^2}{\left[\theta_i^2 T^2 - \left(j+\frac{1}{2}\right)^2 \pi^2\right]^2} - \frac{1}{\theta_i^2 T^2 - \left(j+\frac{1}{2}\right)^2 \pi^2}\right).$$

Now

$$\sum_{j=0}^{n} \frac{4\theta_i^2 T^3 \cos^2 \theta_i T}{\left[\theta_i T^2 - \left(j+\frac{1}{2}\right)^2 \pi^2\right]^2} = \int_{-T}^{T} \sin^2 \theta_i t \, dt = T - \frac{\sin 2\theta_i T}{2\theta_i}. \tag{42}$$

* Note there is no need for considering such sequences for the even solutions ψ_{2i}'s, since they are already $\mathfrak{L}_2$-functions.

In order to sum the second term, observe that the function of complex variable $\tan z$ satisfies the condition of the theorem repeatedly used, and has poles $(j + \frac{1}{2})\pi$, $j = 0, \pm 1, \pm 2, \cdots$, and the residues -1. Hence, using the theorem,

$$-\sum_{j=0}^{\infty} \frac{1}{\theta_i^2 T^2 - \left(j + \frac{1}{2}\right)^2 \pi^2} = \frac{\tan \theta_i T}{2\theta_i T}. \tag{43}$$

Thus, combining the two results,

$$\lim_{n\to\infty} \| R_1^{\frac{1}{2}} \psi_{2i+1,2n+1} \|^2 = \frac{1}{\theta_i^2 T} \left(T + \frac{\sin 2\theta_i T}{2\theta_i} \right). \tag{44}$$

Hence, through the use of the argument in A.4.1, the assertion is proved.

B.4.2 *Orthonormality of* $\{\varphi_k\}$

Define φ_k, $k = 0, 1, 2, \cdots$, by

$$\varphi_{2i} = f_{2i}, \qquad \varphi_{2i+1} = \lim_{l\to\infty} \varphi_{2i+1,l}, \tag{45}$$

where $i = 0, 1, 2, \cdots$, and

$$\varphi_{2i+1,l}(t) = \left(\lim_{l\to\infty} \| R_1 \psi_{2i+1,l} \|^2 \right)^{-\frac{1}{2}} R_1^{\frac{1}{2}} \psi_{2i+1,l}.$$

Then, $\{\varphi_k\}$ is a sequence of orthonormal functions.

Proof: Normality is self-evident. Note, from (30) and (41),

$$(\varphi_{2i}, \varphi_{2m}) = \delta_{im}, \qquad (\varphi_{2i}, \varphi_{2m+1}) = 0, \qquad m = 0, 1, 2, \cdots,$$

and

$$\begin{aligned}(\varphi_{2i+1}, \varphi_{2m+1}) &= 4T f_{2i}(T) f_{2m}(T) \\ &\quad \cdot \sum_{j=0}^{\infty} \frac{\left(j + \frac{1}{2}\right)^2 \pi^2}{\left[\theta_i^2 T^2 - \left(j + \frac{1}{2}\right)^2 \pi^2\right]\left[\theta_m^2 T^2 - \left(j + \frac{1}{2}\right)^2 \pi^2\right]} \\ &= \frac{2 f_{2i}(T) f_{2m}(T)}{\theta_m^2 - \theta_i^2} \sum_{j=0}^{\infty} \left[\frac{\theta_i}{\theta_i T + \left(j + \frac{1}{2}\right)\pi} \right. \\ &\quad + \frac{\theta_i}{\theta_i T - \left(j + \frac{1}{2}\right)\pi} - \frac{\theta_m}{\theta_m T + \left(j + \frac{1}{2}\right)\pi} \\ &\quad \left. - \frac{\theta_m}{\theta_m T - \left(j + \frac{1}{2}\right)\pi} \right].\end{aligned}$$

Thus, from (43) and (31),

$$(\varphi_{2i+1}, \varphi_{2m+1}) = 2f_{2i}(T)f_{2m}(T)\frac{\theta_i T \tan \theta_i T - \theta_m T \tan \theta_m T}{\theta_m^2 - \theta_i^2} = 0$$

B.4.3 $\{\varphi_k\}$ *forms an orthonormal basis of* $\mathfrak{L}_2$

First, note from (30) and (45),

$$\sum_{k=0}^{\infty} (f_{2i}, \varphi_k)^2 = \sum_{j=0}^{\infty} (f_{2i}, f_{2j})^2 = 1, \qquad i = 0, 1, 2, \cdots.$$

Next,

$$\begin{aligned}\sum_{k=0}^{\infty} (f_{2i+1}, \varphi_k)^2 &= \sum_{j=0}^{\infty} (f_{2i+1}, \varphi_{2j+1})^2 \\ &= \sum_{j=0}^{\infty} \frac{4T \cos^2 \theta_j T}{T + \dfrac{\sin 2\theta_j T}{2\theta_j}} \frac{\left(i + \dfrac{1}{2}\right)^2 \pi^2}{\left[\theta_j^2 T^2 - \left(1 + \dfrac{1}{2}\right)^2 \pi^2\right]^2} \\ &= \frac{1}{T} \sum_{k=0}^{\infty} \left[\int_{-T}^{T} \cos\left(i + \frac{1}{2}\right)\frac{\pi}{T} s f_k(s)\, ds\right]^2 \\ &= 1.\end{aligned}$$

Thus, using the argument in A.4.3, the assertion is proved.

B.4.4 *Closed form-expressions of* $R_1^{\frac{1}{2}}\varphi_k$

$$(R_1^{\frac{1}{2}}\varphi_{2i})(t) = d_i \cos \theta_i t, \qquad (R_1^{\frac{1}{2}}\varphi_{2i+1})(t) = d_i \sin \theta_i t, \tag{46}$$

where

$$d_i = \frac{1}{\theta_i T}\left(1 + \frac{1}{1 + \theta_i^2 T^2}\right)^{-\frac{1}{2}}.$$

Proof: The even part of (46) follows immediately from the even parts of (45) and (29). Now, from the odd parts of (45) and (29),*

$$-(R_1^{\frac{1}{2}}\varphi_{2i+1})(t) = \text{l.i.m.}_{n\to\infty} \sum_{j=0}^{n} \frac{2(-1)^j d_i \theta_i T \cos \theta_i T \sin\left(j + \dfrac{1}{2}\right)\dfrac{\pi}{T} t}{\theta_i^2 T^2 - \left(j + \dfrac{1}{2}\right)^2 \pi^2}.$$

* Note, from (34) that

$$T + \frac{\sin 2\theta_i T}{2\theta_i} = T\left(1 + \frac{1}{1 + \theta_i^2 T^2}\right).$$

In order to sum the series, observe that a function of complex variable $\sin z(t/T)/\cos z$ satisfies the condition of the theorem repeatedly used, and has poles $(j + \frac{1}{2})\pi$, $j = 0, \pm 1, \pm 2, \cdots$, and the residues

$$-(-1)^j \sin (j + \tfrac{1}{2})(\pi/T)t.$$

Thus, according to the theorem,

$$\sum_{j=0}^{\infty} \frac{2(-1)^j \sin \left(j + \frac{1}{2}\right) \frac{\pi}{T} t}{\theta_i^2 T^2 - \left(j + \frac{1}{2}\right)^2 \pi^2} = -\frac{\sin \theta_i t}{\theta_i T \cos \theta_i T}.$$

Hence, substitution of the above yields the odd part of (46).

B.4.5 *λ_k and φ_k are eigenvalues and eigenfunctions of $R_1^{-\frac{1}{2}} R_2 R_1^{-\frac{1}{2}}$*

The assertion of A.4.5 holds.

Proof: That λ_{2i} and φ_{2i}, $i = 0, 1, 2, \cdots$, are eigenvalues and eigenfunctions of the extension of $R_1^{-\frac{1}{2}} R_2 R_1^{-\frac{1}{2}}$ is easily seen from (29), (32), (33), (38), and (45).*

For the odd part, i.e., λ_{2i+1} and φ_{2i+1}, we need to show that

$$\lambda_{2i+1} R_1^{\frac{1}{2}} \varphi_{2i+1} = \operatorname*{l.i.m.}_{m \to \infty} R_2 R_1^{-\frac{1}{2}} \varphi_{2i+1,m}. \tag{47}$$

Through direct calculation,

$$\int_{-T}^{T} \exp\left(-\frac{|s-t|}{T}\right) \sin \theta_i s \, ds + T \sin \theta_i T \left[\exp\left(-\frac{T-t}{T}\right) - \exp\left(-\frac{T+t}{T}\right)\right] = \frac{2T}{1 + \theta_i^2 T^2} \sin \theta_i t.$$

Hence, from (37) and (46),

$$\lambda_{2i+1}(R_1^{\frac{1}{2}} \varphi_{2i+1})(t) = d_i \theta_i^2 T^2 \left[\int_{-T}^{T} \exp\left(-\frac{|s-t|}{T}\right) \sin \theta_i s \, ds + T \sin \theta_i T \left[\exp\left(-\frac{T-t}{T}\right) - \exp\left(-\frac{T+t}{T}\right)\right]\right].$$

On the other hand, from (45) and (41),

* Note φ_{2i} is an eigenfunction of $R_1^{-\frac{1}{2}} R_2 R_1^{-\frac{1}{2}}$ itself, without extension to the whole of $\mathfrak{L}_2$.

$$(R_2R_1^{-\frac{1}{2}}\varphi_{2i+1,2n+1})(t) = (R_2R_1^{-\frac{1}{2}}\varphi_{2i+1,2n+2})(t)$$
$$= d_i\theta_i^2T^2\sum_{j=0}^{n}(R_2f_{2j+1})(t)\left[\int_{-T}^{T}\sin\theta_i s\, f_{2j+1}(s)\, ds + 2T\sin\theta_i T\, f_{2j+1}(T)\right].$$

But, since

$$\int_{-T}^{T}\exp\left(-\frac{|s-t|}{T}\right)\sin\theta_i s\, ds = \text{l.i.m.}_{n\to\infty}\sum_{j=0}^{n}(R_2f_{2j+1})(t)\cdot\int_{-T}^{T}\sin\theta_i s\, f_{2j+1}(s)\, ds,$$

we only have to show

$$\exp\left(-\frac{T-t}{T}\right)-\exp\left(-\frac{T+t}{T}\right) = 2\lim_{n\to\infty}\sum_{j=0}^{n}f_{2j+1}(T)(R_2f_{2j+1})(t),$$

which is implied by (28).

Then, by following the argument after (28), (47) is proved.*

The second assertion of A.4.5 is valid in this case also, since $\{\varphi_k\}$ of this example forms an orthonormal basis.

REFERENCES

1. Loéve, M., *Probability Theory*, 2nd ed., Van Nostrand, Princeton, 1960, pp. 478–479.
2. Kadota, T. T., Optimum Reception of Binary Gaussian Signals, B.S.T.J., *43*, Nov., 1964, pp. 2767–2810.
3. Yaglom, A. M., *On the Equivalence and Perpendicularity of Two Gaussian Probability Measures in Function Space*, Proc. Symp. on Time Series Analysis, edited by M. Rosenblatt, John Wiley & Sons, New York, 1963, pp. 327–348.
4. Parzen, E., *Probability Density Functionals and Reproducing Kernel Hilbert Spaces*, Proc. Symp. on Time Series Analysis, edited by M. Rosenblatt, John Wiley & Sons, New York, 1963, pp. 155–169.
5. Root, W. L., *Singular Gaussian Measures in Detection Theory*, Proc. Symp. on Time Series Analysis, edited by M. Rosenblatt, John Wiley & Sons, New York, 1963, pp. 292–315.
6. Huang, R. Y. and Johnson, R. A., Information Capacity of Time-continuous Channels, IRE Trans. Inform. Theory, *IT-8*, No. 5, September, 1962, pp. 191–205.
7. Davenport, W. B. and Root, W. L., *Random Signals and Noise*, McGraw-Hill Book Co., Inc., New York, 1958, pp. 99–101.
8. Whittaker, E. T., and Watson, G. N., *A Course of Modern Analysis*, 4th ed., Cambridge University Press, London, 1962.

* One non-obvious fact needed here is that $\theta_iT > \pi j$, $j = 1, 2, \cdots$, which follows from (31).

Ideal MOS Curves for Silicon

By A. GOETZBERGER

(Manuscript received April 22, 1966)

*Ideal curves of MOS capacity and surface potential are computed for silicon with oxide thickness and doping as a parameter. High-frequency and low-frequency capacity curves are presented for the doping ranges between 1 × 10^{14} and 1 × 10^{17} cm^{-3} and SiO_2 thickness between 100 and 12000 Å. Additional curves give flatband capacitance, minimum capacitance and voltage of the minimum capacitance in the same ranges.**

Measurement of MOS (Metal-Oxide-Semiconductor) capacity vs voltage is a convenient and widely used technique for evaluation of the properties of semiconductor-insulator interfaces.[1,2,3] Most MOS-type measurements require comparison of the experimentally measured curve with the ideal curve. This is usually time consuming because the ideal curve is represented by rather complicated functions and has to be calculated for each value of silicon doping and oxide thickness separately.

The purpose of this work is to facilitate such evaluations by providing a collection of curves embracing all the practically important ranges.

Three sets of curves are furnished.

(*i*) Plots of differential capacity vs voltage with thickness as a parameter and P-doping density N_A varying from plot to plot. The capacity is normalized with respect to the oxide capacity C_{ox}. The dashed lines are the high-frequency branch of the curves.

(*ii*) A plot of surface potential ψ_s corresponding to each of the preceding curves vs applied voltage V. For definition of the surface potential see below.

(*iii*) A set of curves giving a survey of pertinent results of this calculation.

(a) Flatband capacity C_{FB} (defined as capacity for $\psi_s = 0$) vs oxide thickness with doping density as parameter.

(b) The minimum capacitance C_{min}/C_{ox} plotted in the same manner.

* Additional curves covering intermediate doping ranges of 2 × 10^{14} cm^{-3}, 5 × 10^{14}, etc., are available on request.

(c) Voltage at which the minimum capacitance occurs. This is the voltage difference between the point of flatband capacity and minimum capacity.

The entire calculation was done on the IBM 7094 computer. The low-frequency curves were computed for room temperature using the well-known[1,4,5,6] relations between capacitance, surface potential, and applied voltage. Pertinent constants used were: dielectric permittivity of silicon; $\varepsilon_{Si} = 1.06 \times 10^{-12}$ F/cm, dielectric permittivity of SiO_2 ; $\varepsilon_{ox} = 3.4 \times 10^{-13}$ F/cm. The calculation was carried out for p-type silicon and SiO_2 insulator, but the results can be adapted to n-type silicon and insulators other than SiO_2 . The conversion to n-type is achieved simply by changing the sign of the voltage axis, the conversion to other insulators requires scaling of the oxide thickness with the ratio of the dielectric constants of SiO_2 and other insulator

$$d_c = d_a \frac{\varepsilon_{ox}}{\varepsilon_D}$$

where d_c = thickness to be used in these curves, d_a = actual thickness, ε_D = dielectric permittivity of the new dielectric, $\varepsilon_{ox} = 3.4 \times 10^{-13}$ F/cm. Surface potential ψ_s as used here is defined as the amount of band bending from the bulk to the interface in volts. ψ_s is positive, when the bands are bent downwards from the flatband position. It should be noted that the origin of ψ_s is the flatband potential and that its distance from the band edges varies with doping.

The low-frequency curves were calculated under the assumption that minority carriers contribute fully to the capacity. For calculations of the high-frequency capacity, an approximation developed by Sah[7] was used. In this approximation, the space charge region is divided into three parts and their contribution to the capacity separately computed. The high-frequency inversion range was connected with the low-frequency curve by a smooth line.

The curves were computed for doping densities from 1×10^{14} to 5×10^{17} cm^{-3} and oxide thicknesses from 100 to 12000 Å.

For the higher doping ranges, the computation was terminated at an oxide thickness giving a minimum capacitance of about 0.9 of the oxide capacitance. In some of the curves at lower doping overlapping ranges of oxide thickness were plotted in separate graphs to prevent the curves from coming too close to each other. For instance, one plot contains oxide thicknesses 600 Å, 1000 Å, etc., the other 800 Å, 1200 Å, etc.

ACKNOWLEDGMENT

The help of R. S. Reichert with computer plotting routines is gratefully acknowledged.

REFERENCES

1. Lindner, R., Semiconductor Surface Varactor, B.S.T.J., *41*, May, 1962, p. 803.
2. Terman, L. M., Solid State Electronics, *5*, 1962, p. 285.
3. Grove, A. S., Deal, B. E., Snow, E. H., and Sah, C. T., Solid State Electronics, *8*, 1965, p. 145.
4. Garrett, C. G. B. and Brattain, W. H., Phys. Rev., *99*, 1955, p. 376.
5. Kingston, R. H. and Neustadter, S. F., J. Appl. Phys., *26*, 1955, p. 718.
6. Zaininger, K. H., Ph.D. Thesis, El. Eng. Dept., Princeton University, Princeton, New Jersey.
7. Sah, C. T., Solid-State Electronics Laboratory Tech. Report No. 1, El. Eng. Research Laboratories, University of Illinois, Urbana, Illinois, 1964.

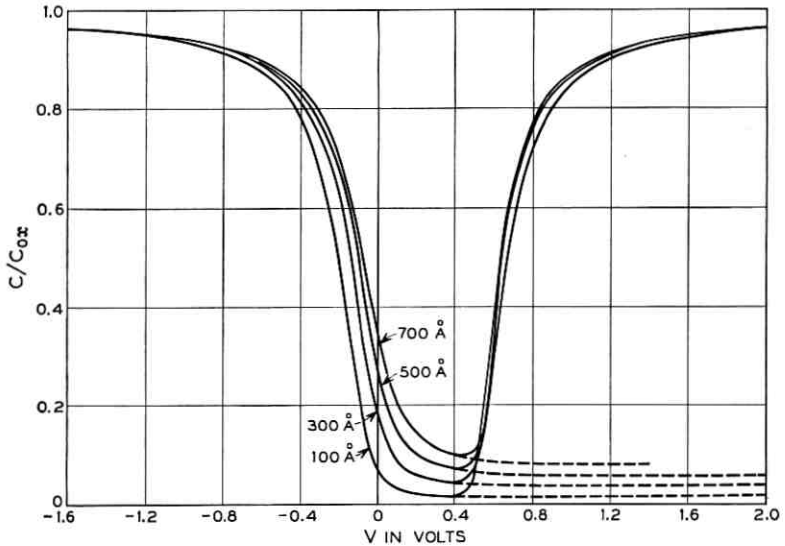

Fig. 1 — MOS capacity vs voltage. Oxide thickness 100–700 Å. ($N_A = 1.0 \times 10^{14}$ cm^{-3})

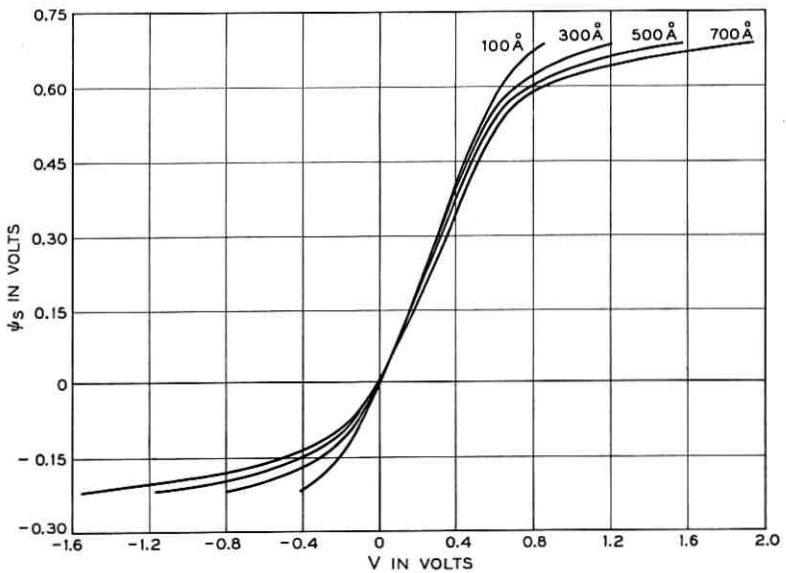

Fig. 2 — Surface potential vs voltage. Oxide thickness 100–700 Å. ($N_A = 1.0 \times 10^{14}$ cm^{-3})

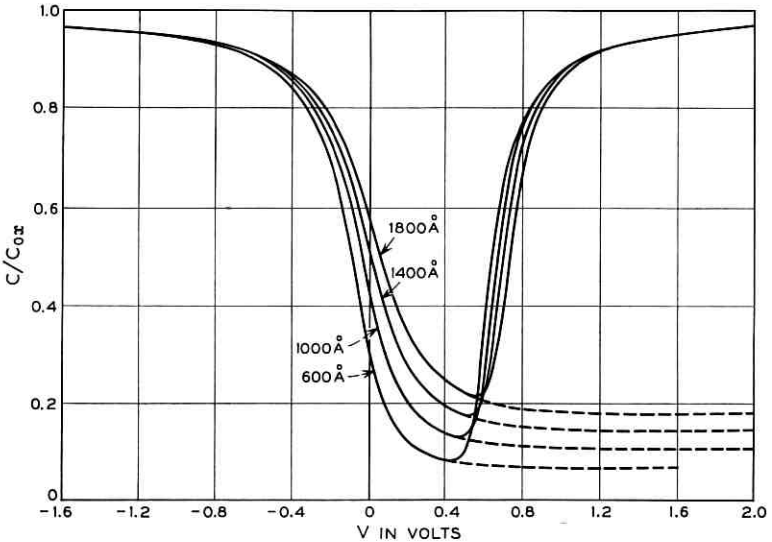

Fig. 3 — MOS capacity vs voltage. Oxide thickness 600–1800 Å. ($N_A = 1.0 \times 10^{14}$ cm^{-3})

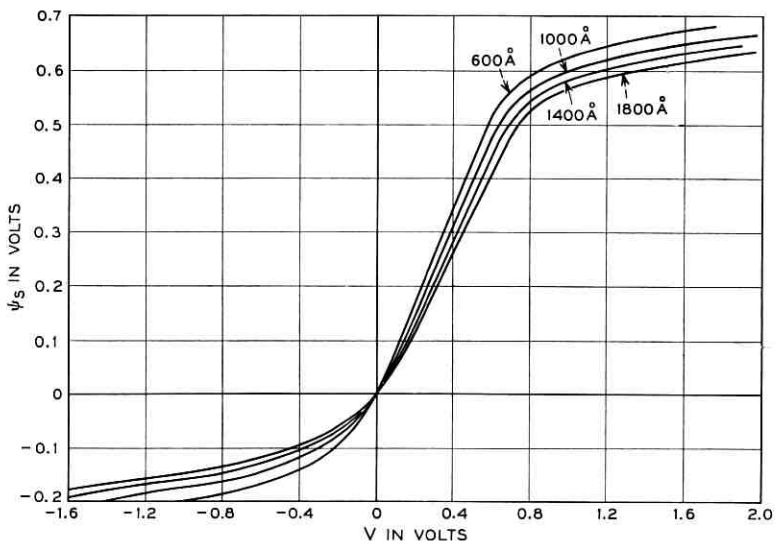

Fig. 4 — Surface potential vs voltage. Oxide thickness 600–1800 Å. ($N_A = 1.0 \times 10^{14}$ cm^{-3})

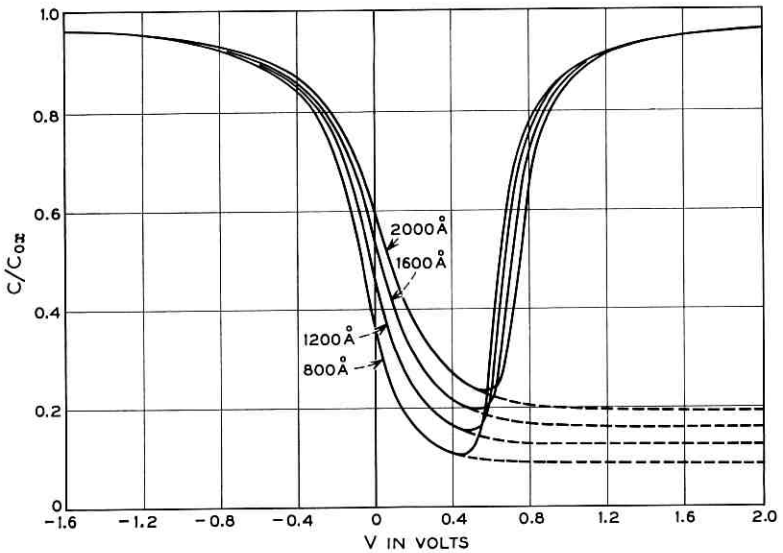

Fig. 5 — MOS capacity vs voltage. Oxide thickness 800–2000. Å ($N_A = 1.0 \times 10^{14}$ cm^{-3})

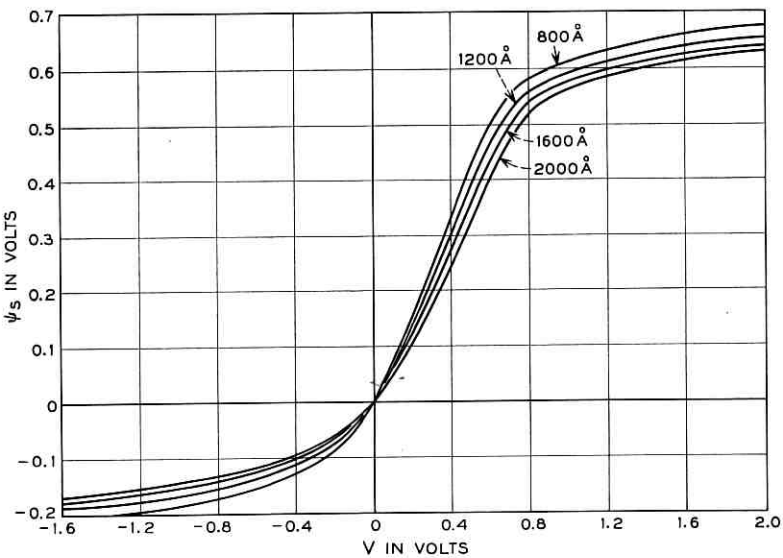

Fig. 6 — Surface potential vs voltage. Oxide thickness 800–2000 Å. ($N_A = 1.0 \times 10^{14}$ cm^{-3})

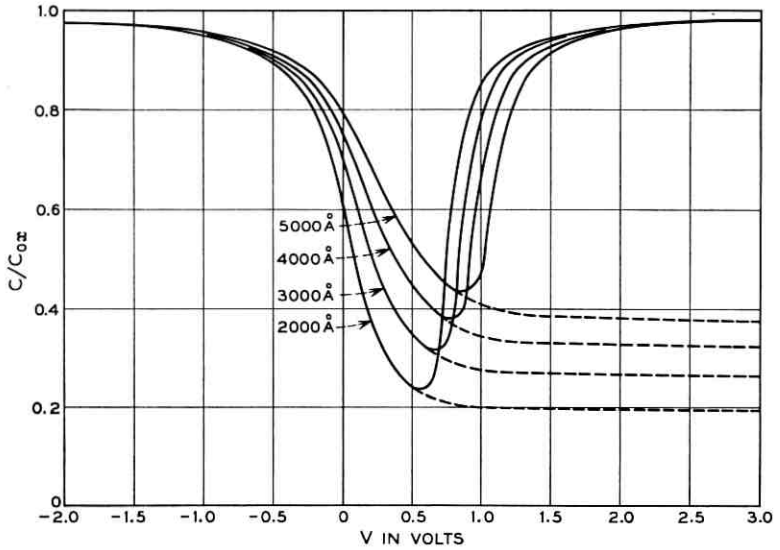

Fig. 7 — MOS capacity vs voltage. Oxide thickness 2000–5000 A. ($N_A = 1.0 \times 10^{14}$ cm^{-3})

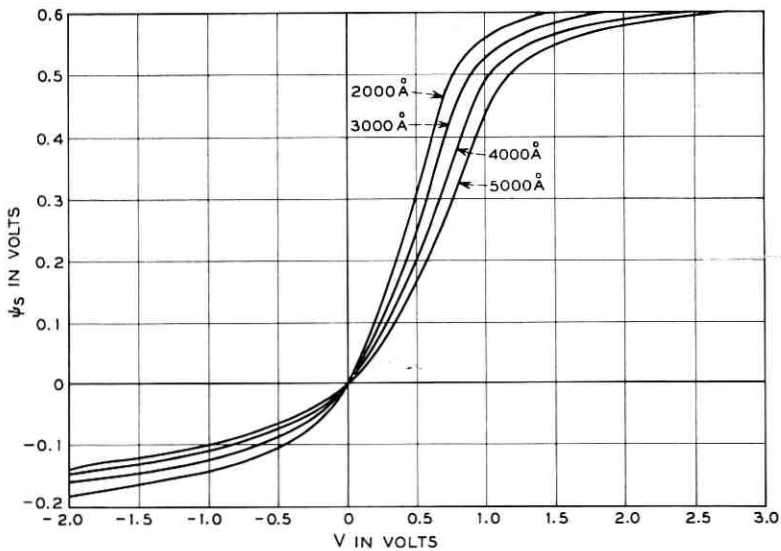

Fig. 8 — Surface potential vs voltage. Oxide thickness 2000–5000 A. ($N_A = 1.0 \times 10^{14}$ cm^{-3})

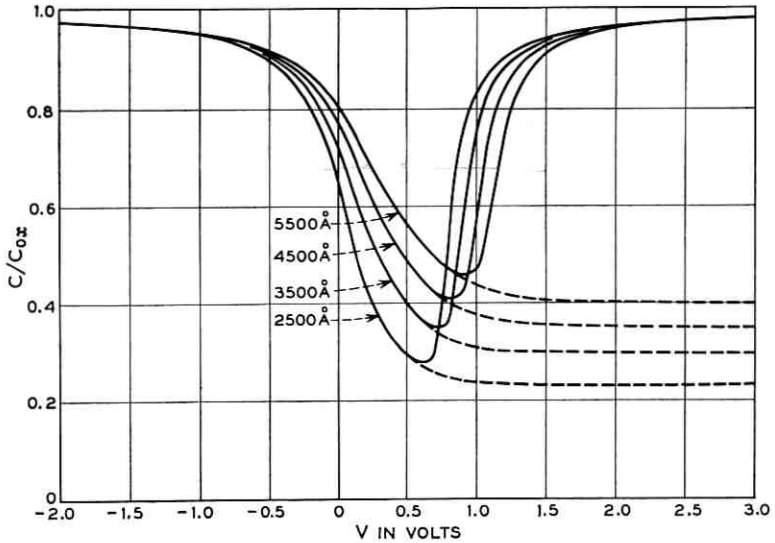

Fig. 9 — MOS capacity vs voltage. Oxide thickness 2500–5500 Å. ($N_A = 1.0 \times 10^{14}$ cm^{-3})

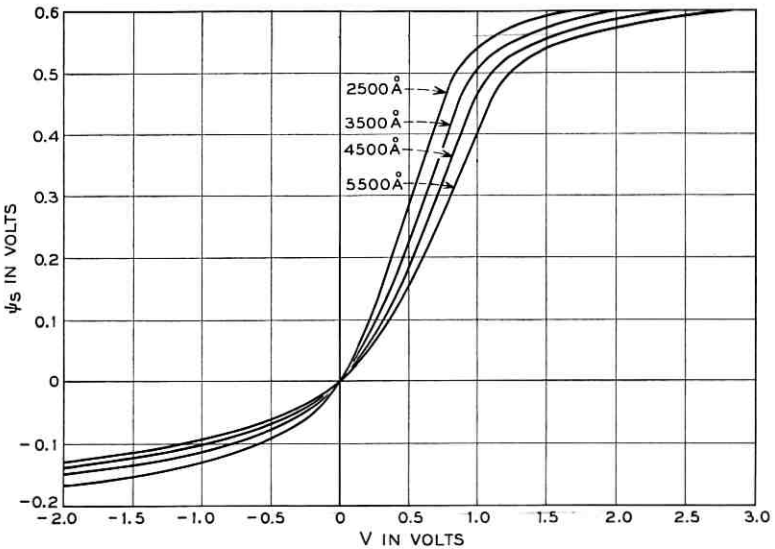

Fig. 10 — Surface potential vs voltage. Oxide thickness 2500–5500 A. ($N_A = 1.0 \times 10^{14}$ cm^{-3})

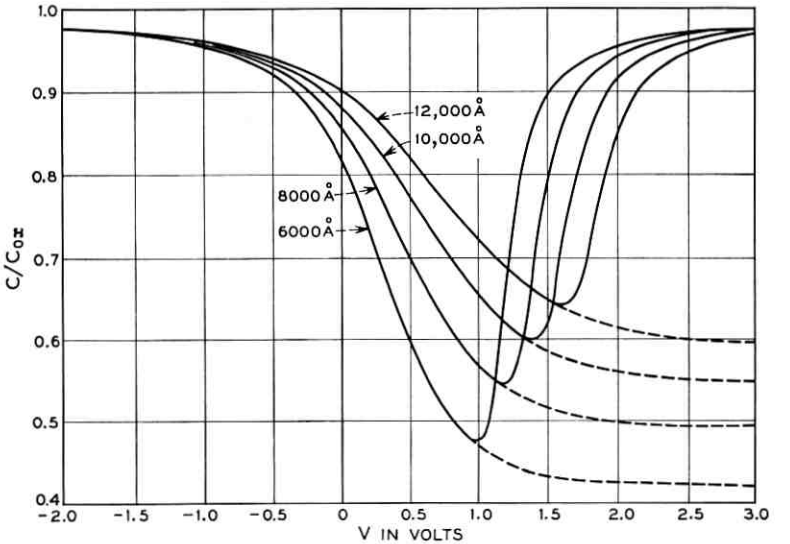

Fig. 11 — MOS capacity vs voltage. Oxide thickness 6000–12,000 A. (N_A = 1.0×10^{14} cm^{-3})

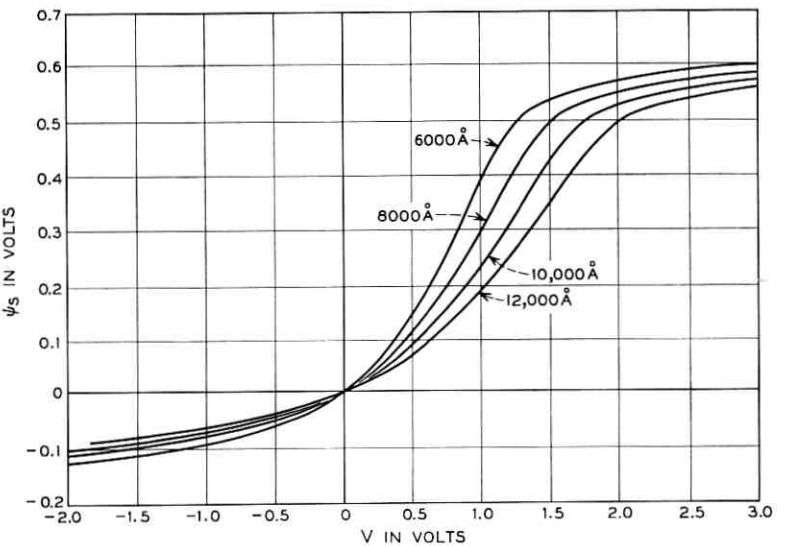

Fig. 12 — Surface potential vs voltage. Oxide thickness 6000–12,000 A. (N_A = 1.0×10^{14} cm^{-3})

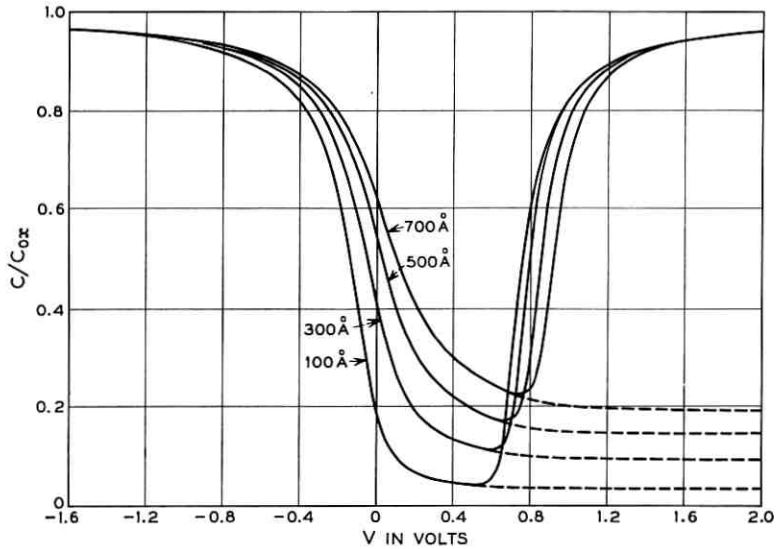

Fig. 13 — MOS capacity vs voltage. Oxide thickness 100–700 Å. ($N_A = 1.0 \times 10^{15}$ cm^{-3})

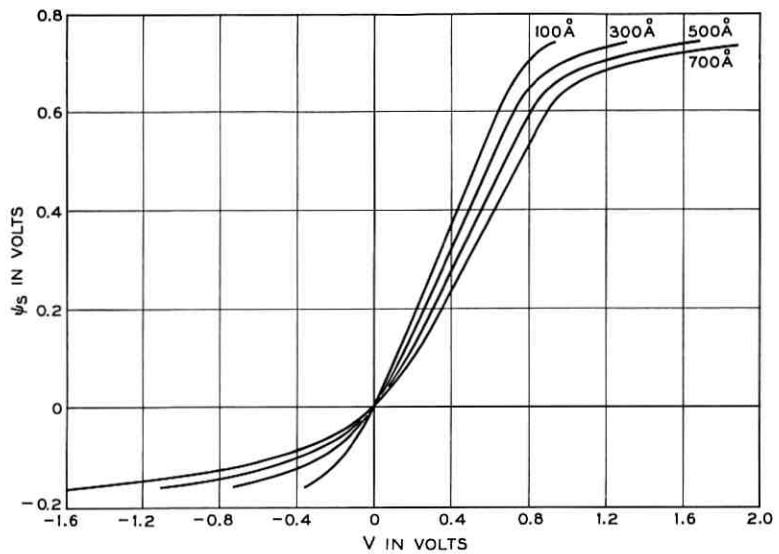

Fig. 14 — Surface potential vs voltage. Oxide thickness 100–700 A. ($N_A = 1.0 \times 10^{15}$ cm^{-3})

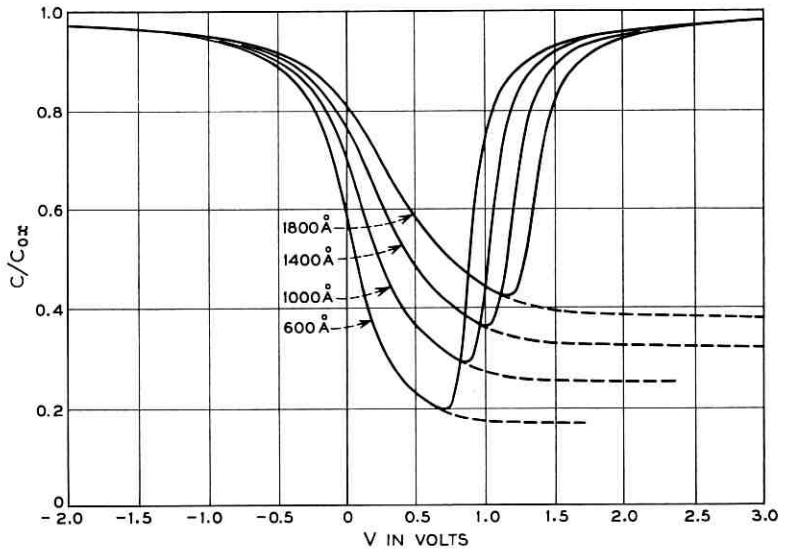

Fig. 15 — MOS capacity vs voltage. Oxide thickness 600–1800 Å. ($N_A = 1.0 \times 10^{15}$ cm^{-3})

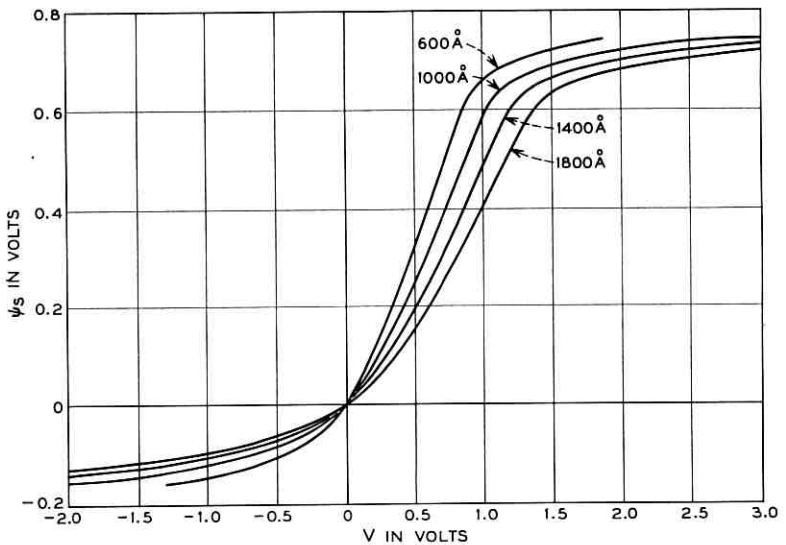

Fig. 16 — Surface potential vs voltage. Oxide thickness 600–1800 Å. ($N_A = 1.0 \times 10^{15}$ cm^{-3})

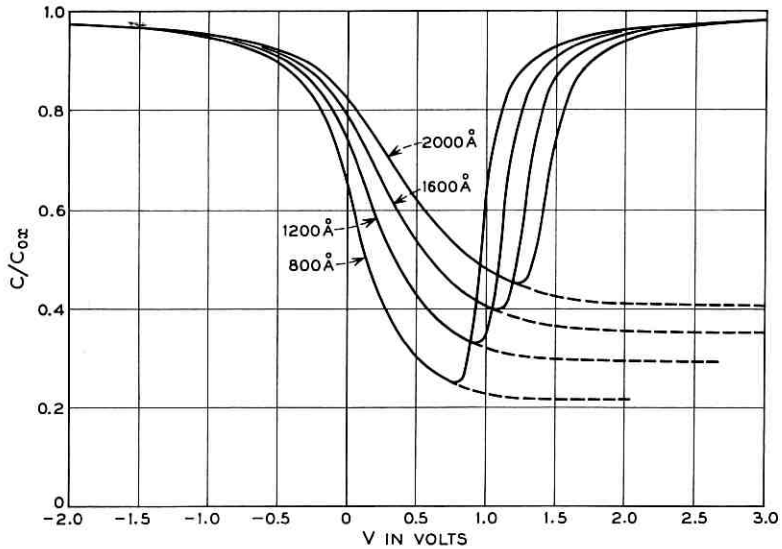

Fig. 17 — MOS capacity vs voltage. Oxide thickness 800–2000 Å. ($N_A = 1.0 \times 10^{15}$ cm^{-3})

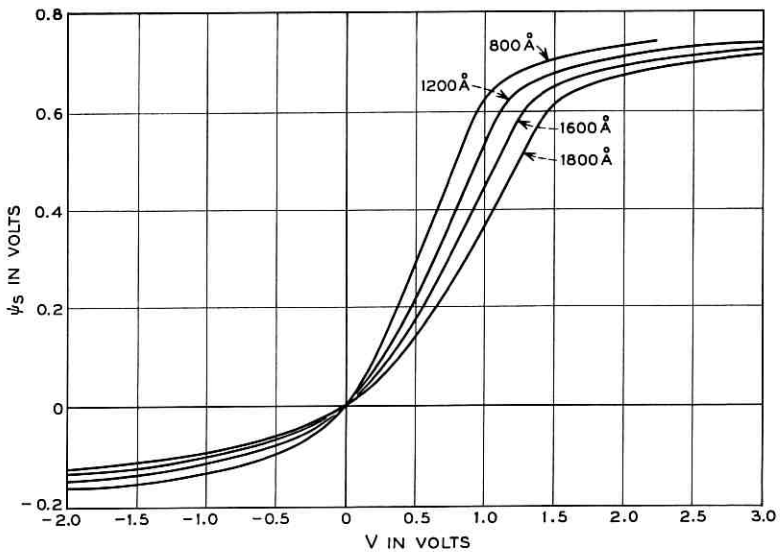

Fig. 18 — Surface potential vs voltage. Oxide thickness 800–2000 A. ($N_A = 1.0 \times 10^{15}$ cm^{-3})

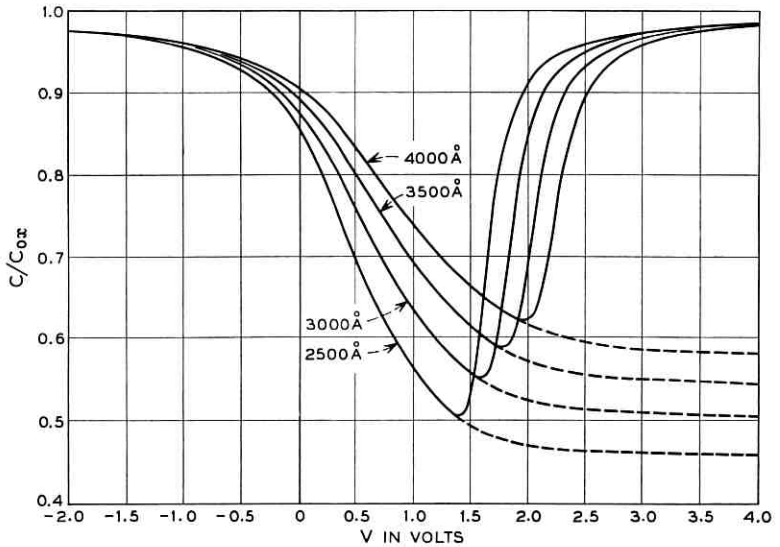

Fig. 19 — MOS capacity vs voltage. Oxide thickness 2500–4000 Å. ($N_A = 1.0 \times 10^{15}$ cm^{-3})

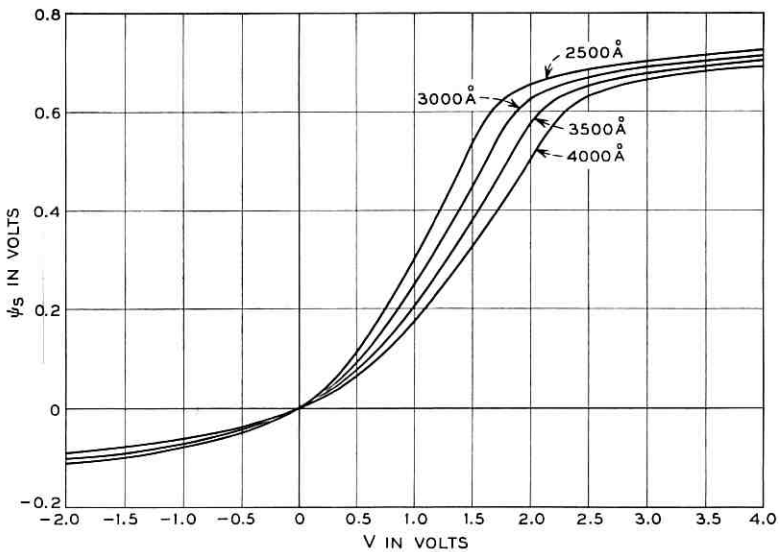

Fig. 20 — Surface potential vs voltage. Oxide thickness 2500–4000 Å. ($N_A = 1.0 \times 10^{15}$ cm^{-3})

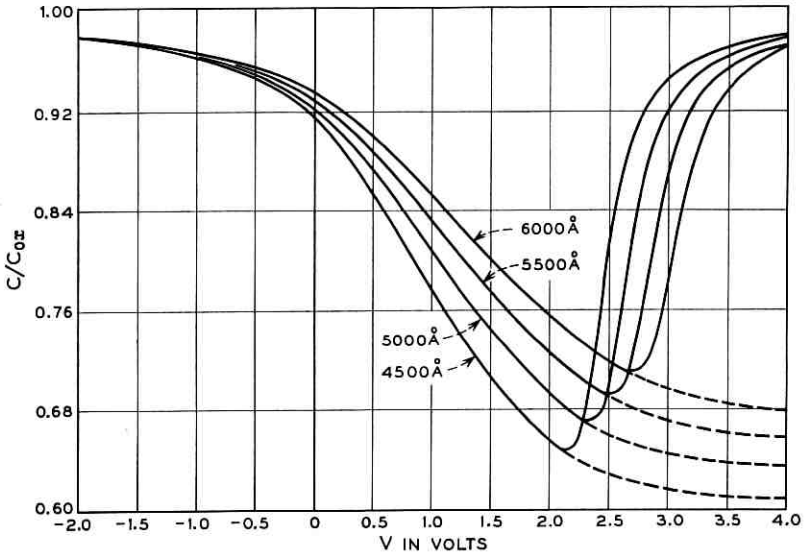

Fig. 21 — MOS capacity vs voltage. Oxide thickness 4500–6000 Å. ($N_A = 1.0 \times 10^{15}$ cm^{-3})

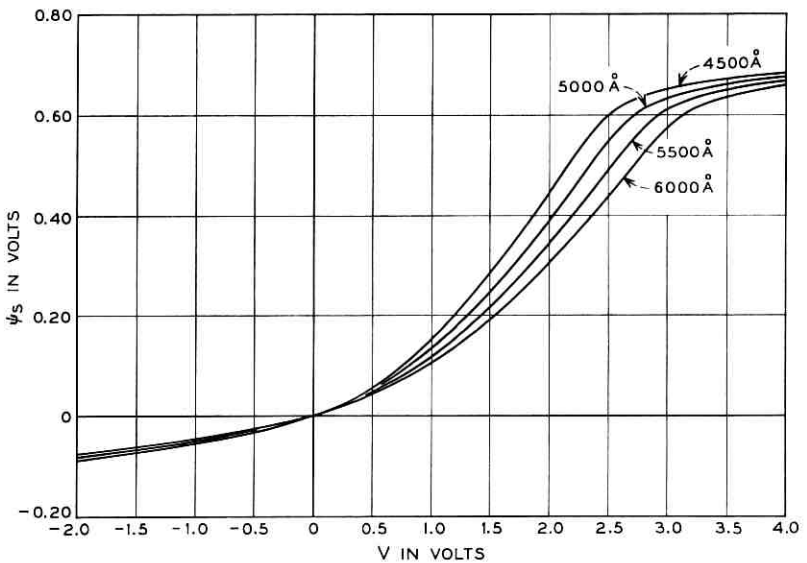

Fig. 22 — Surface potential vs voltage. Oxide thickness 4500–6000 Å. ($N_A = 1.0 \times 10^{15}$ cm^{-3})

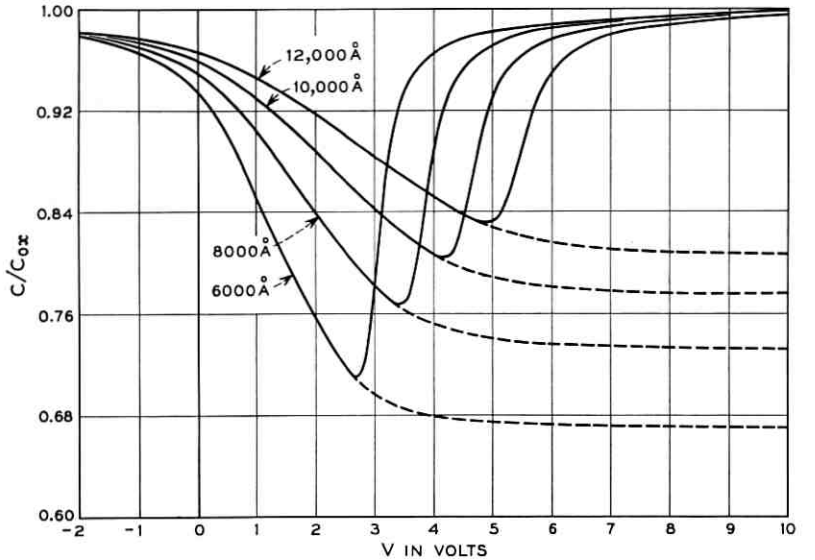

Fig. 23 — MOS capacity vs voltage. Oxide thickness 6000–12,000 Å. (N_A = 1.0×10^{15} cm^{-3})

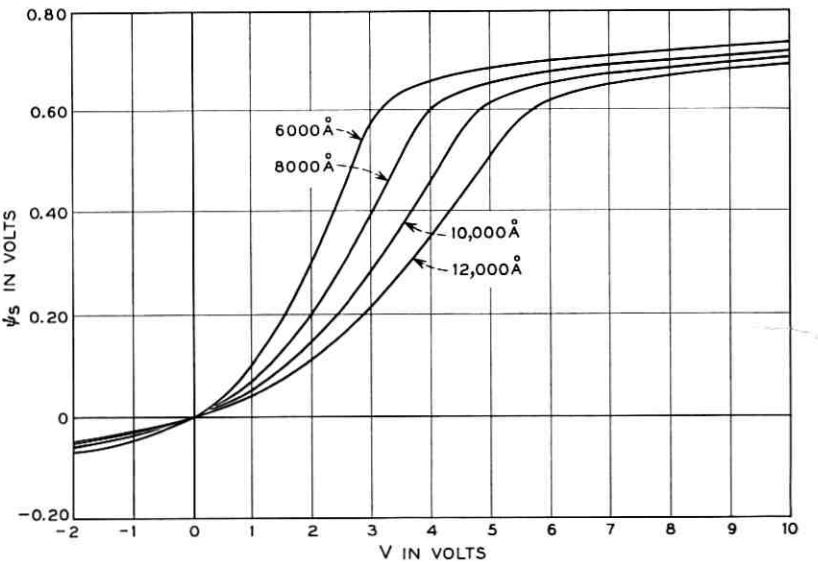

Fig. 24 — Surface potential vs voltage. Oxide thickness 6000–12,000 Å. (N_A = 1.0×10^{15} cm^{-3})

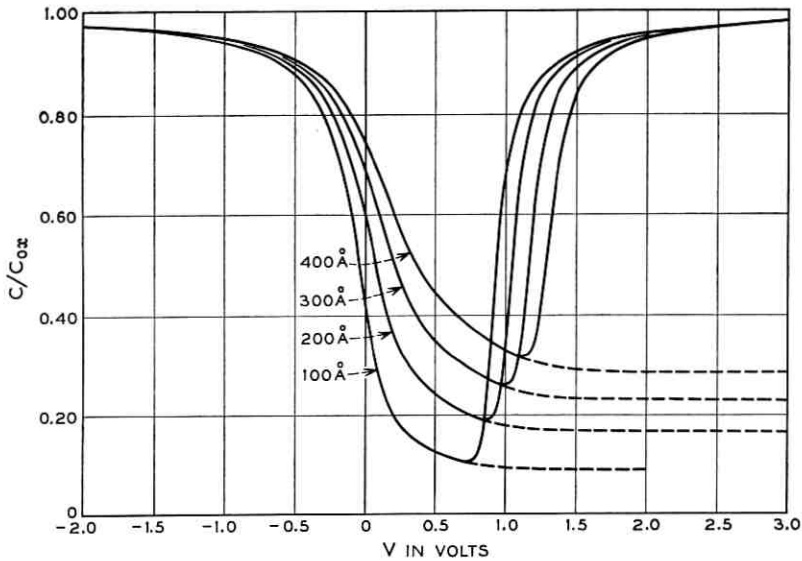

Fig. 25 — MOS capacity vs voltage. Oxide thickness 100–400 A. ($N_A = 1.0 \times 10^{16}$ cm^{-3})

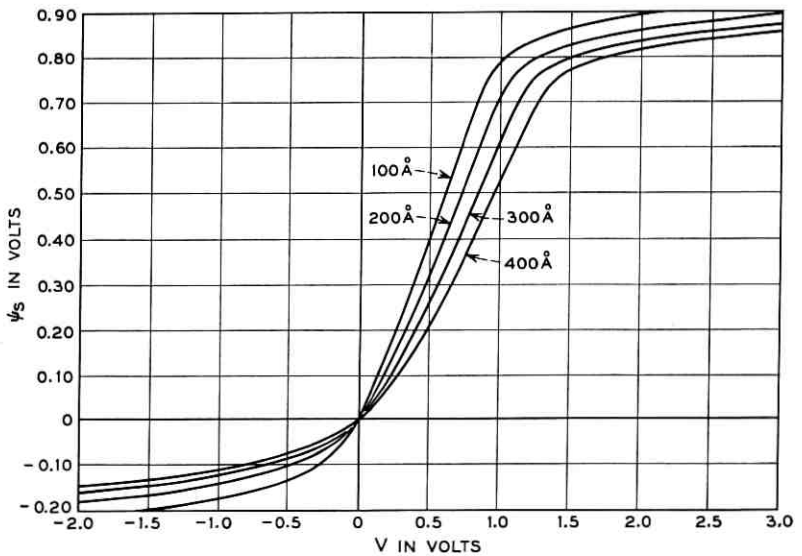

Fig. 26 — Surface potential vs voltage. Oxide thickness 100–400 A. ($N_A = 1.0 \times 10^{16}$ cm^{-3})

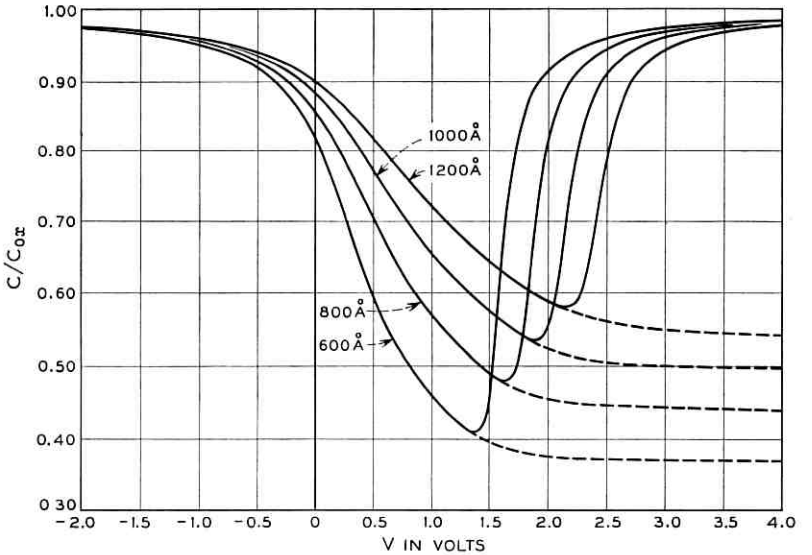

Fig. 27 — MOS capacity vs voltage. Oxide thickness 600–1200 A. ($N_A = 1.0 \times 10^{16}$ cm^{-3})

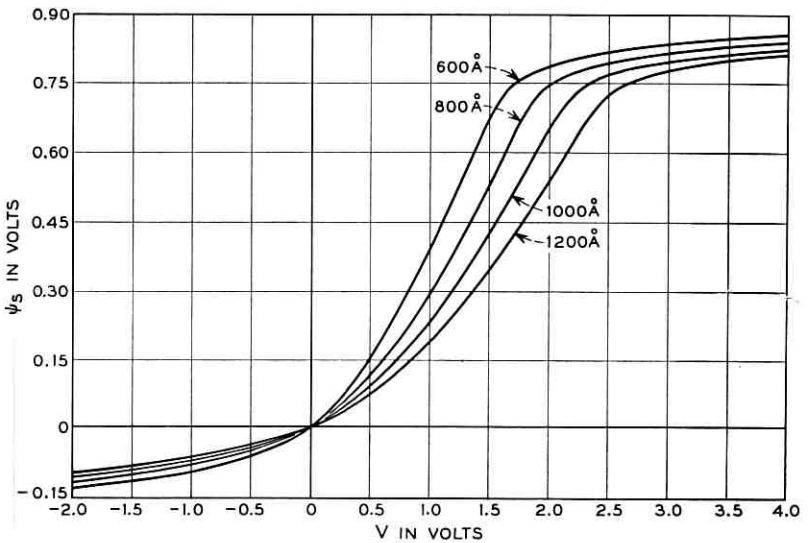

Fig. 28 — Surface potential vs voltage. Oxide thickness 600–1200 A. ($N_A = 1.0 \times 10^{16}$ cm^{-3})

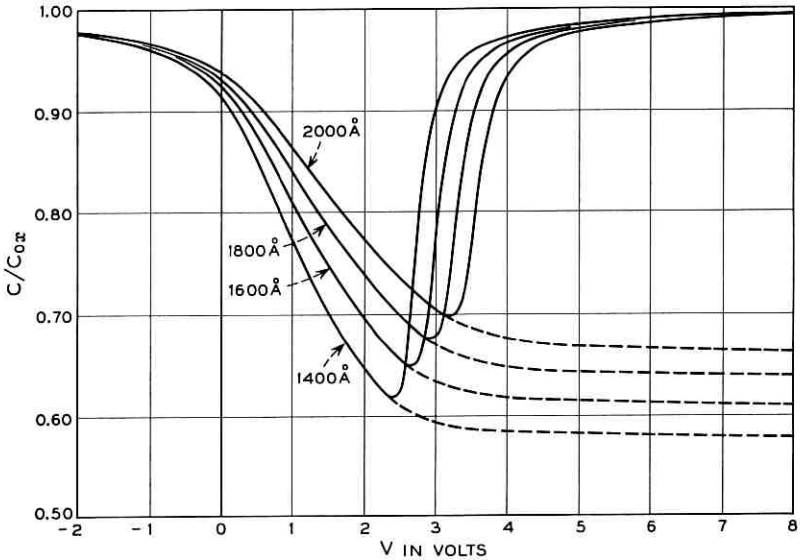

Fig. 29 — MOS capacity vs voltage. Oxide thickness 1400–2000 A. ($N_A = 1.0 \times 10^{16}$ cm^{-3})

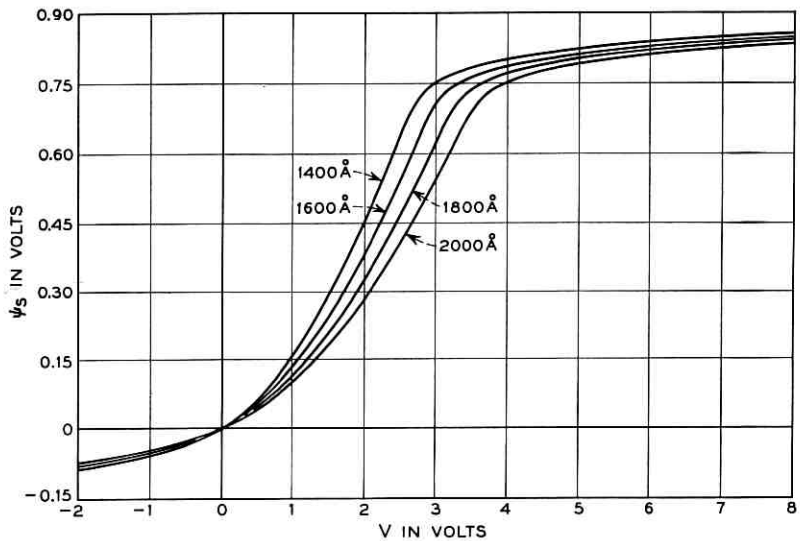

Fig. 30 — Surface potential vs voltage. Oxide thickness 1400–2000 A. ($N_A = 1.0 \times 10^{16}$ cm^{-3})

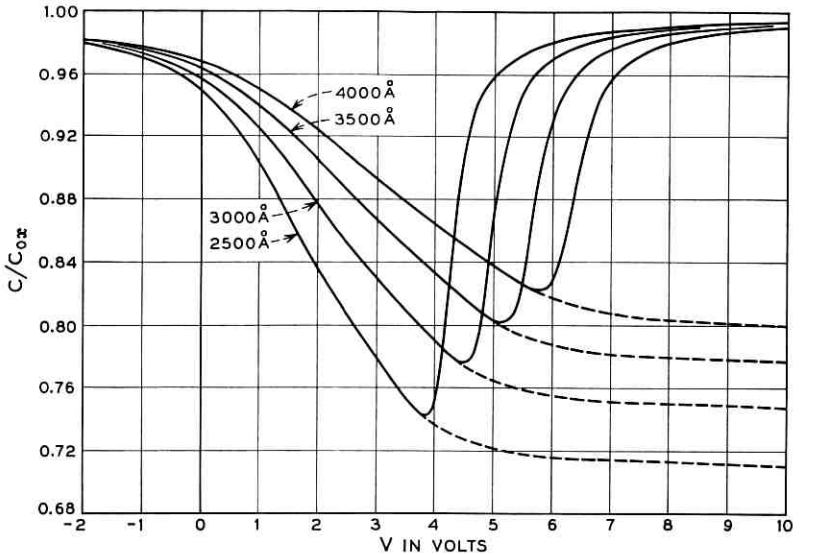

Fig. 31 — MOS capacity vs voltage. Oxide thickness 2500–4000 A. ($N_A = 1.0 \times 10^{16}$ cm^{-3})

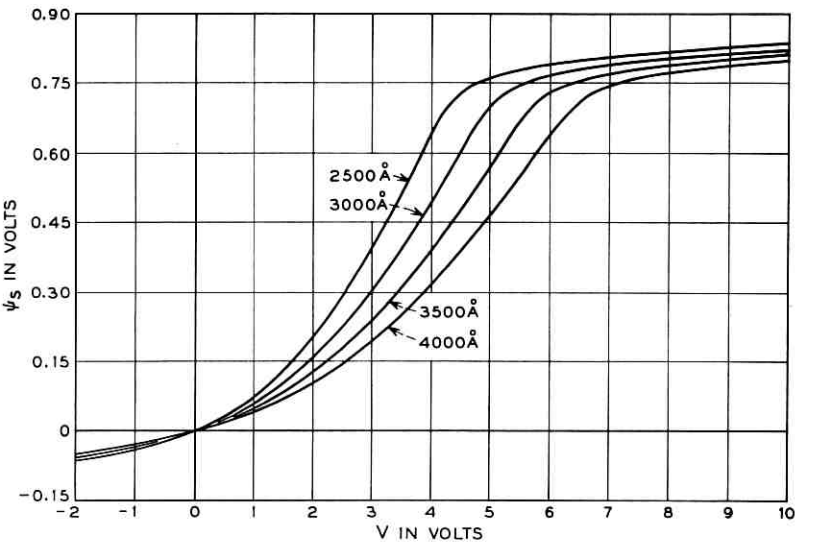

Fig. 32 — Surface potential vs voltage. Oxide thickness 2500–4000 Å. ($N_A = 1.0 \times 10^{16}$ cm^{-3})

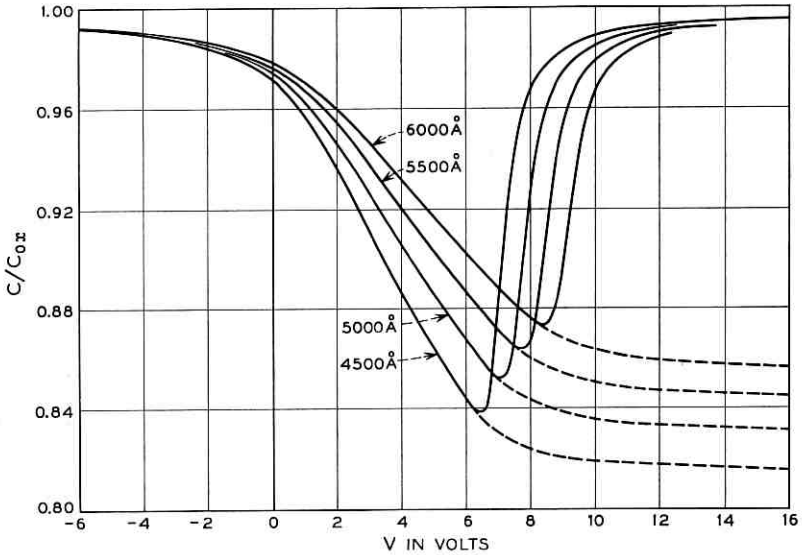

Fig. 33 — MOS capacity vs voltage. Oxide thickness 4500–6000 Å. ($N_A = 1.0 \times 10^{16}$ cm^{-3})

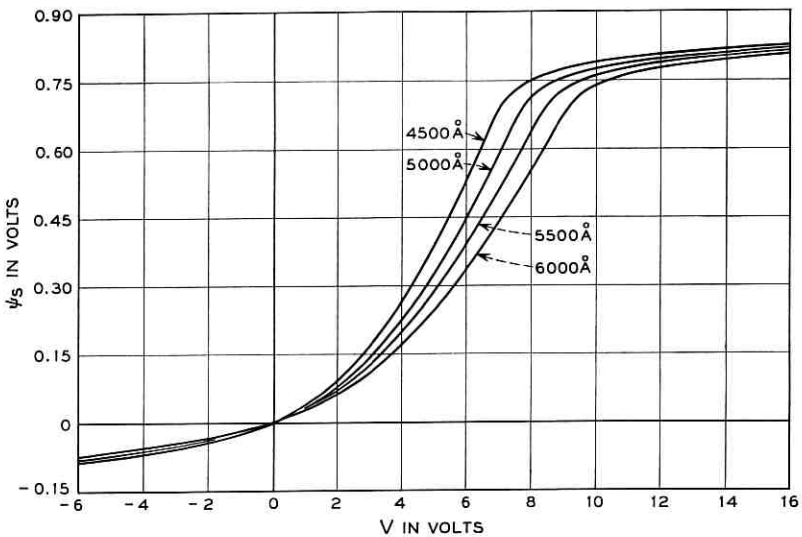

Fig. 34 — Surface potential vs voltage. Oxide thickness 4500–6000 Å. ($N_A = 1.0 \times 10^{16}$ cm^{-3})

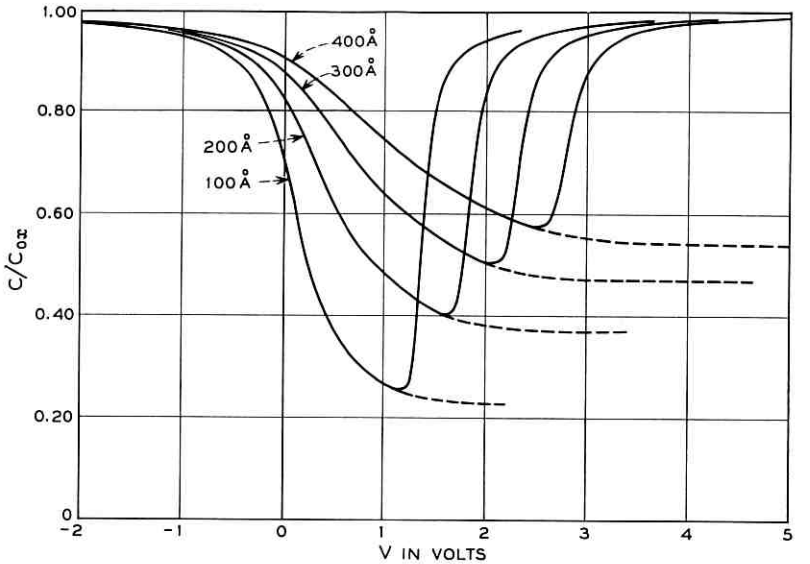

Fig. 35 — MOS capacity vs voltage. Oxide thickness 100–400 Å. ($N_A = 1.0 \times 10^{17}$ cm^{-3})

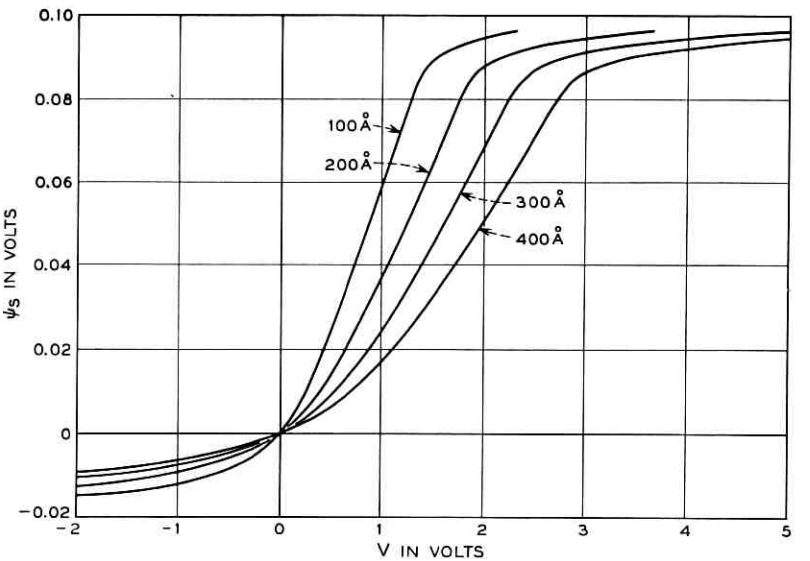

Fig. 36 — Surface potential vs voltage. Oxide thickness 100–400 Å. ($N_A = 1.0 \times 10^{17}$ cm^{-3})

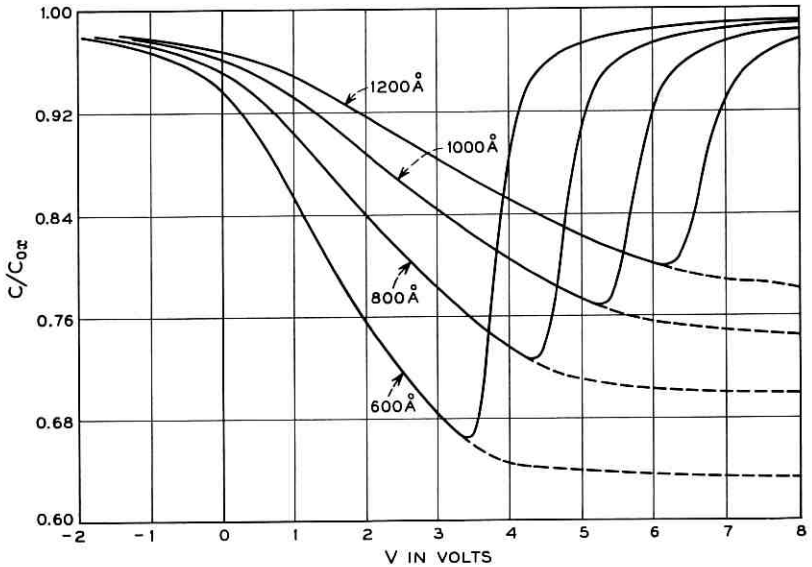

Fig. 37 — MOS capacity vs voltage. Oxide thickness 600–1200 Å. ($N_A = 1.0 \times 10^{17}$ cm^{-3})

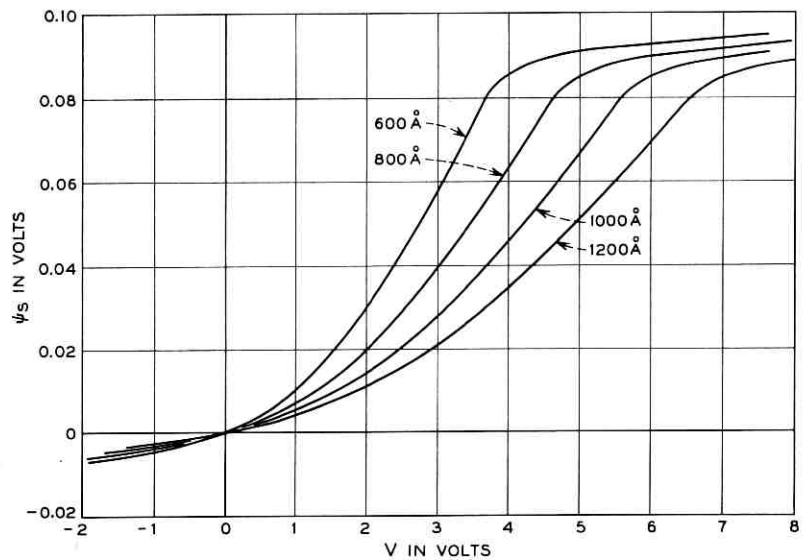

Fig. 38 — Surface potential vs voltage. Oxide thickness 600–1200 Å. ($N_A = 1.0 \times 10^{17}$ cm^{-3})

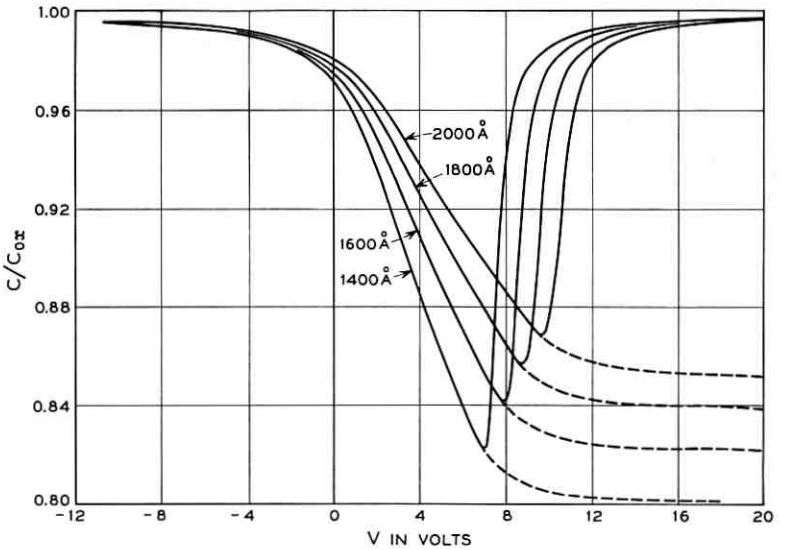

Fig. 39 — MOS capacity vs voltage. Oxide thickness 1400–2000 Å. ($N_A = 1.0 \times 10^{17}$ cm^{-3})

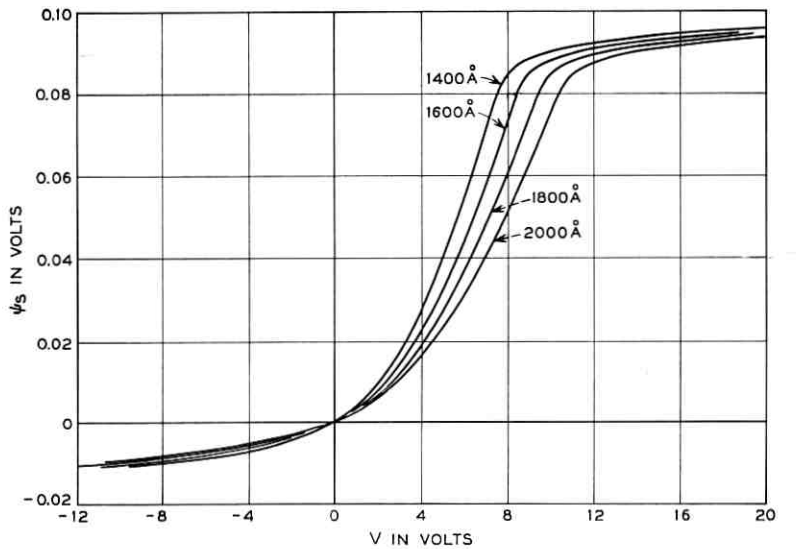

Fig. 40 — Surface potential vs voltage. Oxide thickness 1400–2000 Å. ($N_A = 1.0 \times 10^{17}$ cm^{-3})

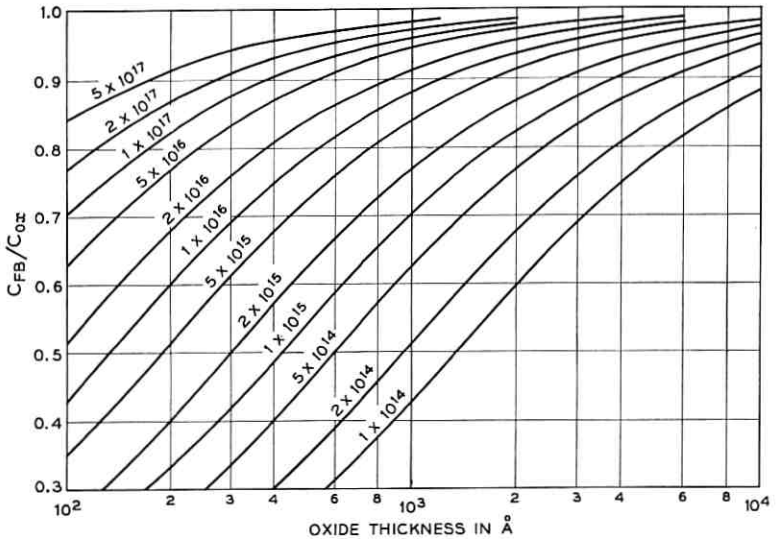

Fig. 41 — Flatband capacity vs oxide thickness I.

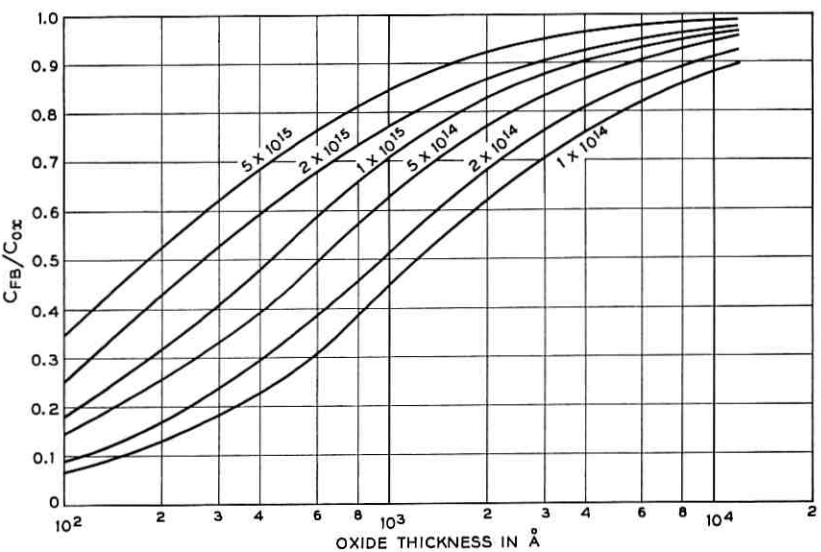

Fig. 42 — Flatband capacity vs oxide thickness II.

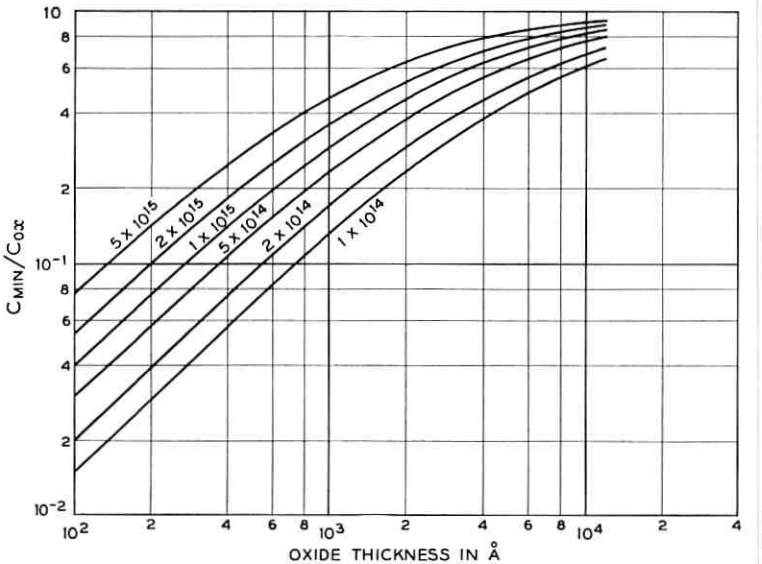

Fig. 43 — Minimum capacity vs oxide thickness. Doping density as parameter 1×10^{14}–5×10^{15} cm^{-3}.

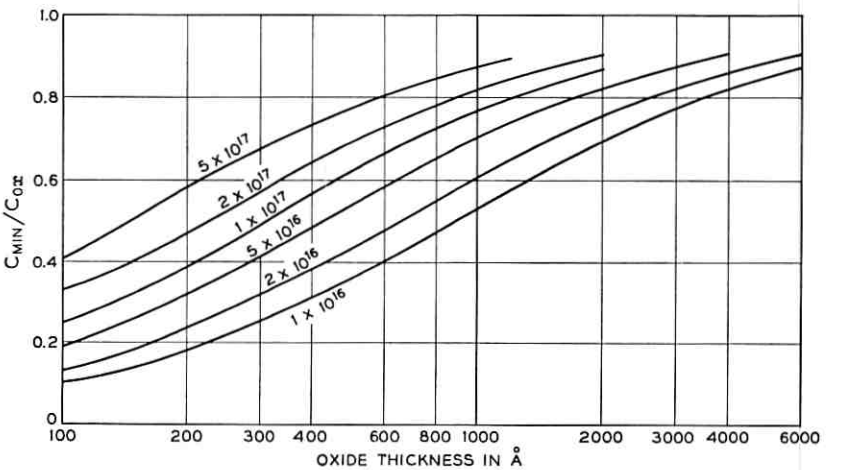

Fig. 44 — Minimum capacity vs oxide thickness. Doping density as parameter 1×10^{16}–5×10^{17} cm^{-3}.

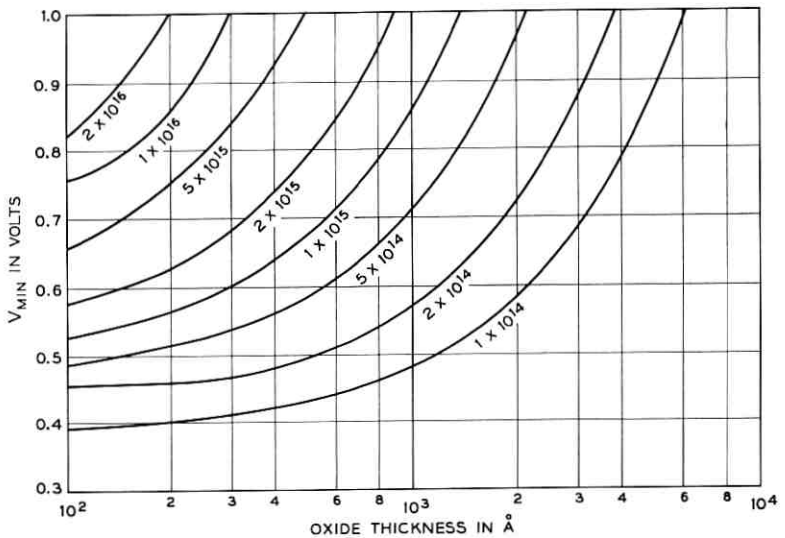

Fig. 45 — Voltage of cap. minimum vs oxide thickness. Doping density a parameter.

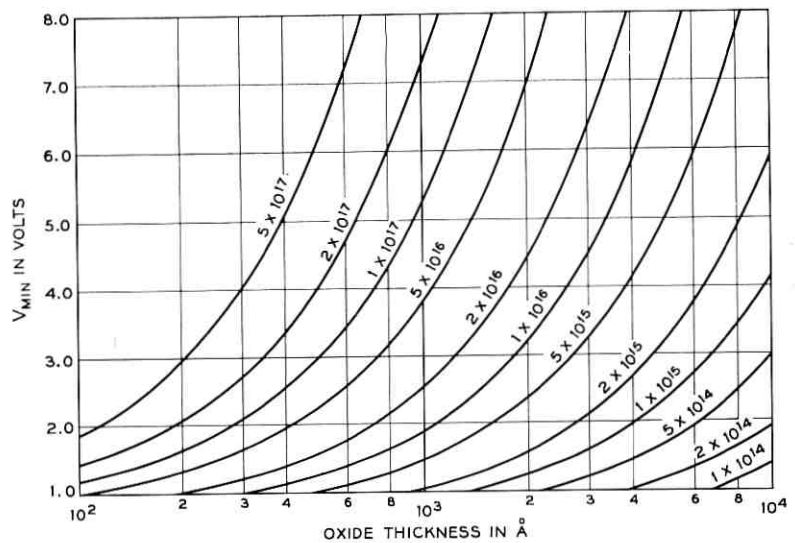

Fig. 46 — Voltage of cap. minimum vs oxide thickness. Doping density as parameter.

Signal-to-Noise and Idle Channel Performance of Differential Pulse Code Modulation Systems – Particular Applications to Voice Signals

By R. A. McDONALD

(Manuscript received April 25, 1966)

Analysis leading to a figure of merit for differential pulse code modulation (DPCM) systems with linear feedback networks is presented. It is shown that the figure of merit can be optimized. Simple DPCM has a 6-dB advantage in signal/quantizing noise ratio over pulse code modulation (PCM) for speech. Optimization yields at most 4 dB more. Computer simulation of the system using actual speech samples leads to data supporting the figure of merit as a useful measure of performance for DPCM systems with four digits or more. The simulation also provides data on the error spectrum as a function of quantizer loading and on the probability density of the quantizer input as a function of loading. Performance of the optimum system as a function of increasing feedback network complexity is also shown.

Idle channel performance of a particular system is analyzed, indicating the presence of inband oscillations in many cases. The best quantizer bias from the point of view of idle channel performance is found. The level of idle channel noise in DPCM is shown to be approximately equivalent to that in PCM.

I. INTRODUCTION

Digital techniques for transmitting analog signals such as voice, television, or facsimile have been known for a long time, and technology has reached the point where some of these methods are commercially feasible. Since cost is a critical factor in determining applicability of these systems, there has been from the beginning an attempt to improve the efficiency of analog-to-digital conversion by reducing the bit rate required for a given accuracy of reproduction. One of the principal methods involves removing inherent signal redundancy through the use

of feedback around the quantizer, and has led to a wide variety of schemes which may all be classed as differential systems. The origins of differential pulse code modulation (DPCM) stem from patents by the N. V. Phillips Company in 1951[1] and by C. C. Cutler in 1952.[2] The ideas also appear in several papers of about that time.[3,4,5] Since that time, considerable research and development work has been reported, and one has only to look at our reference list, which is certainly not complete, to be convinced that the problems have been examined at great length.

The work to be reported here is the result of a fairly extensive investigation of the potential advantages and pitfalls of voice transmission by practical DPCM systems and by alternatives which are essentially variations on the basic theme of PCM or DPCM. The problems are handled analytically as far as is possible. But rather than dilute the result by using an over-simplified model for the input signal, a computer simulation is used to advantage in more than one place. Optimum as well as simple suboptimum systems are considered.

Some of the analysis reported here is applicable to systems other than ones for voice transmission, but the one application is considered throughout since it provided the motivation for the entire project. A similar project was carried out independently by J. B. O'Neal[6] of Bell Telephone Laboratories, but with special consideration given to television signals. The special considerations introduced by the speech signal include the need to investigate performance for a wide range of input signal levels and a need to investigate idle channel performance.

There is considerable overlap with the work of Nitadori.[7] The work in Sections III, IV, and V was influenced heavily by his original work, but is based on broader assumptions. The validity of our assumptions is checked by means of the computer simulation described in Section VI. This simulation may also be construed as a check on the assumptions used by Nitadori and others. Our optimum linear network is developed from a viewpoint different from that of Nitadori.

The analytical results are also essentially parallel to those of Oliver[8] although his work is not directly applicable to the differential systems investigated here.

II. SYSTEM DESCRIPTION

The pulse code modulation (PCM) system shown in Fig. 1 will serve as the basis of comparison for all the others. The input and output shown are sequences of samples, since all the systems under consideration will require sampling. In the PCM system, one high-speed quantizer and

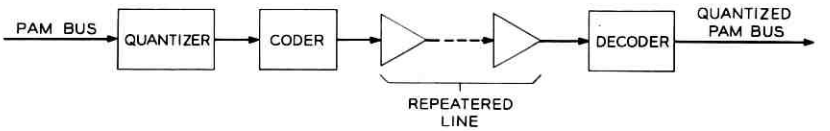

Fig. 1 — Basic PCM system.

coder can be shared among many channels by time division multiplexing the pulses representing the analog samples. There will be greater difficulty multiplexing the inputs to the differential systems, thereby introducing higher costs associated with the terminal portion of the system. It is this fact which controls the economics of the system. If, under an equiperformance criterion, the differential system requires fewer digits per unit time on the transmission portion of the system, but requires a more expensive terminal, there will be a net advantage whenever the repeatered line costs are a large enough portion of the total costs (i.e., long haul systems). It will be assumed throughout the paper that the controlling source of impairment is the quantization noise introduced by the quantizer with a finite number of steps of finite size. The overload noise is hence included here. The measure of performance will be the ratio of the mean squared signal to mean squared noise, or in the case of the idle channel, the mean squared noise alone.

The basic DPCM system which we shall consider is shown in Fig. 2. Without going into the details of operation of the system at this point, we note that the diagram actually represents a wide class of systems, different members of which are obtained with different prediction networks. In actual fact, we shall be restricted in our investigations to linear prediction networks, but this still leaves a rather broad class of systems.

The configuration of Fig. 2 bears a resemblance to several somewhat different systems described in the literature. We refer particularly to the work of Kimme,[9] Kimme and Kuo,[10] and of Spang and Schultheiss.[11]

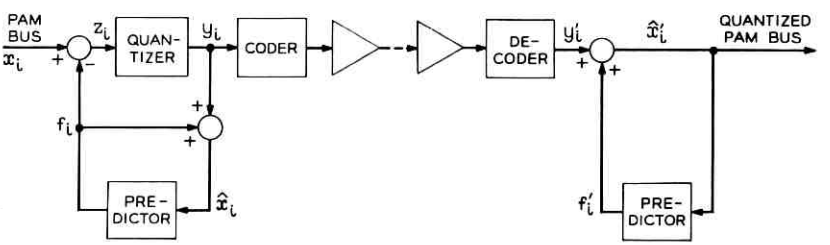

Fig. 2 — Basic DPCM system.

These systems involve quantization noise feedback rather than predictive feedback, and are thought of as shaping the spectrum of the noise rather than removing signal redundancy. It has been shown by Kimme[9] that there is an equivalence between a noise feedback system with predistortion and post-distortion filters and a DPCM system with predistortion and post-distortion filters. That is, given one configuration, there is a transformation which yields transfer functions for the blocks of the other configuration such that the performances are identical. However, we have found the predictive feedback point of view useful in its own right.

III. SIGNAL-TO-NOISE RATIO IMPROVEMENT

Notation needed for the algebraic analysis of DPCM appears in Fig. 2. A stochastic model is assumed for the speech samples, x_i, with a symmetrical zero-mean distribution not dependent on i. The primed quantities on the receiving end differ from the unprimed quantities only when the repeatered line introduces digital errors. For the most part, we shall ignore digital errors, and deal only with the unprimed quantities.

First, the quantizing error is defined as

$$e_i = z_i - y_i. \tag{1}$$

Note that in (1) and in the equations to follow, the index i, which denotes the time order of the samples, decreases to indicate samples further in the past. Unless otherwise stated, it is meant that the equations hold for all integers i.

The other fundamental relationships indicated by the block diagram are

$$z_i = x_i - f_i \tag{2}$$

$$\hat{x}_i = f_i + y_i \tag{3}$$

$$f_i = \sum_{j=1}^{\infty} h_j \hat{x}_{i-j}, \tag{4}$$

where the coefficients h_j are characteristics of the prediction filter. Note that in the last equation only the samples of the output of the assumed linear filter are indicated. This filter may have a continuous time response so long as the samples conform to (4). The absence of an h_0 term in (4) implies the presence of some delay around the loop.

Substitution of (2) and (3) into (1) gives

$$e_i = x_i - \hat{x}_i. \tag{5}$$

Comparison of (1) and (5) indicates a very important point about DPCM. The quantizing error samples, as defined in (1) are identical to the error samples for the overall system, in the absence of digital transmission errors. When quantizing is relatively fine, the successive quantizing error samples are statistically uncorrelated to a good approximation. Therefore, the signal reconstructed from the error samples has a power spectral density which is flat to a good approximation, as in PCM. According to (5), these same statements also hold for the overall system. There is no contradiction here, because e_i in $\hat{x}_i$ is not simply the response of a linear network to the error e_i in y_i. In fact, the feedback introduces error terms in z_i, and these combine with the quantizing error to produce the total error in $\hat{x}_i$. The flat spectrum does not hold for coarse quantization nor when the probability of overload is high. In these cases, neither the PCM nor the DPCM error spectrum would be flat, in general, nor would the two spectra be the same. The spectrum of error which results is discussed in detail later, and is determined by a computer simulation in Section VI.

In order to determine properties of the quantizing error, e_i, it is necessary to determine properties of the quantizer input, z_i. Substitution of (4) and (5) into (2) yield an equation for z_i

$$z_i = x_i - \sum_{j=1}^{\infty} h_j x_{i-j} + \sum_{j=1}^{\infty} h_j e_{i-j} . \tag{6}$$

It is obvious that even if the last term in (6) were neglected, the statistical properties of z_i, and in particular the probability density, depend on joint statistics of the input and past samples of the input. In the case of voice transmission, there exists empirical data on the probability density[12] and spectrum[13,14] of speech signals, but a good model for even the joint statistics of a pair of samples is not known to the author.

At this point, let us discuss the properties of e_i which it is desired to find. The spectral properties of e_i are already known, as mentioned earlier, provided relatively fine quantizing with low overload probability nolds. The probability density of e_i is not considered important, since there is no evidence to indicate a strong dependence of subjective quality on this property. But the most often needed property is the variance of e_i. A well-known[15,16] expression for the error variance of an L step quantizer is in terms of the probabilities of the various quantizer steps, p_{zj}, and the step sizes, Δ_j.

$$E\{e_i^2\} \mid_{\text{DPCM}} = \sum_{j=1}^{L} p_{zj} \frac{\Delta_j^2}{12} . \tag{7}$$

To emphasize the dependence of the step probabilities on the input variable statistics, we use the input variable as a subscript in addition to the step index. This expression is approximate since among other things overload is neglected, but it is most accurate for fine quantizing and low probability of overload. We are interested in comparing this with the quantizing noise in a PCM system with input x_i and step sizes Δ_j'. With the same type of notation the expression is

$$E\{e_i^2\} \mid_{\text{PCM}} = \sum_{j=1}^{L} p_{xj} \frac{\Delta_j'^2}{12}. \tag{8}$$

Although the ratio of the two quantities given by (7) and (8) is a complicated function of the probability densities of z and x, and also of the choice of step sizes, a rough understanding of what determines this ratio can be found in simpler terms. Suppose the step sizes Δ'_j are chosen to have a fixed ratio with the step sizes Δ_j; that ratio being the same as the ratio of the rms values of the two inputs. Then, to the extent that the probabilities p_{xj} and p_{zj} are the same, the variances of the errors will be in the same ratio as the variances of x and z. The probabilities in question will be the same if the probability densities of the normalized variables $x/\sqrt{\overline{x^2}}$ and $z/\sqrt{\overline{z^2}}$ are the same.

Whereas an analytic expression for the probability density of z cannot be derived without a model for the joint statistics of x, empirical evidence will be given later to show a strong similarity between the probability density of normalized speech, and that for normalized z in one important case. It is hence natural to use as a figure of merit the ratio of $\overline{x^2}$ to $\overline{z^2}$, which we shall refer to as SNR IMPROVEMENT.

$$\text{SNR IMPROVEMENT} \equiv \frac{E\{x_i^2\}}{E\{z_i^2\}}. \tag{9}$$

We now return to (6). Under the assumption of vanishingly small statistical correlation among the error samples, and between the error and the input signals, the variance of z_i may be written

$$E\{z_i^2\} = E\left\{\left(x_i - \sum_{j=1}^{\infty} h_j x_{i-j}\right)^2\right\} + E\{e_i^2\} \sum_{j=1}^{\infty} h_j^2. \tag{10}$$

It may be noted that the last term in (10) becomes a negligible fraction of the total for high enough signal-to-noise ratios. We note also that the figure of merit depends on the ability to predict x_i with a linear sum of past samples. In fact, we can optimize the figure of merit by choosing the h_j to be the optimum linear prediction coefficients in the sense of minimum mean square error (see Papoulis, Ref. 17). On the other hand, it

should be noted that the optimum coefficients provide a best match to a particular set of signal properties. But speech signal statistics are not constant from speaker to speaker, nor even for one speaker. Therefore, it is best to investigate as well some suboptimal systems with parameters not dependent on signal properties. We also note in passing, that adaptively controlled prediction coefficients might provide an even better solution to the problem. We do not treat the adaptive case in this paper.

IV. SIMPLE, NONOPTIMAL, DPCM

Historically, most of the investigations of predictive feedback systems have not included general feedback networks. One of the most common systems has an integrator or accumulator in the feedback path. That is,

$$h_1 = 1$$
$$h_j = 0 \qquad j \neq 1. \tag{11}$$

It is easy to show that in this case,

$$f_i = \sum_{j=1}^{\infty} y_{i-j} \tag{12}$$

and

$$z_i = x_i - x_{i-1} + e_{i-1}\,. \tag{13}$$

Then, by (10),

$$E\{z_i^2\} = E\{x_i^2\}\,[2(1 - \rho_1)] + E\{e_{i-1}^2\} \tag{14}$$

where

$$\rho_1 = \frac{E\{x_i x_{i-1}\}}{E\{i^2\}}\,.$$

Neglecting the last term in (14), the figure of merit becomes

$$\text{SNR IMPROVEMENT} \cong \frac{1}{2(1 - \rho_1)}\,. \tag{15}$$

Hence, the figure of merit is greater than unity whenever the normalized adjacent sample correlation of the input signal exceeds 0.5. This result is identical to results obtained by Oliver,[8] Nitadori,[7] and O'Neal,[6] although derived under different assumptions. Empirical work to demonstrate the validity of (15) will be shown in a later section.

This scheme has the advantage that there are no parameters dependent on signal statistics. On the other hand, performance does depend on

signal statistics. If ρ_1 drops below 0.5, the performance is actually worse than PCM. Another disadvantage to this system is that digital channel errors introduce a permanent change in the dc level of $\hat{x}_i'$. In fact, the dc level of $\hat{x}_i'$ will, in the presence of random channel errors, execute an unrestricted random walk until the output saturates. Further discussion of this problem will be found in the next section. In spite of these difficulties, this is the scheme most widely investigated in the literature. In fact, the computer simulation to be reported later will use this system.

V. OPTIMUM LINEAR FEEDBACK NETWORK

As was mentioned previously, the linear feedback coefficients h_j may be optimized in order to minimize the variance of z_i, thus maximizing the figure of merit given by (9). Note that our assumptions have been such as to eliminate the effect of the quantizer nonlinearity from the expressions, and that the solutions given here are optimum only for the cases where our assumptions hold. The problem is somewhat simplified by assuming that the sums in (10) terminate at $j = N$. Since the mutual information between samples usually becomes zero when the samples are remote from each other, the coefficients h_j will approach zero for large j. Therefore, the truncation at $j = N$ does not limit the applicability of the result in cases of interest. Differentiation of the right side of (10) with respect to the variables h_j, and setting the resulting expressions equal to zero gives the following set of linear algebraic equations.

$$\begin{aligned}
\rho_1 &= \left(1 + \frac{1}{K}\right)h_1 + h_2\rho_1 + h_3\rho_2 + \cdots + h_N\rho_{N-1} \\
\rho_2 &= h_1\rho_1 + \left(1 + \frac{1}{K}\right)h_2 + h_3\rho_1 + \cdots + h_N\rho_{N-2} \\
&\vdots \\
\rho_N &= h_1\rho_{N-1} + h_2\rho_{N-2} + h_3\rho_{N-3} + \cdots + \left(1 + \frac{1}{K}\right)h_N,
\end{aligned} \tag{16}$$

where

$$K = E\{x_i^2\}/E\{e_i^2\}$$

is the signal-to-noise ratio, assumed constant, and $\rho_j = E\{x_i x_{i-j}\}/E\{x_i^2\}$. With the exception of the coefficients on the principal diagonal, this is identical to the equations given by Papoulis[17] for determining the optimum linear prediction coefficients. By dividing each equation through by the coefficient on the principal diagonal, the equations are again nor-

malized, with new correlation coefficients. The problem is of course the classical Wiener-Kolmogorov prediction problem in discrete form.

For small N, the algebraic expressions for the solutions are easily obtained. For larger N, a computer solution is more suitable. These solutions may then be put back into the original expression for the error. It is easy to show[17] that the minimum variance of z_i may always be written in the form:

$$E\{z_i^2\}\,|_{\min} = E\{x_i^2\}\left[1 - \sum_{j=1}^{N} h_j\left(\rho_j \Big/ \left(1 + \frac{1}{K}\right)\right)\right]. \quad (17)$$

Hence, the optimum figure of merit becomes

$$\text{SNR IMPROVEMENT}\Big|_{\text{opt.}} = \frac{1}{1 - \sum_{j=1}^{N} h_j\left(\rho_j \Big/ \left(1 + \frac{1}{K}\right)\right)}. \quad (18)$$

It is clear that with fixed sampling rate the minimum error will either remain constant or be monotonically reduced for progressively larger N. That is, each sample further in the past can only add information on which to base a prediction. However, since speech is not perfectly predictable from past samples, it is to be expected that the minimum variance will approach a finite, nonzero, limit as N becomes large. A numerical example showing this relationship, with data from actual speech signals, is given later.

The stability of the closed loop which is present in the DPCM transmission terminal has not been studied in detail. However, the following reasoning clarifies the issue to some extent. Suppose the quantizer granularity is neglected, *i.e.*, assume $y_i \equiv z_i$. Then, using (2), (3), and (4), it is easy to show that

$$x_i \equiv \hat{x}_i$$

$$y_i = z_i = x_i - \sum_{j=1}^{\infty} h_j x_{i-j}.$$

Then the system is stable under a simple criterion requiring the sum of the magnitudes of the h_j's to be finite, and possibly under some weaker criteria. This simple case depends on a *precisely* unity gain amplifier in place of the quantizer. If the gain should remain linear but drift from unity, there exists a forward path from f_i to $\hat{x}_i$. If the gain of this path is sufficient, instability could result. If the granular characteristic of the quantizer is considered, it can be seen that oscillations are possible, in the manner of the bang-bang servo. Some of these cases are investigated

in Section VII. In the cases studied there, the oscillation is bounded, and this means stability in an operational sense.

Because the $N = 1$ case results in considerable simplification, it will be examined a little further. For this case,

$$h_1 = \rho_1 \Big/ \left(1 + \frac{1}{K}\right) \tag{19}$$

and the figure of merit becomes

$$\text{SNR IMPROVEMENT}\Big|_{N=1} = \frac{1}{1 - \left[\rho_1 \Big/ \left(1 + \frac{1}{K}\right)\right]^2}. \tag{20}$$

For large K this is approximately

$$\text{SNR IMPROVEMENT}\Big|_{N=1} \cong \frac{1}{1 - \rho_1^2}. \tag{21}$$

Comparison of (21) and (15) shows a slight advantage for the optimum case over the nonoptimum case, both using one past sample for prediction. Note also that the optimum case always holds an advantage over PCM whereas the nonoptimum case holds an advantage only when $\rho_1 > 0.5$. However, the optimum case requires a parameter adjusted to the assumed signal statistic ρ_1, whereas the nonoptimum case has no such parameters.

It should be noted that when $\rho_1 > 0$, the prediction network for the optimum case with $N = 1$ is merely an attenuation with delay. The overall response of the network from y_i to f_i is that of a "leaky" integrator with delay. This system is one that has been proposed as a means of reducing the problem created by digital channel errors. The effects of digital transmission errors decay exponentially. Hence, the system output does not execute an unrestricted random walk.

VI. COMPUTER SIMULATION — AN EXAMPLE

Because an adequate mathematical model for speech is not available, it was necessary to resort to simulation of the system on the computer, using as input digitized sampled speech, recorded on computer tape. The tape was kindly provided by J. F. Kaiser of Bell Telephone Laboratories. Measuring devices for probability density, variance, and autocorrelation were also simulated on the computer. Knowledge of the autocorrelation function alone is sufficient for evaluation of the figure of merit in each case. But statistics of the derived random variable z are

useful in checking the assumptions leading to our results. Autocorrelation of the quantizing error is also useful in checking our earlier assertions concerning error spectrum.

First, consider the properties of the signal contained on the input tape. The original digitization for computer purposes is linear quantizing with 11 digits. The quantizing error thereby incurred is ignored in further work because quantization introduced in the simulations is much more coarse than this. Table I(a) indicates the normalized autocorrelation of the samples. Note that sampling is at the rate of 9.6 kHz. The spectrum, constructed from this data using a hanning window,[18] is shown in Fig. 3(a) on linear coordinates.

Shown for comparison purposes in Fig. 3(b) is a spectrum constructed as follows. Speech spectra from Dunn and White[14] for men and women are averaged, and the sum multiplied by the attenuation characteristic of a local loop with a 500 telephone set.[19] Although the spectra in Figs. 3(a) and (b) are not precisely the same, the general characteristics are sufficiently close to ascertain the worth of the particular sample. It should be noted that the sample represents only 5 seconds of speech in real time, and cannot be expected to provide a representative average statistic with high precision. However, there is close enough agreement with published statistics to make our point.

Fig. 4 shows the probability density function of the speech samples normalized relative to their RMS value. This was drawn using data obtained by computer processing the input tape. The curve is shown only for positive values of the samples and actually represents an average of both halves of the data. Shown for purposes of comparison are the Laplacian distribution, often used as a speech model,[16] and the Gamma distribution proposed by Richards.[20] The presence of intersyllable and interword quiet time and the presence of low level unvoiced

TABLE I — AUTOCORRELATION COEFFICIENTS — ρ_N

N	(a) 9.6-kHz Samples	(b) 8.0-kHz Samples
0	1.0000	1.0000
1	0.9035	0.8644
2	0.6683	0.5570
3	0.3875	0.2274
4	0.1311	−0.0297
5	−0.0632	−0.1939
6	−0.1939	−0.2788
7	−0.2695	−0.3030
8	−0.3003	−0.2823
9	−0.2980	−0.2208
10	−0.2659	−0.1330

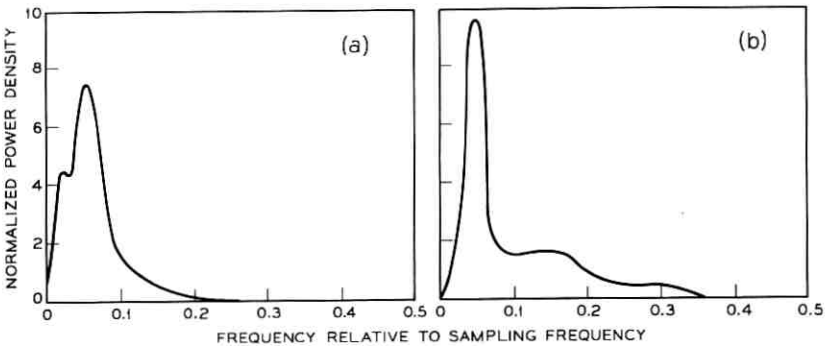

Fig. 3 — Speech spectra; (a) data used in simulation; (b) published data.

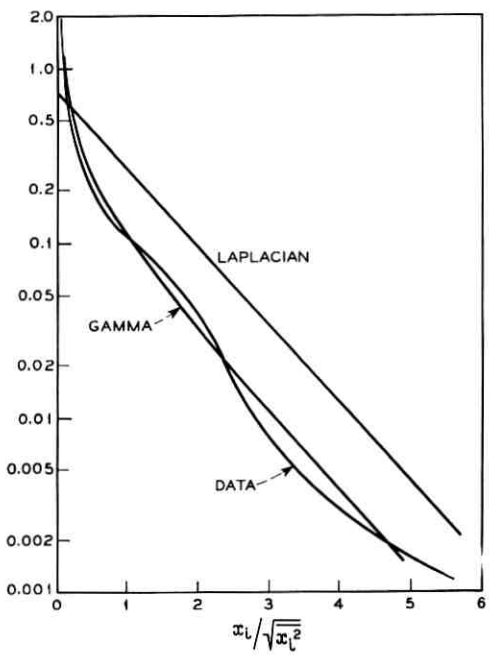

Fig. 4 — Normalized probability density of speech. Symmetrical average of "+" and "−" data.

consonant sounds account for the sharp spike at the origin. The general shape conforms reasonably well to data presented by Davenport.[12]

However, the main reason for using the speech samples is that the second-order statistics are supposed to be representative. It is necessary to take this on faith by extrapolating the favorable comparisons of the first-order statistics and the spectra.

The theory presented in Section IV predicts that the figure of merit for the simple, nonoptimal, DPCM is given by (15). Using ρ_1 from Table I(a), we get

$$10 \log_{10} (\text{SNR IMPROVEMENT}|_{9.6\ \text{kHz}}) = 7.14\ \text{dB}. \quad (22)$$

Under the assumptions developed in Section III, this is the amount by which the overall signal-to-noise ratio will be improved in comparison to PCM, with the same quantizer, comparably loaded.

In Fig. 5(a) are shown curves, determined by the simulation, of signal-to-noise ratio in dB versus input level for PCM and DPCM. The quantizers are 4 digit in each case, and have nonuniform steps conforming to the $\mu = 100$ logarithmic nonlinearity of Smith.[16] In both cases the 0 dB reference input level was determined by trial and error such that the total probability of the two largest quantizer output levels (plus and

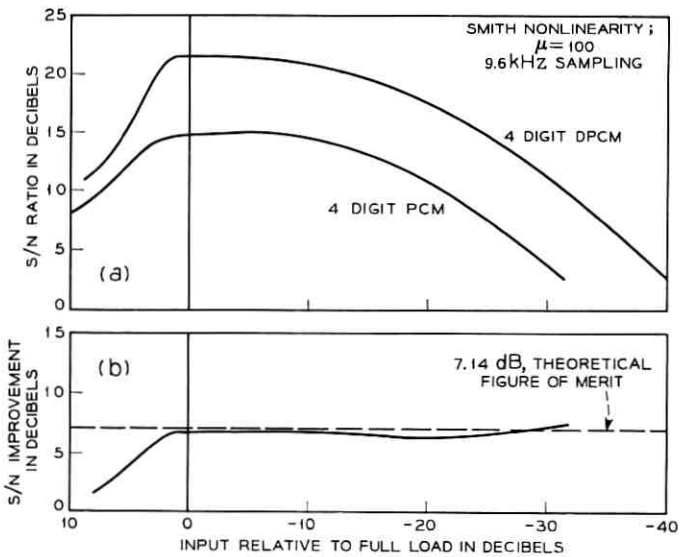

Fig. 5 — (a) Signal-to-noise ratio by simulation. (b) Actual improvement compared to theoretical.

minus) is 0.005. This arbitrary rule was suggested to me by Mr. J. F. Kaiser of Bell Laboratories. The noise includes overload noise, and hence does not conform to the approximate equation (7). Fig. 5(b) shows the difference in dB between the two curves of Fig. 5(a) and also a straight line representing the 7.14 dB difference predicted by the theory. The results indicate that whereas the theory does not predict the exact improvement it does so within about a dB over an input range of about 30 dB. Some improvement in the prediction made by the theory would be expected with quantizers with larger numbers of steps, since the quantizing error term in (14) would then be smaller. This would reduce the discrepancy created by dropping that term in arriving at the figure of merit in (15). But the prediction will never be good in the overload region, because under that condition there is a high probability of large errors, regardless of quantizer step sizes, and the error samples become correlated with each other and with the signal. In addition, some of the discrepancy must be due to the fact that the normalized probability density of z is not the same as that of x. That assumption was made in determining that the figure of merit represented the improvement in signal-to-noise ratio. The assumption that the normalized probability density of z has a particular shape will be poorest under lightly loaded conditions, because the quantizing error becomes a large fraction of the signal z. Even when quantizing error is a negligible component of z, the result depends on the second-order statistics of the input variable x, and these statistics have been guessed at but are not known. The simulation was also carried out using another companding characteristic, with similar results, but those results are not shown here.

Observe in Figs. 6(a), (b), (c), and (d) the normalized probability density of z under various conditions of loading. These curves were obtained from the computer simulation. Note that under progressively lighter loads the probability density changes to bimodal. This can be explained in terms of the oscillation present in DPCM systems under light load when the quantizer is of the midriser type. (See the next section.) The fact that the shape is well maintained in the overload region has not been explained on intuitive or theoretical grounds, but note that in spite of the shape assumption being met, the variances of x and z do not maintain the ratio predicted in (15) because of the error term in z.

Further evidence related to our assumptions is shown in Figs. 7(a), (b), (c), and (d). There the normalized quantizing error power spectral densities for progressively decreased load on the quantizer are shown. In the very lightly loaded case, approximating the idle channel, the oscillation at the half sampling frequency is clearly shown. This was

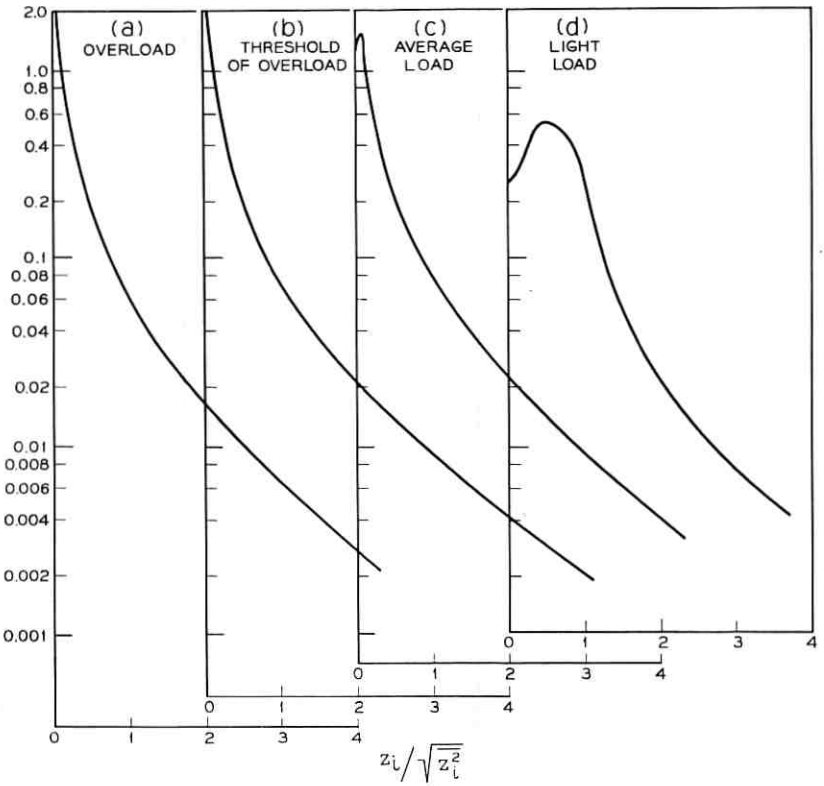

Fig. 6 — Normalized probability densities of z. Symmetrical average of "+" and "—" data; (a) overload; (b) threshold of overload; (c) average load; (d) light load.

mentioned earlier, and is described in full in the next section. The error spectrum remains approximately flat under changing load until the overload phenomena begin. In overload a sharp concentration of energy at low frequencies occurs. No analytical explanation of this has been developed. However, this is not due to a signal correlated component of error because that component was removed computationally in arriving at the spectra shown. It may be due to a statistical dependence more complex than linear correlation, however. The fine structure present on the curves should be ignored, since it is due to the truncation in time of the autocorrelation data used.

Finally, we note one additional point. The simulation was done with a sampling rate of 9.6 kHz. The sampling rate in Bell System voice-fre-

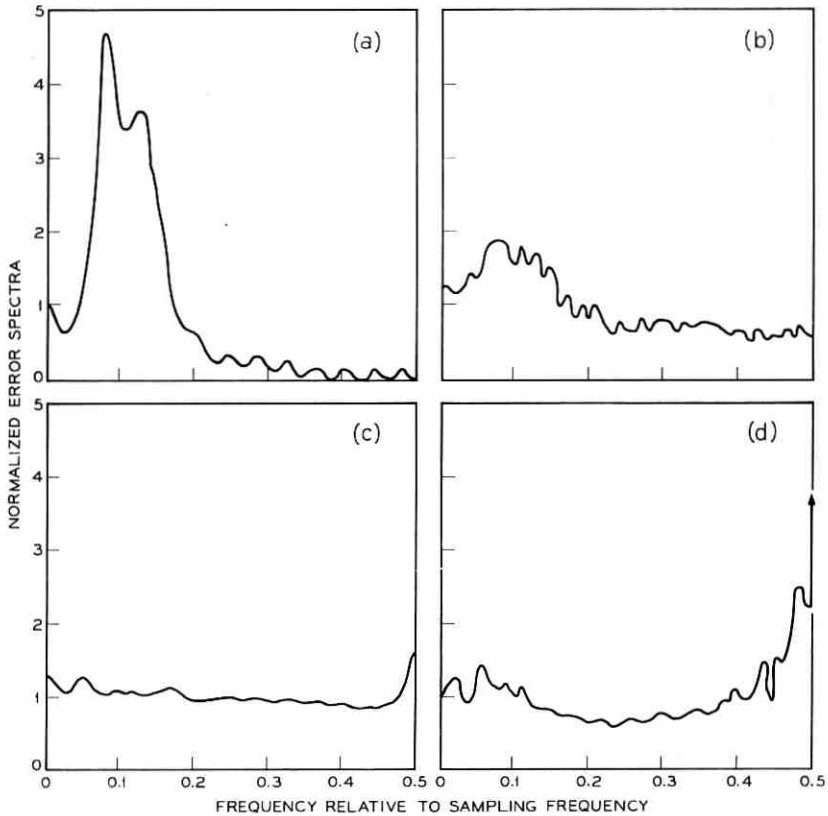

Fig. 7 — Normalized error spectra versus frequency relative to sampling frequency; (a) overload; (b) threshold of overload; (c) average load; (d) light load.

quency PCM equipment, such as the T1 Carrier System, is approximately 8 kHz.[19,21] If the value of ρ_1 for 8-kHz sampling can be determined, a prediction of the advantage of DPCM systems with this sampling rate can be determined. If the autocorrelation function of speech is reconstructed by means of the cardinal series, the value at 0.125 μsec is determined as

$$\rho_1 \mid_{8\text{ kHz}} = 0.8644.$$

All the correlation coefficients determined in this way appear in Table I(b). The figure of merit for nonoptimal DPCM is then

$$10 \log_{10} (\text{SNR IMPROVEMENT} \mid_{8\text{ kHz}}) = 5.7 \text{ dB}. \qquad (23)$$

This means that for the 8-kHz sampling rate, approximately one digit per sample can be saved by using DPCM.

Not considered in the simulations described here are the variations in speech statistics which are known to occur. The usual way of handling the volume variation is to use companding to shape the curve shown in Fig. 5(a). However, the characteristic number ρ_1 will also undoubtedly vary among talkers, perhaps correlated in some way with volume. No statistics on this are known to the author.

With the correlation coefficients given in Table I(b), it is possible to compute the optimum linear feedback coefficients, from (16). Since slightly greater generality is obtained, this will be done for $K \to \infty$. With a signal-to-noise ratio of 30 dB or more, one would expect practically negligible difference. Of great interest is the figure of merit calculated by (18) as a function of N. Fig. 8 shows this relationship. Note that for $N = 1$, the figure of merit is practically 6 dB, just over that attained by the nonoptimal case. For large N the improvement levels off at just over 10 dB, less than 2 digits better than PCM. Better than 9 of the 10 dB are available using only $N = 2$. No simulations have been run for this type of system; hence no check has been made of the assumptions as in the nonoptimal case.

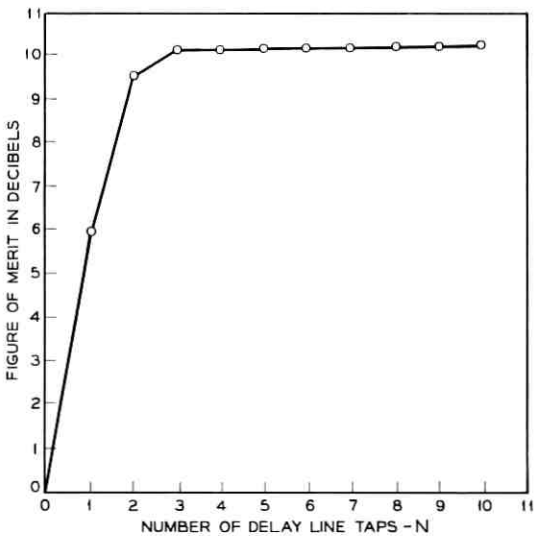

Fig. 8 — Figure of merit vs predictor complexity for 8-kHz sampling.

VII. IDLE CHANNEL PERFORMANCE

Of importance in the design of PCM systems is the so called idle channel performance. Shennum and Gray[22] calculated the output noise of a PCM system with low level thermal noise input, as a function of step size relative to rms noise, and as a function of the bias of the quantizer thresholds nearest the origin. This noise can be larger or smaller than the input thermal noise causing it. A phenomenon with similar causes but different effects occurs in DPCM systems, and these effects are analyzed here.

In this analysis we restrict ourselves to the nonoptimal DPCM described earlier, and represented, for purposes of analysis, in Fig. 9. The Gaussian independent thermal noise samples x_i are the input, and the samples f_i are the output. It is convenient, for analytical purposes, to consider uniform quantizer steps with unit step width and height. It is, of course, common for speech quantizers to be nonuniform, but the steps are generally almost uniform near the origin, the region with which we are concerned. The values computed here for idle channel noise should be compared with those for PCM when the step sizes are the same. Under this condition the systems are approximately equivalent with respect to quantizing noise performance.

The static characteristic of the uniform quantizer we have assumed is shown in Fig. 10, indicating the decision levels b_j, the representation levels a_j, and the biases A and B. The quantizer is assumed to have an infinite number of levels. The biases A and B can represent either drift in the quantizer or a deliberate design, or both. In the overall system, the decoder at the system output, may exhibit a third bias different from A, but that problem is separate from the ones being considered here. There is another factor, similar to these biases, which must be considered; it is the initial condition on the accumulator output at the outset of the idle period. With the exception of the *dc* level created in f_i, and the algebraic sign, the initial condition is identical in its effect to the bias B. Hence, it is no restriction to arbitrarily choose B, if we wish to ignore the *dc*

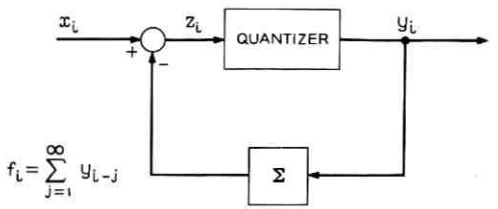

Fig. 9 — Simplified DPCM model.

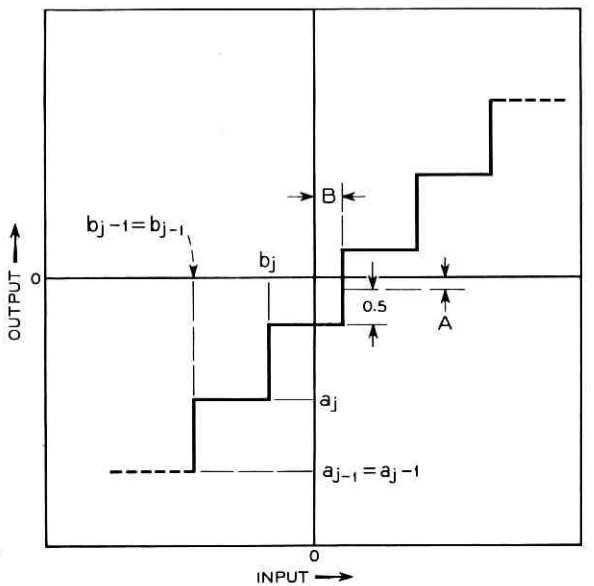

Fig. 10 — Quantizer definitions.

level, as long as the full range of initial conditions is considered. For convenience, choose $A = B$. Then the only two remaining independent parameters are the bias A and the initial value, I.

Under the above set of assumptions we note that the following relations hold.

$$a_j = \frac{b_{j-1} + b_j}{2} \tag{24}$$

$$b_j = a_j + \tfrac{1}{2}; \qquad b_{j-1} = a_j - \tfrac{1}{2} \tag{25}$$

$$y_i = a_j \quad \text{if} \quad a_j - \tfrac{1}{2} \leqq z_i < a_j + \tfrac{1}{2}. \tag{26}$$

For further convenience, let us assume a particular set of a_j's for reference. Let

$$a_j' = j + \tfrac{1}{2} \qquad j = \cdots -2, -1, 0, 1, \cdots. \tag{27}$$

Then

$$a_j = a_j' + A. \tag{28}$$

It is sufficient to study cases covering the range $-\frac{1}{2} \leqq A \leqq \frac{1}{2}$, and in

fact symmetry of the system precludes the necessity of studying half this range.

Of interest is the conditional one step transition probability of the output value f_i. We note this with two subscripts, the second denoting the initial value, the first the subsequent value. The superscript indicates the number of time periods that elapse in the transition.

$$p_{I+a_j,I}^{(1)} = \text{prob}\{a_j - \tfrac{1}{2} \leqq x_i - I < a_j + \tfrac{1}{2}\}. \tag{29}$$

In terms of our previous notations, this may also be written

$$p_{I+A+\frac{1}{2}+j,I}^{(1)} = \text{prob}\{j \leqq x_i - I - A < j + 1\}. \tag{30}$$

Equation (30) is the fundamental equation describing the generation of the samples f_i. However, it still does not give the mean squared value of f_i nor any other statistical characteristics in which we are interested. We may note that the sequence of samples f_i is first order Markov, but this doesn't bring us closer to a solution for our problem.

Let us note that following the initial value I, in one step, there is an enumerable set of possible values of f_i, of the form $\{I + a_j\}$. (Only a small finite subset of this enumerable set have significant probability.) Following each of these possibilities in one more step is another enumerable set of possible outputs; but in general the set of possible outputs is different following each member of the set $\{I + a_j\}$. This makes the state diagram for the sequence of values of f_i extremely complicated in general. It will be necessary to resort to computer simulation to discover what happens in these cases. But under some special assumptions it will be possible to carry the analysis further, and we take those cases first.

Let us first consider the special case, $A = -\frac{1}{2}$, called the midtread case. Then by (28), $a_j = j$, where j is any integer. Under these conditions, the set of possible outputs following I in one step is $\{I + j\}$, including I itself. Following any member of this set in one more step is any member of the *same* set of possible outputs, since the sum of integers is an integer. See Fig. 11 (a) for a flow graph to further clarify this case. Only three output states are shown although an enumerable number is required in general. Any member of the output set may be identified by the integer appearing in the expression for that member. The conditional one step transition probability from any member of the set to any other is written

$$p_{jk}^{(1)} = \text{prob}\{j - k - \tfrac{1}{2} \leqq x_i - I - k < j - k + \tfrac{1}{2}\}. \tag{31}$$

Equation (31) denotes a matrix of values of the conditional transition probabilities, which will be called the one step transition matrix, $P^{(1)}$.

$$P^{(1)} = \begin{bmatrix} \vdots & \vdots & \vdots & \\ \cdots\ p_{-1-1} & p_{-10} & p_{-11} & \cdots \\ \cdots\ p_{0-1} & p_{00} & p_{01} & \cdots \\ \cdots\ p_{1-1} & p_{10} & p_{11} & \cdots \\ \vdots & \vdots & \vdots & \end{bmatrix}. \tag{32}$$

In general, $P^{(1)}$ has enumerable dimensionality, but the probabilities become negligible in cases of interest for large enough magnitude of the indices, hence truncation of the range of the indices creates negligible error.

Similarly, let us consider the special case, $A = 0$, called the midriser case. Here, $a_j = j + \frac{1}{2}$. The first set of possible outputs following I is $\{I + j + \frac{1}{2}\}$, a set which does not include I. The next set of possible outputs, following any member of the above set is $\{I + k\}$ where k is any integer. The third set of possible outputs, following any member of $\{I + k\}$ is the same as the previous set $\{I + j + \frac{1}{2}\}$. Hence, there are two subsets of the total output set, and the output alternates between these subsets. Observe that the flowgraph for this case, Fig. 11 (*b*), has arrows only between the two subsets, none within the subsets. (For convenience the number of members of each subset has been truncated at three.) We may solve the problem of indexing the members of these sets by defining the index in the form

$$l = 2(j + \tfrac{1}{2}) = 2j + 1$$

for the first subset, and

$$l = 2k$$

for the second subset. Now with this notation we may write the one step conditional transition probabilities as before.

$$p_{jk}^{(1)} = \text{prob}\left\{\frac{j-k-1}{2} \leqq x_i - I - \frac{k}{2} < \frac{j-k+1}{2}\right\}, \qquad j - k \text{ odd}$$
$$= 0, \qquad j - k \text{ even}. \tag{33}$$

Because of the alternation between members of two sets, about twice as many possible outputs have to be used in this case as in the first case to make the truncation error negligible.

Cases with larger numbers of output subsets may be found under the

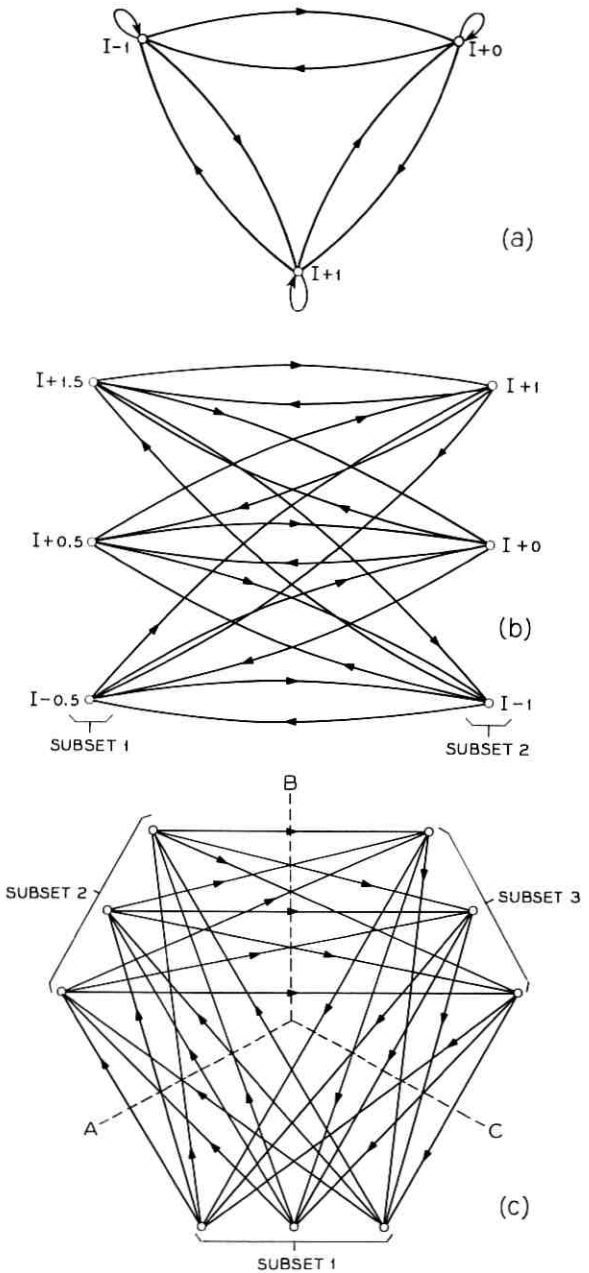

Fig. 11 — (a) Midtread case; $A = -\frac{1}{2}$, $M = 1$. (b) Midriser case; $A = 0$, $M = 2$. (c) $A = -\frac{1}{6}$, $M = 3$.

following conditions. Suppose A is any rational number of the form $\pm m/n$ where $| m/n | \leqq \frac{1}{2}$. Then the number of output subsets is M if M is the smallest integer satisfying

$$M\left(\frac{1}{2} \pm \frac{m}{n}\right) = \text{integer.}$$

The cases for $M = 3, 4, 5$, etc., could be worked out algebraically as we have for $M = 1, 2$, but those cases become unwieldy by the method being used. For clarity, the case $A = -\frac{1}{6}$ $(M = 3)$ is shown in Fig. 11(c), truncated at 3 members of each of the three subsets.

Let us return to the midtread and midriser cases. It is a simple matter to write the conditional probability equations governing the output sequence, and then to arrive at expressions for the output power and autocorrelation function. We write

$$P^{(v)} = P^{(1)} P^{(v-1)}. \tag{34}$$

Equation (34) is a form of the Smoluchowski equation. By iteration, one can easily solve for $P^{(v)}$.

$$P^{(v)} = [P^{(1)}]^v. \tag{35}$$

Let the *a priori* probability of the ith member of the output set be designated C_i, and let the square matrix C be formed with major diagonal elements C_i and other elements zero. The probabilities C_i may be determined from $P^{(1)}$ by simultaneous solution of the following equations:

$$\begin{aligned} C_i &= \sum_{\text{all } k} C_k p_{ik}^{(1)} \qquad \text{for all } i \\ 1 &= \sum_{\text{all } k} C_k . \end{aligned} \tag{36}$$

Equations (36) are an overdetermined system, but in general there is a unique solution, obtainable by not using one of the first group of equations. Now the joint probability of the output at a given step and the output v steps later may be written as the matrix

$$Q^{(v)} = P^{(v)} C \tag{37}$$

and the autocorrelation as a function of v may be written as the quadratic form

$$R(v) = f Q^{(v)} f', \tag{38}$$

where f is a row vector for which the elements are the members of the set of output values, indexed as indicated when developing these sets.

f' is the corresponding column vector. For purposes of defining $R(0)$, $P^{(0)}$ is defined as the unit matrix. All the terms on the right side of (38) may be evaluated by means of the computer, once the transition probability matrix is evaluated. The transition probabilities given by (31) or (33) may be evaluated in terms of the probability function assumed for the samples x_i. It is here that the ratio of variance of x_i to the step size (unity) enters as a parameter. Since the x_i are assumed to be samples of thermal noise, the probability density is assumed Gaussian with zero mean. The most important computed result is $R(0)$, the mean squared output noise relative to the squared step size. The dependence of $R(0)$ on the parameters A, I, and $\overline{x_i^2}$ is shown in Fig. 12. The values shown in Fig. 12 vary between the same maximum and minimum values calculated for PCM by Shennum and Gray.[22] Note that the noise exhibits much more fluctuation as a function of I in the midtread case ($A = -\frac{1}{2}$), although its minimum value is smaller. However, the initial condition I is a parameter which cannot be controlled in the design; hence, midriser

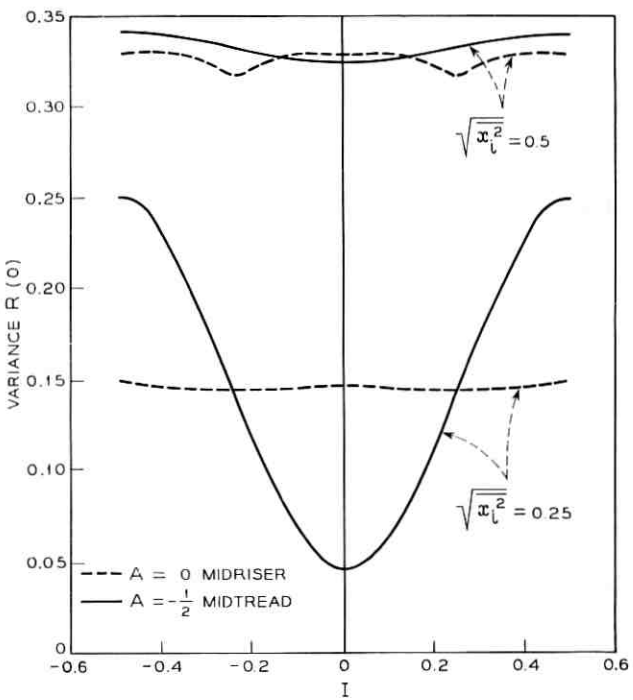

Fig. 12 — Idle channel noise in DPCM system.

operation is a considerably better choice. The other values of $R(v)$ contribute little by way of additional information except to show periodicities and dc values. In the cases studied to this point, these effects were small. Of these two, the midriser case is the only one exhibiting a periodicity. The amplitude of the periodicity depends on the initial value I. The frequency is the half sampling frequency and is easily filtered out in practical systems. This is the same periodicity which showed up in the simulation described in Section VI, and which is indicated in the noise spectrum shown in Fig. 7 (a). Aside from the small dc and periodic components, the output noise samples were uncorrelated.

Other cases, that is those with other values of A, were solved by simulation rather than algebraically. This is because the possible output values become more closely spaced and much higher dimensionality of the matrices is required for accuracy. The simulation is actually quite simple, since all the blocks shown in Fig. 9 are already shown as mathematical operations. The input samples are taken from a so-called Gaussian random number generator program, which produces essentially uncorrelated samples, and having a distribution which is quite accurately Gaussian but which truncates at six times the rms value. The output noise level showed no marked difference from the two cases already presented. Hence, the detailed results will not be shown except for one very interesting case. As indicated earlier, there are particular values of A for which the possible outputs are divided into 3, 4, 5, $\cdots$ etc., subsets. In these cases, the output sequences through these subsets in a definite order, although the particular member is chosen randomly. Clearly there is in general more than one rational fraction A for a given period M, and the pattern followed by the sequence of output subsets may be different for different rational fractions that go with a given value of M. As a consequence, there is a periodicity at $\frac{1}{3}$, $\frac{1}{4}$, $\frac{1}{5}$, $\cdots$ etc., of the sampling frequency respectively. This periodicity falls in the band below the half sampling frequency, and cannot be filtered out as in the midriser case. The sample sequences of the output are not periodic in general because of the randomness of the choice of a particular member of each subset. However, if in each subset there is one highly probable member and others of very small probability, the sample sequences are almost periodic. In the limit of zero input noise, the output sequence is a periodic function. In all cases, the mean and variance are periodic functions of time. As an example, a flowgraph for the case $M = 3$ is shown in Fig. 11(c). At cut A, all the arrows are from subset 1 to subset 2. No other arrows leave subset 1. Similarly, cut B intersects all the arrows from

subset 2 to subset 3, and cut C intersects all those from subset 3 to subset 1.

For the members of a given output subset, *a priori* probabilities may be computed by the methods indicated in (36), and these probabilities can be used to compute the mean and variance for the places in the sequence where that subset applies. The mean and variance for a case where the periodicity is $\frac{1}{20}th$ of the sampling frequency is shown in Fig. 13. In the case of the variance, both the theoretical curve computed from the probabilities and the curve obtained from the simulation are presented. Good agreement is shown.

If the value of A is irrational, the sequence of output subsets does not close on itself as in the cases indicated here. Hence, the period is not an integral multiple of the sampling interval. However, a similar phenomenon takes place with respect to periodicity of the mean and variance of a continuous signal reconstructed from the output sample sequence.

With the simulation method it is possible to study cases with nonuniform quantizing as well as the uniform cases studied to this point. One case with a small amount of nonlinearity was tried but no significantly different phenomena appeared in the results.

It is clear that the model used here for idle channel noise is not ade-

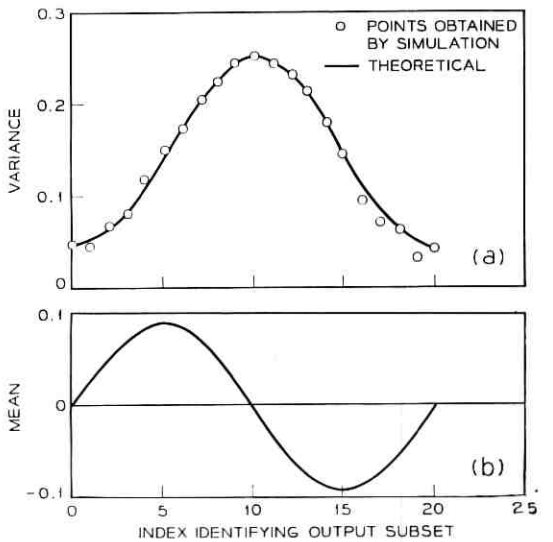

Fig. 13 — Mean and variance of idle channel noise $A = -0.45$; $\sqrt{\overline{x_i^2}} = 0.25$.

quate to describe what goes on in other systems such as DPCM with optimal feedback.

By way of summary, let us note that all evidence presented here points to the midriser case ($A = 0$) as the best one from the system design viewpoint. This is because of the inband periodic component present in the output of all of the other cases except the midtread case. The annoyance created by these inband periodicities will depend on their amplitude and frequency. This could be further studied by the simulation methods, and evaluated with subjective tests. But the midriser design should prove satisfactory, and additional investigation has not been undertaken. The midtread case is the only one showing no periodicity, but it is also the only one showing a high degree of dependence of the output variance on the initial condition I. Since the value of I cannot be controlled by the designer, the midtread case is also unsatisfactory. We note that it is only the quantizer output bias which must be controlled closely in the practical system, since the input bias change is equivalent to a change of initial condition, and we have found no great dependence on this parameter except in the midtread case.

It may be that the midriser design would no longer appear best when one considers crosstalk into an idle channel with a shared coder. Since this has not been investigated, no conclusions are presented on this point.

VIII. PRE-EMPHASIS

Equation (13) shows that in simple DPCM, it is the difference between adjacent input samples which forms the principal component of quantizer input. This leads one to the idea that a similar performance advantage is to be gained by using a pre-emphasis network with PCM. The network should approximate a differentiator. The principal qualitative difference in performance of this system is that an integrator is needed at the output to restore the original signal. This destroys the independence of the error samples and creates a subjective change in the output noise. It is not known whether frequency weighting of the noise will adequately account for the subjective changes. This problem was examined briefly, but is not reported in detail here. The pre-emphasis filter can be optimized, subject to a frequency weighted error criterion. It was found that, using this objective performance measure, an advantage nearly the same as that of simple DPCM can be attained.

Pre-emphasis (and de-emphasis) can also be used with DPCM systems. However, the differential aspect of the system makes use of most of the

advantage to be gained, leaving little additional for the filtering. In other words, the effects are not disjoint.

IX. SUMMARY

The results presented have fallen into approximately three categories. First, an analysis of signal to quantizing noise ratio has been presented, indicating the advantages to be gained by the use of various forms of DPCM, including simple DPCM and optimal DPCM with varying amounts of memory. The analytical results are discussed in the light of results obtained by other authors and the assumptions used. Second, a computer simulation was used to check the assumptions implicit in the present work and that of others. The probability density of the quantizer input and the quantizing error spectrum were studied by the simulation technique. The computer was also used to evaluate the performance to be expected when DPCM is used for speech transmission. It is shown that approximately 6 dB or one digit per sample advantage over PCM is attained by the simplest DPCM system. With optimal linear prediction, 10 dB or less than two digits per sample advantage over PCM is attained. Finally, the performance of the DPCM idle channel is investigated. It is shown that periodicities in the output of the idle channel sometimes are present. Amplitude and frequency depend on the bias of the quantizer output. It is pointed out that the most satisfactory design is the so-called midriser case, where the periodicity is at the half sampling frequency and can be filtered out in a practical system. The idle channel noise of DPCM varies in a different way from that of PCM. The level of the idle channel noise is approximately the same in both PCM and DPCM, when the quantizing noise performance is the same.

X. ACKNOWLEDGMENT

The author wishes to express his appreciation to the many individuals who were of assistance to him in this work. Among these were J. F. Kaiser who provided the computer tape and some programming advice, Miss E. G. Cheatham who helped with the programming, and M. R. Aaron who provided insight and later helped edit the manuscript.

REFERENCES

1. N. V. Phillips, Gloeilampenfabrieken of Holland, French Patent No. 987, 238. Applied for May 23, 1949; Issued August 10, 1951.
2. Cutler, C. C., Differential Quantization of Communication Signals, U. S. Patent No. 2,605,361, July 29, 1952.
3. Schouten, J. F., De Jager, F., and Greefkes, J. A., Delta Modulation, A New

Modulation System for Telecommunication, Phillips Technical Review, March, 1952.
4. Van De Weg, H., Quantizing Noise of a Single Integration Delta Modulation System with an N-digit Code, Phillips Research Reports, *8,* 1953, pp. 367–385.
5. Zetterburg, L., A Comparison Between Delta and Pulse Code Modulation, Ericsson Technics, *2,* No. 1, 1955, pp. 95–154.
6. O'Neal, J. B., Predictive Quantizing Systems (Differential Pulse Code Modulation) for Transmission of Television Signals, B.S.T.J., *45,* May–June, 1966, pp. 689–721.
7. Nitadori, K., Statistical Analysis of Δ-PCM, Electronics and Communications in Japan, *48,* No. 2, February, 1965.
8. Oliver, B. M., Efficient Coding, B.S.T.J., *31,* July, 1952.
9. Kimme, E. G., Methods of Optimal System Design for a PCM Video System Employing Quantization Noise Feedback, Unpublished work.
10. Kimme, E. G. and Kuo, F. F., Synthesis of Optimal Filters for a Feedback Quantization System, IEEE Trans. on C. T., *CT-10,* No. 3, September, 1963, pp. 405–413.
11. Spang, H. A. and Schultheiss, P. M., Reduction of Quantizing Noise by the Use of Feedback, IRE Trans. on Commun. Syst., December, 1962, p. 373.
12. Davenport, W. B., An Experimental Study of Speech-Wave Probability Distributions, J. Acoust. Soc. Amer. *24,* No. 4, July, 1952, pp. 390–399.
13. Purton, R. E., A Survey of Telephone Speech Signal Statistics and Their Significance in the Choice of PCM Companding Law, IEE Paper No. 3773E, January, 1962.
14. Dunn, H. K. and White, S. D., Statistical Measurements on Conversational Speech, J. Acoust. Soc. Amer., *11,* No. 1, January, 1940.
15. Panter, P. F. and Dite, W., Quantization Distortion in Pulse-Count Modulation with Nonuniform Spacing of Levels, Proc. IRE, *39,* January, 1951, pp. 44–48.
16. Smith, B., Instantaneous Companding of Quantized Signals, B.S.T.J., *27,* July, 1948, pp. 446–472.
17. Papoulis, A., *Probability, Random Variables, and Stochastic Processes,* McGraw-Hill Book Company, Inc., 1965, see Chapter 11, p. 385 ff.
18. Blackman, R. B. and Tukey, J. W., *The Measurement of Power Spectra,* Dover Publications, Inc., New York, 1958.
19. Members of Technical Staff of Bell Telephone Laboratories, *Transmission Systems for Communication,* Bell Telephone Laboratories, 1964.
20. Richards, D. L., Statistical Properties of Speech Signals, Proc. IEE, *111,* No. 5, May, 1964.
21. Fultz, K. E. and Pennick, D. B., The T1 Carrier System, B.S.T.J., *44,* September, 1965, p. 1405.
22. Shennum, R. H. and Gray, J. R., Performance Limitations of a Practical PCM Terminal, B.S.T.J., *41,* January, 1962, pp. 143–171.
23. Brainerd, R. C., Subjective Measurement on PCM Noise Feedback Coder for Video Transmission, Unpublished Memorandum.
24. Graham, R. E., Predictive Quantizing of Continuous Sources, Unpublished Memorandum.
25. McDonald, H. S. and Jackson, L. B., A Study of Single Frame Encoding of Pictures by Differential PCM Incorporating a Lossy Integrator, Unpublished Memorandum.
26. Miller, R. L., The Possible Use of Log Differential PCM for Speech Transmission in Unicom, Paper delivered at Globecom Conference in Chicago, 1961.
27. Miller, R. L. and Mounts, F. W., A Comparison of Differential PCM with Normal PCM for Speech Transmission, Unpublished Memorandum.

A Stability Criterion for Nonuniformly Sampled and Distributed Parameter Systems

By B. K. KINARIWALA and A. GERSHO

(Manuscript received May 9, 1966)

This paper presents a stability criterion for distributed parameter and uniformly or nonuniformly sampled systems. Specifically, a finite algorithm is presented which tests whether all the zeros of a function of the form

$$F(s) = \sum_{n=0}^{N} c_n e^{s u_n} ,$$

lie within the interior of the left half s-plane. Thus, the algorithm tests the stability of those systems whose system functions are ratios of finite sums of exponentials. Included in such systems are all distributed systems whose components are uniform, lossless transmission lines and all sampled systems with a periodically varying sampling rate.

This paper presents a stability criterion for distributed parameter and uniformly or nonuniformly sampled systems. Specifically, a finite algorithm is presented which tests whether all the zeros of a function of the form

$$F(s) = \sum_{n=0}^{N} c_n e^{s u_n} , \qquad \begin{pmatrix} c_n \text{ and } u_n \text{ real} \\ u_0 = 0 \\ u_{n+1} > u_n \end{pmatrix} \tag{1}$$

lie within the interior of the left half s-plane. Thus, the algorithm tests the stability of those systems whose system functions are ratios of finite sums of exponentials. Included in such systems are all distributed systems whose components are uniform, lossless transmission lines and all sampled systems with a periodically varying sampling rate.

Criterion: $F(s)$ is of type L_I (i.e., it has all its zeros in the interior of the

left half s-plane) if and only if

$$\Psi_o(s) = \frac{F(s) - F(-s)e^{suN}}{F(s) + F(-s)e^{suN}} = \frac{\sum_{n=0}^{m} a_n e^{sx_n}}{\sum_{n=0}^{m} b_n e^{sx_n}}, \qquad \begin{pmatrix} x_0 = 0 \\ x_{n+1} > x_n \end{pmatrix} \tag{2}$$

reduces to zero/K, (K a constant), under the repeated application of the following

Algorithm:

Given

$$\Psi_{k-1}(s) = \frac{\sum_n a_n e^{sx_n}}{\sum_n b_n e^{sx_n}}, \qquad \begin{pmatrix} x_0 = 0 \\ x_{n+1} > x_n \end{pmatrix}.$$

(*i*) Terminate the algorithm unless $0 < R_k < \infty$ where

$$R_k = -\frac{a_0}{b_0}.$$

(*ii*) Using

$$a_{nu} = R_k b_{nu} = a_n + R_k b_n$$
$$a_{nv} = -R_k b_{nv} = a_n - R_k b_n$$

decompose

$$\Psi_{k-1}(s) = \frac{\sum_n a_{nu} e^{sx_n} + \sum_n a_{nv} e^{sx_n}}{\sum_n b_{nu} e^{sx_n} + \sum_n b_{nv} e^{sx_n}}.$$

(*iii*) Identify the lowest x_n with nonzero a_{nu} as τ_k.

(*iv*) Obtain

$$\Psi_k(s) = \frac{\sum_n a_{nu} e^{s(x_n - \tau_k)} + \sum_n a_{nv} e^{sx_n}}{\sum_n b_{nu} e^{s(x_n - \tau_k)} + \sum_n b_{nv} e^{sx_n}}.$$

The algorithm is repeated for $k = 1, 2, \cdots, M$ until it terminates. The number of steps M is always finite.

Proof: The following three observations based upon the results of Ref. 1 lead to the above criterion.

(*i*) $F(s)$ is of type L_I if and only if $\Psi_o(s)$ is a positive-real function of s.

The Hadamard factorization theorem[2] shows that $e^{su_N}F(-s)/F(s)$ is analytic in the right half s-plane and it is bounded by one on the imaginary axis. Hence, $\Psi_o(s)$ is a positive-real function of s. Alternatively, for real problems (i.e., u_n rational) a mapping $\lambda = \tanh s\tau$ can be used to reduce Ψ_o to a rational function which is positive-real in λ and the conclusion follows.[1]

(*ii*) An odd function of the form (2) is positive-real if and only if it is the impedance function of a SCULL, i.e., a short-circuited cascade of uniform, lossless transmission lines.[1]

This is a special case of the realizability theorem in Ref. 1.

(*iii*) A function of the form (2) is the impedance function of a SCULL if and only if it reduces to (zero/a const.) under a repeated application of the above specified algorithm.[1]

This is actually a synthesis algorithm for the short-circuited cascade structure.

Q.E.D.

Example:

$$F(s) = 10e^{14.3s} - 2e^{8.2s} - e^{6.1s} + 5$$

$$\Psi_o(s) = \frac{5e^{14.3s} - e^{8.2s} + e^{6.1s} - 5}{15e^{14.3s} - 3e^{8.2s} - 3e^{6.1s} + 15}$$

$$\Psi_1(s) = \frac{6e^{6.1s} - 6}{12e^{6.1s} + 12}$$

$$\Psi_2(s) = \frac{\text{zero}}{24}.$$

Hence, $F(s)$ is of type L_I and the associated system is stable.

REFERENCES

1. Kinariwala, B. K., Theory of Cascaded Structures: Lossless Transmission Lines, B.S.T.J., *45*, April, 1966, pp. 631–649.
2. Titchmarsh, E. C., *The Theory of Functions*, Oxford University Press, London, 1939, Chapter VIII, p. 250.

Customer Evaluation of Telephone Circuits with Delay

By GEORGE K. HELDER

(Manuscript received June 9, 1966)

In 1964 tests were begun in which customers making transatlantic calls, to which varying amounts of delay had been added, were interviewed after call completion to determine the circuit quality. These tests were continued in 1965 using the Early Bird satellite which some customers used extensively before being interviewed. During this period a number of different echo suppressors were also tested. Results show that the quality of telephone circuits with echo suppressors decreases with increasing delay, that previous satellite calls have no effect on the customer's opinion of his present call, and that no echo suppressor was superior for all delays although some appear to be better for the longer delays.

I. INTRODUCTION

Echo occurs on any two-wire or combination two-wire, four-wire telephone circuit. The degrading effect of this echo depends on the time it takes for the echo to return to the speaker — the delay time. For very short echo delays — on the order of a few ms — the echo is masked by the sidetone in the telephone receiver. For somewhat longer delays — on the order of a few tens of ms — the echo can be made tolerable by providing loss in the telephone circuit to reduce the level of the echo. For delays longer than this, too much loss is required and echo suppressors are used. Echo suppressors are voice operated devices placed in the four-wire portion of the circuit which insert loss in the return path to suppress the echo.

When an echo suppressor is in its suppression mode, it places a large loss in the echo path which, besides suppressing echo, prevents the speech of the second party of the conversation from reaching the first party if both are speaking at the same time, i.e., double talking. If the echo suppression is removed during double talking, the echo is also heard.

The speech mutilation and imperfect echo suppression during double talking are generally not serious for delays up to about 100 ms. For longer delays, the effects can be easily noticed by many conversants and become increasingly troublesome as the delay increases.

Many tests have been conducted during the past few years to determine the importance of these subjective effects on telephone communications over circuits with long transmission delay. The interest in this subject is related to the introduction of satellite communications systems with their inherently longer delays than terrestrial circuits. Results previously reported have been those gathered in laboratory tests.*

Late in 1963 a program was instituted to obtain the reaction of real users of circuits with different amounts of delay. Initially, the quality of circuits from the United States to Europe over cable and the *Telstar*® and Relay satellites was compared by placing regular commercial telephone calls over circuits on these media. The users of the circuits were interviewed after the completion of the calls and asked whether they had had any difficulty in conversing and asked to rate the call Excellent, Good, Fair or Poor. It was soon evident that the problems of establishing telephone circuits over the experimental satellites were producing quality differences which were confounding the desired test results.

In early 1964, at the request of the Federal Communications Commission and with the advice and knowledge of the National Aeronautics and Space Administration and the Communications Satellite Corporation, a new series of tests was begun. These tests, conducted in cooperation with the telephone administrations in the United Kingdom and France, resulted in some 3000 interviews of customers who completed calls to London and Paris over cable circuits to which varying amounts of delay had been added.

This series of tests was continued in 1965 on circuits over cable and the Early Bird satellite. 4000 more interviews resulted. The telephone administrations in Germany and Italy, in addition to those in the United Kingdom and France, participated in these tests.

This paper discusses the tests conducted in 1964 and 1965.

II. 1964 TESTS

2.1 *Test Description*

From January 27 to April 24, 1964, two non-TASI cable circuits from New York to Paris and two from White Plains to London were equipped

* See, for example, Refs. 1 and 2.

with special echo suppressors and added delay.* The special echo suppressors were used in place of the 1A and, in London, the 6A echo suppressors regularly used on the circuits. A record-reproduce device inserted delay in the outgoing path from the USA as shown in Fig. 1. Four values of total round trip circuit delay were used: 90 ms, 300 ms 600 ms, and 800 ms.† (A small number of interviews were also made using 1000 and 1200 ms delay.)

Two experimental echo suppressors, designated the B and the L, and modified British 6A echo suppressors were used on the White Plains to London circuits; the B, L, and modified Bell System 1A echo suppressors were used on the two circuits from New York to Paris. The echo sup-

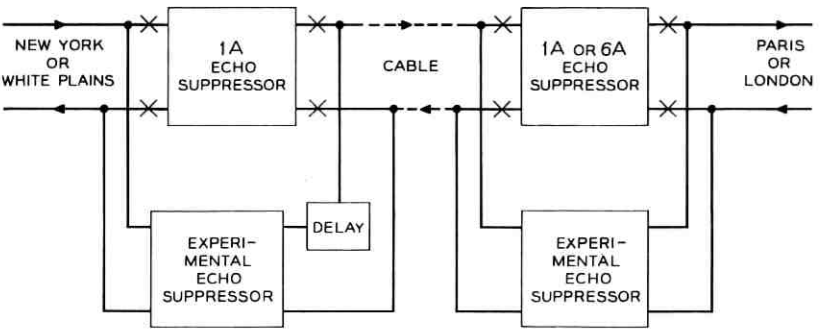

Fig. 1 — Placement of echo suppressors and delay.

pressors were rotated on the circuits so as to prevent any differences in individual circuit quality from biasing the results.

The four circuits had essentially the same transmission characteristics such as bandwidth, noise and transmission loss. The 3 dB down points of the bandwidth were at about 300 and 3100 Hz. The average noise level was about 42 dBrnC at the 0 transmission level point.‡ The circuits

* TASI, which stands for Time Assignment Speech Interpolation, is a technique used to provide more cable channels by time sharing. The circuits used in the 1964 tests were not derived in this manner.

† The 90 ms minimum value is the sum of the 70 ms inherent round trip delay of the cable plus 20 ms, which is the minimum delay introduced by the Echo-Vox. The Echo-Vox delay units were used on all calls including the control, minimum delay, calls. It can be shown that providing a lumped delay equal to the round trip delay in one direction of transmission only is, from the point of view of the speakers and the echo suppressors, equivalent to splitting the delays equally between both directions.

‡ dBrnC is dBrn as measured with a Western Electric 3A Noise Measuring Set with C Message Weighting.

were given special access codes* and were used as first choice circuits for outgoing calls from New York City to London and to Paris between the hours of 9:00 a.m. and 2:00 p.m., New York time, on weekdays. The traffic placed over the circuits was representative of the total traffic occurring during the test hours.

The operators using the circuits had no knowledge of the echo suppressors or delays being used, and they were given no special instructions other than those on the use of the specially coded circuits. The operators noted on the call ticket the access code used in addition to the normal information on party identification, call timing, etc.

2.2 *Echo Suppressor Description*

The pertinent parameter values of the echo suppressors used in the test are shown on Table I. The echo suppressor designated 1 is the modified 1A; 6 is the modified 6A.

Of the four echo suppressors used, the modified 6A and 1A echo suppressors were very similar. Both combined the suppression control and differential action into one circuit.† This does not allow a loud talker to remove suppression caused by a weak talker until the suppression hangover has expired. The modification in the 1A consisted of a 10 dB higher sensitivity and increased suppression loss. The modified 6A had a changed sensitivity frequency characteristic. This change was observed by the British Post Office (BPO) to produce suppression for lower level speech sounds with no increase in operation on noise.

The L echo suppressor, an experimental model of a United States manufacturer, was distinguished by its action during double talking. When this occurs the suppression was removed immediately, and 6-dB attenuation was inserted in both the receive and transmit paths to reduce the echo which was unsuppressed at this time. The hangover on the break-in circuit was about 30 ms. Another unique feature of this echo suppressor was the hysteresis effect present in the suppression and break-in circuits. The signal level required to release from the suppression mode was about 9 dB below that required to operate.

The B experimental echo suppressor, a Bell Laboratories model, was similar to the L in that suppression is removed immediately when double talking was detected. It was, however, unique in the long break-in hang-

* An access code is a three digit number usually associated with one country. When keyed by the overseas operator, it directs the call through the gateway switching machine to the group of circuits to that country. The special access codes here directed the calls to selected subgroups of the circuits to London and Paris.

† For a more complete description of the modified 1A and the B echo suppressors, see Ref. 3.

TABLE I — CHARACTERISTICS OF THE ECHO SUPPRESSORS IN THE 1964 TESTS (NOMINAL OR TYPICAL MEASURED VALUES)

Suppression	Echo Suppressor			
	1	6	B	L
Operate sensitivity*	−41	−26	−31	−32
Release sensitivity	−44	−29	−33	−41
Pick-up time†	10	4	8	1
Hangover time	50	50	50	30
Bandwidth	Peaked at 1000 Hz, 20 dB down at 500 and 2000 Hz	Peaked at 3500 Hz, 7 dB rise from 1000–2000 Hz	Flat over the voice band	Flat over the voice band
Break-In				
Operate sensitivity	−41	−26	−26	−36
Release sensitivity	−44	−29	−27	−41
Pick-up time	50‡	50‡	10	1
Hangover time	20	50	200	30
Bandwidth	Same as Suppression			
Loss During Double Talking				

1 None
6 None
B 6-dB attenuation in transmit path. Speech compressor in the receive path with 0-dB attenuation for a −40 dBm signal and 18-dB attenuation for a 0-dBm signal at the 0 transmission level point.
L 6-dB attenuation in both the receive and transmit paths.

* All sensitivity values are given in terms of the power level of 1000-Hz signal in dBm at the 0 transmission level point.
† All times are in msec and are measured using a 1000-Hz signal level 3 dB above the operate sensitivity.
‡ In the presence of a suppressing signal in the receive path, break-in does not occur until the suppression hangover time expires.

over time (200 ms) and in the insertion of a speech compressor during double talking to reduce the echo.

2.3 *Interviewing*

The method used to determine the subjective evaluation of circuit quality was the customer interview. The parties using the circuits were called back and interviewed by specially trained personnel in New York, London, and Paris after call completion. Fig. 2 gives the form of the questionnaire.* Every effort was made to use the same or equivalent forms and techniques in New York, London and Paris. The interviewers

* Fig. 2 is the form used in the 1965 tests. The wording of the questions on the 1964 form was essentially the same.

No. ☐☐☐☐☐ (1 2 3 4 5) Conv. Start Time ☐☐☐☐ (6 7 8 9) Elapsed Time ☐☐ (10 11)

Time First Attempt Starts ☐☐☐☐ (12 13 14 15) Time Interview Starts ☐☐☐☐ (16 17 18 19)

1. I am Mrs. _____ calling from the telephone company. We are making a study of our overseas connections. Do you have a moment to answer a few brief questions?
   Yes ☐ 20-1
   No ☐ -2

2. Our records show that you made an overseas call to (the United Kingdom, Paris, Germany) a short while ago. Is that correct?
   Yes ☐ 21-1
   No ☐ -2

3. Did you or the person you called have any difficulty talking or hearing over that connection? (Interviewer: If difficulty, probe and record verbatim - distinguish between called and calling parties.)
   No Difficulty ☐ 22-1
   Some Difficulty ☐ -2
   _____ Near ☐☐☐☐☐ (23 24 25 26 27) Far ☐☐☐ (28 29 30)

4. Which of these four words comes closest to describing the quality of that connection: Excellent, Good, Fair or Poor?
   Excellent ☐ 31-1 EX + GD ☐ -2
   Good ☐ -3 GD + FR ☐ -4
   Fair ☐ -5 FR + PR ☐ -6
   Poor ☐ -7 It varies ☐ -0

5. About how many times a month do you talk on the telephone with someone in (the United Kingdom, Paris, Germany)? (Interviewer: If first call, skip to Q.7)
   Calls per month ☐☐ (32 33)
   Other Period Stated _____

6. On your usual call to (the United Kingdom, Paris, Germany) which of these four words comes closest to describing the quality of that connection: Excellent, Good, Fair, or Poor?
   Excellent ☐ 34-1 EX + GD ☐ -2
   Good ☐ -3 GD + FR ☐ -4
   Fair ☐ -5 FR + PR ☐ -6
   Poor ☐ -7 It varies ☐ -0

7. Do you have any other comments you would like to make about your overseas telephone service?
   Yes ☐ 35-1
   No ☐ -2
   ☐☐☐☐☐☐☐☐☐☐ (36 37 38 39 40 41 42 43 44 45)

8. Thank you very much for your help.
   Accent: None ☐ 46-1; Slight ☐ -2; Heavy ☐ -3; Interpreter ☐ -4
   Reasons for non-completion of interview ☐☐☐☐ (47 48 49 50)
   Was any person that answered irritated? Yes ☐ 51-1; No ☐ -2

Time Contact Ended ☐☐☐☐ (52 53 54 55) Number of Interviewer ☐ (56) Number of Coder of Question 3 ☐ (57) No. of Coder of Question 7 ☐ (58)

Circuit Condition ☐ (59) Exposure ☐ 60-1; ☐ -2

Fig. 2 — The interview form used in the 1965 tests.

in New York were employees of a survey firm specializing in this type of work; in London and Paris they were telephone administration personnel who were given special training in interviewing. The interviewer had no knowledge of the type of circuit on which the call was made. No person was interviewed more than once. All interviews were during normal business hours and were completed the day the call was made.

2.4 *Results*

2.4.1 *General*

The primary measures of the subjective effects of transmission delay are the answers to questions 3 and 4 of the interview which concern difficulty in talking or hearing and quality rating. These questions were asked of customers in three locations: New York City, London, and Paris. The interviews in New York City have been separated into those on calls to London through the White Plains gateway and those on calls to Paris through the New York gateway. The customers used circuits with one of four different echo suppressors: 1, 6, B, and L; and had one of four values of delay: 90, 300, 600, and 800 ms. About 60 interviews were completed for each of the combinations of city, echo suppressor and delay. A total of about 3000 interviews resulted.

2.4.2 *Effect of Delay*

The interview results, pooled over echo suppressors and cities, are shown on Fig. 3, where the percentage of interviews reporting difficulty and having a fair or poor rating are plotted.* For delays of 90, 300, 600, and 800 ms each point represents about 750 interviews. The 1000 ms point represents 175 and the 1200 ms point 75 interviews. These last were taken during a two week pilot test prior to the main test and used the L and B echo suppressors only.

It can be seen that the fair or poor rating is similar to the difficulty measure. This similarity is also present when, as below, echo suppressors and cities are separated.

The rating of transmission quality (question 4) as a function of delay is shown in Fig. 4. Data from all cities and suppressors are combined. The percentage of excellent ratings decreases almost linearly with delay while both the poor and fair ratings have steeper slopes at higher delays.

* Also shown are 1965 test results discussed later.

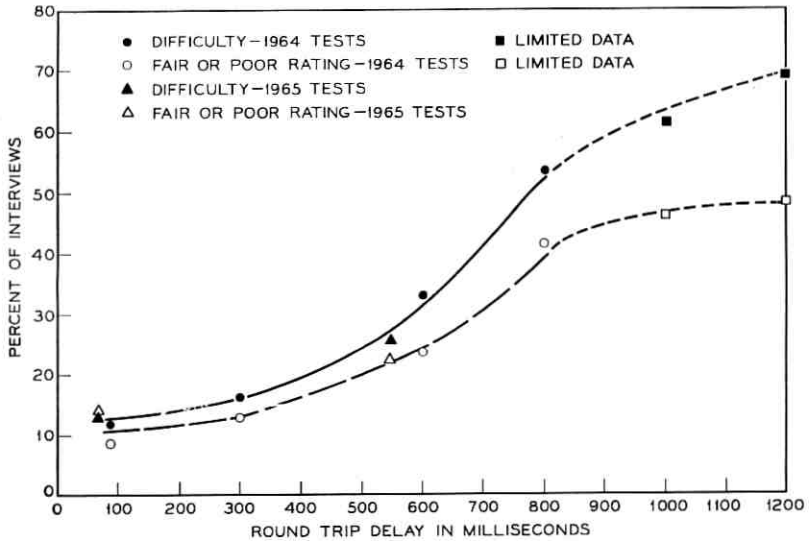

Fig. 3 — Effect of transmission delay.

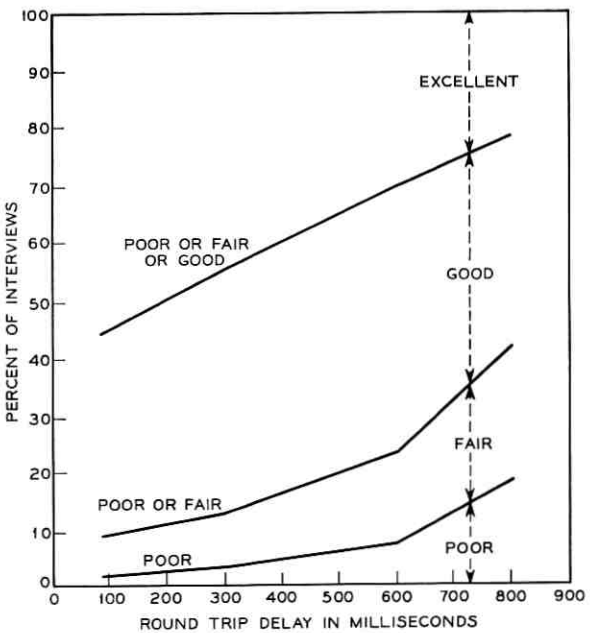

Fig. 4 — Rating of the calls.

2.4.3 *Comparison of Echo Suppressors*

Fig. 5 shows the percentage difficulty broken down for each echo suppressor separately. If the values shown in Fig. 3 are taken as the true mean, for each amount of delay, of the population of all interview results, then all but one of the values shown on Fig. 5 fall within the 95 percent confidence limits on the mean. The implication is that the differences among echo suppressors must be interpreted with caution since it is conceivable that the differences are due to chance sampling. It will be shown later that there is a more significant difference among echo suppressors in the specific types of difficulties they produce.

2.4.4 *Comparison of Cities*

The four "cities" we compare are actually three. Calls were received in London and Paris and were originated in New York City going via the White Plains gateway to London and the New York gateway to Paris. Hence, our four cities, New York (N), Paris (P), White Plains (W) and London (L).

The difficulty percentages combined over echo suppressors are shown on Fig. 6. An analysis of variance shows that, taking all delays into consideration, there is no significant difference among the cities. However, considering 90 ms only, there is a large difference between the

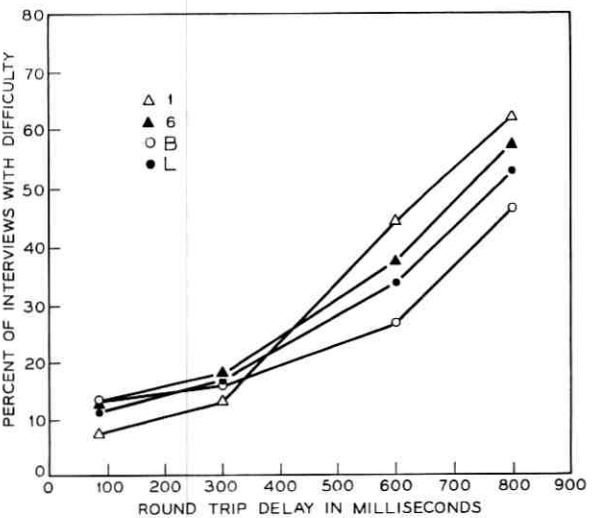

Fig. 5 — Comparison of echo suppressors.

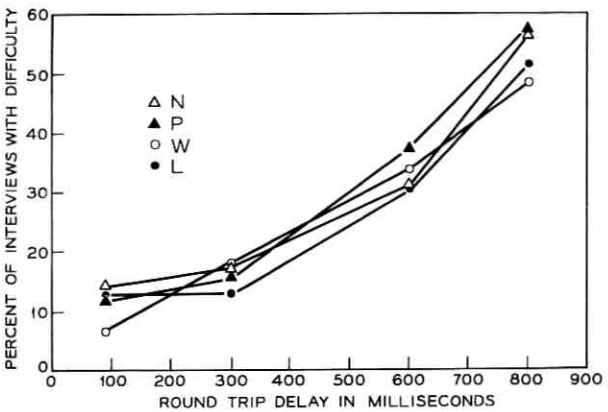

Fig. 6 — Comparison of cities.

results for New York City interviews on calls to London — W interviews, and on calls to Paris — N interviews. This difference also shows up in the usual call rating (Section 2.4.6) and in the 1965 tests (Section 3.4.3).

2.4.5 *Comments*

Those persons who had difficulty generally also described the difficulty they experienced. The difficulties, as stated in the users own words, are not always easy to classify. A three-man committee composed of persons from the Bell Telephone Laboratories, National Aeronautics and Space Administration, and Communications Satellite Corporation, without any knowledge of the echo suppressor or delay relating to each comment, classified the comments into 18 different types. The percentage, by type, of the total comments for all delays, echo suppressors and cities is shown on Fig. 7. Occasionally more than one type comment resulted from one interview.

The comments made by the users are also shown divided into comments they made about their difficulties (near end) and comments made about difficulties experienced by the other party (far end).

The relationship of comments to echo suppressors is shown on Fig. 8. The types of comments shown are those which are grouped on Fig. 7. For each comment four points are shown — one for each delay. The points represent the percentage of *interviews* which both had a "yes" answer to question 3 *and* which had a comment of the type shown, except

for the favorable comment points. In all but one case of favorable comments, no difficulty was reported and the comments were freely given.

Some things are readily apparent from Fig. 8. First, favorable comments generally decrease with delay; second, cutting comments generally increase with delay; third, echo and delay comments occur too rarely to permit meaningful interpretation. There is no clear pattern to most of the rest of the comment types. At the longer delays the B echo suppressor produces less cutting comments than the other echo suppressors. It is believed that this is due to the longer break-in hangover time and the insertion of the speech compressor during double talking.

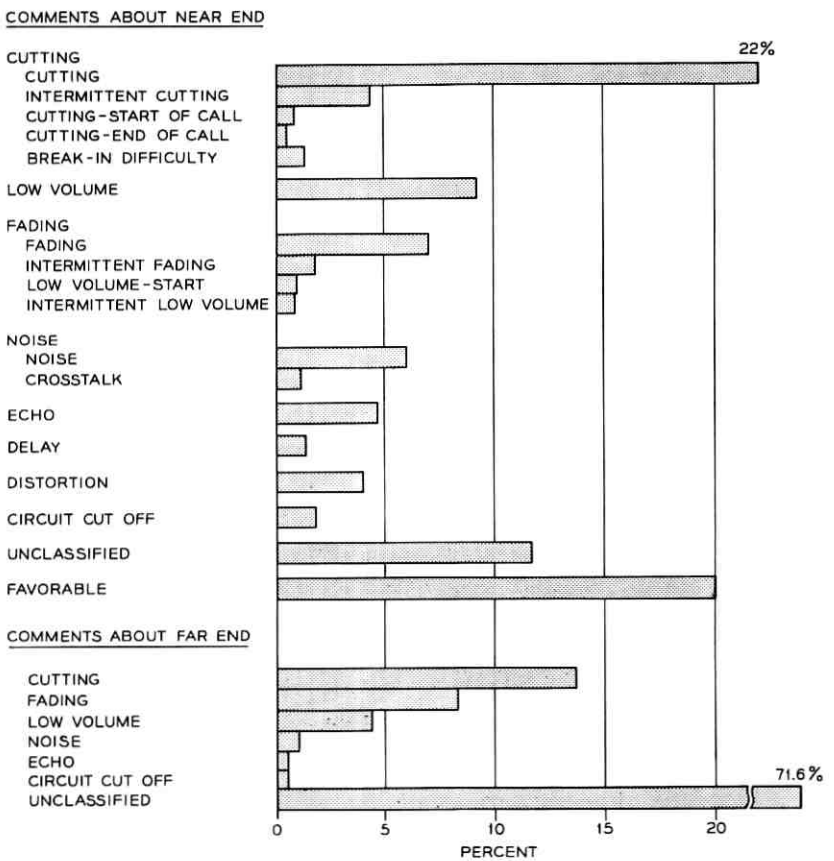

Fig. 7 — Percent of total comments by type.

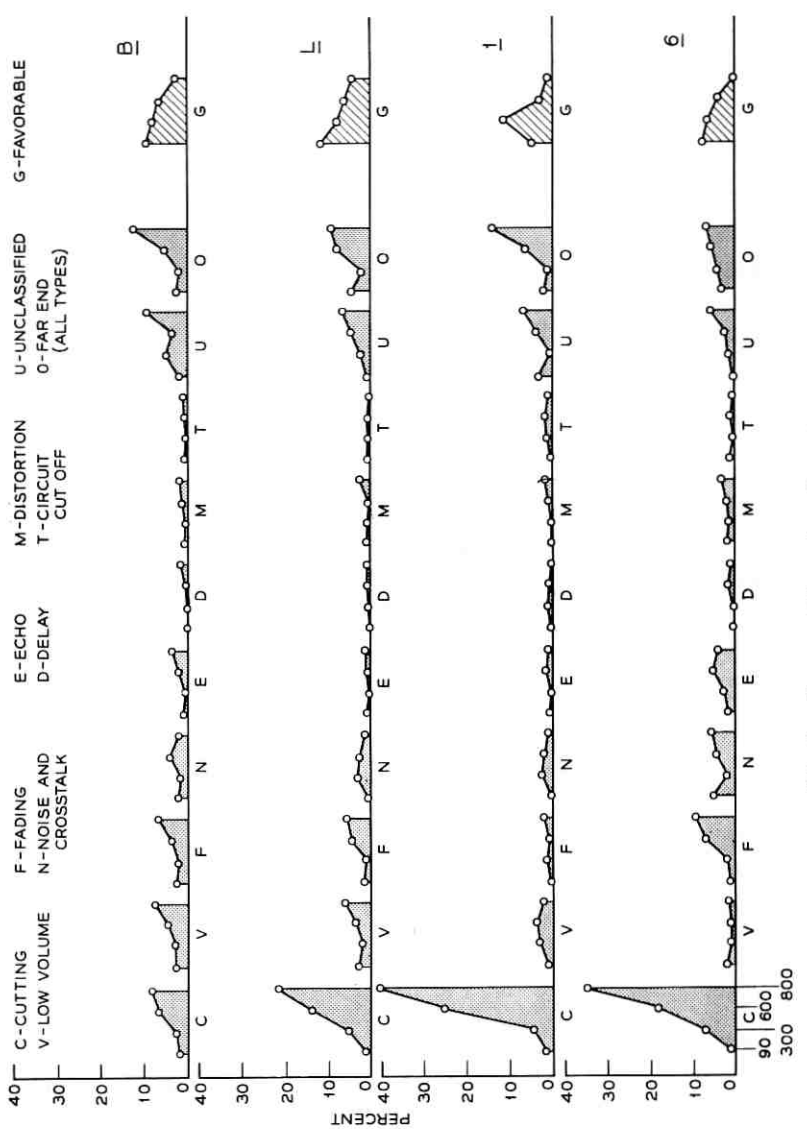

Fig. 8 — Comment types by echo suppressor.

2.4.6 *Rating of Usual Call*

Those interviewed who were not first time users of circuits to London and Paris replied to question 6 on the rating of their usual call. The results are shown on Fig. 9 pooled over cities and echo suppressors where each point represents about 700 interviews. (Also shown are 1965 results discussed later.) The usual call ratings change little with delay while the ratings of the present call, Fig. 4, are strongly affected by delay.

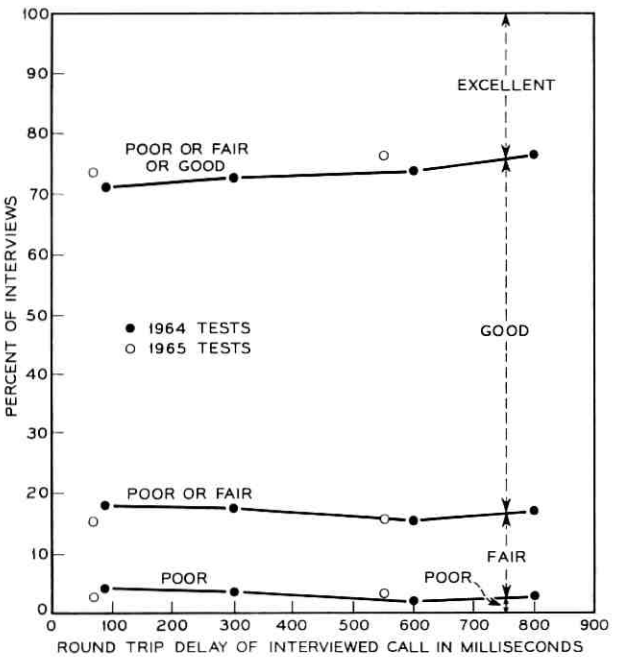

Fig. 9 — Rating of the usual call.

The average rating of the usual call is essentially independent of the average rating of the present call. Also of interest is the rating of the usual call compared with the rating given the present 90 ms call which is very similar in quality to the usual call.* The usual call ratings show fewer excellent and considerably more fair ratings than the present call. The predominant rating of the usual call is good. This may be due to an averaging by the customer of all his previous calls which can range from excellent to poor.

* The usual call is either non-TASI or TASI cable using 1A or equivalent echo suppressors.

The usual call ratings for each city separately, combined over delay and echo suppressors, are shown on Fig. 10. The differences in quality of the usual call to London and Paris for the New York City party (W and N) are consistent with the 90 ms results shown on Fig. 6. The differences between the London and Paris usual call ratings could easily be due to the differences of the population of users in the two cities.

2.4.7 *Length of Conversation*

The length of conversation was not related to the transmission delay as shown on Fig. 11. Prior to the test it was speculated that conversation time might decrease because of decreased satisfaction with the circuit quality, or might increase because of the lost information during times of echo suppressor mutilation and confused situations. Additional analysis shows no significant correlation bewteen the length of conversation and the percentage of customers reporting difficulty.

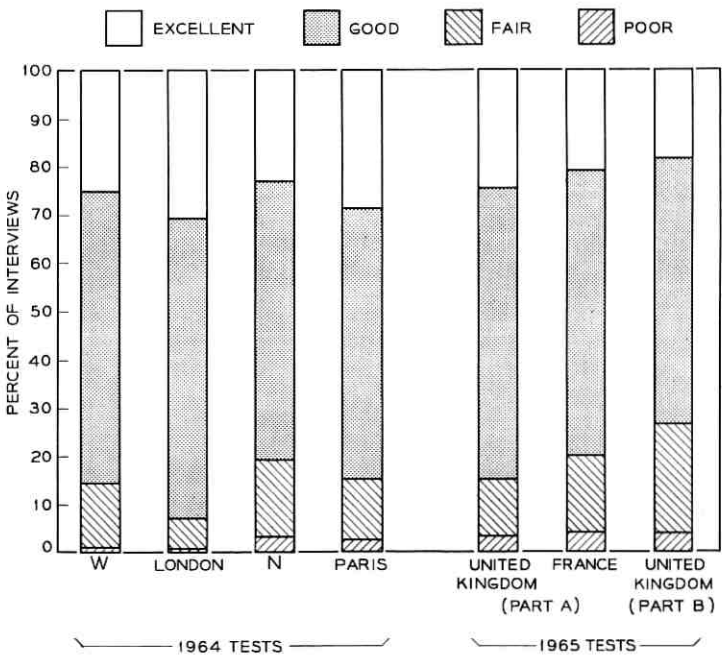

Fig. 10 — Rating of the usual call for each city.

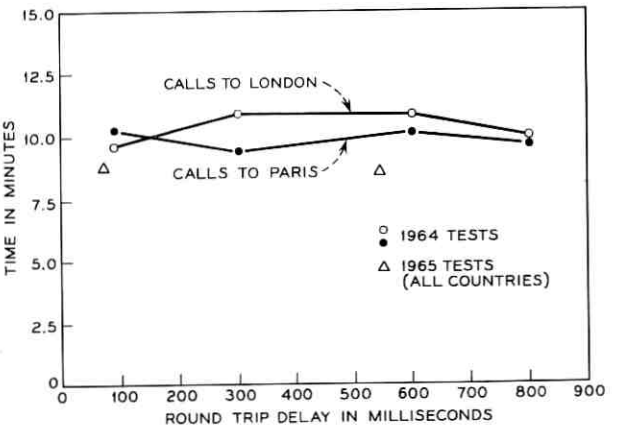

Fig. 11 — Average length of conversation.

2.4.8 *Speech Volume*

Speech volume measurements were made on most calls by craftsmen using VU meters. Some 4500 measurements indicate that the volumes for each delay were very similar. The greatest difference of averages between any two delays was 0.8 dB.

The percentage of customers reporting difficulty as a function of their volume is shown on Fig. 12 where a trend towards more difficulty for higher volumes exists (or conversely, higher volume for more difficulty).

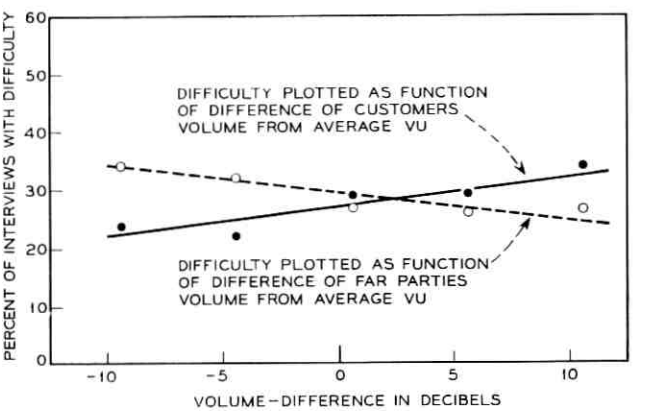

Fig. 12 — Effect of speech volume on difficulty.

Each point shown represents between 64 and 608 volume measurements. Also shown on Fig. 12 is the difficulty as a function of the received volume of the other party (not the interviewee). Here the trend is reversed, the interviewed party having less difficulty as the far party's speech volume increases. Each point represents between 182 and 480 volume measurements.

These trends might reasonably be expected. The louder one party talks, the more likely he will control the echo suppressors and cut off the interrupting speech of the far party. This also is more likely to happen if the far party is a low level talker. Additionally, this low received level itself may cause difficulty for the interviewed customer in the absence of any double talking.

2.4.9 *Interviews at Both Ends*

On 1000 calls it was possible to interview both parties to the conversation. Table II presents the percentage of calls on which the various combinations of difficulty were present.

What one can say is that if either party to the call reported difficulty there is a 50–50 chance the other party also will report difficulty, and if either party reported no difficulty, there is about a four to one chance the other will also report no difficulty. The results for Paris and London separately are very similar.

III. 1965 TESTS

3.1 *General*

In the 1964 tests the customers had only one exposure to long delay before interview. It had long been thought that frequent users of long delay circuits may react differently than those who seldom use them. It was unknown whether these heavy users would accommodate to the delay and echo suppressors or become more critical or neither. The advent of the Early Bird satellite provided the opportunity for investigation.

TABLE II — PERCENTAGE OF CALLS WITH DIFFICULTY

USA end	Europe End	
	Yes difficulty	No difficulty
Yes difficulty	15%	14%
No difficulty	14%	57%

The principal tests in 1965 (termed Part A) were aimed at determining the subjective quality of satellite circuits when:

(*i*) both satellite and cable circuits were in general use,
(*ii*) the presence of both types was common knowledge,
(*iii*) the novelty, if any, of satellite circuits had worn off, and
(*iv*) heavy users of transatlantic circuits had used the satellite extensively.

To provide a baseline for comparison, the quality of non-TASI cable calls was also evaluated and, in a later part of the test, an evaluation of cable circuits derived by TASI was also made.

Another series of tests, termed Part B, was conducted to evaluate a number of different connections, which may be typical in the future, involving satellite circuits with different types of echo suppressors at the two ends or with other echo suppressor-equipped circuits in tandem.

3.2 *Part A Test Description*

Commercial transatlantic telephone communications via the Early Bird satellite began June 28, 1965. From that date until November 12, 1965, all weekday satellite traffic to and from the United Kingdom, France, Germany, and Italy was restricted to that originating or terminating in New York City (except for that in the Part B tests, to be discussed later). A punched card record of each call was kept by each administration from whose national network the call originated. The punched card data included the names and telephone numbers of calling and called parties, test day, call timing, country identification, and customer recall of the originating operator. Copies of all punched cards were regularly forwarded to Bell Telephone Laboratories where they were combined to give the complete satellite calling history of each New York City overseas customer.

The calling history was complete for all weekday calls to and from these four countries for each New York City telephone number. Where different telephone numbers were used by one customer it was sometimes, but not always, possible to relate the calls on each number to the same customer. Calls made on weekends or holidays or to other countries having satellite circuits were not included in the call record cards.* About 50,000 call record cards were kept.

Interviewing of New York City customers began on September 7 for calls on the satellite and on non-TASI cable, and on October 29 for calls

* During the tests, 61 Early Bird circuits to Europe were in use. Two of these, to the United Kingdom, were used in the Part B tests. Of the remaining 59, 46 or 78 per cent were to the four countries involved.

on TASI cable circuits. The interviews continued through November 19. Satellite and non-TASI cable interviews were conducted on calls from the USA to the United Kingdom, France, and Germany; TASI interviews were made on calls to the United Kingdom and France only.

3.3 *Part A Circuit Description*

Essentially the whole group of Early Bird circuits to each country was used for interview calls. The circuits were given special access codes and used for New York City traffic only.

A representative sample of cable circuits — 8 cable circuits to France, 7 to the United Kingdom, and 2 to Germany — were removed from general message use, assigned special access codes and used exclusively for New York City traffic. The cable circuits to France and the United Kingdom were in turn divided into two groups with separate access codes, and the groups were alternately made non-TASI or TASI following a weekly schedule.

The operators handled traffic on all cable and satellite circuits in the same manner and noted on the call ticket the access code used. Subsequent to the interview, the access code was used in the analysis to separate the calls into non-TASI, TASI, and Early Bird calls.

The non-TASI circuits to the United Kingdom were in the Cantat and TAT-3 cables. When derived from TASI, the circuits had equal probabilities of using Cantat, TAT-1 and TAT-3 cable channels. The non-TASI circuits to France used TAT-2, TAT-3, and TAT-4 channels which were also used for the TASI derived circuits. The two non-TASI circuits to Germany used channels in TAT-4.

Noise and loss measurements were made regularly on all channels. Those made at the New York and White Plains testboards are shown in Table III. The noise values are corrected, i.e., those which would have been present had the average loss been zero dB.

The delay at 2000 Hz on two London Early Bird circuits was measured from White Plains when operating with the ground station at Raisting,

TABLE III — NOISE AND LOSS MEASUREMENTS

	Loss		Noise	
	Average (dB)	Std. dev. (dB)	Average (dBrnCO)	Std. dev. (dB)
Early Bird	−0.26	0.98	42.8	2.8
Non-TASI circuits in test	0.17	1.16	43.0	2.0
All channels used in TASI	0.21	1.4	43.2	2.3

Germany and found to be 544 ms round trip. The round trip delay on a TAT-1 circuit was 73.5 ms and for a TAT-3 circuit 86.5 ms. The bandwidth of the Early Bird circuits at the 3 dB down point was about 170 to 3400 Hz; for the TAT-3 cable circuit it was 230 to 3200 Hz.

The normal echo suppressors were used on the cable circuits. These are the Western Electric 1A in the USA and France and Germany, and the GPO 6A in the United Kingdom.* The Western Electric 2A echo suppressor was used at both ends of all Early Bird circuits. Its operation is similar to the B echo suppressor without the 6-dB attenuation in the transmit path.

3.4 *Part A Results*

3.4.1 *Effect of Exposure to Satellite Delays*

The pooled results of interviews made in New York City on calls to the United Kingdom, France, and Germany are shown on Fig. 13. A heavy user is here defined as one who made or received six or more satellite calls prior to being interviewed, including the call leading to the interview if the interview was made after a satellite call. Statistical tests indicate that the differences between the interview results for light and heavy users after both cable and satellite calls are not significant at the 0.05 level. This applies to both the percent difficulty and percent fair or poor.†

Table IV gives a more detailed breakdown of satellite exposure prior to interview. The division between light and heavy users at six satellite cells is arbitrary. On the basis of other divisions, however, one would also probably conclude that there is no significant change in the results with increased exposure.

In all further presentations of results, heavy and light user interviews will be pooled.

3.4.2 *Comparison of Cable And Satellite Circuits*

The interview results for non-TASI, TASI and Early Bird circuits pooled over all countries and over heavy and light users are shown on Fig. 14. The differences between non-TASI and TASI cable are not statistically significant; those between the cable and Early Bird are highly significant.

* See Ref. 3 for a description of the 1A echo suppressor. The 6A is very similar.

† The largest difference is in fair or poor scores on satellite circuits. This difference would have to be 6.4 percent to be significant at the 0.05 level.

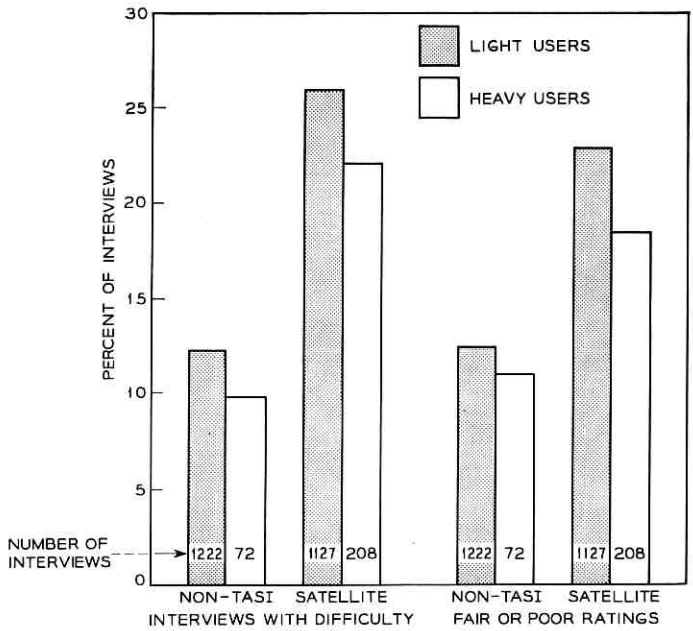

Fig. 13 — Comparison of light and heavy users of satellite circuits.

The rating breakdown is shown on Fig. 15. In addition to the breakdown for all calls, the ratings for those calls on which difficulty was or was not reported is also shown. This was done to see if there was perhaps a difference in the ratings given to calls with difficulty whether on cable or satellite. It was thought that there could be a difference in the severity of the difficulties experienced on the two types of circuits which would

TABLE IV — INTERVIEW RESULTS

No. of satellite calls prior to interview	Cable Interviews			Satellite Interviews		
	No. of interviews	Percent difficulty	Percent fair or poor	No. of interviews	Percent difficulty	Percent fair or poor
0–1	987	12.1	12.7	712	25.3	21.5
2–3	181	13.3	11.6	330	26.4	25.0
4–5	54	13.0	14.8	85	27.1	25.9
6–7	25	12.0	8.0	60	21.7	20.0
8–9	19	10.5	15.8	58	19.0	16.4
10–11	11	9.1	18.2	30	23.3	20.0
12–13	7	14.3	14.3	20	25.0	15.0
14–15	4	0	0	7	0	14.3
16 & Over	6	0	0	33	30.3	21.2

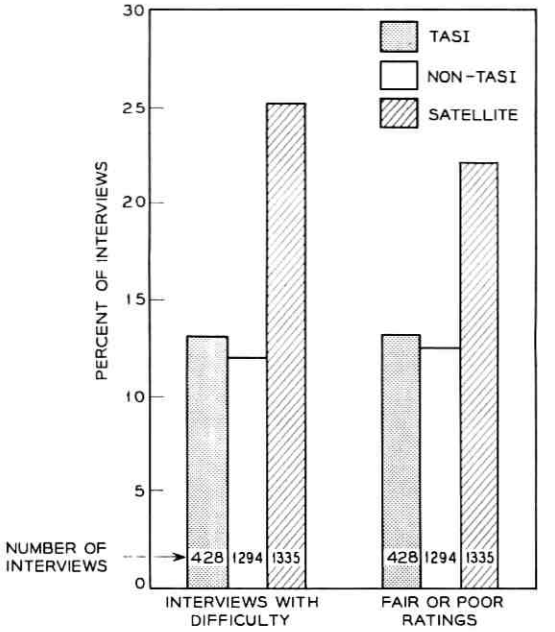

Fig. 14 — Comparison of cable and satellite circuits.

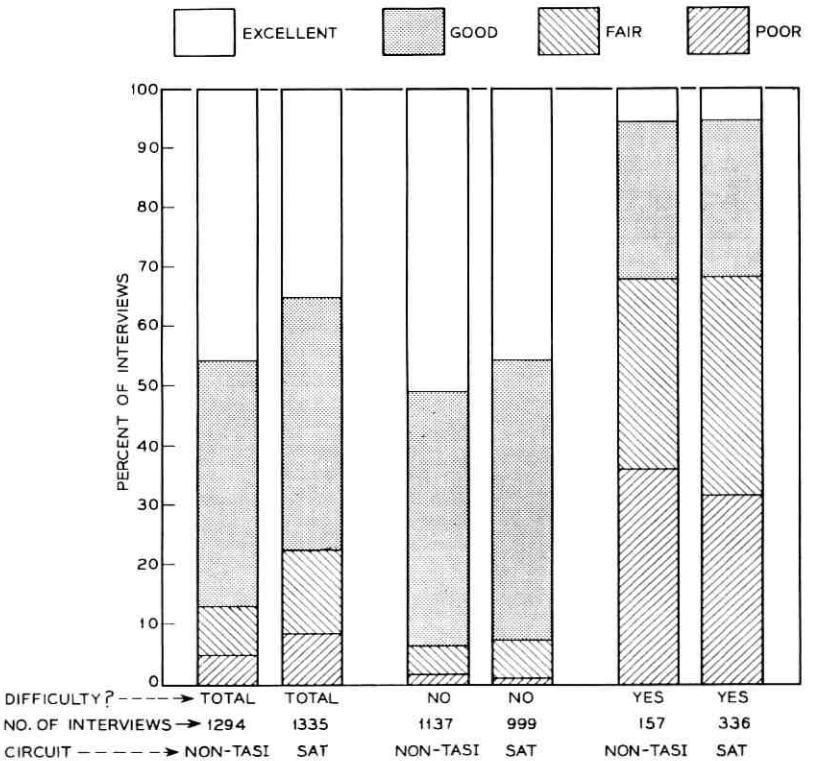

Fig. 15 — Rating of the calls.

show up in the ratings. The similarity of the ratings of the two types of circuits within both 'yes' and 'no' categories of difficulty suggests that there is no difference.

3.4.3 *Comparison of Countries*

The interview results broken down by country of destination are shown on Fig. 16. The following differences between the United Kingdom and France are statistically significant:

(*i*) TASI fair or poor ratings (significant at the 0.01 level).
(*ii*) Non-TASI difficulty (significant at the 0.01 level).
(*iii*) Non-TASI fair or poor (significant at the 0.05 level).

Between the United Kingdom and Germany only the non-TASI diffi-

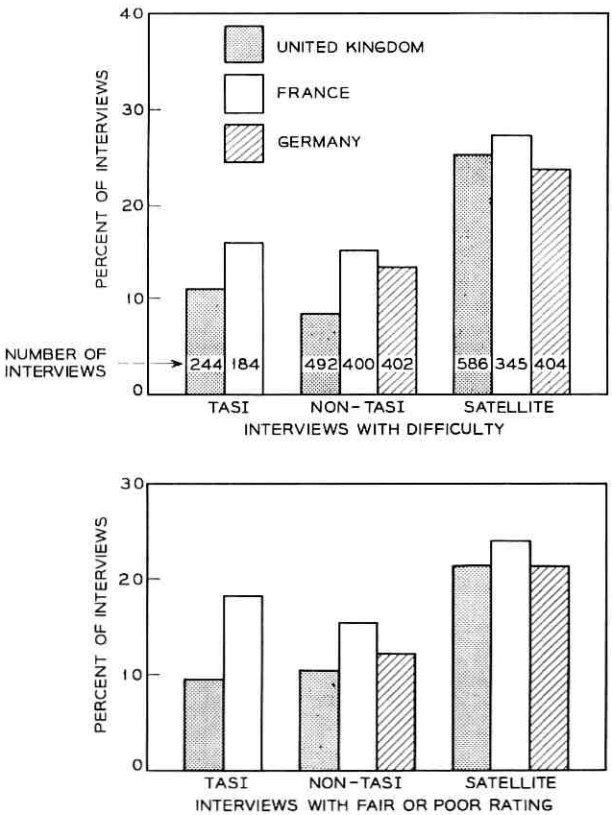

Fig. 16 — Comparison of countries.

culty difference is significant at the 0.05 level. No other differences between countries shown on Fig. 16 are significant. In Section 2.4.4 the differences between interviews on calls to London and Paris for low delays are mentioned.* The reason for this consistent difference is not known.

3.4.4 *Comparison of Ground Stations*

During the test period, the ground stations at Goonhilly Downs, Pleumer-Bodou and Raisting worked with Andover on a weekly rotating basis. The ground stations fed the international gateways in a triangular interconnecting circuit arrangement shown simply on Fig. 17. The ground

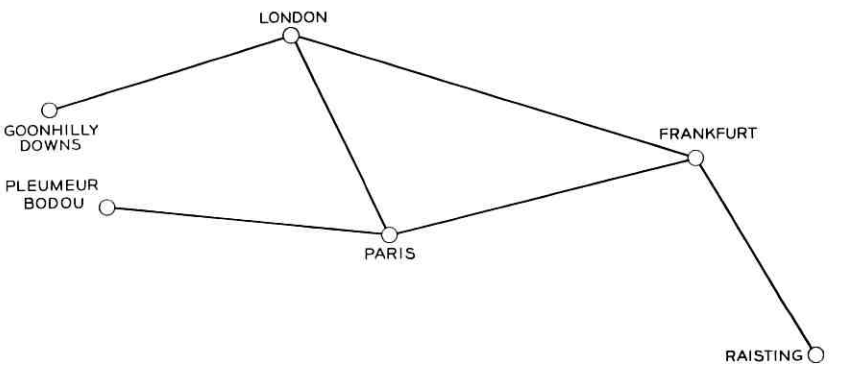

Fig. 17 — Europe Early Bird network.

station at Goonhilly alternately distributed the continental traffic through Frankfurt and Paris via London.

The interview breakdown by ground station, pooled over countries, is shown on Fig. 18. None of the differences are significant. A further analysis for each country separately also fails to yield significant differences, e.g., the United Kingdom results are the same for all ground stations.

3.4.5 *Customer Comments*

Prior to the 1965 tests, the comments made in the 1964 tests were analyzed to determine the most descriptive words. These descriptive

* In the 1965 tests 84 percent of the interviews on United Kingdom circuits were on calls to London and 90 percent of the interviews on France circuits were on calls to Paris.

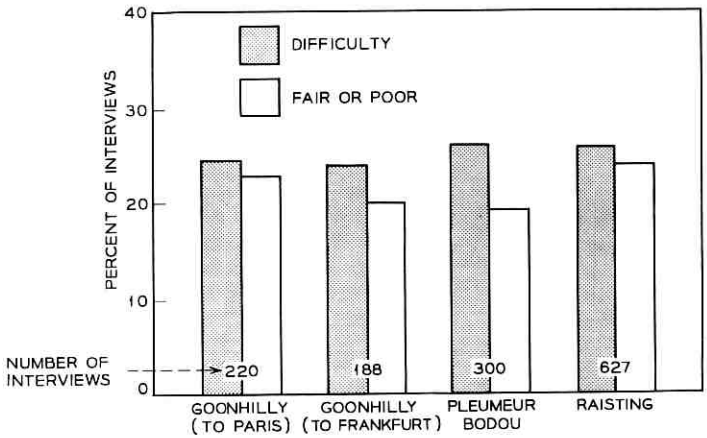

Fig. 18 — Comparison of ground stations.

words were then related to nine categories of difficulty and one favorable category, and a dictionary was prepared. The categories were a collapsed version of those used for the 1964 test as shown below.

Dictionary coding	1964 cable test coding
1 Cutting	Cutting on and off
	Cutting at start
	Cutting intermittent
	Break-in difficulty
	Cutting at end
2 Low Volume	Low volume
	Low volume at start
	Low volume intermittent
3 Fading	Fading
	Fading intermittent
4 Noise	Noise
5 Echo	Echo
6 Distortion	Distortion
7 Delay	Delay
8 Crosstalk	Crosstalk
9 Unclassified	Unclassified
	Circuit cut off
10 Favorable	Favorable

The interview supervisor, a senior interviewer, coded the comments made in the 1965 test into these ten categories using the dictionary as a guide. Fig. 19 presents the frequency of each type of comment in terms of the percent of all interviews having comments of the type shown. These include comments relating to the difficulties encountered by the near (interviewed) party and by the far party as described by the near party. In some cases interviews had comments classifiable into more than one category and occasionally both the near and far parties had

the same type of difficulty. About five percent of the customers who stated they had no difficulty, and were recorded as such, also made a classifiable comment about difficulty on the circuit. These data are included. On about two percent of the interviews, a favorable comment was made about transmission for one party along with difficulty comments about transmission for the other party.

It can be seen that in general the differences between the percentages shown are small and not consistent when comparing non-TASI and TASI. When comparing cable and satellite circuits the differences are consistent and, in many cases, statistically significant. The troubles experienced by the users of the satellite circuits appear to be caused in large part by the action of the echo suppressor as evidenced by the large increase in the cutting, fading, and echo comments. The delay *per se* of satellite circuits does not appear to be noted by the customers, but rather it is the delay in combination with the necessary echo suppressors.

3.4.6 *Rating of the Usual Call*

The customer's rating of the usual call was asked in each interview in order to be able to interpret his rating of the present call relative to

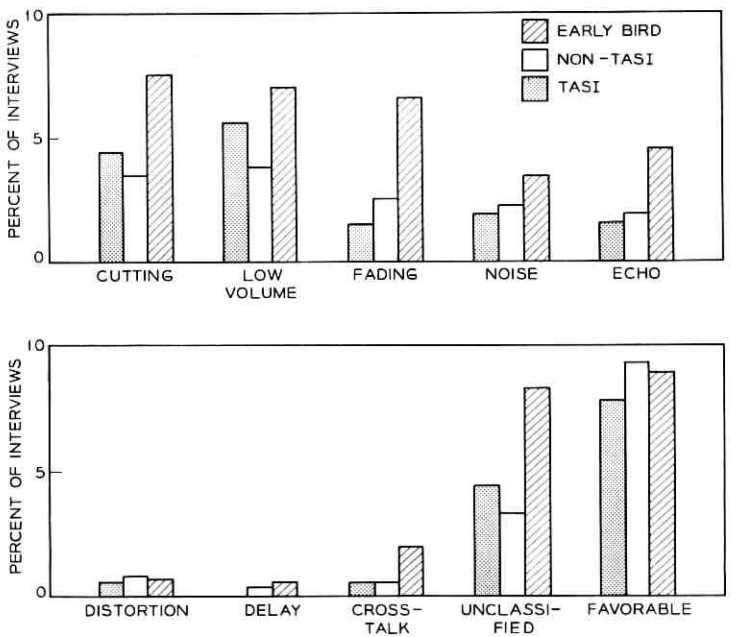

Fig. 19 — Customer comments.

his rating of his usual call to the same city. The usual call ratings for interviews on cable and satellite are shown on Fig. 9 where it is seen that they are very similar to those of the 1964 tests.

The relation between present and usual call ratings is shown on Fig. 20 in terms of the percentage of people who rated the present call one, two or three rating steps better or worse than their usual call. The satellite interviews have more present calls rated one, two or three steps poorer than the usual call than do the cable interviews. On both satellite and cable interviews, however, there are more cases in which the present call is rated better than the usual call than cases where the present call is rated worse than the usual call.

The usual call ratings for each country separately, combined over cable and satellite interviews, are shown on Fig. 10. A comparison of the W and United Kingdom and the N and France bars shows good agreement between the 1964 and the 1965 Part A tests and suggests that the population of customers and the usual call quality are the same in both tests.

As mentioned in Section 2.4.6, the respondents tend to give their usual (presumably cable) call a predominant rating of good and this

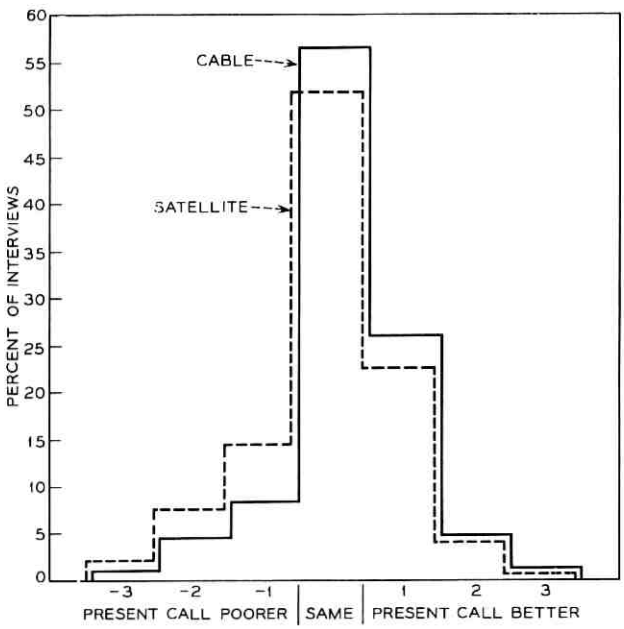

Fig. 20 — Rating of the present call expressed as the difference in rating steps from the usual call.

differs from the rating given present cable calls from essentially the same population of calls. This difference in ratings has been noted in several other tests. Because of this effect it is not appropriate to compare ratings of the usual calls and ratings of present calls using different facilities to determine relative transmission quality without compensating for the above described tendency.

3.4.7 *Length of Conversations*

As shown on Fig. 11, the average conversation length was essentially the same for cable and satellite calls.

3.4.8 *Time of Conversation*

Almost all interviews were made on calls which occurred between the hours of 8 a.m. and 2 p.m. New York time. These hours include the busiest traffic hours and an hour or so of lighter traffic before and after the busy hours. The assumption that the rate of customer difficulty increases with traffic density was tested. The following positive significant correlations with traffic density were found:

(*i*) Difficulty and fair or poor on United Kingdom TASI circuits.
(*ii*) Fair or poor on United Kingdom non-TASI circuits.
(*iii*) Fair or poor on France non-TASI circuits.
(*iv*) Difficulty on France Early Bird circuits.
(*v*) Fair or poor on German non-TASI circuits.

The reason for these correlations is not known. The correlations are not consistently associated with any country or type of circuit.

3.5 *Part B Test Description*

The Part B tests were conducted on two Early Bird circuits to London equipped with special echo suppressors. Traffic between the United Kingdom, excluding London, and 21 numbering plan areas surrounding but excluding New York City was placed on these circuits and the parties were interviewed after call completion. Confinement to the 21 NPA's prevented the inclusion of tandem echo suppressors in the United States Direct Distance Dialing (DDD) network.

3.6 *Part B Echo Suppressors*

The echo suppressor combinations used on the circuits are shown on Fig. 21. The 2A and 6A echo suppressors have already been described. (The 6AF is a full version of the 6AS used on cable circuits.) When used as split (6AS) echo suppressors, condition 6, 2-ohms delay was inserted between the two 6AS echo suppressors and −50 dBmO (psophometric) of noise was injected.

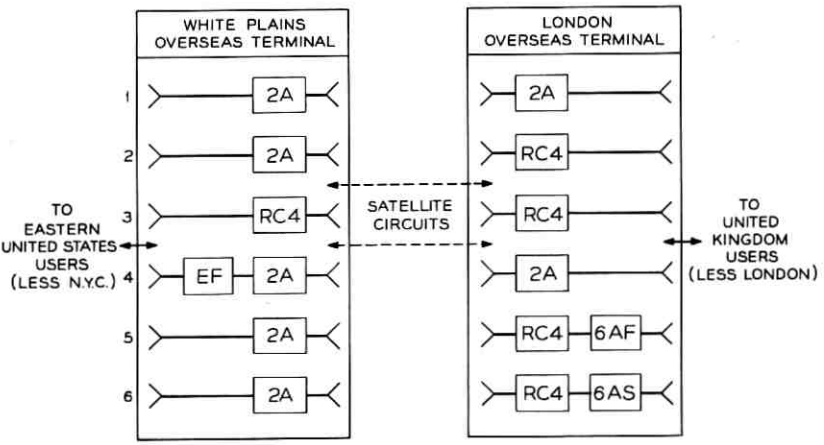

Fig. 21 — Part B circuit combinations.

The RC4 is a British Post Office experimental echo suppressor designed for long delay circuits. Its distinguishing features are a shaped frequency response in the control circuit path (like the modified 6A of Table I), a break-in hangover of 300 ms and 6 dB of loss inserted in the receive path during double talking.

The EF echo suppressor, a Bell Laboratories experimental model, is a full echo suppressor proposed as a replacement for the present Western Electric 1A in most domestic applications. It is much like two 2A echo suppressors back to back without speech compressors in the transmission paths.

3.7 *Part B Test Results*

3.7.1 *Comparison of Echo Suppressor Conditions*

The Part B results of interviews in the United States only are shown on Fig. 22. An analysis of variance shows that, taken as a group, there are no significant differences among the six conditions.

The average percentage difficulty for all conditions in the Part B tests was 42.4 and the average percentage fair or poor was 27.9. These values are close to those for condition 1 which used 2A echo suppressors only. It will be noted that these percentages are considerably different from those in the Part A tests for calls to the United Kingdom which were 25.1 percent difficulty and 21.6 percent fair or poor. The reason for this is not known. The populations of users were different in that the

Part A customers were in New York City and conversed, in most cases, with someone in London, while the Part B customers were in the eastern United States and conversed with someone in the United Kingdom excluding London. This may result in somewhat poorer circuit quality. Speech volume readings were made at the London gateway by the British Post Office, and the average transmitted volume to New York was 2.3 dB lower in the Part B tests than in Part A. As discussed in Section 3.4.8, this contributes to poorer quality. The ratings of the usual calls are also lower in Part B than in Part A.

3.7.2 *Rating of the Usual Call*

The usual call ratings are shown on Fig. 10 along with those Part A calls to the United Kingdom. This shows the higher percentage of fair ratings and lower percentage of excellent and good ratings in the Part B tests. No interviews were made on cable calls in the Part B tests so no comparison can be made between usual and present calls.

3.7.3 *Customer Comments*

One way of comparing the types of difficulties produced by the combinations is as follows. Combinations 1, 2, and 3 involve no tandem echo suppressors and the comments are therefore pooled. Combination 4 has

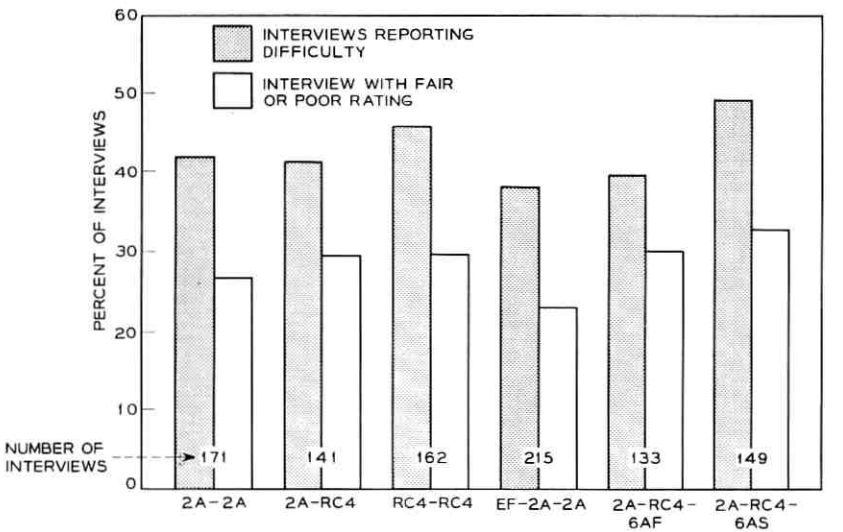

Fig. 22 — Comparison of circuits.

a tandem suppressor at the near end. Combinations 5 and 6 have tandem suppressors at the far end, and these comments are pooled. Taking the sum of all customer comments (excluding favorable) for each of the three classes of circuits above, one can then determine the percentage of the difficulty comments falling into each category, rather than the percentage of interviews having comments in each category. This has been done and is shown on Fig. 23. As would be expected, the tandem echo suppressor combinations generally produce a greater proportion of cutting and fading comments and fewer echo and crosstalk comments. (A customer comment about fading can relate to echo suppressor action, and echo is sometimes described by the customer as "other voices on the line," i.e., crosstalk.)

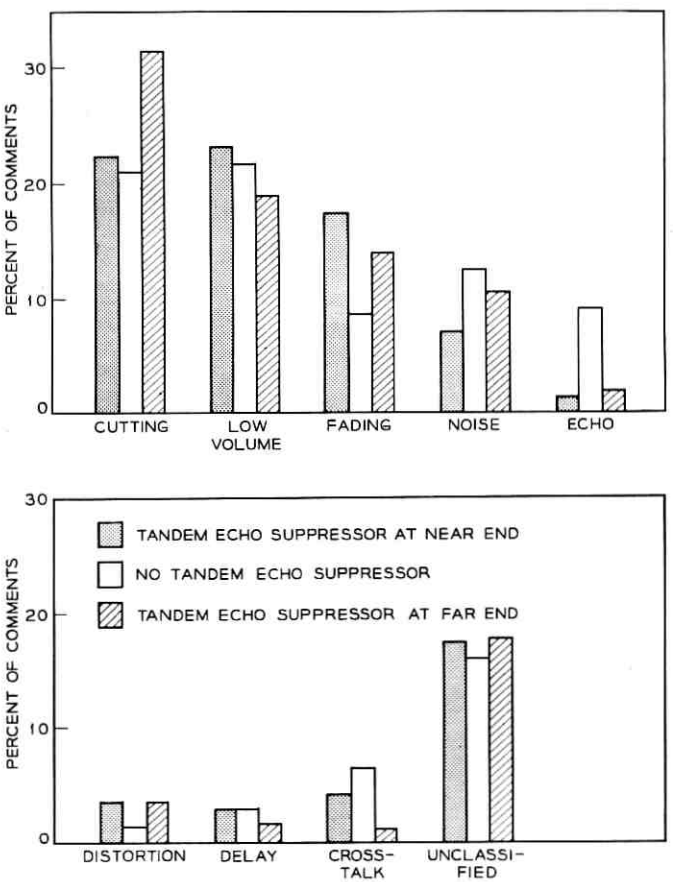

Fig. 23 — Comment breakdown.

IV. INTERVIEWING

4.1 *Technique*

Most of the interviewers in 1964 and 1965 were housewives who interviewed on a part-time basis. They had previous training in interviewing by their employer and were given two days of specialized training for these tests.

The interview took an average of 2.1 minutes to complete. About 0.6 percent of the customers in 1965 expressed some irritation about being interviewed. Although no count was taken, a sizable percentage of interviewees expressed some pleasure about being interviewed.

In 1964, the average time from call completion to interview completion was considerably less than one hour and in many cases only a few minutes. During the much more complex 1965 tests, the average time was greater than one hour. Some 81 percent of all interview attempts in 1964 resulted in a completed interview and this high percentage is due mainly to those interviews conducted within a few minutes. In 1965, this rate dropped to 65 percent.

The main reasons for non-completion of interviews appear in Table V.

4.2 *Comparison of Interviewers*

Five interviewers conducted most of the interviews in the 1965 Part A tests (one interviewer made $\frac{2}{3}$ of the interviews in the Part B tests and no Part A interviews). The Part A interviewers are compared on Fig. 24. Generally, the differences among interviewers are small compared with the differences among circuits, although in one case the cable ratings were lower for the cable than the satellite — the fair or poor ratings for interviewer number 4.

V. COMPARISON OF 1964 AND 1965 TEST RESULTS

The differences between the 1964 and 1965 tests, particularly in echo suppressors, make comparisons difficult. However, as discussed below,

TABLE V — REASONS FOR NOT COMPLETING INTERVIEWS

No answer	23%
Customer busy	66%
Customer refused all interviews	1%
Language barrier	1%

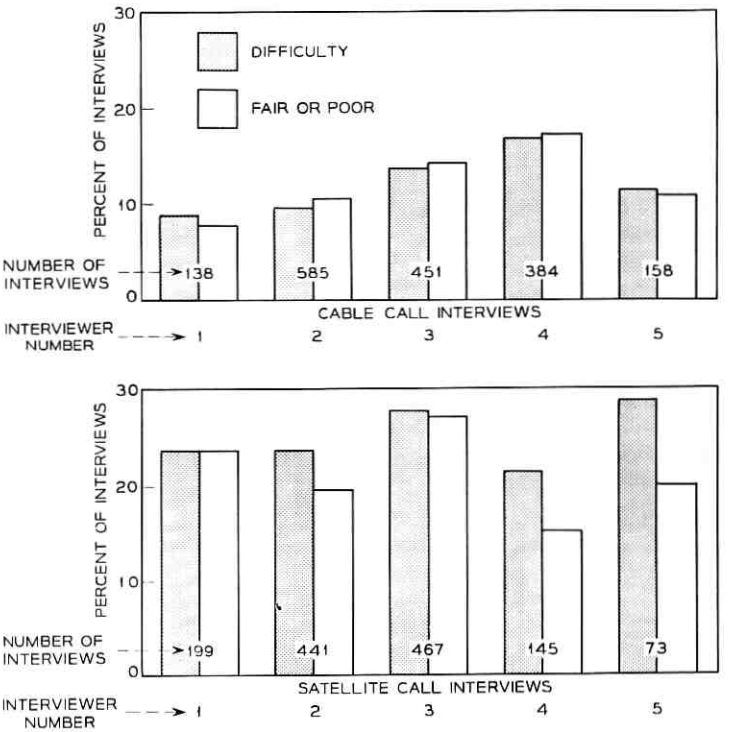

Fig. 24 — Comparison of interviewers.

those comparisons which seem most reasonable show the results of the two tests to be very similar.

In 1965, the Part A tests used the 2A echo suppressor, which is very similar to the B echo suppressor of the 1964 tests, and the interviews were in New York City only. The 1964 interviews in New York City only using the B echo suppressor are shown on Bar 1 on Fig. 25 while the 1965 results are shown on Bar 5. (The 1964 test results have been linearly extrapolated to the 545 ms delay of Early Bird. There is no extrapolation of the low cable delays.) Comparison of Bars 1 and 5 for both cable and satellite delays shows close similarity.

Since some of the 1965 interviews are on calls to Germany, these have been removed in Bar 4 to provide interviews to the United Kingdom and France only. The same comparisons can be made.

In the 1964 tests there was no consistent difference among the echo suppressors, and to increase the sample size the New York City inter-

views for all suppressors have been combined in Bar 2. There were also no significant differences among cities. Thus, Bar 3 represents all interviews in the 1964 tests (at the delays shown).

The data represented by each bar is summarized below:

Bar number 1 represents 1964 interviews in New York only on calls to London and Paris using the B echo suppressor.

Bar number 2 represents 1964 interviews in New York only to London and Paris using all echo suppressors.

Bar number 3 represents 1964 interviews in all cities using all echo suppressors.

Bar number 4 represents 1965 New York interviews on calls to the United Kingdom and France only.

Bar number 5 represents 1965 New York interviews on calls to the United Kingdom, France and Germany.

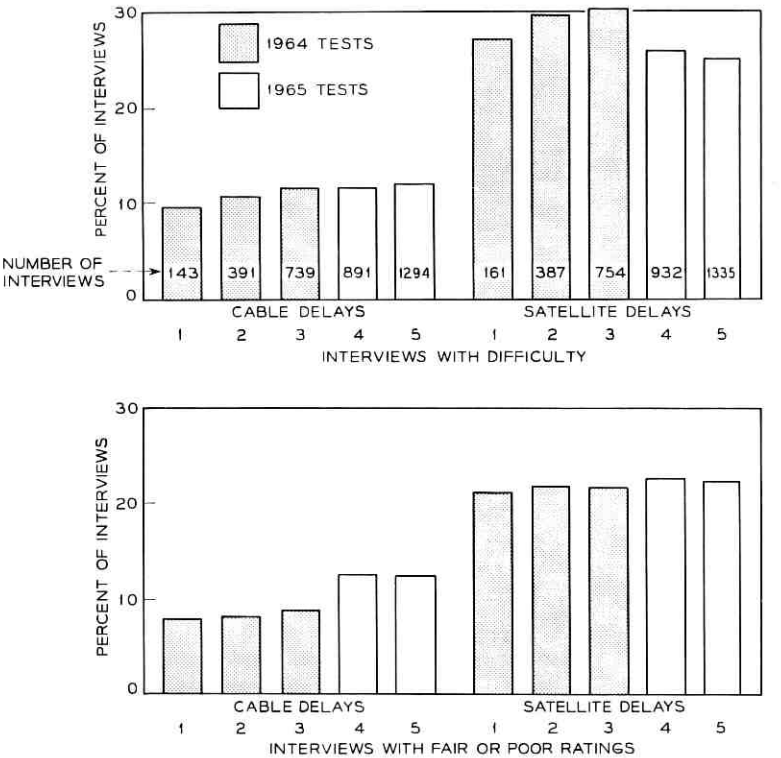

Fig. 25 — Comparison of 1964 and 1965 tests.

The close agreement between all comparisons for comparable amounts of delay suggests that the data can be combined as was done on Fig. 3.

VI. SUMMARY AND CONCLUSIONS

The following statements summarize the more important results of the tests.

(*i*) The quality of telephone circuits with echo suppressors decreases with increasing transmission delay.

(*ii*) Previous satellite calls, for the rates of exposure tested, have no effect on the customer's opinion of his present call.

(*iii*) There is no conclusive evidence that the echo suppressors and combinations of echo suppressors tested produce significant quality differences. It should not be inferred, however, that other echo suppressors would produce the same results.

(*iv*) The customer's rating of his usual call is relatively independent of the quality of his present call.

(*v*) Interviewing, as a method of evaluating circuit quality, provides consistent results.

(*vi*) There is enough variability among interviewers to require an experimental design which minimizes interviewer differences.

The customer opinion of circuit quality for any delay cannot be considered static. New advances in echo suppressors are not inconceivable, and this may improve the quality. On the other hand, historically telephone customers have come to expect continuing improvements in telephony, and this may tend to lower customer satisfaction. It should also be stressed that the customer's opinion of transatlantic circuits with delay does not necessarily reflect his opinion on other routes. Long delay circuits to hard-to-reach places may be infinitely better than none at all. Conversely, long delay circuits in the domestic network may be much less satisfactory than the presently used circuits.

VII. ACKNOWLEDGMENTS

I am at a loss to properly acknowledge the contributions made by literally hundreds of people. Let me just say that I am indebted to the many craftsmen, operators, interviewers, engineers, psychologists, administrators, and others from all the organizations in this country and in Europe whose interest and effort assured the success of the tests.

Without reducing in any way my appreciation for this widespread cooperation, I feel obliged to make special mention of Mr. Edmund T. Klemmer of Bell Telephone Laboratories who contributed so much to

the development of the interview technique and to Mr. Bernard Strassburg of the Federal Communications Commission who initially proposed the use of interviewing.

REFERENCES

1. Riesz, R. R. and Klemmer, E. T., Subjective Evaluation of Delay and Echo Suppressors in Telephone Communications, B.S.T.J., *42,* November, 1963, pp. 2919–2941.
2. Gardner, Mark B. and Nelson, John R., Combating Echo in Speech Circuits with Long Delay, J. Acoust. Soc. Am., *35,* November, 1963, p. 1762.
3. Brady, P. T. and Helder, G. K., Echo Supressor Design in Telephone Communications, B.S.T.J., *42,* November, 1963, pp. 2893–2918.

Contributors to This Issue

IRWIN DORROS, S.B., S.M., 1956, Massachusetts Institute of Technology; Eng.Sc.D., 1962, Columbia University; Bell Telephone Laboratories, 1956—. Mr. Dorros first joined Bell Laboratories as a MIT-Co-op student with assignments involving military communications, early data communications, and Electronic Switching Systems (ESS). He stayed on in ESS development where his work covered characterization of transistors for small functional circuits, circuit design for remote line concentrators, initial design of ferreed switches, and program and system "debugging" for the Morris ESS Trial. As Supervisor, Data Communications Development, Mr. Dorros was involved with a feasibility study of a narrow band system for multiple data channels over a single voice channel, and development for manufacture of the B1 Data Trunking System for deriving six narrow band data channels from a single voice channel. As Head, PCM Repeater Department, he was responsible for the development of the 224 Mb/s experimental repeatered line, design of the T2 repeatered line at 6.3 Mb/s, and equipment design for digital lines and terminals. He is currently Director of the Transmission Engineering Planning Center.

A. GERSHO, B.S., 1960, M.I.T.; M.S., 1961, Ph.D., 1963, Cornell University; Bell Telephone Laboratories, 1963—. Mr. Gersho is now Assistant Professor of Electrical Engineering at the City College of the City University of New York. He has been engaged in research in automatic and adaptive equalization for digital communications, synchronization of remote clocks, and synthesis of distributed networks.

A. GOETZBERGER, Ph.D. in Science, 1955, University of Munich; Bell Telephone Laboratories, 1963—. Mr. Goetzberger is a supervisor in the metal insulator semiconductor group. Prior to 1963, he was with the Shockley Laboratory in Palo Alto, where he worked on junction imperfections and avalanche breakdown phenomena in silicon. He also participated in the development of the power transistor. Member, American Physical Society, IEEE, Electrochemical Society.

RONALD L. GRAHAM, B.S., 1958, University of Alaska; M.A., Ph.D.,

1962, University of California (Berkeley); Bell Telephone Laboratories, 1962—. Mr. Graham has been engaged in research into a variety of problems arising in coding theory, graph theory and combinatorial geometry. Member, American Mathematical Society, Mathematical Association of America, Sigma Xi.

GEORGE K. HELDER, B.S. (Business), 1952, B.S.E.E., 1958, University of Colorado; M.E.E., 1960, New York University; Bell Telephone Laboratories, 1958—. Mr. Helder was first engaged in exchange area transmission, including methods of subscriber loop testing. More recently he has been concerned with the problems of echo control on telephone connections and in studies to determine the effects of transmission over long delay circuits. At present he supervises a group dealing with the transmission aspects of the local telephone network and echo control in the toll network. Member, Tau Beta Pi, Eta Kappa Nu, IEEE.

T. T. KADOTA, B.S., 1953, Yokahama National University (Japan); M.S., 1956, Ph.D., 1960, University of California (Berkeley); Bell Telephone Laboratories, 1960—. Mr. Kadota has been engaged in the study of noise theory with application to optimum detection theory. Member, Sigma Xi, SIAM.

B. K. KINARIWALA, B.S., 1951, Benares University (India); M.S., 1954, and Ph.D., 1957, University of California; Bell Telephone Laboratories, 1957–1966. Mr. Kinariwala is now Professor of Electrical Engineering at the University of Hawaii. He was first engaged in research in circuit theory involving, in particular, active and time-varying networks. More recently, he has been concerned with problems in communication systems. Member, IEEE, Sigma Xi.

JESSIE MACWILLIAMS (Mrs. F.J.), B.A., 1939, M.A., 1941 Cambridge, (England), Ph.D., 1962, Harvard; Bell Telephone Laboratories, 1956—. Mrs. MacWilliams has worked in transmission networks development, data communications engineering, and is now in the mathematics and statistics research center. Member, Mathematical Association of American, American Mathematical Society.

RICHARD A. MCDONALD, B.E. (EE), 1956, M.E. (EE), 1957 and D.E. (EE), 1961, Yale University; 1961–64, Assistant Professor of Engineering and Applied Science, Yale University; Bell Telephone Lab-

oratories, 1964—. Mr. McDonald has been concerned with aspects of the development of digital communication systems such as PCM, Differential PCM, and Deltamodulation for speech and video signals. Member, IEEE, Sigma Xi, Tau Beta Pi, ASEE.

JACK M. SIPRESS, B.E.E., M.E.E., and D.E.E., Polytechnic Institute of Brooklyn, 1956, 1957, and 1961, respectively; Bell Telephone Laboratories, 1958—. Previously employed by the Sperry Gyroscope Corp. and the Microwave Research Institute of the Polytechnic Institute of Brooklyn. At Bell Telephone Laboratories he was concerned with the design of active networks. Recently, he has supervised a group responsible for the systems design of digital transmission lines containing waveguide, coaxial cable, and paired cable media.

F. D. WALDHAUER, B.E.E., 1948, Cornell University, M.S.E.E., 1960, Columbia University; Radio Corporation of America, 1948–1955; Bell Telephone Laboratories, 1956—. At RCA, Mr. Waldhauer was engaged in transistor circuit development and in the prosecution of patent applications in the United States Patent Office. At Bell Telephone Laboratories he has been engaged in the exploratory development of the T1 PCM short haul carrier system and in broadband solid state analog-to-digital conversion for experimental 224 Mb/s PCM terminals, including fundamental development of feedback amplifiers. More recently, he has been in charge of a group responsible for the development of an experimental 224 Mb/s digital repeatered line.

E. J. WELDON, JR., B.S.E.E., 1958, Manhattan College; M.S.E.E., 1960 and Ph.D., 1963, University of Florida; Bell Telephone Laboratories, 1963—. Mr. Weldon has been concerned with the construction and analysis of error-correcting codes and the equipment necessary to implement them in data transmission systems. He is presently on a leave of absence at the University of Hawaii. Member, IEEE, Eta Kappa Nu.